

**SYNTHESIS AND CATALYTIC APPLICATIONS OF METAL  
OXIDE BASED MATERIALS IN PARTICULATE FORM**

**PARTİKÜL FORMUNDA METAL OKSİT BAZLI  
MALZEMELERİN SENTEZİ VE KATALİTİK  
UYGULAMALARI**

**KADRIYE ÖZLEM HAMALOĞLU**

**PROF. DR. S. ALİ TUNCEL**  
**Supervisor**

Submitted to Institute of Graduate School of Science and Engineering of  
Hacettepe University as a Partial Fulfillment to the Requirements for the  
Award of the Degree of Doctor of Philosophy in Chemical Engineering

2015



This work named “**Synthesis and Catalytic Applications of Metal Oxide Based Materials In Particulate Form**” by **KADRİYE ÖZLEM HAMALOĞLU** has been approved as a thesis for the Degree of **DOCTOR OF PHILOSOPHY IN CHEMICAL ENGINEERING** by the below mentioned Examining Committee Members.

Prof. Dr. Gürkan KARAKAŞ

Head

.....

Prof. Dr. S. Ali TUNCEL

Supervisor

.....

Prof. Dr. Halil KALIPÇILAR

Member

.....

Prof. Dr. Zümriye AKSU

Member

.....

Prof. Dr. Hülya YAVUZ ERSAN

Member

.....

This thesis has been approved as a thesis for the Degree of **DOCTOR OF PHILOSOPHY IN CHEMICAL ENGINEERING** by Board of Directors of the Institute of Graduate School of Science and Engineering.

Prof. Dr. Fatma SEVİN DÜZ

Director of the Institute of  
Graduate School of Science and Engineering

*'Imagination is more important than knowledge.'*

*Albert Einstein*

*To my valuable family and precious husband...*

## **ETHICS**

In this thesis study, prepared in accordance with the spelling rules of Institute of Graduate School of Science and Engineering of Hacettepe University,

I declare that

- all the information and documents have been obtained in the base of academic rules
- all audio-visual and written information and results have been presented according to the rules of scientific ethics
- in case of using other Works, related studies have been cited in accordance with the scientific standards
- all cited studies have been fully referenced
- I did not do any distortion in the data set
- and any part of this thesis has not been presented as another thesis study at this or any other university.

25/06/2015

KADRIYE ÖZLEM HAMALOĞLU

## **ABSTRACT**

# **SYNTHESIS AND CATALYTIC APPLICATIONS OF METAL OXIDE BASED MATERIALS IN PARTICULATE FORM**

**Kadriye Özlem HAMALOĞLU**

**Doctor of Philosophy, Department of Chemical Engineering**

**Supervisor: Prof. Dr. S. Ali TUNCEL**

**June 2015, 161 pages**

In this thesis, new sol-gel templating methods for the synthesis of titanium dioxide (TiO<sub>2</sub>) based catalysts in both bare and magnetic forms with or without gold nanoparticle decoration were developed, and their photocatalytic activity and plasmonic catalytic activity were investigated.

In the first part of this thesis, monodisperse-porous bare titania microbeads were synthesized by new sol-gel templating method by using sodium sulfonate (-SO<sub>3</sub>Na) attached-polymethacrylate microbeads as template. Newly synthesized monodisperse-porous poly(3-chloro-2-hydroxypropyl methacrylate-co-ethylene dimethacrylate), poly(HPMA-Cl-co-EDMA) microbeads 5.4 μm in size were used as starting material for the preparation of -SO<sub>3</sub>Na attached-polymethacrylate template. The new sol-gel templating protocol was applied by treating -SO<sub>3</sub>Na attached-polymethacrylate microbeads with the titania precursor, titanium chloride (TiCl<sub>4</sub>) in an aqueous medium and washing subsequently with ammonia to obtain

titania-polymer composite microbeads. The composite microbeads were calcined to have monodisperse-porous bare titania microbeads. The bare titania microbeads in the size range of 3.0-5.0  $\mu\text{m}$  with crater-like or fine porous structures with the specific surface areas ranging between 50-91  $\text{m}^2/\text{g}$  were obtained by changing the concentration and crosslinking density of  $-\text{SO}_3\text{Na}$  attached-polymethacrylate template microbeads and the calcination temperature. The selection of a polymethacrylate template decomposed at lower temperatures with respect to poly(styrene-co-divinylbenzene), poly(S-co-DVB) templates, commonly used for synthesis of porous titania microbeads, allowed to perform the calcination of titania-polymer composite microbeads at lower temperatures. Hence, monodisperse-porous titania microbeads with higher specific surface area and a crystalline structure with higher percent of anatase phase could be obtained by performing calcination at lower temperatures.

A new sol gel templating protocol was also first developed for the synthesis of monodisperse-porous titania microbeads in the magnetic form. For this purpose, the magnetic polymer template was obtained by co-precipitation of iron salts onto the primary amine attached-poly(HPMA-Cl-co-EDMA) microbeads and alkaline reduction of iron salts to magnetic iron oxide nanoparticles immobilized within the polymethacrylate microbeads. For the synthesis of magnetic titania microbeads, the method proposed for bare titania microbeads was applied with some modifications. The magnetic titania microbeads in the monodisperse-porous form 5.5  $\mu\text{m}$  in size were achieved by the calcination of titania-magnetic polymethacrylate composite microbeads at 450°C.

As a new plasmonic catalyst or photocatalyst, AuNP decorated forms of the bare and magnetic titania microbeads were also synthesized via the methods developed in this thesis. For this purpose, AuNPs synthesized by Turkevich and Martin methods 20 and 3 nm in size, respectively were decorated onto the primary amine attached forms of bare and magnetic titania microbeads in the monodisperse and porous form.

The bare, magnetic and AuNP decorated forms of bare and magnetic titania microbeads were characterized in terms of scanning electron microscopy, x-ray diffraction spectrophotometry, elemental analysis, vibrating sample magnetometry

and surface area and pore-size analysis via nitrogen adsorption-desorption method.

The photocatalytic activities of bare and magnetic titania microbeads and their AuNP decorated forms were determined in batch fashion including a textile dye, RB5 as an organic contaminant. The effects of operational parameters such as pH, catalyst amount, crystal composition and surface area, initial substrate concentration on the photocatalytic degradation of RB5 dye with bare and magnetic titania microbeads were determined. The complete removal of RB5 dye was achieved with both bare and magnetic titania microbeads. The decoration of Martin AuNPs instead of Turkevich AuNPs markedly enhanced the photocatalytic activity of titania microbeads. The decoration with AuNPs with lower size resulted in a significant enhancement in the photocatalytic degradation rate due to electron transfer characteristics of AuNPs with lower size. However, an enhancement could not be achieved with the Martin AuNP decorated magnetic titania microbeads.

The photocatalytic behaviours of bare and magnetic titania microbeads and their AuNP decorated forms were also studied using phenol as a more common organic contaminant in batch fashion. The effects of pH, catalyst amount, initial substrate concentration on the photocatalytic degradation of phenol with bare titania microbeads were determined. The complete photocatalytic degradation of phenol was obtained only using bare titania microbeads. In contrast to the bare titania microbeads, the complete phenol removal could not be achieved with magnetic titania microbeads. On the other hand, the decoration of Martin and Turkevich AuNPs onto the bare and magnetic titania microbeads resulted in reduced photocatalytic activities for both photocatalysts.

The plasmonic catalytic activity of AuNP decorated magnetic titania microbeads was determined by using 4-NP as the organic contaminant. In these runs, the effects of AuNP size, Au loading, catalyst amount, initial substrate concentration and temperature on the photocatalytic degradation of 4-NP were determined in batch fashion. A significant enhancement in the plasmonic catalytic activity was obtained with Martin AuNP decorated magnetic titania microbeads, in which AuNP size was smaller, compared to Turkevich AuNP decorated magnetic titania microbeads. Using this plasmonic catalyst, 4-NP in an aqueous solution could be converted into 4-AP within 2 min.



The results showed that the new sol-gel methods developed with the polymethacrylate based templates were adequate for the synthesis of both bare and magnetic titania microbeads. Higher photocatalytic degradation rates for an azo-dye and phenol and higher plasmonic catalytic degradation rate for 4-nitrophenol were observed with the new titania based catalysts compared to the literature.

**Keywords:** Bare and magnetic titania microbeads; Sol-gel templating method; Gold nanoparticle decoration, Photocatalysis; Plasmonic catalysis, RB5 dye degradation, Phenol degradation, 4-Nitrophenol reduction.

## ÖZET

### **PARTİKÜL FORMUNDA METAL OKSİT BAZLI MALZEMELERİN SENTEZİ VE KATALİTİK UYGULAMALARI**

**Kadriye Özlem HAMALOĞLU**

**Doktora, Kimya Mühendisliği Bölümü**

**Tez Danışmanı: Prof. Dr. S. Ali TUNCEL**

**Haziran 2015, 161 sayfa**

Bu tez kapsamında, altın nanopartiküllerle (AuNP) dekore edilmiş ya da edilmemiş hem titanyum dioksit ( $TiO_2$ ) hem de manyetik titanyum dioksit katalizörlerinin sentezi için yeni sol-jel kalıplama yöntemi geliştirilmiş, ve bu katalizörlerin fotokatalitik ve plazmonik katalitik aktiviteleri incelenmiştir.

Tezin ilk kısmında, eş boyutlu-gözenekli titanyum dioksit mikroküreler yeni bir sol-jel kalıplama yöntemi ile sodyum sülfonat ( $-SO_3Na$ ) bağlı polimetakrilat mikrokürelerin kalıp olarak kullanılmasıyla sentezlenmiştir.  $-SO_3Na$  bağlı polimerik kalıpların hazırlanması için başlangıç materyali olarak  $5.4 \mu m$  boyutlarında sentezlenmiş olan eş boyutlu-gözenekli poli(3-kloro-2-hidroksipropil metakrilat-co-etilen dimetakrilat), poli(HPMA-Cl-co-EDMA) mikroküreler kullanılmıştır.

Titanyum dioksit-polimer kompozit mikrokürelerinin elde edilmesi için,  $-SO_3Na$  bağlı polimetakrilat mikrokürelerin titanyum klorür ( $TiCl_4$ ) prekürsörü ile sulu

ortamda etkileştirilmesi ve daha sonra da amonyak ile yıkanması üzerine kurulu yeni bir sol-jel kalıplama yöntemi geliştirilmiştir. Yöntemin en son basamağında eşboyutlu-gözenekli titanyum dioksit mikroküreleri elde etmek için kompozit mikroküreler kalsine edilmiştir.

3.0-5.0 µm boyut aralığında, kratere-benzer ya da küçük gözenekli yapılarda, spesifik yüzey alanları 50-91 m<sup>2</sup>/g aralığında olan titanyum dioksit partiküller; -SO<sub>3</sub>Na bağlı polimetakrilat mikrokürelerin konsantrasyonunun, polimetakrilat mikrokürelerin çapraz bağlayıcı yoğunluğunun ve kalsinasyon sıcaklığının değiştirilmesi ile elde edilmiştir.

Titanyum dioksit mikrokürelerin sentezinde yaygın olarak kullanılan poli(stiren-ko-divinilbenzen), poli(S-co-DVB) tipindeki kalıpların yerine, düşük sıcaklıklarda termal olarak bozulan polimetakrilat kalıpların seçilmesi; titanyum dioksit-polimer kompozit mikrokürelerin kalsinasyonunun düşük sıcaklıklarda yapılmasına olanak sağlamıştır. Bu sebeple, kalsinasyonun düşük sıcaklıklarda yapılması ile daha yüksek spesifik yüzey alanına ve yüksek oranlarda anataz faz içeren kristal yapıya sahip eşboyutlu-gözenekli titanyum dioksit partiküller elde edilmiştir.

Manyetik formda eş boyutlu-gözenekli titanyum dioksit mikrokürelerin sentezi için de yeni bir sol-jel kalıplama protokolü geliştirilmiştir. Bu amaçla, demir tuzlarının ikili çöktürme yöntemi ile birincil amin bağlı-(HPMA-Cl-co-EDMA) mikrokürelerine çöktürülmesiyle manyetik polimerik mikroküreler elde edilmiştir.

Manyetik titanyum dioksit mikrokürelerin sentezi için, titanyum dioksit mikrokürelerinin üretiminde kullanılan sentez metodunda bazı modifikasyonlar yapılmıştır. Titanyum dioksit-manyetik polimetakrilat kompozit mikrokürelerin 450°C'de kalsinasyonu ile 5.5 µm boyutlarında, eş boyutlu-gözenekli manyetik titanyum dioksit mikrokürler elde edilmiştir.

Yeni bir plazmonik katalizör ya da fotokatalizör olarak AuNP dekore edilmiş titanyum dioksit ve manyetik titanyum dioksit mikroküreler, bu tez kapsamında geliştirilen metodlarla sentezlenmiştir. Bu amaçla, Turkevich ve Martin metodlarıyla sentezlenen, sırasıyla 20 ve 3 nm boyutlarında olan AuNP'ler birincil amin bağlı, eş boyutlu-gözenekli titanyum dioksit ve manyetik titanyum dioksit mikrokürelerin üzerine dekore edilmiştir.

AuNP dekore edilmiş ve edilmemiş titanyum dioksit ve manyetik titanyum dioksit mikroküreler, taramalı elektron mikroskobu, X-ışını kırınım spektrofotometresi, elementel analiz, örnek titreşimli manyetometre ve azot adsorpsiyon-desorpsiyon yoluyla yüzey alanı/gözenek boyut analizi ile karakterize edilmiştir.

AuNP dekore edilmiş ve edilmemiş titanyum dioksit ve manyetik titanyum dioksit mikrokürelerin fotokatalitik aktiviteleri, organik bir kirletici olan RB5 tekstil boyasını içeren kesikli sistemde belirlenmiştir. pH, katalizör miktarı, kristal kompozisyonu ve yüzey alanı, başlangıç substrat konsantrasyonu gibi çalışma koşullarının RB5 boyasının fotokatalitik degradasyonuna etkisi, titanyum dioksit ve manyetik titanyum dioksit mikroküreleri ile belirlenmiştir. RB5 boyasının tam fotokatalitik degradasyonu, hem titanyum dioksit hem de manyetik titanyum dioksit mikroküreleri ile elde edilmiştir. Turkevich AuNP'lerin yerine Martin AuNP'lerin dekore edilmesiyle, titanyum dioksit mikrokürelerin fotokatalitik aktiviteleri önemli derecede geliştirilmiştir. Küçük boyutlardaki AuNP'lerin elektron transfer karakteristiklerinden dolayı, bu partiküllerin titanyum dioksit mikrokürelere dekore edilmesi fotokatalitik degradasyon hızında önemli bir gelişme sağlamıştır. Fakat, Martin AuNP dekore edilmiş manyetik titanyum dioksit mikroküreler ile bir gelişme elde edilememiştir.

AuNP dekore edilmiş ve edilmemiş titanyum dioksit ve manyetik titanyum dioksit mikrokürelerin fotokatalitik davranışları; daha yaygın bir organik kirletici olan fenol kullanılarak da kesikli sistemde çalışılmıştır. pH, katalizör miktarı, kristal kompozisyonu ve yüzey alanı, başlangıç substrat konsantrasyonu gibi çalışma koşullarının fenolün fotokatalitik degradasyonuna etkisi titanyum dioksit mikroküreleri ile belirlenmiştir. Fenolün tam fotokatalitik degradasyonu sadece titanyum dioksit mikrokürelerle elde edilmiştir. Titanyum dioksit mikrokürelerin aksine, fenolün tam fotokatalitik degradasyonu manyetik titanyum dioksit mikroküreler ile elde edilememiştir. Ancak, titanyum dioksit ve manyetik titanyum dioksit mikrokürelere Martin ve Turkevich AuNP'lerin dekore edilmesi her iki katalizör için de fotokatalitik aktivitede azalmaya neden olmuştur.

AuNP dekore edilmiş manyetik titanyum dioksit mikrokürelerinin plazmonik katalitik aktivitesi, organik kirletici olan 4-NP kullanılarak belirlenmiştir. Bu deneylerde; AuNP boyutunun, Au yüklemesinin, katalizör miktarının, başlangıç substrat

konsantrasyonunun ve sıcaklığın 4-NP'nin fotokatalitik degradasyonu üzerine etkisi kesikli sistemde belirlenmiştir.

Turkevich AuNP ile dekore edilmiş manyetik titanyum dioksit mikrokürelerin yerine daha küçük boyutlardaki Martin AuNP ile dekore edilmiş manyetik titanyum dioksit mikrokürelerin kullanılmasıyla, plazmonik katalitik aktivitede önemli bir gelişme elde edilmiştir. Bu plazmonik katalizörü kullanarak sulu çözeltideki 4-NP 4-AP'ye 2 dakikada dönüştürülmüştür.

Sonuçlar polimetakrilat bazlı yapılarla geliştirilen sol-jel yöntemlerinin titanyum dioksit ve manyetik titanyum dioksit mikrokürelerin sentezi için uygun olduğunu göstermiştir. Literatürle karşılaştırıldığında, yeni titanyum dioksit bazlı katalizörlerle azo-boya ve fenol için daha yüksek fotokatalitik degradasyon hızları ve 4-nitrofenol için daha yüksek plazmonik katalitik degradasyon hızı gözlemlenmiştir.

**Anahtar Kelimeler:** Titanyum dioksit ve manyetik titanyum dioksit mikroküreler; Sol-jel kalıplama yöntemi; Altın nanopartikül dekorasyonu, Fotokataliz; Plazmonik Kataliz, RB5 boya degradasyonu, Fenol degradasyonu, 4-Nitrofenol indirgenmesi.

## ACKNOWLEDGMENTS

*At the end of my thesis, it is a pleasure for me to express my thanks to all those who contributed in many ways to the success of this study and made it an unforgettable experience for me.*

*I would like to express my deepest gratitude and special thanks to my supervisor Prof. Dr. S. Ali TUNCEL for his academic guidance, valuable support and patience. Under his guidance I overcame many difficulties and learned a lot. In spite of being extraordinarily busy, he always guided and kept me on the correct path to carry out my PhD studies successfully.*

*I would also like to greatly acknowledge my Ph.D. Examining Committee members, Prof. Dr. Zümriye Aksu, Prof. Dr. Hülya Yavuz Ersan for their enlightening comments and directions.*

*I would also like to show my gratitude to Dr. Bekir Çelebi, Doç. Dr. Ömür Çelikkıçak, Doç. Dr. Lokman Uzun for their valuable tutorship.*

*I would like to thank my best friends, Aslıhan Gökaltun, Çiğdem Kıp, Özge Yüksel Orhan and Pınar Kodal for always being with me. Without their presence I wouldn't be able to make it this far.*

*I would like to thank my best crony, Ebru Sağ for being around me at any time I need.*

*I would like to acknowledge my lab mates, Güneş Kibar, Gülçin Günal, Eda Öğüt, Tuncay Şimşek, Erhan Şenlik, Aykut Bilir, Hasan İlhan, Kourosh Salimi, Duygu Deniz Usta, İlknur Durukan and Eda Beldek for supporting me with a nice working environment and their great friendship.*

*I sincerely acknowledge THE SCIENTIFIC AND TECHNOLOGICAL RESEARCH COUNCIL OF TURKEY (TÜBİTAK) for the scholarship which encouraged me and provided financial assistance during my PhD studies.*

*I owe a special gratitude to my whole family for their great encouragement, support and assistance during my Ph.D studies and for raising me to become who I am today. Also I would like to thank my soulmate Burcu Kaya for always supporting and being with me. Finally I would like to thank my husband Cem Hamaloğlu for his personal support, patience at all times and for his great encouragement.*

*Kadriye Özlem Hamaloğlu*

## TABLE OF CONTENTS

ABSTRACT .....	i
ÖZET .....	v
ACKNOWLEDGMENTS .....	ix
TABLE OF CONTENTS .....	x
LIST OF TABLES .....	xvii
LIST OF FIGURES .....	xix
SYMBOLS AND ABBREVIATIONS .....	xxvi
1. INTRODUCTION.....	1
2. LITERATURE REVIEW.....	4
2.1. Titanium dioxide (Titania) .....	4
2.1. Synthesis .....	8
2.1.1. Sol–gel method .....	9
2.1.1.1. Low–temperature sol–gel process.....	10
2.1.1.2. Sol-gel Templating Method.....	11
2.2. Synthesis of Polymeric Templates .....	12
2.2.1. Dispersion Polymerization .....	12
2.2.2. Multistep Microsuspension Polymerization for Synthesis of Functional, Monodisperse Porous Particles.....	15
2.3. Applications of Titanium Dioxide Particles .....	16
2.3.1. Support for catalysis .....	18
2.3.2. Photocatalysis .....	19
2.3.2.1. General mechanism of photocatalytic reaction process.....	20
2.4. Factors affecting the photocatalytic process .....	21
2.4.1. Structural and morphological properties of TiO <sub>2</sub> .....	21
2.4.1.1. Crystal structure of TiO <sub>2</sub> .....	22
2.4.1.2. Surface area of TiO <sub>2</sub> .....	22
2.4.1.3. Particle dimensions of TiO <sub>2</sub> .....	22

2.4.2. Operational parameters.....	22
2.4.2.1. Catalyst loading.....	23
2.4.2.2. Substrate concentration.....	23
2.4.2.3. pH.....	23
2.4.2.4. Temperature.....	23
2.4.2.5. Oxygen supply.....	24
2.4.2.6. Light Intensity.....	24
2.5. Trends to improve TiO <sub>2</sub> activity.....	24
2.5.1. TiO <sub>2</sub> doping.....	24
2.5.1.1. Gold Nanoparticle (AuNP) Synthesis.....	25
2.5.1.1.1. Turkevich Method.....	25
2.5.1.1.2. Martin Method.....	25
2.5.1.2. Magnetic Nanoparticle Synthesis.....	26
2.5.1.2.1. Co-precipitation method.....	26
3. EXPERIMENTAL METHODS.....	27
3.1. Synthesis of Monodisperse-Porous poly(HPMA-Cl-co-EDMA) Microbeads...	27
3.1.1. Materials.....	27
3.1.2. Synthesis of GMA Seed Latex.....	28
3.1.3. Synthesis of Monodisperse-Porous Poly(HPMA-Cl-co-EDMA) Microbeads by Multistep Microsuspension Polymerization.....	29
3.2. Derivatization of Monodisperse-Porous Poly(HPMA-Cl-co-EDMA) Microbeads .....	31
3.2.1. Materials.....	31
3.2.2. Derivatization of poly(HPMA-Cl-co-EDMA) microbeads with sodium bisulfite.....	31
3.2.3. Derivatization of poly(HPMA-Cl-co-EDMA) microbeads with EDA.....	32
3.3. Synthesis of magnetic poly(HPMA-Cl-co-EDMA) microbeads.....	33
3.3.1. Materials.....	33



3.3.2. Magnetization of amine attached-poly(HPMA-Cl-co-EDMA) microbeads.....	33
3.4. Synthesis of Monodisperse-Porous Bare and Magnetic Titania Microbeads .	35
3.4.1. Materials.....	35
3.4.2. Synthesis of Monodisperse-Porous Bare and Magnetic Titania Microbeads by Sol-Gel Templating Method.....	35
3.5. Synthesis of Gold Nanoparticle Decorated Monodisperse-Porous Bare and Magnetic Titania Microbeads.....	36
3.5.1. Materials.....	36
3.5.2. Derivatization of Monodisperse-Porous Bare and Magnetic Titania Microbeads with Aminopropyltriethoxysilane.....	37
3.5.3. Synthesis of AuNPs.....	38
3.5.4. .... Synthesis of AuNPs via Turkevich Method.....	38
3.5.4.1. Synthesis of AuNPs via Martin Method.....	38
3.5.5. Decoration of Monodisperse-Porous Bare or Magnetic Titania Microbeads with AuNPs.....	39
3.6. Characterization of Monodisperse-Porous Bare and Magnetic Poly(HPMA-Cl-co-EDMA) and Titania Microbeads.....	40
3.7. Catalysis Runs.....	42
3.7.1. Materials.....	42
3.7.2. Photocatalysis of Remazol Black 5 Dye.....	43
3.7.2.2. Photocatalysis of Remazol Black 5 Dye with AuNP Decorated-Bare Titania Microbeads.....	44
3.7.2.2.1. AuNP Decorated Bare Titania Microbeads by Turkevich Method.....	44
3.7.2.2.2. AuNP Decorated Bare Titania Microbeads by Martin Method.....	45
3.7.2.3. Photocatalysis of Remazol Black 5 Dye with Magnetic Titania Microbeads.....	45
3.7.2.4. Photocatalysis of Remazol Black 5 Dye with AuNP Decorated Magnetic Titania Microbeads.....	46
3.7.2.4.1. AuNP Decorated Magnetic Titania Microbeads by Turkevich Method...	46
3.7.2.4.2. AuNP Decorated Magnetic Titania Microbeads by Martin Method.....	47

3.7.2.5. Catalyst recovery and reuse.....	48
3.7.3. Photocatalysis of Phenol.....	48
3.7.3.1. Photocatalysis of Phenol with Bare Titania Microbeads.....	48
3.7.3.2. Photocatalysis of Phenol with AuNP Decorated Bare Titania Microbeads.....	49
3.7.3.2.1. AuNP Decorated Bare Titania Microbeads by Turkevich Method.....	49
3.7.3.2.2. AuNP Decorated Bare Titania Microbeads by Martin Method.....	49
3.7.3.3. Photocatalysis of Phenol with Magnetic Titania Microbeads.....	50
3.7.3.4. Photocatalysis of Phenol with AuNP Decorated Magnetic Titania Microbeads.....	51
3.7.3.4.1. AuNP Decorated Magnetic Titania Microbeads by Turkevich Method...51	
3.7.3.4.2. AuNP Decorated Magnetic Titania Microbeads by Martin Method.....51	
3.7.3.5. Catalyst recovery and reuse.....	51
3.7.4. Plasmonic Catalysis of 4-Nitrophenol.....	52
3.7.4.1. Plasmonic Catalysis of 4-Nitrophenol with AuNP Decorated Monodisperse-Porous Bare and Magnetic Titania Microbeads.....	52
3.7.4.1.1. Plasmonic Catalysis of 4-Nitrophenol with Turkevich AuNP Decorated Monodisperse-Porous Bare and Magnetic Titania Microbeads .....	52
3.7.4.2. Plasmonic Catalysis of 4-Nitrophenol with Turkevich AuNP Decorated Magnetic Titania Microbeads.....	52
3.7.4.2.1. Plasmonic Catalysis of 4-Nitrophenol with Martin AuNP Decorated Magnetic Titania Microbeads.....	53
3.7.4.3. Catalyst recovery and reuse.....	54
4. RESULTS and DISCUSSION .....	55
4.1. Synthesis and Characterization of Monodisperse-Porous poly(HPMA-Cl-co-EDMA) Microbeads .....	56
4.1.1. Synthesis and Characterization of Sodium Bisulfite Functionalized Poly(HPMA-Cl-co-EDMA) Microbeads .....	58
4.1.2. Synthesis and Characterization of Monodisperse-Porous Bare Titania Microbeads.....	60

4.1.2.1. Effect of crosslinking agent feed concentration on bare titania microbeads.....	60
4.1.2.2. Effect of concentration of polymeric template on titania microbeads.....	63
4.1.2.3. Effect of calcination temperature on titania microbeads.....	64
4.2. Synthesis and Characterization of Monodisperse-Porous and Magnetic Titania Microbeads.....	69
4.2.2. Synthesis and Characterization of Magnetic poly(HPMA-Cl-co-EDMA) Microbeads.....	69
4.2.3. Properties of Magnetic Titania Microbeads.....	72
4.3. Synthesis and Characterization of AuNP Decorated Bare/Magnetic Titania Microbeads.....	75
4.3.1. Synthesis and Characterization of Amine Functionalized Bare/Magnetic Titania Microbeads.....	75
4.3.2. Properties of AuNP Decorated Magnetic Titania Microbeads.....	79
4.4. Photocatalytic Activity Measurements.....	83
4.4.1. Photocatalytic Degradation of Remazol Black 5 Dye with Bare Titania Microbeads.....	83
4.4.1.1. Effect of Calcination Temperature.....	85
4.4.1.2. Effect of pH.....	87
4.4.1.3. Effect of Catalyst Amount.....	88
4.4.1.4. Effect of Initial RB5 Dye Concentration.....	90
4.4.1.5. Effect of Au Loading.....	91
4.4.1.5.1. Determination of appropriate pH.....	92
4.4.1.5.2. Determination of appropriate AuNP size.....	93
4.4.1.5.3. Effect of AuNP loading at the appropriate pH and appropriate AuNP size.....	94
4.4.1.6. Reusability.....	97
4.4.2. Photocatalytic Degradation of RB5 with Magnetic Titania Microbeads.....	98
4.4.2.1. Effect of pH.....	98
4.4.2.2. Effect of Catalyst Amount.....	100

4.4.2.3. Effect of RB5 Dye Concentration.....	101
4.4.2.4. Effect of Au Loading.....	102
4.4.2.4.1. Effect of pH.....	102
4.4.2.4.2. Effect of Gold Nanoparticle Size.....	103
4.4.2.4.3. Effect of of Au Loading.....	104
4.4.2.5. Reusability.....	105
4.4.3. .Photocatalytic Degradation of Phenol with Bare Titania Microbeads.....	106
4.4.3.1. Effect of pH.....	109
4.4.3.2. Effect of Catalyst.....	111
4.4.3.3. Effect of Phenol Concentration.....	112
4.4.3.4. Effect of Au Loading.....	113
4.4.3.4.1. Effect of AuNP Size.....	114
4.4.3.4.2. Effect of Au Loading.....	115
4.4.3.5. Reusability.....	116
4.4.4. Photocatalytic Degradation of Phenol with Magnetic Titania Microbeads..	117
4.4.4.1. Effect of Au Loading.....	118
4.5. Plasmonic Catalytic Activity Measurements.....	119
4.5.1. Reduction of 4-Nitrophenol.....	119
4.5.2. Plasmonic catalysis of 4-NP with Turkevich AuNP Decorated Bare and Magnetic Titania Microbeads.....	120
4.5.2.1. Plasmonic catalysis of 4-NP with Turkevich AuNP Decorated Magnetic Titania Microbeads.....	122
4.5.2.1.1. Effect of Catalyst Amount.....	122
4.5.2.1.2. Effect of Temperature.....	123
4.5.2.1.3. Effect of Initial 4-NP Concentration.....	124
4.5.3. . Enhancement on the Plasmonic Catalytic Activity.....	125
4.5.3.1. .Effect of AuNP Size.....	125
4.5.3.2. .Effect of Au loading.....	127
4.5.4. Reusability.....	128

5. CONCLUSION .....	130
REFERENCES.....	133
CURRICULUM VITAE.....	160

## LIST OF TABLES

Table 2.1. Some physical properties for different crystal structures of titania [50,51]. .....	6
Table 3.1. Experimental conditions of dispersion polymerization of GMA monomer for the synthesis poly(GMA) seed latex. ....	28
Table 3.2. Experimental conditions of synthesized poly(HPMA-Cl-co-EDMA) microbeads with different crosslinking agent feed concentrations.....	31
Table 3.3. Experimental conditions for Au loading (% w/w) on bare and magnetic titania microbeads. ....	40
Table 3.4. Experimental conditions and parameters changed in the photocatalysis of RB5 dye with monodisperse-porous bare titania microbeads.....	43
Table 3.5. Experimental conditions and parameters changed in the photocatalysis of RB5 dye with Turkevich AuNP decorated monodisperse-porous bare titania microbeads.....	44
Table 3.6. Experimental conditions in the photocatalysis of RB5 dye with Martin AuNP decorated bare titania microbeads.....	45
Table 3.7. Experimental conditions and parameters changed in the photocatalysis of RB5 dye with monodisperse-porous magnetic titania microbeads. ....	46
Table 3.8. Experimental conditions in the photocatalysis of RB5 dye with Turkevich AuNP decorated magnetic titania microbeads.....	47
Table 3.9. Experimental conditions in the photocatalysis of RB5 dye with Martin AuNP decorated magnetic titania microbeads.....	47
Table 3.10. Experimental conditions in the photocatalysis of phenol with bare titania microbeads. ....	48
Table 3.11. Experimental conditions in the photocatalysis of phenol with Martin AuNP decorated bare titania microbeads.....	50
Table 3.12. Experimental conditions in the reduction of 4-NP with Turkevich AuNP decorated-magnetic titania microbeads.....	53
Table 3.13. Experimental conditions in the plasmonic catalysis of 4-NP with Martin AuNP decorated magnetic titania microbeads.....	54
Table 4.1. The size and specific surface areas of poly(HPMA-Cl-co-EDMA) microbeads obtained with different volume percent of crosslinking agent (EDMA). .....	57

Table 4.2. The size and specific surface areas of bare titania microbeads prepared by using -SO <sub>3</sub> Na attached-poly(HPMA-Cl-co-EDMA) microbeads produced with different crosslinking agent feed concentrations (EDMA).....	61
Table 4.3. The size and specific surface areas of bare titania microbeads obtained with different concentrations of poly(HPMA-Cl-co-EDMA) microbeads (volume percent of crosslinking agent: % 30). .....	64
Table 4.4. Size properties and specific surface areas of poly(HPMA-Cl-co-EDMA) and magnetic poly(HPMA-Cl-co-EDMA) microbeads. ....	70
Table 4.5. Size properties and specific surface areas of monodisperse-porous bare and magnetic titania microbeads.....	73
Table 4.6. Specific surface areas of Turkevich and Martin AuNP decorated bare titania microbeads with different Au loadings. ....	77
Table 4.7. Specific surface area values of Turkevich and Martin AuNP decorated magnetic titania microbeads with different with different Au loadings.....	80

## LIST OF FIGURES

Figure 2.1. Band diagram of semiconductors.....	7
Figure 2.2. Scheme of the sol–gel processing options [76]. .....	9
Figure 2.3. Schematical description of the stages of dispersion polymerization [115]. .....	14
Figure 2.4. Schematical description of seed latex preparation and multistep microsuspension polymerization [115]. .....	15
Figure 2.5. Applications of TiO <sub>2</sub> photocatalysis [123]. .....	17
Figure 2.6. Schematic representation of photochemical process in and on a titania particle [153]. .....	21
Figure 3.1. Synthesis of poly(HPMA-Cl-co-EDMA) microbeads by multistep microsuspension polymerization. ....	29
Figure 3.2. Reaction mechanism for the derivatization of poly(HPMA-Cl-co-EDMA) microbeads with NaHSO <sub>3</sub> . .....	32
Figure 3.3. Reaction mechanism for the derivatization of poly(HPMA-Cl-co-EDMA) microbeads with EDA. ....	32
Figure 3.4. Synthesis of magnetic poly(HPMA-Cl-co-EDMA) microbeads by in-situ co-precipitation method. ....	34
Figure 3.5. Synthesis of monodisperse-porous (A): bare and (B): magnetic titania microbeads by sol-gel templating method. ....	35
Figure 3.6. Reaction mechanism for the derivatization of monodisperse-porous bare and magnetic titania microbeads with APTES. ....	37
Figure 3.7. Synthesis of AuNPs via Turkevich method. ....	38
Figure 3.8. Synthesis of AuNPs via Martin Method. ....	39
Figure 3.9. Decoration of monodisperse-porous bare or magnetic titania microbeads with AuNPs. ....	39
Figure 3.10. The equipments used for the characterization of poly(HPMA-Cl-co-EDMA) microbeads (A) Quanta 200 FEG SEM, (B) Perkin Elmer 2400, (C) Quantachrome Nova 2200 BET. ....	41
Figure 3.11. Devices used for the characterization of poly(HPMA-Cl-co-EDMA) microbeads (A) DSC, Diamond DSC, Perkin Elmer, (B) TGA, TG/DTA 6300 SII EXSTAR 6000, Perkin Elmer, (C) XRD, Rigaku, D/Max-2200. ....	42



Figure 4.1. SEM photographs of monodisperse-porous poly(HPMA-Cl-co-EDMA) microbeads obtained with different volume percent of crosslinking agent (v/v %): (A):15 , (B): 30, (C): 50, (D): 70, (E): 85. Magnifications: Larger images: X20.000, Smaller images: X4000. ....	57
Figure 4.2. The effect of HPMA-Cl feed concentration on -SO <sub>3</sub> Na content of polymethacrylate microbeads and fractional conversion of chloropropyl groups in the poly(HPMA-Cl-co-EDMA) microbeads.....	59
Figure 4.3. SEM photographs of monodisperse-porous bare titania microbeads prepared by using -SO <sub>3</sub> Na attached-poly(HPMA-Cl-co-EDMA) microbeads produced with different volume percent of crosslinking agent (v/v %): (A):15, (B): 30, (C): 50, (D): 70, (E): 85. Magnifications: Larger images: X25000, Smaller images: X2500. ....	60
Figure 4.4. The effect of crosslinking agent feed concentration on the specific surface area of -SO <sub>3</sub> Na attached-poly(HPMA-Cl-co-EDMA) microbeads and bare titania microbeads. ....	62
Figure 4.5. SEM photographs of bare titania microbeads prepared by using different concentrations of -SO <sub>3</sub> Na attached-poly(HPMA-Cl-co-EDMA) microbeads (g/L) A: 3.3 g/L, B: 6.7 g/L, C: 10 g/L, D: 13.3 g/L. (feed concentration of crosslinking agent: 30 % v/v). Magnifications: Larger images: X25.000, Smaller images: X2500. ....	63
Figure 4.6. TGA curves of monodisperse-porous poly(HPMA-Cl-co-EDMA) microbeads.....	65
Figure 4.7. DSC curve of monodisperse-porous poly(HPMA-Cl-co-EDMA) microbeads.....	66
Figure 4.8. The variation of specific surface area of bare titania microbeads with the calcination temperature. Template: -SO <sub>3</sub> Na attached-poly(HPMA-Cl-co-EDMA) microbeads.....	67
Figure 4.9. XRD patterns for monodisperse-porous bare titania microbeads calcined at different temperatures (450°C, 500°C, 550°C, 600°C). Template: -SO <sub>3</sub> Na attached poly(HPMA-Cl-co-EDMA) microbeads.....	68
Figure 4.10. SEM photographs of (A): poly(HPMA-Cl-co-EDMA) microbeads, (B): magnetic poly(HPMA-Cl-co-EDMA) microbeads. Magnifications: Images on the left side: X16000, Images on the right side: X80000. ....	70

Figure 4.11. XRD patterns of poly(HPMA-Cl-co-EDMA) and magnetic poly(HPMA-Cl-co-EDMA) microbeads.....	71
Figure 4.12. VSM curve of magnetic poly(HPMA-Cl-co-EDMA) microbeads. ....	72
Figure 4.13. SEM photographs of (A): bare titania microbeads, (B): magnetic titania microbeads. Magnifications: Images on the left side (microbeads): X16.000, Images on the right side (surface): X80.000.....	73
Figure 4.14. XRD patterns of bare and magnetic titania microbeads. ....	74
Figure 4.15. VSM curve of magnetic titania microbeads. ....	75
Figure 4.16. SEM photograph of Turkevich AuNP decorated bare titania microbeads with an Au loading of 5 % (%w/w).....	76
Figure 4.17. UV-Vis spectra of Turkevich and Martin AuNP solutions.....	77
Figure 4.18. XRD patterns of bare titania microbeads, Turkevich and Martin AuNP decorated bare titania microbeads. ....	78
Figure 4.19. SEM photograph of monodisperse-porous Turkevich AuNP decorated magnetic titania microbeads with an Au loading of 5.0 % (%w/w).....	80
Figure 4.20. XRD patterns of magnetic titania microbeads, Turkevich and Martin AuNP decorated magnetic titania microbeads.....	81
Figure 4.21. VSM curve of Turkevich and Martin GNP decorated magnetic titania microbeads.....	82
Figure 4.22. Molecular structure of RB5.....	83
Figure 4.23. UV-Vis spectra at different times during the decolorization of RB5 dye solution. (Conditions: pH: 7, catalyst amount: 80 mg, calcination temperature: 450°C, RB dye solution: 25 ppm, 100 mL) .....	84
Figure 4.24. The variation of RB5 dye concentration with the time during the photocatalytic degradation. (Conditions: pH: 7, catalyst amount: 80 mg, calcination temperature: 450°C, RB5 dye solution: 25 ppm, 100 mL). ....	85
Figure 4.25. Effect of calcination temperature on the photocatalytic degradation of RB5 dye with bare titania microbeads. (Conditions: catalyst amount: 80 mg, RB5 dye solution: 25 ppm, 100 mL, pH: 3.5).....	86
Figure 4.26. Effect of pH on the photocatalytic degradation rate of RB5 with bare titania microbeads.(Conditions: catalyst amount: 80 mg, calcination temperature: 450°C, RB5 dye solution: 25 ppm, 100 mL). ....	88

Figure 4.27. Effect of catalyst amount on the photocatalytic degradation rate of RB5 with bare titania microbeads.(Conditions: calcination temperature: 450°C, RB5 dye solution: 25 ppm, 100 mL, pH: 3.5).....	89
Figure 4.28. Effect of initial RB5 dye concentration on the photocatalytic degradation rate of RB5 dye with bare titania microbeads. (Conditions: catalyst amount: 80 mg, calcination temperature: 450°C, pH: 3.5).....	91
Figure 4.29. Effect of pH on the photocatalytic degradation rate of RB5 dye with Turkevich AuNP decorated bare titania microbeads. (Conditions: catalyst amount: 80 mg, Au loading (w/w): 5 %, RB5 dye solution: 25 ppm, 100 mL).....	92
Figure 4.30. Effect of AuNP size on the photocatalytic degradation rate of RB5 dye. (Conditions: catalyst amount: 80 mg, Au loading (w/w): 5 %, RB dye solution: 25 ppm, 100 mL, pH: 7).....	93
Figure 4.31. Effect of weight percent of Au loading on the photocatalytic degradation rate of RB5 dye with Turkevich AuNP decorated bare titania microbeads. (Conditions: catalyst amount: 80 mg, RB5 dye solution: 25 ppm, 100 mL, pH: 7).....	95
Figure 4.32. Effect of weight percent of Au loading on the photocatalytic degradation rate of RB5 dye with Martin AuNP decorated bare titania microbeads. (Conditions: catalyst amount: 80 mg, RB dye solution: 25 ppm, 100 mL, pH: 7)..	96
Figure 4.33. Reusability of Martin AuNP decorated bare titania microbeads in decolorization of RB5 dye solution. (Conditions: catalyst amount: 80 mg, Au loading (%w/w): 5 %, RB5 dye solution: 25 ppm, 100 mL, pH: 7). .....	97
Figure 4.34. Effect of pH on the photocatalytic degradation rate of RB5 dye with magnetic titania microbeads. (Conditions: catalyst amount: 80 mg, calcination temperature: 450°C, RB dye solution: 25 ppm, 100 mL). .....	99
Figure 4.35. Effect of catalyst amount on the photocatalytic degradation rate of RB5 dye with magnetic titania microbeads. (Conditions: calcination temperature: 450°C, RB dye solution: 25 ppm, 100 mL, pH: 3.5).....	100
Figure 4.36. Effect of initial dye concentration on the photocatalytic degradation rate of RB5 dye in the presence of magnetic titania microbeads (Conditions: catalyst amount: 80 mg, calcination temperature: 450°C, pH: 3.5).....	101
Figure 4.37. Effect of pH on the photocatalytic degradation rate of RB5 dye with Turkevich AuNP decorated magnetic titania microbeads. (Conditions: catalyst amount: 80 mg, Au loading (w/w): 5 %, RB dye solution: 25 ppm, 100 mL).....	103

Figure 4.38. Effect of AuNP size on the photocatalytic degradation rate of RB5 dye. (Conditions: catalyst amount: 80 mg, Au loading (w/w): 5 %, RB5 dye solution: 25 ppm, 100 mL, pH: 7). .....	104
Figure 4.39. Effect of Au loading on the photocatalytic degradation rate of RB5 with Martin AuNP decorated magnetic titania microbeads. (Conditions: catalyst amount: 80 mg, RB dye solution: 25 ppm, 100 mL, pH: 7). .....	105
Figure 4.40. Reusability of magnetic titania microbeads in the decolorization of RB5 dye solution. (Conditions: catalyst amount: 80 mg, calcination temperature: 450°C, RB5 dye solution: 25 ppm, 100 mL, pH: 3.5) .....	106
Figure 4.41. A proposed model for the photocatalytic degradation of phenol. ....	107
Figure 4.42. HPLC chromatograms obtained at different times during the photocatalytic degradation of phenol. (Conditions: catalyst amount: 160 mg, calcination temperature: 450°C, phenol solution: 50 ppm, 100 mL, pH: 7). .....	108
Figure 4.43. The variation of phenol concentration with the time in the degradation of phenol with bare titania microbeads. (Conditions: catalyst amount: 160 mg, calcination temperature: 450°C, Phenol solution: 50 ppm, 100 mL, pH: 7). .....	109
Figure 4.44. Effect of pH on the photocatalytic degradation rate of phenol with bare titania microbeads. (Conditions: catalyst amount: 160 mg, calcination temperature: 450°C, phenol solution: 50 ppm, 100 mL). .....	110
Figure 4.45. Effect of catalyst amount on the photocatalytic degradation rate of phenol with bare titania microbeads. (Conditions: Calcination temperature: 450°C, phenol solution: 50 ppm, 100 mL, pH : 7). .....	112
Figure 4.46. Effect of initial phenol concentration on the photocatalytic degradation rate of phenol with bare titania microbeads. (Conditions: Catalyst amount: 160 mg, Calcination temperature: 450°C, pH :7). .....	113
Figure 4.47. Effect of AuNP size on the photocatalytic degradation rate of phenol. (Conditions: Catalyst amount: 160 mg; Calcination temperature: 450°C; Au loading (w/w %) : 5 %; Phenol solution: 50 ppm, 100 mL; pH : 7). .....	114
Figure 4.48. Effect of Au loading on the photocatalytic degradation rate of phenol with Martin AuNP decorated bare titania microbeads. (Conditions: Catalyst amount: 160 mg; Calcination temperature: 450°C; Phenol solution: 50 ppm, 100 mL; pH :7). .....	115

Figure 4.49. Reusability of bare titania microbeads in the photocatalytic degradation of phenol. (Conditions: Catalyst amount: 160 mg; Calcination temperature: 450°C; Phenol solution: 50 ppm, 100 mL; pH :7). .....	116
Figure 4.50. Comparison of the photocatalytic activity of bare and magnetic titania microbeads. (Conditions: Catalyst amount: 160 mg; Calcination temperature: 450°C; Phenol solution: 50 ppm, 100 mL; pH :7). .....	117
Figure 4.51. Effect of Au loading on the photocatalytic degradation rate of phenol with magnetic titania microbeads. (Conditions: Catalyst amount: 160 mg; Calcination temperature: 450°C; Au loading (w/w %) : 5 %; Phenol solution: 50 ppm, 100 mL; pH :7).....	118
Figure 4.52. Model reaction for the reduction of 4-NP to 4-AP.....	119
Figure 4.53. UV-Vis spectra at different times during the reduction of 4-NP. (Conditions: Catalyst: Turkevich AuNP decorated magnetic titania microbeads, Catalyst amount: 1 mg, Calcination temperature: 450°C, Au loading (w/w %) : 5 %; 4-NP solution: 7.5 ppm, 24 mL, Temperature: 20°C) .....	120
Figure 4.54. 4-NP concentration with time. (Conditions: Catalysts: Turkevich AuNP decorated bare and magnetic titania microbeads, Catalyst amount: 1 mg, Calcination temperature: 450°C, Au loading (w/w %) : 5 %; 4-NP solution: 7.5 ppm, 24 mL, Temperature: 20°C).....	121
Figure 4.55. Effect of catalyst amount on the plasmonic catalytic degradation rate of 4-NP with Turkevich AuNP decorated magnetic titania microbeads. (Conditions: Calcination temperature: 450°C,Au loading (w/w %): 5 %;4-NP solution: 7.5 ppm, 24 mL, Temperature: 20°C )......	122
Figure 4.56. Effect of temperature on the plasmonic catalytic degradation rate of 4-NP with Turkevich AuNP decorated magnetic titania microbeads. (Conditions: Catalyst amount: 1 mg; Calcination temperature: 450°C; Au loading (w/w %) : 5 %; 4-NP solution: 7.5 ppm, 24 mL).....	124
Figure 4.57. Effect of initial 4-NP concentration on the plasmonic catalytic degradation rate of 4-NP with Turkevich AuNP decorated magnetic titania microbeads. (Conditions: Catalyst amount: 1 mg; Calcination temperature: 450°C; Au loading (w/w %) : 5 %; Temperature: 20°C).....	125
Figure 4.58. Effect of AuNP size on the plasmonic catalytic degradation rate 4-NP. (Conditions: Catalyst amount: 1 mg; Calcination temperature: 450°C; Au loading (w/w %) : 5 %; 4-NP solution: 7.5 ppm, 24 mL; Temperature: 20°C).....	126

Figure 4.59. The variation of 4-NP concentration during the reduction of 4-NP with initial concentrations of 7.5 and 15 ppm with Martin AuNP decorated magnetic titania microbeads. (Conditions: Catalyst amount: 1 mg, Calcination temperature: 450°C, Au loading (w/w %) : 5 %; Temperature: 20°C) .....	127
Figure 4.60. Effect of Au loading on the plasmonic degradation rate of 4-NP with Martin AuNP decorated magnetic titania microbeads. (Conditions: Catalyst amount: 1 mg; Calcination temperature: 450°C; 4-NP solution: 7.5 ppm, 24 mL; Temperature: 20°C).....	128
Figure 4.61. Reusability of Martin AuNP decorated magnetic titania microbeads in the reduction of 4-NP solution. (Conditions: Catalyst amount: 1 mg; Calcination temperature: 450°C; Au loading (w/w %) : 5 %; 4-NP solution: 7.5 ppm, 24 mL; Temperature: 20°C).....	129

## SYMBOLS AND ABBREVIATIONS

### Symbols

$C_v$	Coefficient of variation
pKa	Logarithmic acid dissociation constant

### Abbreviations

AIBN	2,2'-azobisisobutyronitrile
AOPs	Advanced Oxidation Processes
APTES	Aminopropyltriethoxysilane
Au	Gold
AuNP	Gold nanoparticle
BET	Brunauer-Emmet-Teller
BPO	Benzoyl peroxide
CTAB	Hexadecyltrimethylammonium bromide
DDI	Distilled deionized water
DVB	Divinylbenzene
EB	Ethylbenzene
EDA	Ethylenediamine
EDMA	Ethylene glycol dimethacrylate
EtOH	Ethanol
GMA	Glycidyl methacrylate
HCl	Hydrochloric acid
HPLC	High Pressure Liquid Chromatography
HPMA-Cl	3-chloro-2-hydroxypropyl methacrylate
IsOH	Isopropanol
NaBH <sub>4</sub>	Sodiumborohydride
NaHSO <sub>3</sub>	Sodium bisulfite
NaOH	Sodium hydroxide

NH <sub>4</sub> OH	Ammonium hydroxide
4-Nitrophenol	4-NP
Poly(HPMA-Cl-co-EDMA)	Poly(3-chloro-2-hydroxypropyl methacrylate-co-ethylene dimethacrylate)
Poly(S-co-DVB)	Poly(styrene-co-divinyl benzene)
PVA	Poly(vinyl alcohol)
PVP-K30	Poly(vinyl pyrrolidone)
RB5	Remazol Black 5
S	Styrene
SDS	Sodium lauryl sulfate
SEM	Scanning Electron Microscope
SO <sub>3</sub> Na	Sodium sulfonate
SSA	Specific Surface Area (m <sup>2</sup> /g)
TEA	Triethylamine
THF	Tetrahydrofuran
TIP	Titanium isopropoxide
TiCl <sub>4</sub>	Titanium chloride
TiO <sub>2</sub>	Titanium chloride
UV	Ultraviolet-visible



## 1. INTRODUCTION

In the last century, conventional physical, biological and chemical processes were used to remove organic compounds from contaminated water [1]. Due to the limitations of these processes, a lot of research has been done in the last decades about a new class of oxidation processes which is called as Advanced Oxidation Processes (AOPs). AOPs consists of different processes like; chemical oxidation processes (ozone ( $O_3$ ), ozone/hydrogen peroxide( $O_3/H_2O_2$ ), Fenton photochemical oxidation processes (UV/ $O_3$ , UV/ $H_2O_2$ ) and photocatalytic processes (UV/ $TiO_2$ ) [2]. Each process is based on the formation of hydroxyl radicals and reaction of these hydroxyl radicals with organic contaminants. Heterogeneous photocatalysis, in which semiconductor metal oxides are used instead of oxidants like  $H_2O_2$  and  $O_3$  with UV light, is a promising method for the degradation of organic compounds due its low cost and high efficiency [3-6].

Among the semiconductors that have been used for photocatalysis,  $TiO_2$  is the most suitable one due to high activity, low cost and non-toxicity [7-10]. Accordingly, titania nanoparticles with a high porosity have attracted much attention due to its usability in heterogeneous photocatalysis for decomposing many kinds of organic compounds like textile dyes [11-18] and phenolic compounds [18-24]. Two of the most important factors affecting on the photocatalytic activity of titania beads are specific surface area and crystallinity [25, 26]. The higher surface areas can be obtained with titania nanoparticles, however the removal of nanoparticles from solutions is a serious problem after the catalytic reaction. From the viewpoint of practical applications, in addition to high surface area, easy removal, controllable shape and size are also important for developing convenient porous titania beads. Hence, magnetic titania beads have attracted much attention due to ease of removal from the reaction medium [27-30].

Using polymeric templates, which controls the morphological property such as pore size, outer shape and size, has a great importance for the synthesis of monodisperse porous titania beads [31]. The sol-gel templating is a suitable method for the preparation of titania beads with controlled morphology and structure. This method involves sol-gel chemistry of pure metal alkoxides within the porous polymeric template. The template is removed from the composite

structure after formation of inorganic structure. By using this method, Caruso and co-workers demonstrated the use of porous poly(styrene-co-divinylbenzene), poly(S-co-DVB) microbeads as template and  $\text{TiCl}_4$  as precursor in the production of titania microbeads [32, 33]. Meyer et al used non-functionalized and hydroxyl/amine functionalized poly(S-co-DVB) microbeads as template and titanium isopropoxide (TIP) as precursor for the preparation of titania microbeads [34]. Wang and co-workers also used the same particles but in larger size to synthesize titania macrobeads by using titanium(IV) sulfate ( $\text{Ti}(\text{SO}_4)_2$ ) as precursor [35]. Qi and co-workers prepared hollow microbeads of titania, with commercial porous polymer beads (Sephadex G-100 beads) as template and  $\text{TiCl}_4$  as precursor [36]. The calcination temperature for the titania/poly(S-co-DVB) composite microbeads was 550 °C in the related articles [32-35].

The effects of calcination temperature on the surface area and crystalline structure of the ultrafine (<10 nm) titania powders synthesized by sol-gel method were studied by Guo and coworkers [37]. Qi and co-workers changed the calcination temperature and showed its effect on the surface area of hollow microbeads of titania [36]. However, the effects of calcination temperature on the structural properties of titania microbeads synthesized by using sol-gel templating method were not studied yet.

In this thesis, a new protocol was proposed for the preparation of monodisperse-porous bare and magnetic titania microbeads with prescribed particle size, crystallinity and specific surface area by using monodisperse  $-\text{SO}_3\text{Na}$  attached-polymethacrylate microbeads as template and  $\text{TiCl}_4$  as precursor. Using a polymethacrylate template with low degradation temperature allowed the synthesis of monodisperse-porous bare and magnetic titania microbeads with higher specific surface areas. Calcination at lower temperatures resulted in different crystalline structures for bare and magnetic titania microbeads. To obtain the plasmonic catalysts and enhance the photocatalytic activity of bare and magnetic titania microbeads, decoration of gold nanoparticles (AuNPs) was achieved by subsequent derivatizations. The photocatalytic activity of monodisperse-porous bare or magnetic titania microbeads was investigated by the degradation of a textile dye, Remazol black 5 (RB5) and phenol under UV-irradiation in terms of operational conditions like pH, catalyst concentration, crystal structure, surface

area of the catalyst and initial substrate concentration. The effect of AuNP loading on the photocatalytic activity of bare or magnetic titania microbeads was examined. The plasmonic catalytic activity of AuNP decorated bare and magnetic titania microbeads were studied by reduction of 4-nitrophenol (4-NP) depending on AuNP size, weight percent of Au loading, catalyst concentration, initial substrate concentration and temperature, using excess amount of  $\text{NaBH}_4$ .

## 2. LITERATURE REVIEW

### 2.1. Titanium dioxide (Titania)

Titanium dioxide is a non-toxic semiconductor metal oxide and used as pigment or filler in many industrial fields like paint, plastic, medicine and food [37-39]. As an UV absorber, it is also used in cosmetics and skin care. In addition to these areas, titania has attracted a significant interest in recent years because of its unique photocatalytic properties which can be used for the removal of organic and inorganic pollutants in water, the degradation of harmful organic contaminants such as endocrine disrupters, pesticides, and textile dyes, photoreduction of  $N_2$  or  $CO_2$ , killing of bacteria and harvesting of solar energy [40-44].

In the 1790s,  $TiO_2$  was discovered in the form of black sand on the beaches of Cornwall, England. William Gregor found out that the black grains were separated from the silica sand with a magnet. He treated these black grains with hydrochloric acid which resulted in a white residue. After treating this residue with sulphuric acid and soda he performed a calcination and at last he obtained a white powder:  $TiO_2$  [45].

Today,  $TiO_2$  is produced by sulfate or chlorine processes. In sulfate process, ilmenite, which is found in metamorphic rocks, is turned into iron and titanium sulfates by the treatment with sulfuric acid. Then, titanium hydroxide is precipitated by hydrolysis and calcinated at high temperature. In the chlorine process, the seed crystals are generated by alkaline hydrolysis and reacted with chlorine to produce titanium tetrachloride. Then, titanium tetrachloride is purified and reoxidized to yield very pure  $TiO_2$  [45].

Anatase, rutile and brookite are the crystal structures of titania that can be found in nature [46]. The reasons of the difference on the crystal structure are the distortion of each  $TiO_2$  octahedral and the assemblage patterns of the octahedral chains. The crystal structures of these three different forms of titania are illustrated in Figure 2.1. In anatase phase, the octahedrals are connected by their vertices, while in rutile phase, the edges are connected. In brookite phase, both vertices and edges are connected [47].

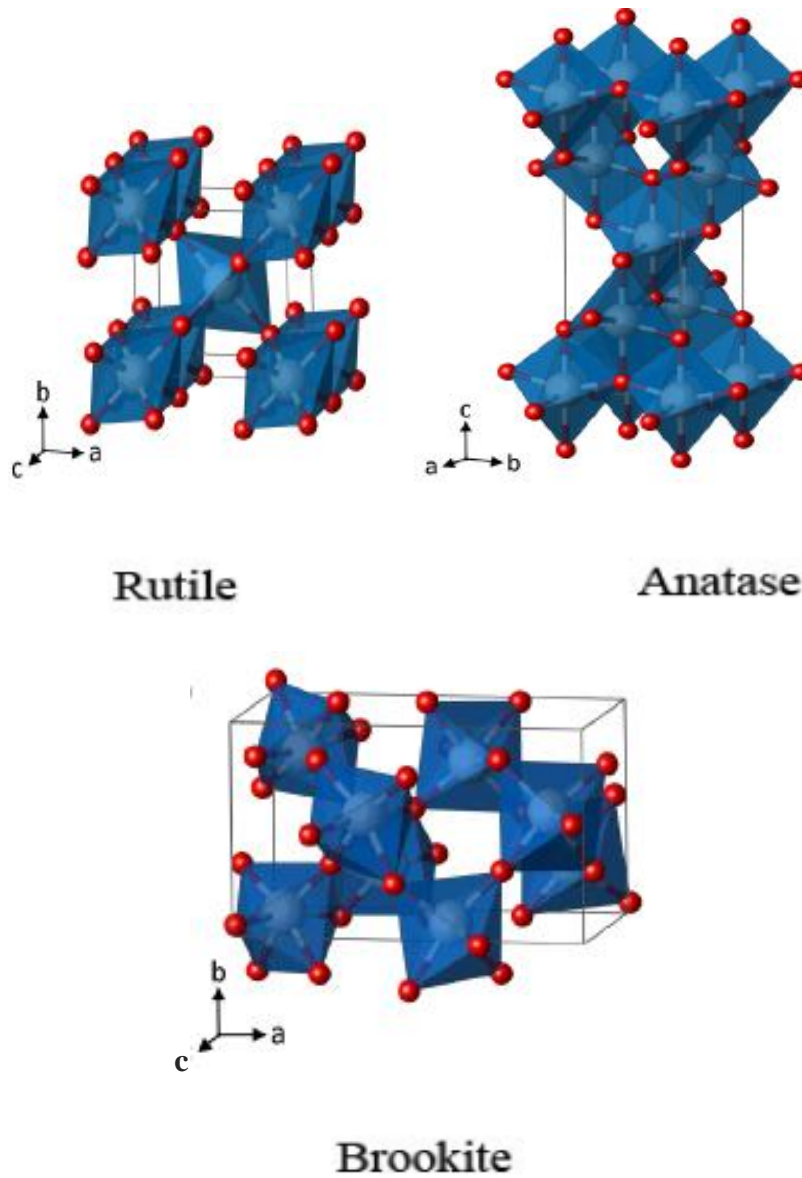


**Figure 2.1.** Representations of the crystal structures for rutile, anatase and brookite [48].

The physical properties regarding to the crystal structures are shown in Table 2.1. [49].

**Table 2.1.** Some physical properties for different crystal structures of titania [50,51].

	<b>Rutile</b>	<b>Anatase</b>	<b>Brookite</b>
<b>Crystal structure</b>	tetragonal	tetragonal	orthorhombic
<b>Band gap energy (eV)</b>	3.0	3.2	3.2 to 3.8
<b>Refractive index</b>	2.49	2.61	2.58
<b>Density (g/cm<sup>3</sup>)</b>	4.13	3.79	3.99
<b>Lattice constants (Å)</b>	a=4.5936 c=2.9587	a=3.784 c=9.515	a=9.184 b=5.447 c=5.145
<b>Ti-O bond length (Å)</b>	1.949(4) 1.980(2)	1.937(4) 1.965(2)	1.87~2.04
<b>O-Ti-O bond angle</b>	81.2° 90.0°	77.7° 92.6°	81.2°~90.0°

Rutile and anatase phases have a tetragonal structure, whereas brookite has orthorhombic structure. The band gap energies for anatase and rutile phases are 3.2 eV and 3.0 eV, respectively. Although the band gap of rutile phase is lower than the band gap of anatase phase, anatase phase shows higher photocatalytic activity due to reduced recombination of photogenerated electron-hole pairs [39, 52]. Among these phases, rutile and anatase have been used in most of the photocatalytic investigations [53]. Rutile phase is chemically more stable but is less active in photocatalysis when compared with anatase phase [54, 55]. However, it was reported that TiO<sub>2</sub> with a large quantity of anatase phase and a small quantity of rutile phase exhibits a higher photocatalytic activity than pure anatase phase [56, 57].

Titania received a great attention especially on photocatalysis among other semiconductors due to its chemical stability, non-toxicity and low cost. As a result it is the most preferred photocatalyst that is used both in laboratory and pilot plant studies for photocatalysis of organic molecules [39].

The electrical conductivity of conductors is around  $10^7 (\Omega\text{m})^{-1}$  which is a high value for electrical conductivity. Unlike conductors, the electrical conductivity of insulators is ranging between  $10^{-10}$  and  $10^{-20} (\Omega\text{m})^{-1}$ . Semiconductors are defined to have electrical conductivity values in between the electrical conductivity values of conductors and insulators [38].

The energy band diagram of a semiconductor which shows the levels of energies of electrons is illustrated in Figure 2.2. Valence band ( $E_{VB}$ ) is the lower energy level of a semiconductor and the next higher energy band is called conduction band ( $E_{CB}$ ), where the electrons are considered to be free. There is a band gap ( $E_g$ ) between the valence and conduction band and the Fermi level for a semiconductor band structure lies in the band gap. The electrons are forbidden to exist in this band gap and therefore an electron should absorb an energy which is higher than the band gap to be excited from valence band to conduction band.

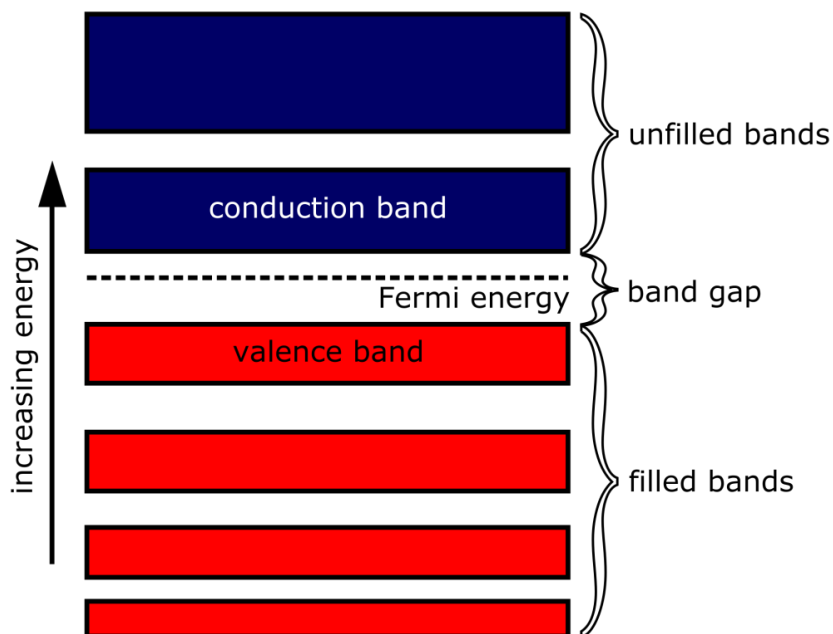


**Figure 2.1.** Band diagram of semiconductors.

The semiconductors with lower band gaps have higher probabilities for the excitation of a valence electron into the conduction band which results in more conduction electrons and higher electrical conductivity. The excitation of an electron leaves behind an empty space for another electron and it is called a hole ( $h^+$ ). Consequently, the excitation of an electron results in not only an electron in the conduction band but also a hole in the valence band. Thus, both the electron and hole can be used in photocatalytic reactions [38].

## **2.1. Synthesis**

TiO<sub>2</sub> can be produced in different forms like powder, crystals or thin films. Each form can be synthesized in a broad size range from few nanometers to several micrometers. The important point is that the physical and chemical properties of TiO<sub>2</sub> depend on the conditions of preparation method. Generally the preparation methods can be divided into two groups: gas-phase methods and solution methods.

For the preparation of thin TiO<sub>2</sub> films, usually the gas-phase methods are preferred. The main techniques for the gas-phase methods are: chemical vapor deposition (CVD) [58] and physical vapor deposition (PVD) [59]. Recently, some other complicated techniques based on gas-phase methods have been used: ion implantation [60], sputtering [61], molecular beam epitaxy [62] and dynamic ion beam mixing [63]. These new techniques provided the production of materials with high purity and controllable film growth. However high energy consumption is a disadvantage when compared with other techniques.

The solution methods are usually used for the synthesis of powders. There are several advantages for this method: the possibility to control stoichiometry, production of homogeneous materials, possibility of formation of complex shapes, and preparation of composite materials. On the contrary, long processing times and use of expensive precursors are the disadvantages of the solution methods.

The solution methods include precipitation and coprecipitation [64, 65], solvothermal and hydrothermal methods [66, 67], microemulsion [68], combustion and electrochemical synthesis [69, 70] and sol-gel method [71]. The sol-gel method is the most popular technique for the synthesis of titania in different forms



due to its advantages over other techniques. The introduction to TiO<sub>2</sub> composite materials [72] and TiO<sub>2</sub>-doped materials [73] is made with this process.

### 2.1.1. Sol–gel method

In the sol–gel method, the solid product is formed by gelation different from crystallization or precipitation. It is described as the process to form materials via a sol, gelation of the sol and finally removal of the solvent [74]. A “sol” is a stable suspension of colloidal solid particles in a liquid. A “gel” is a solid network formed by agglomeration of colloidal solid particles [74, 75].

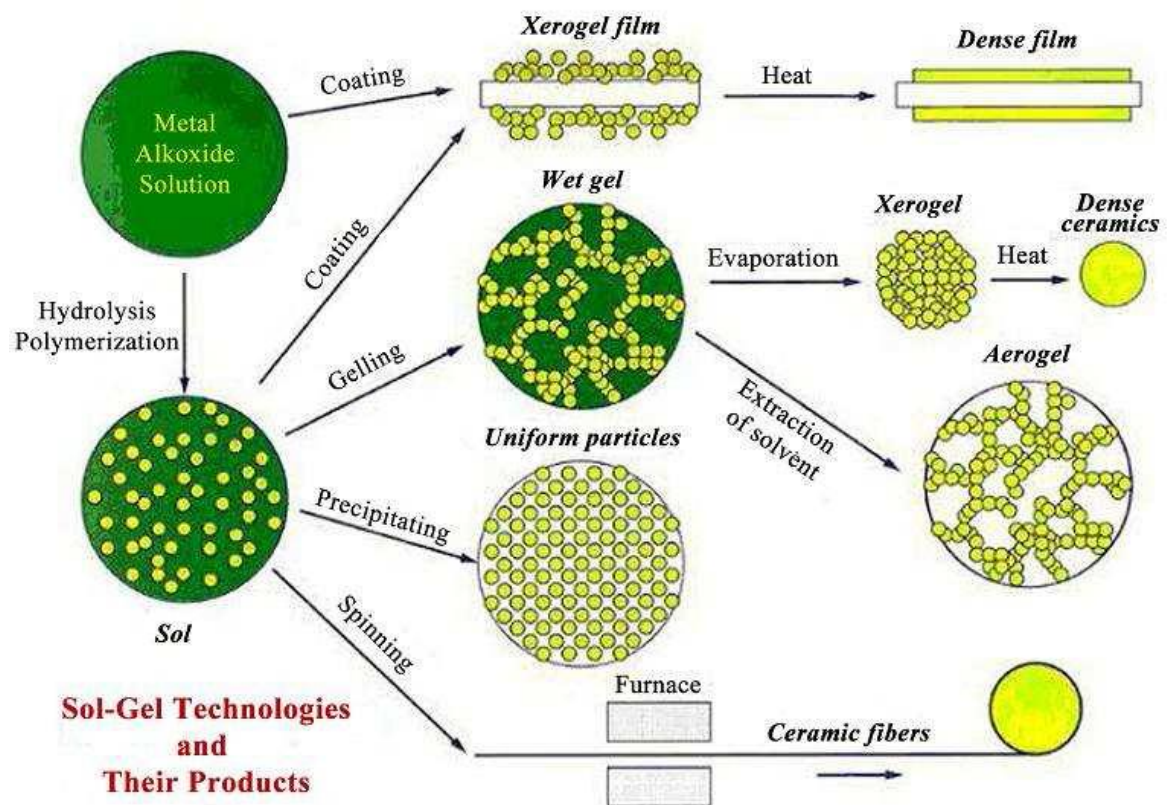


**Figure 2.2.** Scheme of the sol–gel processing options [76].

The scheme of different process routes leading from the sol to a variety of materials is shown in Figure 2.3. By applying different processes to the sol, which is formed by the hydrolysis of precursor, products in different forms (dense films, dense ceramics, wet gels, xerogels, aerogels, uniform particles, ceramic fibers) are obtained [75]. Many materials like catalysts, catalyst supports, ceramic fibers, electroceramic powders, and insulating materials are synthesized by using sol-gel

method. There are some reasons to choose the sol–gel method for the synthesis of such materials [76]:

1. Highly porous materials and crystalline materials can be synthesized.
2. The particle size, pore size and porosity of the final material can be adjusted by controlling the rates of hydrolysis and condensation.
3. By controlling drying and calcination conditions, pore size, porosity and mechanical properties can be controlled.

TiO<sub>2</sub> can be produced by alkoxide or non-alkoxide sol-gel routes depending on the precursor used. In the non-alkoxide (inorganic) sol-gel route, inorganic salts such as nitrates, chlorides, acetates are used as precursors and it requires an additional removal of the inorganic anion [77]. In the alkoxide (organic) sol-gel route, the precursors that are used are metal alkoxides like titanium ethoxide, titanium isopropoxide (TIP) and titanium n-butoxide. Inorganic compounds such as TiCl<sub>4</sub>, Ti(SO<sub>4</sub>)<sub>2</sub> as precursors for titanium dioxide are easily available and more economical than alkoxides [78, 79]. The sol–gel process can be divided in two different categories according to temperature: high–temperature preparation (using calcination treatment) and low–temperature preparation (crystallinity is achieved without calcination treatment).

#### **2.1.1.1. Low–temperature sol–gel process**

By usual sol–gel chemistry in solvent mixtures, only amorphous titania could be synthesized [80]. In most of the studies, calcination of amorph titanium dioxide was performed around 300–400°C to obtain titanium dioxide in anatase form [81]. By performing the calcination at higher temperatures, highly crystalline structures can be obtained, however higher thermal energy leads to the collapse of mesoporous frameworks which results in lower surface areas [82]. Liu et al. synthesized TiO<sub>2</sub> hydrosols by chemical precipitation–peptization method by using titanium sulfate as precursor and metatitanic acid as peptizing agent under different peptizing conditions. The effect of peptizing conditions on the photocatalytic activity was investigated. It was reported that the preparation of TiO<sub>2</sub> particles at low temperatures (< 100 °C) has several advantages such as (1) TiO<sub>2</sub> particles with uniform particle size distribution; (2) higher interfacial adsorption ability; and (3) easy coating on various supporting materials. It was also reported

that the photocatalytic activity of TiO<sub>2</sub> particles depend on some factors such as crystal structure, particle size and surface area [83]. Lee and Liu reported an acid–hydrolysis method for the synthesis of crystalline TiO<sub>2</sub> sol at low temperatures to avoid calcination at high temperatures. TiCl<sub>4</sub> was used as a precursor and hydrochloric acid (HCl) as a peptizing agent. The effects of some parameters such as pH, HCl concentration and storage temperature were investigated [84]. Addamo et al. prepared TiO<sub>2</sub> particles in nanometer size by controlling the hydrolysis of TiCl<sub>4</sub> without calcination. In the study, the effect of concentration of TiCl<sub>4</sub>, preparation procedure and boiling time on the properties of TiO<sub>2</sub> was investigated. It was shown that the photocatalytic activity of TiO<sub>2</sub> samples depended on the crystallinity and particle size [85]. Hydrated titanium dioxide was prepared by Randorn et al. by using TiCl<sub>4</sub> and concentrated NH<sub>4</sub>OH solution without calcination. The crystal structure of the prepared powders consisted of amorphous phase with a small amount of anatase phase. The photocatalytic degradation of methylene blue dye was investigated with prepared powders [86]. Although the low–temperature sol-gel synthesis (<100 °C) eliminates the calcination step [81, 85, 86], the main problem due to low temperature is the low crystallinity and therefore the low photocatalytic activity of the titania particles [81].

#### **2.1.1.2. Sol-gel Templating Method**

Sol-gel templating method is an alternative approach that uses templates to control the morphology of titania particles. Generally, templates can be divided into two groups, soft and hard. Soft templates are flexible and usually organic or biologic molecules are used such as microemulsions, micelles, or proteins. Unlike soft templates, hard templates have rigid structures such as inorganic colloids or polymeric beads. Using polymeric templates, which controls the morphological property such as pore size, outer shape and size, has a great importance for the synthesis of monosized porous titania beads [31]. The sol-gel templating is a suitable method for the preparation of titania beads with controlled morphology and structure. This method involves sol-gel chemistry of pure metal alkoxides within porous polymeric template. The template is removed from the composite structure by calcination or extraction [87, 88]. By using this method, Caruso and co-workers demonstrated the use of porous poly(S-co-DVB) microbeads as template and TiCl<sub>4</sub> as precursor in the production of titania microbeads [32, 33].

Meyer et al. used non-functionalized and hydroxyl/amine functionalized poly(S-co-DVB) microbeads as template and titanium isopropoxide (TIP) as precursor for the preparation of titania microbeads [34]. Wang and co-workers also used the same particles but larger in size to synthesize titania macrobeads by using  $\text{Ti}(\text{SO}_4)_2$  as precursor [35]. Qi and co-workers prepared hollow microbeads of titania, with commercial porous polymer beads (Sephadex G-100 beads) as template and  $\text{TiCl}_4$  as precursor [36]. The calcination temperature for the titania/poly(S-co-DVB) composite microbeads was 550 °C [32-36]. Caruso and coworkers successfully prepared a novel titania material by using cuboid agarose gel block as template [89, 90]. Although the pore structure was perfectly replicated and controllable, the final material showed poor mechanical stability because the agarose fibers were only coated with a thin titania film. The shortcomings would seriously limit their application as chromatographic packing. Sun and co-workers synthesized porous titania beads by an improved sol-gel templating procedure using agarose gel as template [91].

## **2.2. Synthesis of Polymeric Templates**

Polymeric particles can be synthesized in the broad size range from nanometer to micrometer scale by using different types of liquid-phase heterogeneous free-radical polymerizations: emulsion polymerization, microemulsion polymerization, mini emulsion polymerization, dispersion polymerization and suspension polymerization [92, 93].

### **2.2.1. Dispersion Polymerization**

Dispersion polymerization is a free-radical polymerization technique and used for the production of polymer particles in micron-size range with a narrow size distribution [94]. The size of the polymeric particles obtained with dispersion polymerization is usually between 1 to 10 microns. The most important property that separates the dispersion polymerization from other techniques is the synthesis of highly monodisperse particles. Dispersion polymerization has received a great interest for the synthesis of monodisperse polymeric particles used in industry, health care and various research areas [95-98]

In the literature, the dispersion polymerization was first developed by Osmond and coworkers and then it was reviewed by Barrett [94]. For the production of non-

aqueous dispersions of polymeric particles, acrylic and vinylic monomers were polymerized in hydrocarbons with polymeric stabilizers. Almog et al. used polar solvents to obtain monodisperse polymeric microspheres, using hydrolyzed polyvinyl alcohol (PVA) as a colloidal stabilizer and a quaternary ammonium salt as an electrostatic co-stabilizer [99]. This work extended the field of dispersion polymerization and as a result it became a popular method for the synthesis of polymeric particles [100, 101].

In the dispersion polymerization, the monomer is polymerized in the presence of a suitable stabilizer which is also soluble in the reaction medium. The selection of solvent is important as the solvent should dissolve both the monomer and the stabilizer, but should not dissolve the polymer being formed. Therefore, in the early stages of dispersion polymerization the polymerization solution is homogeneous. As the polymerization continues and the monomer conversion increases, the sterically stabilized polymeric particles are formed by the precipitation. The mechanism of the dispersion polymerization is very complicated, since at the beginning of polymerization it is like a solution polymerization and then in a short time it changes to a heterogeneous polymerization [92, 93, 102-105]. The size and the molecular weight of the polymeric particles formed by dispersion polymerization depend on polymerization kinetics, particle growth process and all other reaction parameters [92, 93, 102-104, 106-109]. There are three steps in the particle formation in dispersion polymerization: (1) self-nucleation [110], (2) aggregative nucleation [111], and (3) nucleation from micelles [112].

The mechanism for the dispersion polymerization of methyl methacrylate in *n*-dodecane was obtained by Barrett and Thomas [113]. A kinetic model for the prediction of particle size in dispersion polymerization was developed by Paine et al [102, 114]. The mechanism for the polymerization of micron-size polymeric particles in the dispersion polymerization of methyl methacrylate (MMA) in methanol with polyvinylpyrrolidone (PVP) as the stabilizer was investigated by Shen et al. by monitoring the change in the average particle size during the polymerization [104]. Tseng et al. proposed a mechanism for the particle formation in dispersion polymerization of polystyrene in ethyl alcohol with PVP with different co-stabilizers [108]. The schematical description of the dispersion polymerization is given in Figure 2.4.

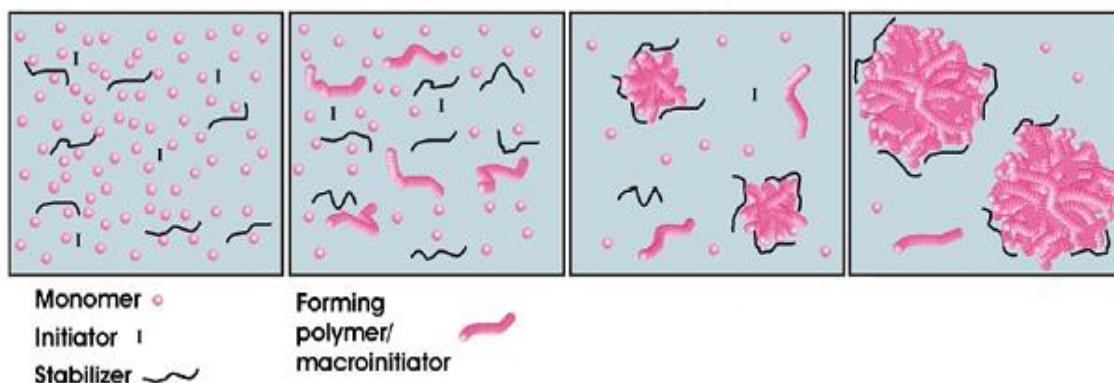


**Figure 2.3.** Schematic description of the stages of dispersion polymerization [115].

According to the studies given in literature [104, 108, 113], the mechanism can be summarized in four steps.

- 1) At the beginning, monomer, initiator and polymeric stabilizer are dissolved in the solvent and the solution is homogeneous.
- 2) After heating the solution, the initiator decomposes to form free radicals and these free radicals react with the monomer to form oligomers, which are still soluble in solvent.
- 3) By reaching the critical chain length, the polymer chains start to precipitate and form the nuclei that are stabilized by the polymeric stabilizer. Then the nuclei aggregate into larger particles by absorbing stabilizer and co-stabilizer from the medium till the stable particles are formed.
- 4) The polymerization occurs within the monomer-swollen particles. This process continues until all of the oligomers and nuclei are consumed in the reaction medium [115].

As reported in different studies, the nuclei are formed throughout the dispersion polymerization and the number of particles is determined at the early stages. After the particle formation stage is completed, only the particle size increase as the polymerization proceeds [92, 93, 104, 116, 117]. According to various researchers, the number of stable particle is determined by the aggregation rate of nuclei and the stabilization kinetics. Also nuclei formed at later stages of the reaction become incorporated into the larger particles already present in the reaction [103, 104, 106, 108]. The stabilizer has an important role in the particle formation during the polymerization and the stable particles can not be formed in the absence of

stabilizer [93, 114]. Therefore, the nucleation kinetics determines the initial number of particles and the stabilizer controls the particles size and size distribution.

### 2.2.2. Multistep Microsuspension Polymerization for Synthesis of Functional, Monodisperse Porous Particles

The multistage polymerization protocols give the opportunity to obtain functional polymeric particles. For the introduction of functional groups into the structure of relatively hydrophobic polymeric particles, hydrophilic acrylate or methacrylate based monomers are mostly preferred [115]. In the late 1970s, Ugelstad et al. reported that polymeric particles could absorb hydrophilic agents up to 100 times of their own volume and form stable emulsions [118]. The schematical description of seed latex preparation and multistep microsuspension polymerization is given in Figure 2.5.

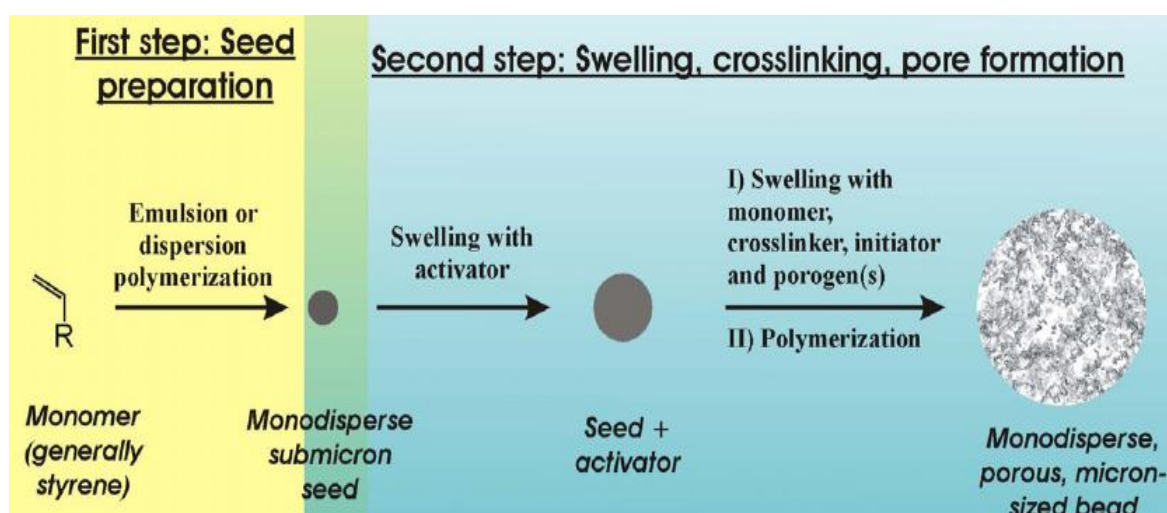


**Figure 2.4.** Schematical description of seed latex preparation and multistep microsuspension polymerization [115].

The first step shown in Figure 2.5. is the seed latex preparation from monomer(s) by emulsion or dispersion polymerization. The second step shows the description of multistep microsuspension polymerization, in which the seed latex is swollen by an activator (i.e. ethylbenzene) in the first stage. In the second stage, the swollen seed latex is reswollen by an organic mixture containing functional monomer, crosslinker and initiator. In the last stage the polymerization of monomer phase within the swollen seed latex particles is performed. The multistep

microsuspension polymerization results in large, porous and monodisperse polymeric particles [115].

The work reported by Frechet and co-workers is a typical example for the multistep microsuspension polymerization [119]. In this work, polystyrene seed latex was first prepared by emulsion polymerization and the seed latex was swollen by dibutylphthalate, to activate the seed latex before the swelling stage with the monomers of propargyl acrylate and EDMA. At the end of the polymerization, monodisperse functional microbeads 5  $\mu\text{m}$  in size were obtained. With a similar polymerization procedure uniform the polystyrene particles with different functionalities (carboxyl, amine, amide, hydroxyl, aldehyde) were also obtained [120]. Tuncel and co-workers reported a multistage approach for the preparation of monodisperse porous functional polymeric particles [121]. In the referred study, nonporous seed latex was produced by dispersion polymerization. Then the seed latex was subsequently swollen by using a diluent in the first stage. In the second stage, the monomer phase was adsorbed by the swollen seed latex. Finally, the repolymerization of the monomer phase was achieved in the swollen seed latex [121].

The multistep microsuspension polymerization bands together the advantages of emulsion/dispersion polymerizations and suspension polymerization to form functional monodisperse porous polymeric particles in different sizes. However, multi-step polymerization requires a good knowledge and experience to obtain the desired particles [122].

### **2.3.Applications of Titanium Dioxide Particles**

Mesoporous titanium dioxide particles have been extensively used in many products like sunscreens, paints, ointments and toothpaste. After the discovery of photocatalytic splitting of water on a  $\text{TiO}_2$  electrode under UV light, many studies has been bent on the application areas of  $\text{TiO}_2$  materials (Figure 2.6.) like photocatalysis, air/water purification, solar cells and hydrogen evolution [123].



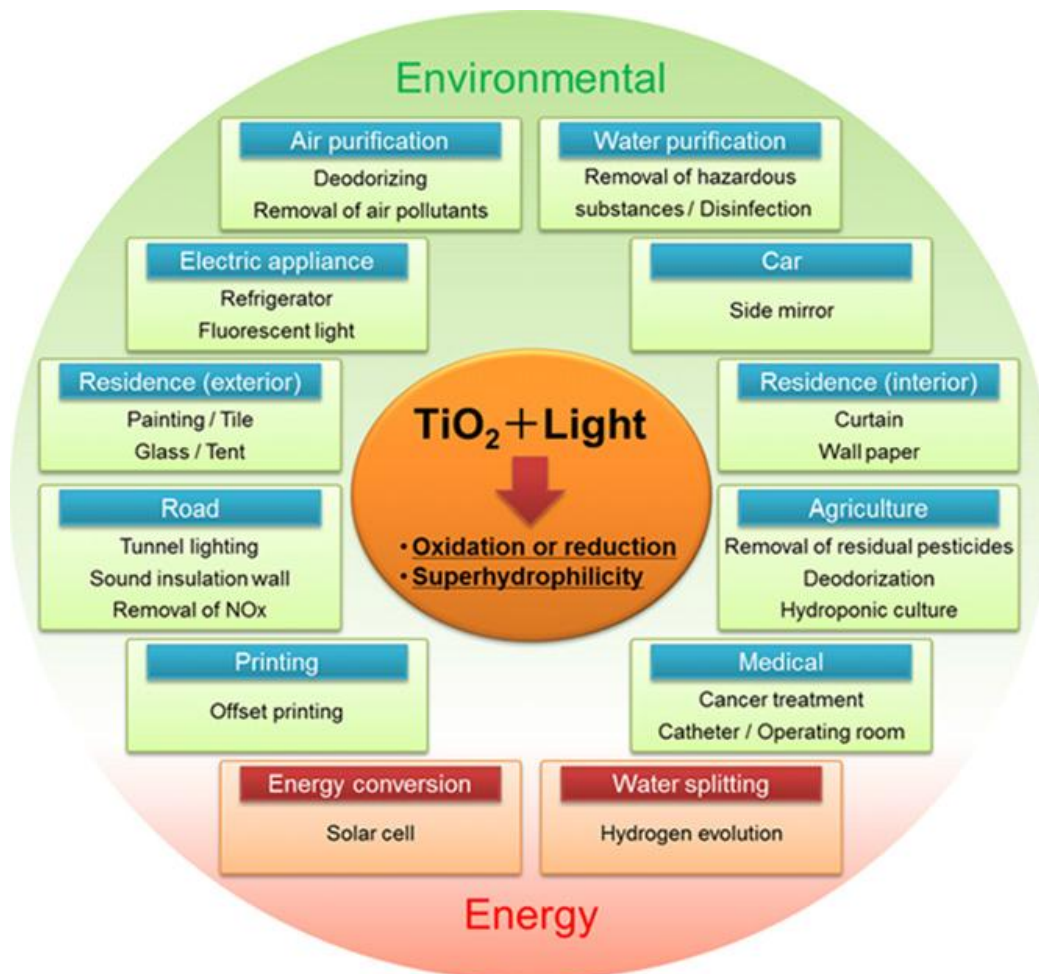


**Figure 2.5.** Applications of  $\text{TiO}_2$  photocatalysis [123].

As the morphology and crystal structure of mesoporous titania materials will differ in different applications, controlling the morphological and structural properties of mesoporous titania is greatly important.

Peng et al reported a method for the hydrothermal synthesis of mesoporous titania nanoparticles by using a surfactant as a structure-directing agent. The titania nanoparticles had a high surface area and exhibited high photocatalytic activity for oxidation of Rhodamine B [124].

Thermally stable mesoporous anatase with high crystallinity, large surface area and large pore size (10 nm) was synthesized by Zhou et al [125]. The photocatalytic activity of this material was tested by the degradation of 2,4-dichlorophenol under UV irradiation. Dai et al used the La-doped mesoporous titania nanoparticles for the degradation of phoxim, which is a high toxic pesticide [126].

One of the most popular materials used in dye sensitized solar cells (DSSCs) is also titanium dioxide. As the particle size and shape of titanium dioxide is important for the efficiency of DSSCs [127], titanium dioxide types with different shapes, such as nanoparticles, nanotubes, nanowires and nanofibers were used in the fabrication of the porous film electrodes [128–130]. Khan et al showed that the conversion efficiency of DSSCs was affected by surface area and pore volume of nanocrystalline titania containing anatase phase [131]. Zhao et al investigated the effect of annealing temperature of porous electrodes, which are fabricated with mesoporous titania nanoparticles, on the photoelectrochemical properties of DSSCs [132]. They also reported that the mesostructures of mesoporous titania nanoparticles improved the dye adsorption and thus the photoelectrochemical properties of DSSCs. Recently, mesoporous titania has been used in the gas sensor studies. Benkstein and Semancik showed that mesoporous titania films could be used as gas sensor materials [133]. Devi et al prepared hydrogen (H<sub>2</sub>) and carbon monoxide (CO) sensors with mesoporous titania and reported that the sensors were more sensitive due to their higher surface areas [134]. Despite the other application areas, a little work has been published about the biomedical applications. Recently, Wu et al have reported the biomedical application for mesoporous titania. The viability tests showed that titania material had a good biocompatibility till a concentration of 0.4 g. L<sup>-1</sup>. They also showed that the synthesized titania was an excellent drug delivery platform [135].

### **2.3.1. Support for catalysis**

In classical heterogeneous catalysis, the catalysts (often a metal, an oxide, or a sulfide) are in the form of small particles in the nanometer range. The reason of using catalysts in small size is to obtain higher surface areas as the catalytic reactions occur on the surface of the particles. Unfortunately, the particles in nanometer scale are not stable and they tend to agglomerate. To overcome this disadvantage, different supports with high surface areas can be used to keep the active catalyst in the dispersed state in the reaction medium [136].

There are different studies in literature concerning the gold nanoparticle supported titania catalyst for the reduction reactions [137-140].

Camargo and co-workers described a facile approach for the decoration gold nanoparticles on titania spheres and investigated the catalytic activity of the gold nanoparticle decorated titania spheres as a function of composition and particle size by employing the reduction of 4-NP as a model reaction [141].

Yazid et al prepared gold nanoparticles supported on titania for the reduction of nitrophenol by deposition-precipitation method. The effect of gold nanoparticle size and pH on the catalytic activity was investigated [142].

### **2.3.2. Photocatalysis**

The research of Fujishima and Honda, which figured out the possibility of water splitting with titania, reported in 1972 contributed an understanding in the heterogeneous photocatalytic processes [143]. In heterogeneous photocatalysis, semiconductor metal oxides are used as a photocatalysts with UV irradiation [5]. Heterogeneous photocatalysis can be considered under AOPs and is a promising method for the degradation of toxic organic molecules [145]. Different from other AOPs, the semiconductor metal oxides are used as a catalyst in photocatalysis instead of oxidants like  $H_2O_2$  and  $O_3$  which are expensive reactants [5].

For a heterogeneous photocatalysis, the overall process can be summarized in independent steps given below [146]:

- i. Diffusion of the reactants to the surface of the photocatalyst;
- ii. Adsorption of the reactants;
- iii. Reaction in the adsorbed phase;
- iv. Desorption of the products;
- v. Removal of the products from the photocatalyst.

Organic compounds like alkanes or alkenes, phenolic compounds, aromatics, textile dyes can be degraded with heterogeneous photocatalysis under ambient temperatures[147]. In the literature, many studies in different application areas were made about heterogeneous photocatalysis with titania [11-24, 148, 149].

The advantages of the heterogeneous photocatalysis are:

- 1) no additives are required,
- 2) cheap chemicals can be used for the preparation of photocatalysts,

3) total mineralization is achieved for most of the organic compounds [150].

### 2.3.2.1. General mechanism of photocatalytic reaction process

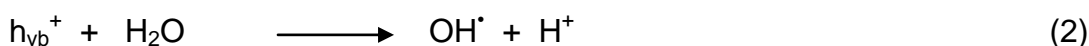
The redox reaction which undergoes after UV-irradiation of the semiconductor metal oxide material provides the degradation of organic pollutants. When a photon with an energy higher than the band gap value of the semiconductor is absorbed by a particle, an electron excited from the valance band to the conduction band by generating a photogenerated hole ( $h_{vb}^+$ ) in the valance band and a photogenerated electron ( $e_{cb}^-$ ) in the conduction band [151, 152].

The mechanism of the photocatalytic reaction process of titania is given by the Equations 1–12.

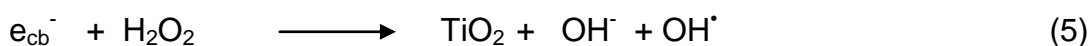
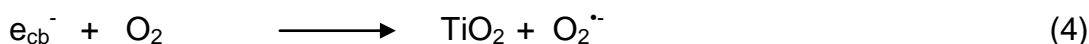
#### Electron-hole pair formation:



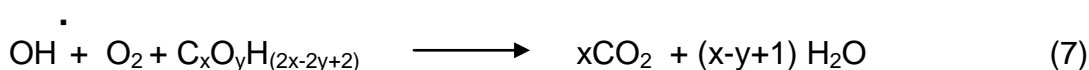
#### Hole trapping:



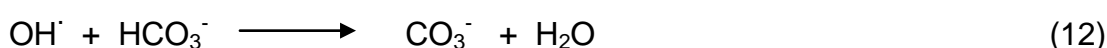
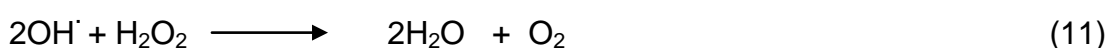
#### Electron removal from the conduction band:



#### Oxidation of organic pollutant molecules:



#### Non-productive radical reactions:



The  $e_{cb}^-$  and the  $h_{vb}^+$  can recombine on the surface or in the bulk of the titania particle in a short times (Eqn. (8)) or can be trapped in surface states where they can react with donor (D) or acceptor (A) species adsorbed or close to the surface of the titania particle (Figure 2.7.).

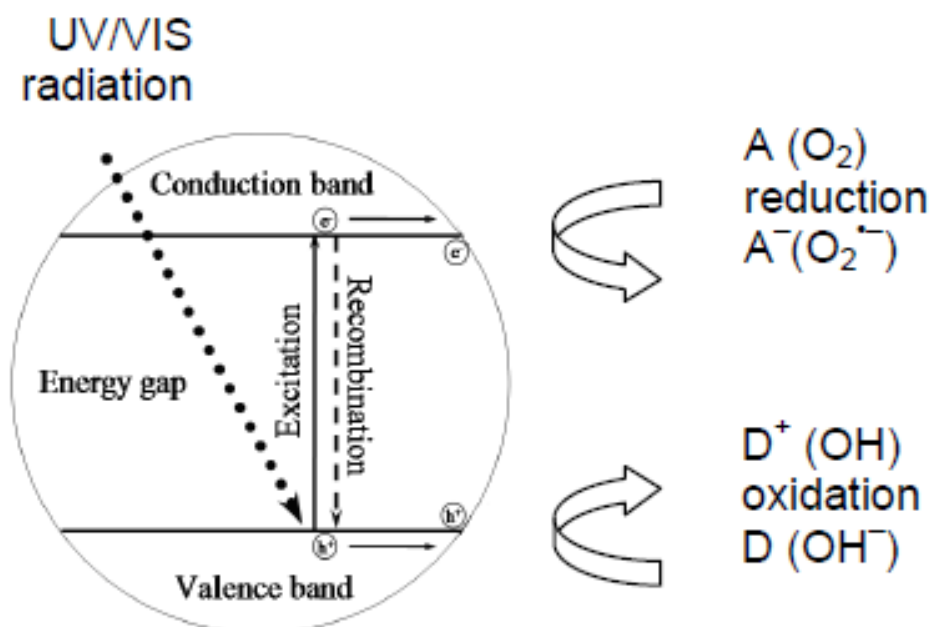


**Figure 2.6.** Schematic representation of photochemical process in and on a titania particle [153].

Principally it is accepted that the initial step for photocatalytic degradation is the formation of reactive hydroxyl radicals ( $\bullet\text{OH}$ ) by hole trapping (Eqns. (2), (3)). The  $\bullet\text{OH}$  is formed on the highly hydroxylated semiconductor surface. This process is immediately followed by the reduction of adsorbed oxygen species, derived either from dissolved oxygen molecules, or by other electron acceptors available.

## 2.4. Factors affecting the photocatalytic process

### 2.4.1. Structural and morphological properties of $\text{TiO}_2$

The photocatalytic activity of titania should be investigated by considering the effects of the crystal structure, surface area, pore size and the pore size distribution.

#### **2.4.1.1. Crystal structure of TiO<sub>2</sub>**

The most active crystalline phase of titania is accepted as the anatase form. The higher efficiency obtained with anatase phase of titania can be attributed to the higher degree of hydroxylation compared to rutile phase. Also, the higher surface area of anatase phase of titania is another reason for the superior efficiency. However, some studies showed that pure anatase did not always perform the best photocatalytic performance [56, 57, 154]. The results obtained from different studies can be concluded that the presence of rutile phase may introduce mesoporosity and a wider pore size distribution.

#### **2.4.1.2. Surface area of TiO<sub>2</sub>**

The surface area of titania photocatalysts is directly related with the concentration of active sites for adsorption and reaction. A large surface area can be resulted in large amounts of substrate adsorption, which is an important factor in photodegradation reactions. However, titania with higher surface areas are associated with the crystal lattice defects, which leads to a poor photocatalytic activity [155]. It was reported that a morphous titania did not show a photocatalytic activity which means that crystalline structure is an important factor [156]. Therefore, to obtain the maximum photocatalytic activity the surface area and crystallinity of the photocatalyst should be adjusted.

#### **2.4.1.3. Particle dimensions of TiO<sub>2</sub>**

The particle size plays an important role in the photocatalytic activity of the titania, since the electron/hole recombination process depends on the particle size dependent. Also the particle size is an important parameter in heterogeneous photocatalysis as it directly changes the specific surface area and the number of active surface sites of the photocatalyst [157, 158].

#### **2.4.2. Operational parameters**

It is obvious that operational parameters related with each agent (water, organic substrate, catalyst, light and oxygen) involved in photocatalytic reactions may affect the photocatalytic activity. There are several operating conditions that affect the photocatalytic activity including catalyst loading, substrate concentration, pH, temperature, oxygen supply and light intensity.

#### **2.4.2.1. Catalyst loading**

The mass of the photocatalyst is directly proportional to the initial reaction rate in photocatalytic processes. However, the reaction rate becomes independent of the mass of photocatalyst after a certain amount of photocatalyst. The reason of this limitation is that in each reaction medium there is a maximum amount of photocatalyst in which all of the particles are fully illuminated. Therefore, in photocatalytic applications it is important to obtain the optimum photocatalyst amount to avoid using excess photocatalyst [147].

#### **2.4.2.2. Substrate concentration**

The photocatalytic reactions occur on the surface of the photocatalysts, therefore, higher amount of substrate adsorbed on the photocatalyst is favored. In kinetic modelling studies, it was reported that most of the photocatalytic reactions follow a Langmuir-Hinshelwood kinetic rate model, which means that at high initial substrate concentration the catalytic sites of photocatalysts are occupied. As a result, increasing the initial substrate concentration after a certain concentration decreases the observed rate constant. Also the photocatalytic reaction intermediates adsorbed on photocatalysts affect the rate constant negatively [159, 160].

#### **2.4.2.3. pH**

The change in the pH directly affects the surface charge of titania particles due to the amphoteric (point of zero charge at pH~6.5) nature of titania particles. The surface of titania particles are protonated or deprotonated under acidic and alkaline conditions, respectively. Also, the pH affects the surface charge of the substrate depending on its pKa. Therefore, the electrostatic interaction between the titania particles and substrate accordingly the adsorption of substrate on titania particles directly changes with pH. It can be concluded that pH is an important parameter that influences photocatalytic reaction rate [161].

#### **2.4.2.4. Temperature**

Heating is not required in photocatalytic reactions due to photonic activation, thus photocatalytic reactions occur at room temperature. This is a crucial point in the purification systems as there is no need to apply energy to photocatalytic systems [6].

#### **2.4.2.5. Oxygen supply**

In liquid phase reactions it is assumed that dissolved oxygen (according to Henry's law) adsorbs on titania particles from the liquid phase. If oxygen is continuously supplied to the medium, it can be assumed that its coverage at the surface of  $\text{TiO}_2$  is constant which results in a constant reaction rate [147]. Increasing the amount of dissolved oxygen can reduce the unwanted electron and hole recombinations, but also it can decrease the adsorption of substrate according to the concentration.

#### **2.4.2.6. Light Intensity**

The light source and light intensity is an important parameter that should be taken into consideration in the design of the reactor [162]. In the literature there are some studies that investigated the effect of light intensity on photocatalysis [163,164].

### **2.5. Trends to improve $\text{TiO}_2$ activity**

As mentioned before titania is the most preferred semiconductor in photocatalysis applications as it is the most active photocatalyst. However, it was observed that a great effort has been shown to improve photocatalytic activity of titania in recent studies including modifications by metal doping, mixing with other semiconductors and addition of inert supports [10, 165].

#### **2.5.1. $\text{TiO}_2$ doping**

Doping titania with transition metals may result in an enhancement on the photocatalytic activity. In literature it was reported that several metals like Au, Ag, Sn were doped on titania to increase the photocatalytic activity by decreasing the value of band gap of titania [166-169]. The dopants can increase the photocatalytic activity by working as hole and electron traps or compromising interfacial charge transfer. When the dopant works as an electron trap, the lifetime of the generated charge carriers will increase and as a result an enhancement was observed in the photocatalytic. However, longer lifetimes may result in lower redox potential and as a result inhibition was observed in the photocatalytic activity of the photocatalyst.



Also the concentration of the metal dopant on the titania is an important parameter on the photocatalytic activity. The space-charge region, in which electron/hole pairs are separated by a large electric field before recombination, becomes narrower by increasing the concentration of the metal dopant. Therefore, at higher concentrations of the metal dopant the recombination of electron/hole pairs in the titania increases due to narrow space-charge region which is detrimental for the photocatalytic activity. It can be concluded that there should be an optimum concentration for the metal dopants [167-169].

#### **2.5.1.1. Gold Nanoparticle (AuNP) Synthesis**

Gold nanoparticles (AuNPs) are synthesized with different methods but generally different reducing agents are used for the reduction of chloroauric acid ( $\text{HAuCl}_4$ ) [170-175]. In these reduction processes  $\text{Au}^{3+}$  is reduced to form gold nanoparticles. In Turkevich method, citrate ions were used both for the reduction of  $\text{Au}^{3+}$  and the stabilization of obtained AuNPs in water [173]. AuNPs in low sizes were obtained in organic liquids with Brust method [174]. The Martin method introduced a new route for the synthesis of AuNPs in which “naked” monodisperse AuNPs are generated in water due to the reduction of  $\text{HAuCl}_4$  by sodium borohydride ( $\text{NaBH}_4$ ) [175].

##### **2.5.1.1.1. Turkevich Method**

This method was initiated in 1951 by Turkevich [173, 176]. Later on the method was improved by G. Frens in 1970 [177, 178]. In this method AuNPs were formed by the reduction of chloroauric acid with citrate ions, which is used as both reducing and stabilizing agent. The size of spherical AuNPs obtained with this method varies between 10-20 nm depending on citrate concentration. Decreasing the concentration of citrate ions results in nanoparticles with larger sizes.

##### **2.5.1.1.2. Martin Method**

This new method was introduced to literature in 2010 [175] and in this method  $\text{NaBH}_4$  was used as reducing agent for the reduction of  $\text{HAuCl}_4$  to form AuNPs. As a result monodispersed AuNPs were obtained in the size of 3-5 nm without a stabilizing agent. It should be noted that stabilized aqueous solutions of  $\text{HAuCl}_4$  and  $\text{NaBH}_4$  were prepared by using HCl and NaOH solutions, respectively.

### **2.5.1.2. Magnetic Nanoparticle Synthesis**

Different methods have been used for the synthesis magnetic nanoparticles (MNPs), including co-precipitation, sol-gel synthesis, microemulsion synthesis, hydrothermal reaction, thermal decomposition [179-183]. Co-precipitation method is the classical method, in which iron salts in a stoichiometric ratio are used to prepare iron oxide nanoparticles [184]. The operational parameters like pH, reaction temperature influences the morphology and size of the MNPs.

#### **2.5.1.2.1. Co-precipitation method**

The co-precipitation method, which was found by Massart [185], is the simplest classical method to synthesize iron oxide nanoparticles. In this method  $\text{Fe}^{2+}$  and  $\text{Fe}^{3+}$  ions in a molar ratio of 1:2 are co-precipitated in a basic solution to form iron oxide nanoparticles. As the iron ions are sensitive to oxidation, an inert gas is purged to the reaction medium to prevent the transformation of magnetite form to maghemite. Unfortunately, the control of nanoparticle size in co-precipitation synthesis method is not good which means that agglomerations can occur. To obtain nanoparticles in narrow size distribution, the nucleation time should very short and nucleation step should be separated from growth step, which is shown in LaMer diagram [186]. The size and the morphology of the magnetic nanoparticles can be varied by changing the solution pH, type of iron salts, temperature, and reaction time.

### 3. EXPERIMENTAL METHODS

In this thesis, a new sol-gel templating method was constructed by using  $-\text{SO}_3\text{Na}$  attached-poly(HPMA-Cl-co-EDMA) microbeads and magnetic poly(HPMA-Cl-co-EDMA) microbeads as templates for the synthesis of bare and magnetic titania microbeads, respectively. Multistep microsuspension polymerization method was used for the preparation of monodisperse-porous poly(HPMA-Cl-co-EDMA) microbeads. The surface morphology, size, porous structure and specific surface area of the monodisperse-porous poly(HPMA-Cl-co-EDMA) were varied by changing the feed concentration of crosslinking agent.

Monodisperse-porous bare titania microbeads in different sizes, porous structures and specific surface areas were obtained by using  $-\text{SO}_3\text{Na}$  attached poly(HPMA-Cl-co-EDMA) microbeads with different feed concentrations and crosslinking densities. On the other hand, monodisperse-porous magnetic titania microbeads were obtained by using magnetic poly(HPMA-Cl-co-EDMA) microbeads as the template material.

AuNP decorated bare and magnetic titania microbeads were also synthesized by the treatment of gold nanoparticle solutions with the amine attached bare and magnetic titania microbeads. These materials were tested as catalysts in photocatalytic and plasmonic catalytic activity measurements. The photocatalytic and plasmonic catalytic activity measurements of  $\text{TiO}_2$  based materials were carried out by considering operational parameters such as pH, catalyst concentration, crystal composition and surface area, initial reactant concentration, temperature, AuNP size and Au loading.

#### 3.1. Synthesis of Monodisperse-Porous poly(HPMA-Cl-co-EDMA) Microbeads

##### 3.1.1. Materials

For the synthesis of monodisperse-porous poly(3-chloro-2-hydroxypropyl methacrylate-co-ethylene glycol dimethacrylate) [poly(HPMA-Cl-co-EDMA)] microbeads; the monomers, glycidyl methacrylate (GMA), 3-chloro-2-hydroxypropyl methacrylate (HPMA-Cl), the crosslinking agent, ethylene dimethacrylate (EDMA), and the diluent, ethylbenzene (EB) were supplied from

Aldrich Chem. Corp., USA. The initiator, benzoyl peroxide (BPO), the stabilizers, polyvinyl alcohol (PVA, 87–89 % hydrolyzed, Mw= 85,000–146,000 Da) and polyvinylpyrrolidone (PVP K-30, Sigma, average molecular weight: 40.000 Da), the emulsifier, sodium dodecyl sulfate (SDS) were supplied from Aldrich. The initiator, BPO was dried under vacuum at 30 °C before use. 2,2-azobisisobutyronitrile (AIBN) supplied from Across Organics, USA were recrystallized from methanol before use. Ethanol (EtOH, HPLC grade, Merck A.G., Darmstadt, Germany) and tetrahydrofuran (THF, HPLC grade, Aldrich) were used as the solvents. Distilled deionized (DDI) water (Direct-Q 3 UV (Type 1), Millipore, USA) with a resistivity of 18 MΩ cm was used during all synthesis runs.

### 3.1.2. Synthesis of GMA Seed Latex

Monodisperse poly(GMA) seed latex particles 2.5 μm in size were obtained by the dispersion polymerization of GMA monomer.

The conditions of the dispersion polymerization were given in Table 3.1.

**Table 3.1.** Experimental conditions of dispersion polymerization of GMA monomer for the synthesis poly(GMA) seed latex.

<b>Materials</b>		<b>Amount</b>
<b>Solvent</b>	Absolute Ethanol	30 mL
<b>Stabilizer</b>	PVPK-30	0.45 g
<b>Monomer</b>	GMA	3 mL
<b>Initiator</b>	AIBN	0.24 g
<b>Polymerization conditions</b>		
<b>Temperature</b>		70 °C
<b>Time</b>		24 h
<b>Shaking rate</b>		120 rpm

PVPK-30 (0.45 g), as stabilizer, was dissolved in 30 mL absolute ethanol in a glass polymerization reactor. The monomer, GMA (3 mL) and the initiator, AIBN were added to the solution and sonicated in ultrasonic bath (Bransonic 200, UK) till

AIBN was dissolved. Then the glass polymerization reactor was sealed carefully and placed in a temperature-controlled shaking water bath (Memmert Type WB 14, Germany) at room room temperature. The temperature-controlled shaking water bath with a shaking rate of 120 cpm was heated to 70 °C and the polymerization was carried out under these conditions. After 24 hours, the sealed glass polymerization reactor was taken from the temperature-controlled shaking water bath and cooled down to room temperature. Poly(GMA) seed latex was isolated by centrifugation (2000 rpm, 3 min) and then washed with EtOH and DDI water for several times and finally dispersed in DDI water [187]. The amount of poly(GMA) seed latex in a certain volume was obtained by gravimetric analysis. For this purpose, 1 mL of poly(GMA) seed latex solution was dried in a container at 70 °C for 24 h. The change in the weight of the container gave the amount of solid in 1 mL of poly(GMA) seed latex solution.

### 3.1.3. Synthesis of Monodisperse-Porous Poly(HPMA-Cl-co-EDMA) Microbeads by Multistep Microsuspension Polymerization

For the synthesis of monodisperse-porous poly(HPMA-Cl-co-EDMA) microbeads ‘multistep microsuspension polymerization’ was used. The scheme of the multistep microsuspension polymerization is given in Figure 3.1.

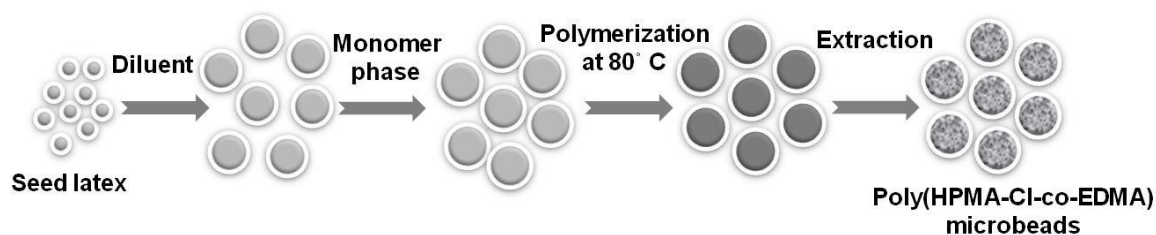


**Figure 3.1.** Synthesis of poly(HPMA-Cl-co-EDMA) microbeads by multistep microsuspension polymerization.

In the first stage, poly(GMA) seed latex particles were swollen by an organic diluent in an aqueous emulsion medium by preserving the monodispersity of the seed latex particles. For this purpose, SDS (0.125 g) was dissolved in distilled water (50 mL); and the diluent (EB, 2.5 mL) was added into this solution. The resulting medium was sonicated for 8 min for dispersion of EB in the form of micron-size droplets in the aqueous medium. After emulsification, the aqueous

dispersion of poly(GMA) seed latex particles (0.3 g) was added to the emulsion and sonicated for 4 minutes. The medium was stirred at room temperature for 24 h for complete absorption of EB by the seed latex particles. In the second stage, the diluent swollen seed latex particles were reswollen by the monomer phase, containing HPMA-Cl (3.5 mL) and EDMA (1.5 mL) and the initiator, BPO (0.3 g). For this purpose, the monomer phase was emulsified in water (50 mL) containing SDS (0.125 g) by sonication for 12 minutes. After sonication, the emulsion was added to the aqueous dispersion of diluent-swollen seed latex particles prepared in the first step. The resulting dispersion was stirred at room temperature for 24 h for complete absorption of monomer phase by the seed particles. Then, the stabilizer PVA (0.8 g in 10 mL DDI water) was added to the resulting dispersion. In the last stage, the monomer phase was polymerized within the swollen seed latex particles. For this purpose, the temperature was increased to 80 °C and the polymerization was performed in a temperature-controlled shaking water bath kept at this temperature with a shaking rate of 120 rpm for 24 h [188].

The monodisperse-porous poly(HPMA-Cl-co-EDMA) microbeads were isolated by centrifugation and then washed with EtOH several times and extracted with THF. The polymer microbeads were then extensively washed with EtOH and DDI water and finally dispersed in DDI water. The amount of poly(HPMA-Cl-co-EDMA) microbeads in a certain volume was obtained by gravimetric analysis.

In order to obtain monosized-porous titania microbeads with different size and porous properties, poly(HPMA-Cl-co-EDMA) microbeads prepared with different crosslinking agent feed concentrations. For this purpose, the feed concentration of EDMA in the monomer phase (*i.e.* HPMA-Cl + EDMA) was changed between 15-100 % v/v by keeping the total volume of monomer phase constant.

Experimental conditions of poly(HPMA-Cl-co-EDMA) microbeads synthesized with different crosslinking agent feed concentrations are given in Table 3.2.

**Table 3.2.** Experimental conditions of synthesized poly(HPMA-Cl-co-EDMA) microbeads with different crosslinking agent feed concentrations.

Volume percents of crosslinking agent of poly(HPMA-Cl-co-EDMA) microbeads (% v/v)	Poly(GMA) seed latex (g)	HPMA-Cl (mL)	EGDMA (mL)	EB (mL)	BPO (g)	PVA (g/10 mL)
15	0.3	4.25	0.75	2.5	0.3	0.8
30	0.3	3.50	1.50	2.5	0.3	0.8
50	0.3	2.50	2.50	2.5	0.3	0.8
70	0.3	1.50	3.50	2.5	0.3	0.8
85	0.3	0.75	4.25	2.5	0.3	0.8

Conditions: Poly(GMA) seed latex: 0.3 g; EB: 2.5 mL; SDS: 0.25 % (w/w) both in diluent and monomer swelling stages; PVA: 0.8 g. Diluent and monomer swelling , 22 °C, 24 h, and 250 rpm stirring rate; polymerization, 80 °C, 24 h, and 120 rpm shaking rate.

### 3.2. Derivatization of Monodisperse-Porous Poly(HPMA-Cl-co-EDMA) Microbeads

#### 3.2.1. Materials

Sodium bisulfite (NaHSO<sub>3</sub>, Sigma Chemical Co., St. Louis, MO, USA) and ethylene diamine (EDA, Sigma Chemical Co., St. Louis, MO, USA) was used for the derivatization of poly(HPMA-Cl-co-EDMA) microbeads with NaHSO<sub>3</sub> and EDA, respectively. Distilled deionized (DDI) water (Direct-Q 3 UV (Type 1), Millipore, USA) with a resistivity of 18 MΩ cm was used during all derivatizations.

#### 3.2.2. Derivatization of poly(HPMA-Cl-co-EDMA) microbeads with sodium bisulfite

Poly(HPMA-Cl-co-EDMA) microbeads were derivatized with NaHSO<sub>3</sub> for the synthesis of a polymeric template with strong cation-exchanger functionality. The reaction mechanism for the derivatization of poly(HPMA-Cl-co-EDMA) microbeads with NaHSO<sub>3</sub> is given in Figure 3.2.

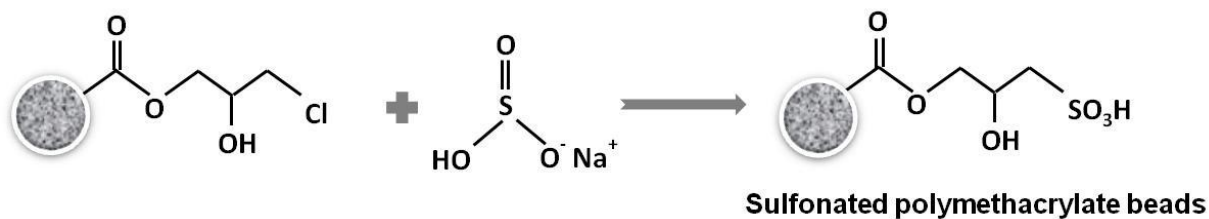


**Figure 3.2.** Reaction mechanism for the derivatization of poly(HPMA-Cl-co-EDMA) microbeads with NaHSO<sub>3</sub>.

For this purpose, poly(HPMA-Cl-co-EDMA) microbeads (1.5 g) were treated with NaHSO<sub>3</sub> solution (20 mL, %5 w/v) in a sealed glass reactor. The reactor was kept in a temperature-controlled shaking water bath at 80 °C for 24 h with a shaking rate of 120 rpm. After derivatization, -SO<sub>3</sub>Na attached-poly(HPMA-Cl-co-EDMA) microbeads were washed with DDI water by centrifugation (5000 rpm, for 3 min) and decantation for several times. -SO<sub>3</sub>Na attached-poly(HPMA-Cl-co-EDMA) microbeads were dispersed in DDI water and the amount of microbeads in a certain volume was obtained by gravimetric analysis.

### 3.2.3. Derivatization of poly(HPMA-Cl-co-EDMA) microbeads with EDA

Poly(HPMA-Cl-co-EDMA) microbeads were derivatized with EDA for the generation of primary amine groups within the particles for the impregnation of iron ions. The reaction mechanism for the derivatization of poly(HPMA-Cl-co-EDMA) microbeads with EDA is given in Figure 3.3.

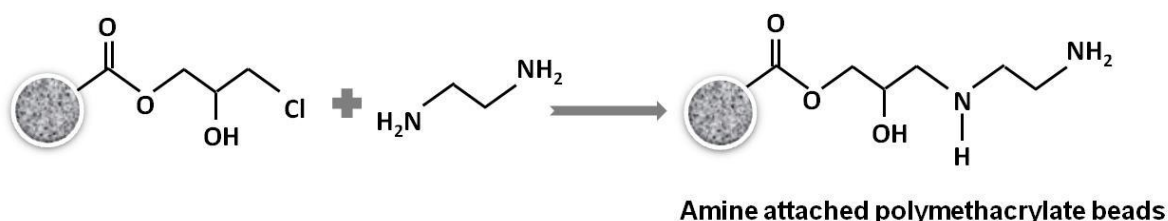


**Figure 3.3.** Reaction mechanism for the derivatization of poly(HPMA-Cl-co-EDMA) microbeads with EDA.

For this purpose, poly(HPMA-Cl-co-EDMA) microbeads (2 g) were treated with EDA solution (12.5 mL, %60 v/v) in a sealed glass reactor. The reactor was kept in a temperature-controlled shaking water bath at 80 °C for 12 h [189]. After



derivatization, amine attached-poly(HPMA-Cl-co-EDMA) microbeads were washed with DDI water by centrifugation (5000 rpm, for 3 min) and decantation for several times to remove the excess EDA. Finally, amine attached-poly(HPMA-Cl-co-EDMA) microbeads were dispersed in DDI water and the amount of microbeads in a certain volume was obtained by gravimetric analysis.

### **3.3. Synthesis of magnetic poly(HPMA-Cl-co-EDMA) microbeads**

#### **3.3.1. Materials**

For the synthesis of magnetic poly(HPMA-Cl-co-EDMA) microbeads  $\text{FeCl}_3 \cdot 6\text{H}_2\text{O}$  (Sigma Chemical Co., St. Louis, MO, USA) and  $\text{FeCl}_2 \cdot 4\text{H}_2\text{O}$  (Sigma Chemical Co., St. Louis, MO, USA) were used as iron salts. Ammonium hydroxide solution ( $\text{NH}_4\text{OH}$ , 26 % w/w), used for the reduction of iron salts, was also purchased from Sigma. Hydrochloric acid (HCl, 37 % w/w) was obtained from Sigma Chemical Co., St. Louis, MO, USA. Distilled deionized (DDI) water (Direct-Q 3 UV (Type 1), Millipore, USA) with a resistivity of 18 M $\Omega$  cm was used during the synthesis and washing steps.

#### **3.3.2. Magnetization of amine attached-poly(HPMA-Cl-co-EDMA) microbeads**

Magnetic poly(HPMA-Cl-co-EDMA) microbeads were obtained by in-situ co-precipitation method by using iron salts and primary amine attached-poly(HPMA-Cl-co-EDMA) microbeads. The scheme for the synthesis of magnetic poly(HPMA-Cl-co-EDMA) microbeads by in-situ co-precipitation method is given in Figure 3.4.

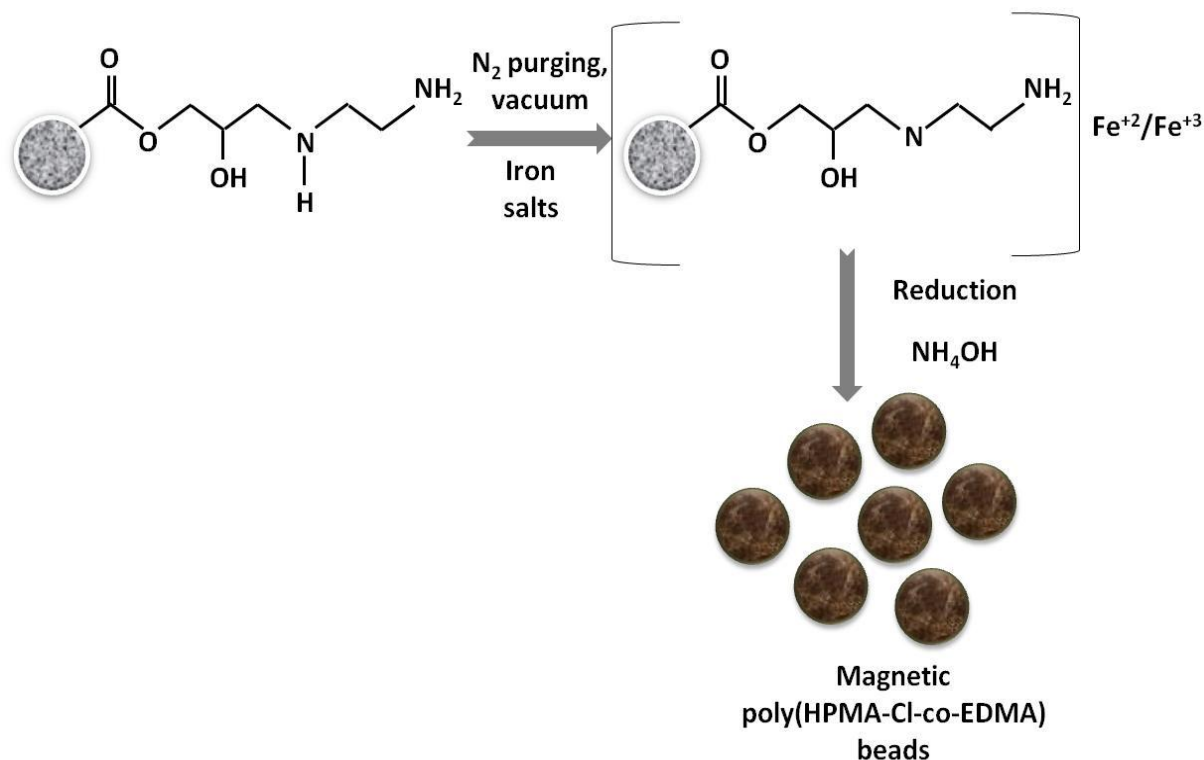


**Figure 3.4.** Synthesis of magnetic poly(HPMA-Cl-co-EDMA) microbeads by in-situ co-precipitation method.

Typically, 2 g of primary amine attached-poly(HPMA-Cl-co-EDMA) microbeads were added into a flask containing 100 mL water. The mixture was cooled in a water bath under nitrogen gas bubbling.  $\text{FeCl}_3 \cdot 6\text{H}_2\text{O}$  (3 mmol, 0.8 g) and  $\text{FeCl}_2 \cdot 4\text{H}_2\text{O}$  (2.7 mmol, 0.536 g) were dissolved in 20 mL  $\text{H}_2\text{O}$ . Then the iron ions solution was added to the flask and a light brown color mixture was obtained. The ice bath was removed and the flask was continuously evacuated with the mixture kept stirring until no further foaming in the mixture was observed. The evacuation was stopped and flask was immersed in a preheated water bath at 85 °C. 25 mL of  $\text{NH}_4\text{OH}$  was then added. The reaction mixture turned gradually to black. The mixture was kept stirring at 85 °C for 1 h, then cooled to room temperature. The resultant magnetic microbeads were centrifuged and thoroughly washed with water and 0.1M HCl [189]. Finally, magnetic microbeads were dispersed in DDI water and the amount of magnetic microbeads in a certain volume was obtained by gravimetric analysis.

### 3.4. Synthesis of Monodisperse-Porous Bare and Magnetic Titania Microbeads

#### 3.4.1. Materials

For the synthesis of monodisperse-porous bare and magnetic titania microbeads, titanium chloride ( $\text{TiCl}_4$ , Sigma Chemical Co., St. Louis, MO, USA) as precursor, ammonium hydroxide solution ( $\text{NH}_4\text{OH}$ , 26 % w/w, Sigma Chemical Co., St. Louis, MO, USA) and hexadecyltrimethylammonium bromide (CTAB, Sigma Chemical Co., St. Louis, MO, USA) were used. Distilled deionized (DDI) water (Direct-Q 3 UV (Type 1), Millipore, USA) with a resistivity of 18  $\text{M}\Omega$  cm was used during all synthesis.

#### 3.4.2. Synthesis of Monodisperse-Porous Bare and Magnetic Titania Microbeads by Sol-Gel Templating Method

The syntheses of bare and magnetic titania microbeads were performed by sol-gel templating method using  $-\text{SO}_3\text{Na}$  attached and magnetic poly(HPMA-Cl-co-EDMA) microbeads as template, respectively. The schematical representation of the sol-gel templating method for the synthesis of monodisperse-porous bare and magnetic titania microbeads is given in Figure 3.5.

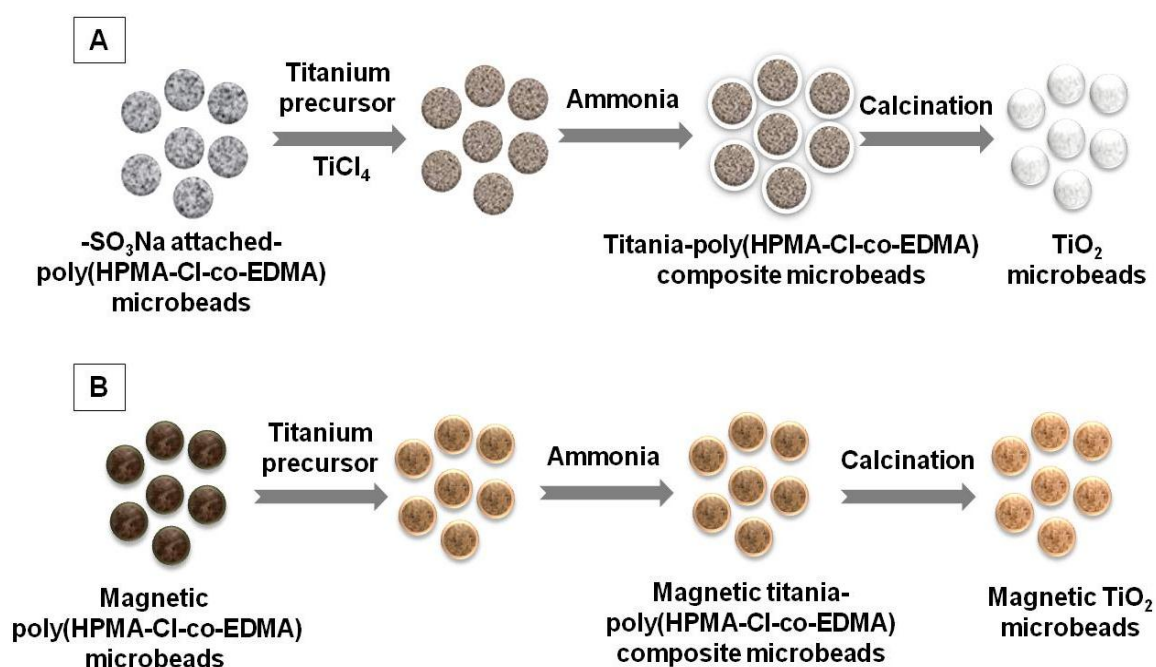


**Figure 3.5.** Synthesis of monodisperse-porous (A): bare and (B): magnetic titania microbeads by sol-gel templating method.

The proposed procedure consists of two steps. In the first step, the hydrous titanium dioxide ( $\text{TiO}_2 \cdot n\text{H}_2\text{O}$ ) nanoparticles were formed via the hydrolysis reaction by the dissolution of precursor ( $\text{TiCl}_4$ ) in an aqueous medium (60 mL, 0.1 M). Then,  $-\text{SO}_3\text{Na}$  attached or magnetic poly(HPMA-Cl-co-EDMA) microbeads (0.4 g) were dispersed within the precursor solution and stirred at 250 rpm at room temperature for 24 h.  $-\text{SO}_3\text{Na}$  attached or magnetic poly(HPMA-Cl-co-EDMA) microbeads, in which hydrous titanium dioxide ( $\text{TiO}_2 \cdot n\text{H}_2\text{O}$ ) nanoparticles were adsorbed, were extensively washed with DDI water. In the second step, microbeads were treated with ammonia solution (60 mL, 1 M) containing CTAB (0.3 g) and the solution was stirred at 250 rpm at room temperature for 6 h. Upon the treatment with ammonia solution, the hydrous titanium oxide ( $\text{TiO}_2 \cdot n\text{H}_2\text{O}$ ) nanoparticles were precipitated into the pores of  $-\text{SO}_3\text{Na}$  attached or magnetic poly(HPMA-Cl-co-EDMA) microbeads to form bare or magnetic titania-polymer composite microbeads. To remove the excess chloride ions, bare and magnetic titania-polymer composite microbeads were washed with DDI water by centrifugation and decantation for several times. The hydrolysis and ammonia precipitation steps were repeated twice in order to get integrated bare or magnetic titania microbeads. Before the calcination, bare or magnetic titania-polymer composite microbeads were dried at 70 °C under vacuum for 12 h. The polymeric templates were removed from the bare or magnetic titania-polymer composite microbeads by calcination [190]. The calcination of bare titania-polymer composite microbeads was made at different temperatures (450 °C, 500 °C, 550 °C, 600 °C) for 4 h with a heating ramp of 2 °C/min, under air atmosphere. However, the calcination of magnetic titania-polymer composite microbeads was performed only at 450 °C.

### **3.5. Synthesis of Gold Nanoparticle Decorated Monodisperse-Porous Bare and Magnetic Titania Microbeads**

#### **3.5.1. Materials**

Aminopropyltriethoxysilane (APTES, Sigma Chemical Co., St. Louis, MO, USA), triethylamine (TEA, Sigma Chemical Co., St. Louis, MO, USA) was used for the derivatization of monodisperse-porous bare and magnetic titania microbeads with amine groups. Isopropanol (IsOH, HPLC grade, Aldrich) was used as the solvent.

For the synthesis of gold nanoparticles (AuNPs), chloroauric acid-trihydrate ( $\text{HAuCl}_4 \cdot 3\text{H}_2\text{O}$ , Sigma Chemical Co., St. Louis, MO, USA), trisodium citrate (TSS, Sigma Chemical Co., St. Louis, MO, USA), sodium borohydride ( $\text{NaBH}_4$ , Sigma Chemical Co., St. Louis, MO, USA) were used. Sodium hydroxide ( $\text{NaOH}$ , Sigma Chemical Co., St. Louis, MO, USA) and hydrochloric acid ( $\text{HCl}$ , %37 w/w, Sigma Chemical Co., St. Louis, MO, USA) were used for the preparation of  $\text{NaBH}_4$  and  $\text{HAuCl}_4$  solutions, respectively. Distilled deionized (DDI) water (Direct-Q 3 UV (Type 1), Millipore, USA) with a resistivity of 18  $\text{M}\Omega \text{ cm}$  was used.

### 3.5.2. Derivatization of Monodisperse-Porous Bare and Magnetic Titania Microbeads with Aminopropyltriethoxysilane

Monodisperse-porous bare or magnetic titania microbeads were derivatized with APTES for the preparation of amine attached bare or magnetic titania microbeads. The reaction mechanism for the derivatization of monodisperse-porous bare or magnetic titania microbeads with APTES was given in Figure 3.6.

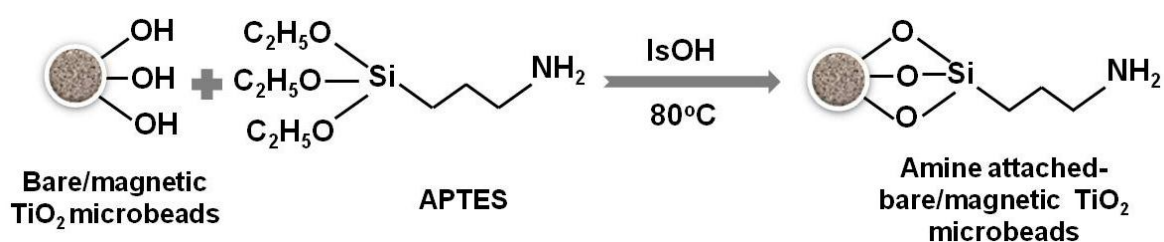


**Figure 3.6.** Reaction mechanism for the derivatization of monodisperse-porous bare and magnetic titania microbeads with APTES.

The monodisperse-porous bare or magnetic titania microbeads (0.4 g) were degassed at 250 °C for 6 h to remove physically adsorbed water vapor before reaction with APTES. The microbeads (0.4 g) were then dispersed within Iso-PrOH (20 mL), to which APTES (3 mL) and TEA (0.3 mL) were added by ultrasonication, in a sealed glass reactor. Then, the reactor was kept in a temperature-controlled shaking water bath at 80 °C for 24 h. After derivatization, amine attached bare or magnetic titania microbeads were washed with Iso-PrOH by centrifugation (5000 rpm, for 3 min) and decantation for several times to remove the excess APTES. Then amine attached bare or magnetic titania microbeads were washed with DDI water and finally dispersed in DDI water. The

amount of amine attached-bare or magnetic titania microbeads in a certain volume was obtained by gravimetric analysis.

### 3.5.3. Synthesis of AuNPs

AuNPs are synthesized with two different methods using different reducing agents. In these processes,  $\text{Au}^{3+}$  is reduced to form AuNPs. In Turkevich method, citrate ions were used both for the reduction of  $\text{Au}^{3+}$  and the stabilization of resulting AuNPs in water. In the Martin method, AuNPs in relatively smaller sizes are generated in water due to the reduction of  $\text{HAuCl}_4$  by  $\text{NaBH}_4$ .

### 3.5.4. Synthesis of AuNPs via Turkevich Method

A solution of  $\text{HAuCl}_4$  ( $1.0 \times 10^{-3} \text{ M}$ , 24 mL) was magnetically stirred and heated until boiling. Then 2.0 mL of sodium citrate solution (1.75 % (w/v)) was added. The reduction of gold ions by citrate was completed within 5 min which was evident by the color change to deep red. The boiling was continued for further 15 min [173, 176]. The solution was removed from the heating element and stirred magnetically at 250 rpm until it was cooled down to room temperature.

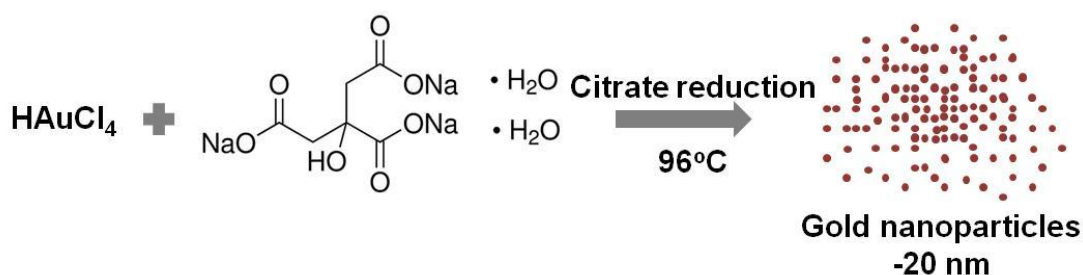


**Figure 3.7.** Synthesis of AuNPs via Turkevich method.

#### 3.5.4.1. Synthesis of AuNPs via Martin Method

An aqueous stock solution of 50 mM gold chloride anions ( $\text{AuCl}_4^-$ ) in a glass vial was prepared by dissolving  $\text{HAuCl}_4 \cdot 3\text{H}_2\text{O}$  with the same molar amount of HCl. An aqueous stock solution of 50 mM borohydride anions ( $\text{BH}_4^-$ ) in a glass vial was prepared by dissolving  $\text{NaBH}_4$  with the same molar amount of NaOH. For the nanoparticles of 3.2 nm in diameter, 200  $\mu\text{L}$  of the  $\text{AuCl}_4^-/\text{H}^+$  solution was added to 40 mL of water in a glass vial and later 600  $\mu\text{L}$  of the  $\text{BH}_4^-/\text{OH}^-$  solution was injected all at once, while stirring for uniform mixing at 250 rpm. The concentration of gold ions in the final solution was 0.50 mM. The solution changed color from

light yellow to orange immediately, and then to red while the vial was stirred for 1 min to release hydrogen [175].

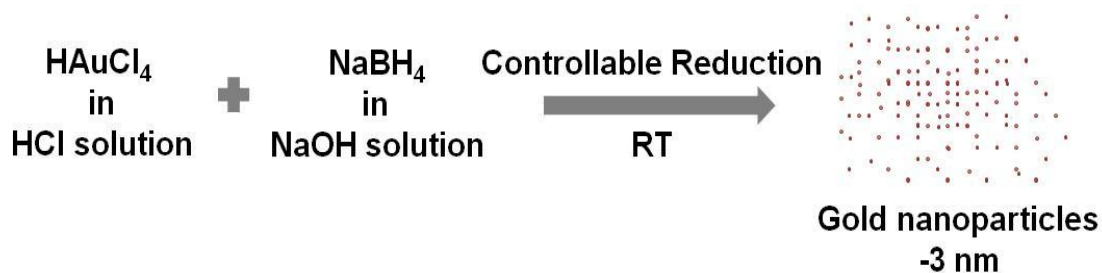


**Figure 3.8.** Synthesis of AuNPs via Martin Method.

### 3.5.5. Decoration of Monodisperse-Porous Bare or Magnetic Titania Microbeads with AuNPs

For decoration of monodisperse-porous bare or magnetic titania microbeads with AuNPs, amine attached bare and magnetic titania microbeads were put into AuNP solutions obtained with Turkevich and Martin methods and stirred at 250 rpm for 6 h at room temperature.

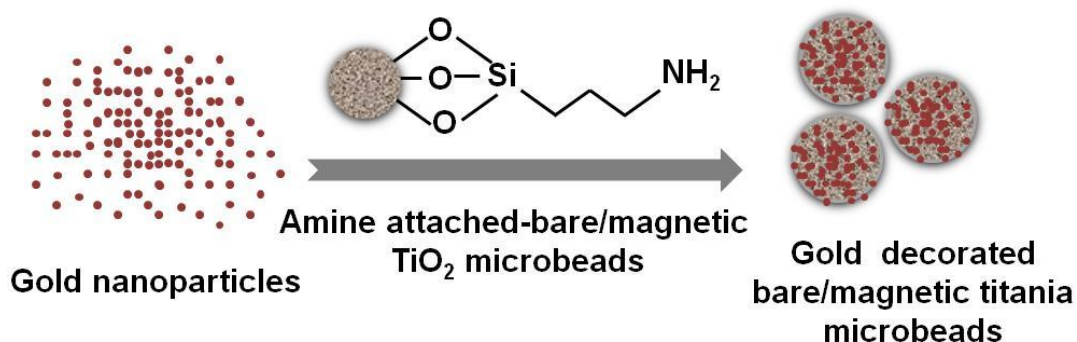


**Figure 3.9.** Decoration of monodisperse-porous bare or magnetic titania microbeads with AuNPs.

To change the Au loading (% w/w) on bare or magnetic titania microbeads, different amounts of amine attached bare or magnetic titania microbeads were put into the same volume of AuNP solutions synthesized with Turkevich and Martin methods. The details of experimental conditions showing the Au loading (% w/w) on bare or magnetic titania microbeads are given in Table 3.3.

**Table 3.3.** Experimental conditions for Au loading (% w/w) on bare and magnetic titania microbeads.

<b>Turkevich Method</b>		<b>Martin Method</b>	
<b>AuNP loading on bare/magnetic TiO<sub>2</sub> microbeads (% w/w)</b>	<b>Amount of bare/magnetic TiO<sub>2</sub> microbeads (g)</b>	<b>AuNP loading on bare/magnetic TiO<sub>2</sub> microbeads (% w/w)</b>	<b>Amount of bare/magnetic TiO<sub>2</sub> microbeads (g)</b>
2.5	0.20	2.5	0.16
5.0	0.10	5.0	0.08
10.0	0.05	10.0	0.04

Conditions: Turkevich AuNP solution volume: 24 mL; Martin AuNP solution volume: 80 mL; Stirring: 250 rpm, 6 h.

### **3.6. Characterization of Monodisperse-Porous Bare and Magnetic Poly(HPMA-Cl-co-EDMA) and Titania Microbeads**

The size distribution properties and the surface morphology of bare and magnetic poly(HPMA-Cl-co-EDMA) microbeads and bare and magnetic titania microbeads were determined by scanning electron microscopy (SEM; JEM 1200EX, JEOL, Akishima, Tokyo, Japan). For sample preparation, certain amount of dried microbeads were dispersed in an aqueous SDS solution (0.1 w/v) by sonication for several minutes. Then 0.1 mL of dispersion was dropped onto a carbon tape and dried at room temperature. The dried samples were coated with gold by physical vapor deposition.

The specific surface areas (SSAs) of bare and magnetic poly(HPMA-Cl-co-EDMA) and titania microbeads were determined by surface area and pore size analyzer (Quantachrome, Nova 2200E, UK) using the Brunauer–Emmett–Teller (BET) equation. All samples were degassed under vacuum at 250 °C for 6 h in the port of the adsorption analyzer. After degassing the analysis were made at 77 K. The BET specific surface area was calculated from nitrogen adsorption data in the relative pressure range from 0.05 to 0.2.

The functional group content of -SO<sub>3</sub>Na attached-poly(HPMA-Cl-co-EDMA) microbeads was determined by potentiometric titration. The functional group



content of amine attached-poly(HPMA-Cl-co-EDMA) and amine-attached-titania microbeads were determined by elemental analysis (Thermo-Scientific, Flash 2000, A.B.D.).

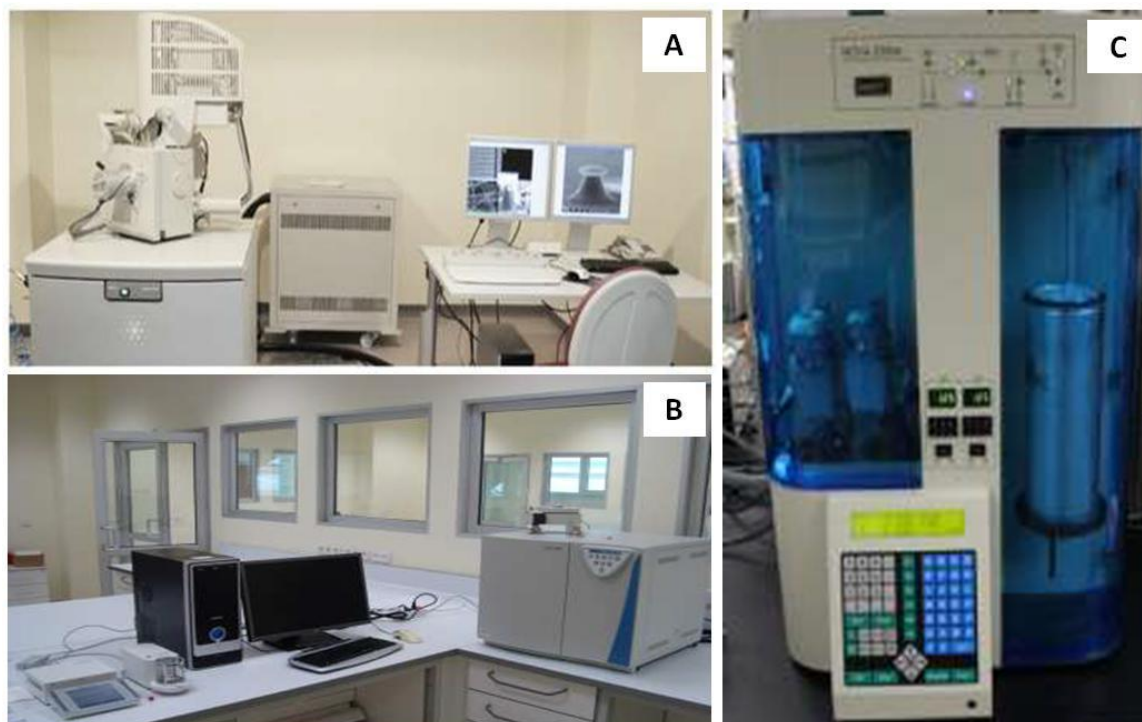


**Figure 3.10.** The equipments used for the characterization of poly(HPMA-Cl-co-EDMA) microbeads (A) Quanta 200 FEG SEM, (B) Perkin Elmer 2400, (C) Quantachrome Nova 2200 BET.

Thermal decomposition behaviour of poly(HPMA-Cl-co-EDMA) microbeads was characterized by differential scanning calorimeter (DSC, Diamond DSC, Perkin Elmer, USA) and Thermal Gravimetric Analysis (TGA, TG/DTA 6300 SII EXSTAR 6000, Perkin Elmer, USA). The runs were carried out under nitrogen flow using a heating rate of 5 °C/min. The chemical structure of poly(HPMA-Cl-co-EDMA) and titania microbeads were investigated by X-ray diffraction spectroscopy (XRD, Rigaku, D/Max-2200, USA). Diffraction patterns were collected in the range 0° – 90° (2 $\theta$ ) with a step size of 0.02°.

The magnetic properties of magnetic poly(HPMA-Cl-co-EDMA) microbeads and magnetic titania microbeads were measured at room temperature by vibrating sample magnetometer (VSM, Quantum Design, Model P525, USA).

AuNPs were analyzed using a UV-visible spectrophotometer (UV-Vis, Shimadzu, UV-1601, Japan). Each batch of AuNPs were analyzed by spectral scan in the range of 400-800 nm to identify the characteristic peak and for uniform size distribution.



**Figure 3.11.** Devices used for the characterization of poly(HPMA-Cl-co-EDMA) microbeads (A) DSC, Diamond DSC, Perkin Elmer, (B) TGA, TG/DTA 6300 SII EXSTAR 6000, Perkin Elmer, (C) XRD, Rigaku, D/Max-2200.

### 3.7. Catalysis Runs

#### 3.7.1. Materials

In the photocatalytic activity runs, a textile dye Remazol Black 5 (RB5, Aldrich Chem. Corp., USA) and an organic contaminant, phenol (Aldrich Chem. Corp., USA) were used as target molecule to be degraded.

In the plasmonic catalysis runs, 4-Nitrophenol (4-NP, Aldrich Chem. Corp., USA) and sodiumborohydride (NaBH<sub>4</sub>, Aldrich Chem. Corp., USA) were used. The pH of the reaction medium was adjusted by 0.1 M HCl and 0.1 M NaOH. Distilled deionized (DDI) water (Direct-Q 3 UV (Type 1), Millipore, USA) with a resistivity of 18 MΩ cm was used in all runs.

### 3.7.2. Photocatalysis of Remazol Black 5 Dye

#### 3.7.2.1. Photocatalysis of Remazol Black 5 Dye with Bare Titania Microbeads

Photocatalytic activity of monodisperse-porous bare titania microbeads was investigated by photodegradation of RB5 dye by changing calcination temperature, pH of reaction medium, catalyst concentration and RB5 dye concentration. Experimental conditions used in the photocatalytic degradation of RB5 dye by monodisperse-porous bare titania microbeads are given in Table 3.4.

**Table 3.4.** Experimental conditions and parameters changed in the photocatalysis of RB5 dye with monodisperse-porous bare titania microbeads.

Experimental conditions	Parameter	Range
80 mg catalyst, pH 3.5, 25ppm RB5 dye	Calcination temperature (°C)	450, 500, 550, 600
80 mg catalyst, 25 ppm RB5 dye, Calcination at 450°C	pH	3.5, 5.0, 7.0, 9.0
25 ppm RB5 dye, pH 3.5 Calcination at 450°C	Catalyst amount (mg)	20, 40, 80
80 mg catalyst, pH 3.5 Calcination at 450°C	Dye concentration (ppm)	12.5, 25.0, 50.0

Reaction volume: 100 mL

Typically, bare titania microbeads (calcined at 450°C, 80 mg) were added into an aqueous solution of RB5 dye (25 ppm, 100 mL) and the resulting dispersion was ultrasonicated for 5 min at 200 W. pH was adjusted to a desired value in the range of 3.5-9.0 by adding HCl or NaOH solution (0.1 M). The dispersion was irradiated

from the top with a UV light-source (Osram, Ultra-vitalux lamp, 300 W) under magnetic stirring with 300 rpm at 25°C within a metal box equipped with a temperature-control system. For the determination of dye concentration in the aqueous medium at a certain time, the sample withdrawn from the reactor (2 mL) was centrifuged at 5000 rpm for 5 min in the dark. The concentration of RB5 dye was monitored by measuring the absorption of supernatant at 598 nm using UV-Vis spectrophotometer (UV-1601, Shimadzu, Japan).

### 3.7.2.2. Photocatalysis of Remazol Black 5 Dye with AuNP Decorated-Bare Titania Microbeads

#### 3.7.2.2.1. AuNP Decorated Bare Titania Microbeads by Turkevich Method

The photocatalytic activity of AuNP decorated-bare titania microbeads was investigated by photodegradation of RB5 dye by changing pH of solution and Au loading on bare titania microbeads. Experimental conditions and parameters in the photocatalysis of RB5 dye with AuNP decorated-bare titania microbeads by Turkevich Method are given in Table 3.5.

**Table 3.5.** Experimental conditions and parameters changed in the photocatalysis of RB5 dye with Turkevich AuNP decorated monodisperse-porous bare titania microbeads.

Experimental conditions	Variable	Range
80 mg catalyst, 25ppm RB5 dye,	pH	3.5, 5.0, 7.0, 9.0
80 mg catalyst, 25 ppm RB5 dye, pH 7	Au loading (% w/w)	2.5, 5.0, 10.0

Calcination temperature: 450 °C, Reaction volume: 100 mL

The same experimental procedure explained in Section 3.7.2.1 was applied for the photodegradation of RB5 dye with AuNP decorated-bare titania microbeads with Turkevich method.

### 3.7.2.2.2. AuNP Decorated Bare Titania Microbeads by Martin Method

The photocatalytic activity of AuNP decorated bare titania microbeads by Martin method was investigated by the photodegradation of RB5 dye by changing Au loading on titania microbeads. Experimental conditions in the photocatalysis of RB5 dye with Martin AuNP decorated bare titania microbeads are given in Table 3.6.

**Table 3.6.** Experimental conditions in the photocatalysis of RB5 dye with Martin AuNP decorated bare titania microbeads.

Experimental Conditions	Parameter	Range
80 mg catalyst, 25ppm RB5 dye, pH 7	Au loading (%w/w)	2.5, 5.0, 10.0

Calcination temperature: 450 °C, Reaction volume: 100 mL

The same experimental procedure explained in Section 3.7.2.1. was applied for the photodegradation of RB5 with Martin AuNP decorated bare titania microbeads.

### 3.7.2.3. Photocatalysis of Remazol Black 5 Dye with Magnetic Titania Microbeads

The photocatalytic activity of monodisperse-porous magnetic titania microbeads was investigated by photodegradation of RB5 dye by changing pH of solution, catalyst amount and RB5 dye concentration. Experimental conditions in the photocatalysis of RB5 dye with magnetic titania microbeads are given in Table 3.7.

**Table 3.7.** Experimental conditions and parameters changed in the photocatalysis of RB5 dye with monodisperse-porous magnetic titania microbeads.

Experimental Conditions	Parameter	Range
80 mg catalyst, 25 ppm RB5 dye	pH	3.5, 5.0, 7.0, 9.0
25ppm RB5 dye, pH 3.5	Catalyst amount (mg)	20, 40, 80
80 mg catalyst, pH 3.5	Dye concentration (ppm)	12.5, 25.0, 50.0

Calcination temperature: 450 °C, Reaction volume: 100 mL

Typically, magnetic titania microbeads (calcined at 450°C, 80 mg) were added into an aqueous solution of RB5 dye (25 ppm, 100 mL) and the resulting dispersion was ultrasonicated for 5 min at 200 W. pH was adjusted to a desired value in the range of 3.5-9.0 by adding HCl or NaOH solution (0.1 M). The dispersion was irradiated from the top with a UV light-source (Osram, Ultra-vitalux lamp, 300 W) under mechanical stirring with 300 rpm at 25°C within a metal box equipped with a temperature-control system. For the determination of dye concentration in the aqueous medium at a certain time, 2 mL of sample was withdrawn from the reactor and magnetic titania microbeads were separated by an external magnet. The concentration of RB5 dye was monitored by measuring the absorption of supernatant at 598 nm using UV-Vis Spectrophotometer (UV-1601, Shimadzu, Japan).

### **3.7.2.4. Photocatalysis of Remazol Black 5 Dye with AuNP Decorated Magnetic Titania Microbeads**

#### **3.7.2.4.1. AuNP Decorated Magnetic Titania Microbeads by Turkevich Method**

The photocatalytic activity of Turkevich AuNP decorated magnetic titania microbeads was investigated by photodegradation of RB5 dye by changing the pH of reaction medium. Experimental conditions in the photocatalysis of RB5 dye with

Turkevich AuNP decorated monodisperse-porous magnetic titania microbeads are given in Table 3.8.

**Table 3.8.** Experimental conditions in the photocatalysis of RB5 dye with Turkevich AuNP decorated magnetic titania microbeads.

Experimental Conditions	Parameter	Range
80 mg catalyst, 25ppm RB5 dye, Au loading (5 % w/w)	pH	3.5, 5.0, 7.0, 9.0
Calcination temperature: 450°C, Reaction volume: 100 mL.		

The same experimental procedure explained in Section 3.7.2.3. was applied for the photodegradation of RB5 dye with Turkevich AuNP decorated-magnetic titania microbeads.

#### 3.7.2.4.2. AuNP Decorated Magnetic Titania Microbeads by Martin Method

The photocatalytic activity of Martin AuNP decorated monodisperse-porous magnetic titania microbeads was investigated by photodegradation of RB5 dye by changing the Au loading on monodisperse-porous magnetic titania microbeads. Experimental conditions in the photocatalysis of RB5 dye with Martin AuNP decorated magnetic titania microbeads are given in Table 3.9.

**Table 3.9.** Experimental conditions in the photocatalysis of RB5 dye with Martin AuNP decorated magnetic titania microbeads.

Experimental Conditions	Parameter	Range
80 mg catalyst, 25ppm RB5 dye, pH 7	Au loading (%w/w)	2.5, 5.0, 10.0
Calcination temperature: 450°C		

The same experimental procedure explained in Section 3.7.2.3. was applied for the photodegradation of RB5 dye with Martin AuNP decorated magnetic titania microbeads.

### 3.7.2.5. Catalyst recovery and reuse

Only the reusability of the Martin AuNP decorated-titania microbeads was investigated since it was chosen as the best catalyst for the photocatalytic degradation of RB5 dye. At the end of the photocatalytic degradation of RB5 dye (80 mg catalyst, 25 ppm RB5, pH 7, 450°C calcination temperature), the suspensions were centrifuged (5000 rpm, 5 min) and rinsed with water for several times to recover the catalyst particles. The recovered catalyst was then reused in photocatalytic degradation of RB5 dye under the same experimental conditions. The degradation-recovery cycle was repeated for 5 times to examine the reusability of the catalyst.

### 3.7.3. Photocatalysis of Phenol

#### 3.7.3.1. Photocatalysis of Phenol with Bare Titania Microbeads

The photocatalytic activity of bare titania microbeads was investigated by phenol degradation by changing pH of solution, catalyst amount and phenol concentration. Experimental conditions in the photocatalysis of phenol with bare titania microbeads are given in Table 3.10.

**Table 3.10.** Experimental conditions in the photocatalysis of phenol with bare titania microbeads.

Experimental Conditions	Parameter	Range
160 mg catalyst, 50 ppm Phenol	pH	4, 5, 7, 9
50 ppm Phenol, pH 7	Catalyst amount (mg)	80, 160, 240
160 mg catalyst, pH 7	Phenol concentration (ppm)	25, 50, 100

Calcination temperature: 450°C, Reaction volume:100 mL.

In a typical experiment, bare titania microbeads (160 mg) were added into an aqueous solution of phenol (50 ppm,100 mL) in a batch reactor enveloped by an aluminum foil and the resulting dispersion was ultrasonicated for 5 min at 200 W.



The medium pH was adjusted to a desired value in the range of 4.0-9.0 by adding HCl or NaOH solution (0.1 M). Then the dispersion was left to equilibrium in the dark under magnetic stirring with 300 rpm at 25°C for 20 min within a metal box equipped with a temperature-control system. At the end of this period, to obtain the initial concentration of phenol 2 mL sample was taken from the reactor and centrifuged at 5000 rpm for 5 min in the dark for solid separation. Oxygen at constant flow was supplied to the reactor as an oxidative agent before the irradiation of the dispersion with a UV light-source (Osram, Ultra-vitalux lamp, 300 W) from the top. For the determination of phenol concentration in the aqueous medium at a certain time, the sample withdrawn from the reactor (2 mL) was centrifuged at 5000 rpm for 5 min in the dark. Phenol concentration was followed by High Pressure Liquid Chromatography (HPLC, Shimadzu, LC-10AD, Japan) equipped with UV-vis detector using a homemade octadecylamine attached-poly(HPMA-Cl-co-EDMA) column (2 mm × 250 mm). Mobile phase was water/acetonitrile (60:40) at a flow rate of 0.2 mL/min.

### **3.7.3.2. Photocatalysis of Phenol with AuNP Decorated Bare Titania Microbeads**

#### **3.7.3.2.1. AuNP Decorated Bare Titania Microbeads by Turkevich Method**

The photocatalytic activity of Turkevich AuNP decorated bare titania microbeads was investigated by the photodegradation of phenol solution (50 ppm, 100 mL) at pH 7 using 160 mg of Turkevich AuNP decorated bare titania microbeads with an Au loading of 5 % w/w. The same experimental procedure explained in Section 3.7.3.1. was applied for the photodegradation of phenol with Turkevich AuNP decorated bare titania microbeads.

#### **3.7.3.2.2. AuNP Decorated Bare Titania Microbeads by Martin Method**

The photocatalytic activity of Martin AuNP decorated bare titania microbeads was investigated by the photodegradation of phenol by changing Au loading on monodisperse-porous bare titania microbeads. Experimental conditions in the photocatalysis of phenol with Martin AuNP decorated bare titania microbeads are given in Table 3.11.

**Table 3.11.** Experimental conditions in the photocatalysis of phenol with Martin AuNP decorated bare titania microbeads.

Experimental Conditions	Parameters	Range
160 mg catalyst, pH 7, 50 ppm phenol	Au loading (%w/w)	2.5, 5.0, 10.0

Calcination temperature: 450°C, Reaction volume: 100 mL.

The same experimental procedure explained in Section 3.7.3.1. was applied for the photodegradation of phenol with Martin AuNP decorated monodisperse-porous bare titania microbeads.

### 3.7.3.3. Photocatalysis of Phenol with Magnetic Titania Microbeads

The photocatalytic activity of magnetic titania microbeads was investigated by photodegradation of phenol solution (50 ppm, 100 mL) at pH 7 using 160 mg of monodisperse-porous magnetic titania microbeads.

In a typical experiment, monodisperse-porous magnetic titania microbeads (160 mg) were added into an aqueous solution of phenol (50 ppm, 100 mL) in a batch reactor enveloped by an aluminum foil. The dispersion was ultrasonicated for 5 min at 200 W. pH was adjusted to a desired value in the range of 4.0-9.0 by adding HCl or NaOH solution (0.1 M). Then the dispersion was left to equilibrium in the dark under mechanical stirring with 300 rpm at 25°C for 20 min within a metal box equipped with a temperature-control system. To obtain the initial concentration of phenol, 2 mL sample was taken from the reactor and magnetic titania microbeads were separated with an external magnet.

Oxygen as oxidative agent was supplied to the reactor at constant flow before the irradiation of dispersion with a UV light-source (Osram, Ultra-vitalux lamp, 300 W) from the top. For the determination of phenol concentration in the aqueous medium at a certain time, the sample was taken from the reactor (2 mL) and magnetic titania microbeads were separated with a magnet. Phenol concentration was followed by HPLC (Schimadzu, LC-10AD, Japan) equipped with UV-vis detector using a home-made octadecylamine attached-poly(HPMA-Cl-co-EGDMA) column (2 mm × 250 mm). The mobile phase was water/methanol (60:40) at a flow rate of 0.2 mL/min.

### **3.7.3.4. Photocatalysis of Phenol with AuNP Decorated Magnetic Titania Microbeads**

#### **3.7.3.4.1. AuNP Decorated Magnetic Titania Microbeads by Turkevich Method**

The photocatalytic activity of Turkevich AuNP decorated magnetic titania microbeads was investigated by photodegradation of phenol solution (50 ppm, 100mL) at pH 7 using 160 mg of Turkevich AuNP decorated magnetic titania microbeads with an Au loading of 5 % w/w. The experimental procedure explained in Section 3.7.3.3. was applied for the photodegradation of phenol with Turkevich AuNP decorated magnetic titania microbeads.

#### **3.7.3.4.2. AuNP Decorated Magnetic Titania Microbeads by Martin Method**

The photocatalytic activity of Martin AuNP decorated magnetic titania microbeads was investigated by photodegradation of phenol solution (50 ppm, 100 mL) at pH 7 using 160 mg of Martin AuNP decorated magnetic titania microbeads with an Au loading of 5 % w/w. The experimental procedure explained in Section 3.7.3.3. was applied for the photocatalytic degradation of phenol with Martin AuNP decorated magnetic titania microbeads.

#### **3.7.3.5. Catalyst recovery and reuse**

Only the reusability of the monodisperse-porous bare titania microbeads was investigated as it was chosen as the optimal catalyst for the photocatalytic degradation of phenol. At the end of the photocatalytic degradation of phenol (160 mg catalyst, 50 ppm phenol, pH 7), the suspensions were centrifuged (5000 rpm, 5 min) and rinsed with water for several times to recover the catalyst particles. The recovered catalyst was then reused in photocatalytic degradation of phenol in the same experimental conditions. This degradation-recovery cycle was repeated for 5 times to achieve the reusability of the catalyst.

### **3.7.4. Plasmonic Catalysis of 4-Nitrophenol**

#### **3.7.4.1. Plasmonic Catalysis of 4-Nitrophenol with AuNP Decorated Monodisperse-Porous Bare and Magnetic Titania Microbeads**

##### **3.7.4.1.1. Plasmonic Catalysis of 4-Nitrophenol with Turkevich AuNP Decorated Monodisperse-Porous Bare and Magnetic Titania Microbeads**

The plasmonic catalytic activity of Turkevich AuNP decorated monodisperse-porous bare and magnetic titania microbeads was investigated by reduction of 4-NP solution (7.5 ppm, 24mL) at 20°C by using 1 mg of Turkevich AuNP decorated monodisperse-porous bare and magnetic titania microbeads with an Au loading of 5 % w/w.

In a typical experiment, NaBH<sub>4</sub> (0.2 g) was added into an aqueous solution of 4-NP (7.5 ppm, 24 mL) in a batch reactor. The solution was left to be stirred with 300 rpm at 20°C till evolution of H<sub>2</sub> gas was finished. After a certain time, 2 mL of sample was taken from the reactor to obtain the initial concentration of 4-NP. Then Turkevich AuNP decorated monodisperse-porous bare and magnetic titania microbeads (1 mg) were added to the solution of 4-NP. For the determination of 4-NP concentration in the aqueous medium at a certain time, the sample was taken from the reactor (2 mL) and Turkevich AuNP decorated bare titania microbeads were centrifuged at 5000 rpm for 5 min in the dark for solid separation while Turkevich AuNP decorated magnetic titania microbeads were separated with a magnet. 4-NP concentration was monitored by measuring the absorption of supernatant at 400 nm using UV-Vis Spectrophotometer (UV-1601, Shimadzu, Japan).

#### **3.7.4.2. Plasmonic Catalysis of 4-Nitrophenol with Turkevich AuNP Decorated Magnetic Titania Microbeads**

The plasmonic catalytic activity of Turkevich AuNP decorated monodisperse-porous magnetic titania microbeads was investigated by reduction of 4-NP by changing catalyst amount, temperature and 4-NP concentration. Experimental conditions in the reduction of 4-NP with Turkevich AuNP decorated magnetic titania microbeads are given in Table 3.12.

**Table 3.12.** Experimental conditions in the reduction of 4-NP with Turkevich AuNP decorated-magnetic titania microbeads.

Experimental Conditions	Parameter	Range
7.5 ppm 4-NP, 20°C	Catalyst Amount (mg)	1.0, 2.5, 5.0, 10.0
1 mg catalyst, 7.5 ppm 4-NP	Temperature (°C)	10, 20, 30, 40
1 mg catalyst, 20°C	4-NP concentration (ppm)	3.75, 7.50, 15.00

Calcination temperature: 450°C, Reaction volume: 24 mL

In a typical experiment, NaBH<sub>4</sub> (0.2 g) was added into an aqueous solution of 4-NP (7.5 ppm, 24 mL) in a batch reactor. The solution was stirred mechanically with 300 rpm at 20°C till evolution of H<sub>2</sub> was finished. After a certain time, 2 mL of sample was taken from the reactor to obtain the initial concentration of 4-NP. Then Turkevich AuNP decorated magnetic titania microbeads (1 mg) were added to the solution of 4-NP. For the determination of 4-NP concentration in the aqueous medium at a certain time, the sample was taken from the reactor (2 mL) and Turkevich AuNP decorated magnetic titania microbeads were separated with an external magnet. 4-NP concentration was monitored by measuring the absorption of supernatant at 400 nm using UV-Vis Spectrophotometer (UV-1601, Shimadzu, Japan).

#### **3.7.4.2.1. Plasmonic Catalysis of 4-Nitrophenol with Martin AuNP Decorated Magnetic Titania Microbeads**

The plasmonic catalytic activity of Martin AuNP decorated magnetic titania microbeads was investigated by reduction of 4-NP by changing Au loading on magnetic titania microbeads. Experimental conditions in the plasmonic catalysis of 4-NP with Martin AuNP decorated magnetic titania microbeads are given in Table 3.13.

**Table 3.13.** Experimental conditions in the plasmonic catalysis of 4-NP with Martin AuNP decorated magnetic titania microbeads.

Experimental conditions	Parameter	Range
1 mg catalyst, 20°C, 7.5 ppm 4-NP	Au loading (% w/w)	2.5, 5.0, 10.0
Au loading (5 % w/w), 20 °C, 1 mg catalyst, 15 ppm 4-NP		

Calcination temperature: 450°C, Reaction volume: 100 mL

The same experimental procedure explained in Section 3.7.4.2. was applied for the reduction of 4-NP with Martin AuNP decorated magnetic titania microbeads.

#### **3.7.4.3. Catalyst recovery and reuse**

Only the reusability of Martin AuNP decorated magnetic titania microbeads was investigated as it was selected as the best catalyst in the reduction of 4-NP. At the end of the plasmonic catalysis of 4-NP (1 mg catalyst, 7.5 ppm 4-NP, 20°C), the suspension was centrifuged (5000 rpm, 5 min) and rinsed with water for several times to recover the catalyst particles. The recovered catalyst was then reused in the degradation of 4-NP under the same experimental conditions. This degradation-recovery cycle was repeated for 5 times to achieve the reusability of the catalyst.

## 4. RESULTS and DISCUSSION

In this study, a new sol–gel templating method for the synthesis of monodisperse-porous bare titania microbeads was proposed by using  $-\text{SO}_3\text{Na}$  attached poly(HPMA-Cl-co-EDMA) microbeads as template. Monodisperse-porous poly(HPMA-Cl-co-EDMA) microbeads were obtained by multistage microsuspension polymerization using monodisperse poly(GMA) beads as seed latex. Monodisperse-porous poly(HPMA-Cl-co-EDMA) microbeads were then reacted with  $\text{NaHSO}_3$  to generate  $-\text{SO}_3\text{Na}$  functionality on the polymethacrylate based microbeads. For the synthesis of bare titania microbeads via sol-gel templating method,  $-\text{SO}_3\text{Na}$  attached poly(HPMA-Cl-co-EDMA) microbeads were interacted with the titania precursor,  $\text{TiCl}_4$  in the aqueous medium and then washed with aqueous ammonia solution to remove chloride ions generated by the hydrolysis of precursor. Hence, bare titania-polymer composite microbeads in the spherical form were obtained. Then the monodisperse-porous bare titania microbeads were obtained by the calcination of composite microbeads.

For the synthesis of monodisperse-porous magnetic titania microbeads, magnetic poly(HPMA-Cl-co-EDMA) microbeads were used as template. Poly(HPMA-Cl-co-EDMA) microbeads were reacted with EDA to generate amine functionality on the polymethacrylate based microbeads before magnetization. Magnetic poly(HPMA-Cl-co-EDMA) microbeads obtained by precipitating iron salts on amine attached poly(HPMA-Cl-co-EDMA) microbeads by in-situ co-precipitation method. In sol-gel templating method, magnetic poly(HPMA-Cl-co-EDMA) microbeads were interacted with the titania precursor,  $\text{TiCl}_4$  in the aqueous medium and then washed with aqueous ammonia solution to obtain magnetic titania-polymer composite microbeads. Then magnetic titania microbeads were obtained by the calcination of composite microbeads.

The bare and magnetic titania microbeads were treated with APTES to obtain amine attached bare and magnetic titania microbeads. Then amine attached bare and magnetic titania microbeads were put into AuNP solutions for the decoration of monodisperse-porous bare and magnetic titania microbeads with AuNPs synthesized with Turkevich and Martin methods.

The photocatalytic activity of monodisperse-porous bare and magnetic titania microbeads were achieved by the degradation of RB5 dye and phenol. The effect of Au loading on the photocatalytic activity of monodisperse-porous bare and magnetic titania microbeads was investigated. The plasmonic catalytic activity of Turkevich and Martin AuNP decorated monodisperse-porous bare and magnetic titania microbeads were achieved by the reduction of 4-NP.

#### **4.1. Synthesis and Characterization of Monodisperse-Porous poly(HPMA-Cl-co-EDMA) Microbeads**

Monodisperse-porous poly(HPMA-Cl-co-EDMA) microbeads were obtained by multistage microsuspension polymerization using monodisperse poly(GMA) microbeads as the starting material. The surface morphology, size, porous structure and specific surface area (SSA) of the monodisperse-porous poly(HPMA-Cl-co-EDMA) microbeads were varied by changing the feed concentration of crosslinking agent of the poly(HPMA-Cl-co-EDMA) beads.

The SEM photographs of poly(HPMA-Cl-co-EDMA) microbeads obtained with different crosslinking agent feed concentrations (% v/v) are shown in Figure 4.1. The size properties and the specific surface areas of poly(HPMA-Cl-co-EDMA) microbeads are given in Table 4.1.



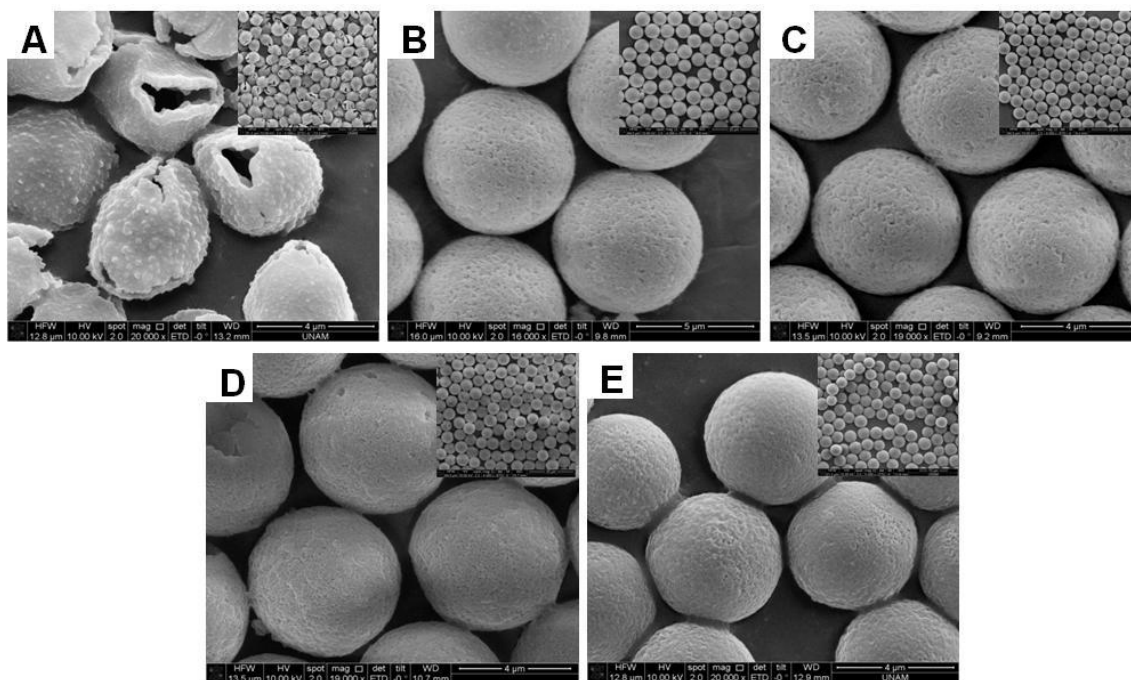


**Figure 4.1.** SEM photographs of monodisperse-porous poly(HPMA-Cl-co-EDMA) microbeads obtained with different volume percent of crosslinking agent (v/v %): (A):15 , (B): 30, (C): 50, (D): 70, (E): 85. Magnifications: Larger images: X20.000, Smaller images: X4000.

**Table 4.1.** The size and specific surface areas of poly(HPMA-Cl-co-EDMA) microbeads obtained with different volume percent of crosslinking agent (EDMA).

<b>Volume percents of crosslinking agent of poly(HPMA-Cl-co-EDMA) microbeads (% v/v)</b>	<b>Diameter (<math>\mu\text{m}</math>)</b>	<b>CV (%)</b>	<b>SSA (<math>\text{m}^2/\text{g}</math>)</b>
15	4.3	6.5	1.0
30	6.3	4.9	14.7
50	5.5	3.3	60.0
70	5.4	4.5	65.2
85	4.3	4.3	147.5

As seen in Figure 4.1., spherical, nearly monodisperse and porous poly(HPMA-Cl-co-EDMA) microbeads were achieved with all EDMA concentrations except the lowest EDMA concentration (Figure 4.1.). As seen from Table 4.1., the size and

the coefficient of variation of size distribution were not affected much by changing the feed concentration of crosslinking agent. As also seen in Table 4.1, SSA increased with the increasing crosslinking agent feed concentration. This finding showed that the mean pore size decreased and the mesopore fraction became more dominant with the increasing feed concentration of crosslinking agent [188].

#### **4.1.1. Synthesis and Characterization of Sodium Bisulfite Functionalized Poly(HPMA-Cl-co-EDMA) Microbeads**

In the literature, poly(S-co-DVB) microbeads were used as template for the synthesis of monodisperse-porous titania microbeads [32-35]. In our case,  $-\text{SO}_3\text{Na}$  attached-poly(HPMA-Cl-co-EDMA) microbeads were selected as the template material for the sol-gel templating synthesis of monodisperse-porous titania microbeads. It was considered that higher amount of hydrous titanium dioxide ( $\text{TiO}_2 \cdot n\text{H}_2\text{O}$ ) nanoparticles could be adsorbed by the template material with strong cation exchange character with respect to the plain template. The strong cation exchanger form of the poly(HPMA-Cl-co-EDMA) microbeads was obtained via a simple reaction between reactive chloropropyl group of poly(HPMA-Cl-co-EDMA) microbeads and  $\text{NaHSO}_3$  (Figure 4.2.).

The functional group content of the  $-\text{SO}_3\text{Na}$  attached-poly(HPMA-Cl-co-EDMA) microbeads was determined by potentiometric titration. The effect of HPMA-feed concentration on the  $-\text{SO}_3\text{H}$  content of polymethacrylate microbeads and fractional conversion of chloropropyl groups in the poly(HPMA-Cl-co-EDMA) microbeads are given in Figure 4.2.

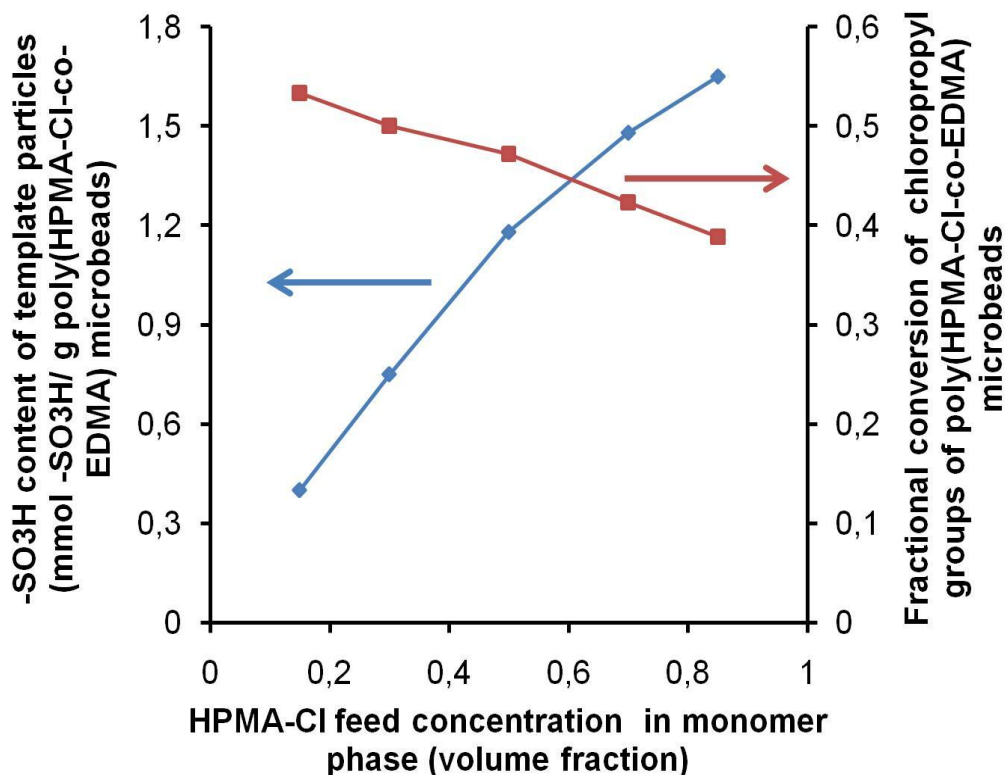


**Figure 4.2.** The effect of HPMA-Cl feed concentration on  $-\text{SO}_3\text{Na}$  content of polymethacrylate microbeads and fractional conversion of chloropropyl groups in the poly(HPMA-Cl-co-EDMA) microbeads.

As expected  $-\text{SO}_3\text{H}$  content of polymethacrylate microbeads increased with the increasing feed concentration of HPMA-Cl in the monomer phase. In other words, an increase in the chloropropyl content of poly(HPMA-Cl-co-EDMA) microbeads resulted in an increase in the  $-\text{SO}_3\text{H}$  content of polymethacrylate template.

On the other hand, the fractional conversion of chloropropyl groups decreased with the increasing HPMA-Cl feed concentration from 0.56 to 0.39 (Figure 4.2.). As the reaction took place in the aqueous medium, the interaction of bisulfite anions with the chloropropyl groups should be strongly related to the water penetration into the microbeads. The partial consumption of chloropropyl groups can be explained by the intraparticle diffusion limitation for water diffusion within the polymethacrylate microbeads.

## 4.1.2. Synthesis and Characterization of Monodisperse-Porous Bare Titania Microbeads

### 4.1.2.1. Effect of crosslinking agent feed concentration on bare titania microbeads

The SEM photographs of bare titania microbeads obtained by  $\text{-SO}_3\text{Na}$  attached-poly(HPMA-Cl-co-EDMA) microbeads with different crosslinking agent feed concentrations (% v/v) are shown in Figure 4.3. The size properties and SSAs of bare titania microbeads are given in Table 4.2.

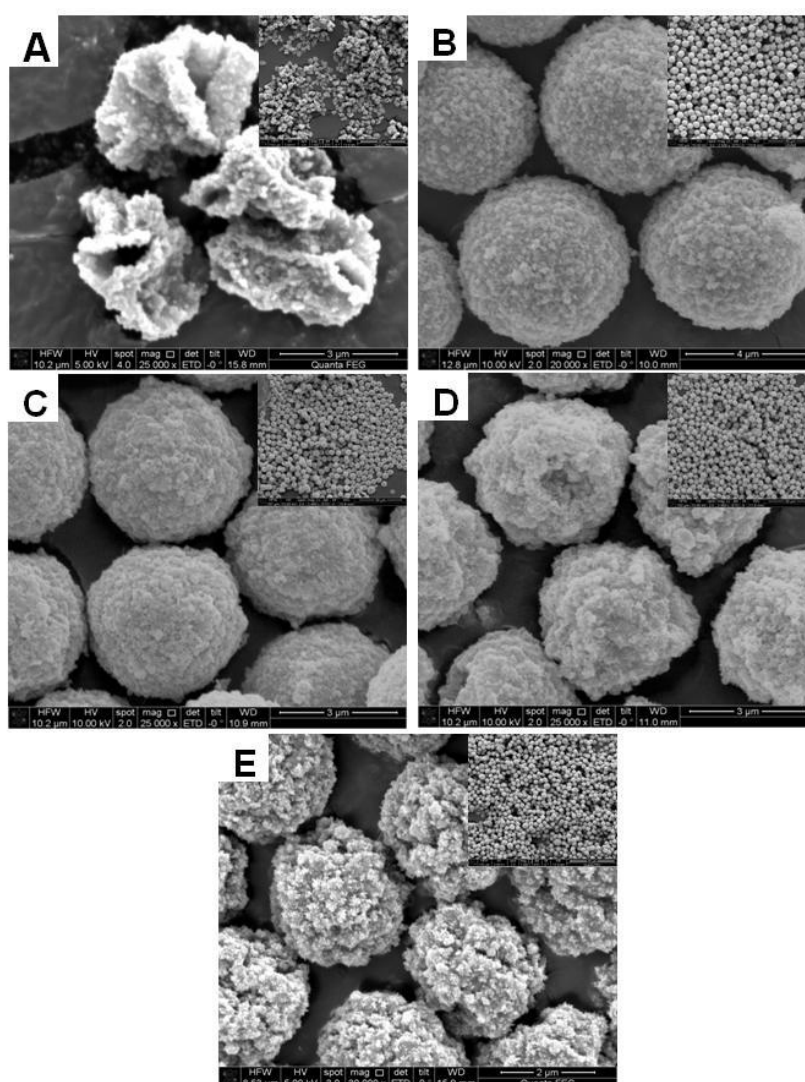


**Figure 4.3.** SEM photographs of monodisperse-porous bare titania microbeads prepared by using  $\text{-SO}_3\text{Na}$  attached-poly(HPMA-Cl-co-EDMA) microbeads produced with different volume percent of crosslinking agent (v/v %): (A):15, (B): 30, (C): 50, (D): 70, (E): 85. Magnifications: Larger images: X25000, Smaller images: X2500.

**Table 4.2.** The size and specific surface areas of bare titania microbeads prepared by using -SO<sub>3</sub>Na attached-poly(HPMA-Cl-co-EDMA) microbeads produced with different crosslinking agent feed concentrations (EDMA).

<b>Crosslinking agent feed concentration for poly(HPMA-Cl-co-EDMA) microbeads (% v/v)</b>	<b>Diameter (μm)</b>	<b>CV (%)</b>	<b>SSA (m<sup>2</sup>/g)</b>
15	4.1	7.0	60.2
30	5.4	5.2	63.3
50	3.9	4.7	52.3
70	3.7	4.9	44.8
85	3.1	4.5	42.8

Calcination temperature: 550°C,

As seen in Figure 4.3. (B) and (C), spherical bare titania microbeads could be obtained with the crosslinking agent feed concentrations of 30 and 50 % v/v. Irregular titania beads were obtained with the template synthesized with the lowest EDMA feed concentration. This finding should be explained by the relatively lower porosity and SSA of the template obtained with the lowest EDMA feed concentration [188]. The lower porosity involves less TiO<sub>2</sub> nanoparticle deposition on the polymeric template. It should be also noted that irregular titania microbeads were also obtained with the high crosslinking agent feed concentrations (*i.e.* Figure 4.2. (E) and (F)). The higher porosity of the -SO<sub>3</sub>Na attached-poly(HPMA-Cl-co-EDMA) microbeads obtained with the higher crosslinking agent feed concentration should be probably the reason of the excessive shrinkage of bare titania microbeads. Then both the SSA and the porosity of template should be suitable for either the sufficient TiO<sub>2</sub> nanoparticle deposition onto the template and to prevent excessive shrinking during calcination. Hence, the titania microbeads in spherical form can be achieved. Based on these results the polymeric templates synthesized with the EDMA feed concentrations of 30 and 50 % (v/v) had more suitable for obtaining spherical titania microbeads.

As also seen from Table 4.2., the average size of bare titania microbeads was slightly smaller with respect to the size of corresponding template probably due to the shrinkage occurred by the removal of template during calcination. The average size of bare titania microbeads decreased with the increasing crosslinking agent feed concentration depending upon the extent of shrinkage in the calcination stage. However, no significant change was observed in the coefficient of variation for size distribution since the size distribution of titania microbeads should be dominantly controlled by the weight ratio of  $\text{TiCl}_4$ /polymethacrylate microbeads.

The effect of crosslinking agent feed concentration used in the preparation of  $-\text{SO}_3\text{Na}$  attached-poly(HPMA-Cl-co-EDMA) microbeads on the SSA of bare titania microbeads is given in Figure 4.4.

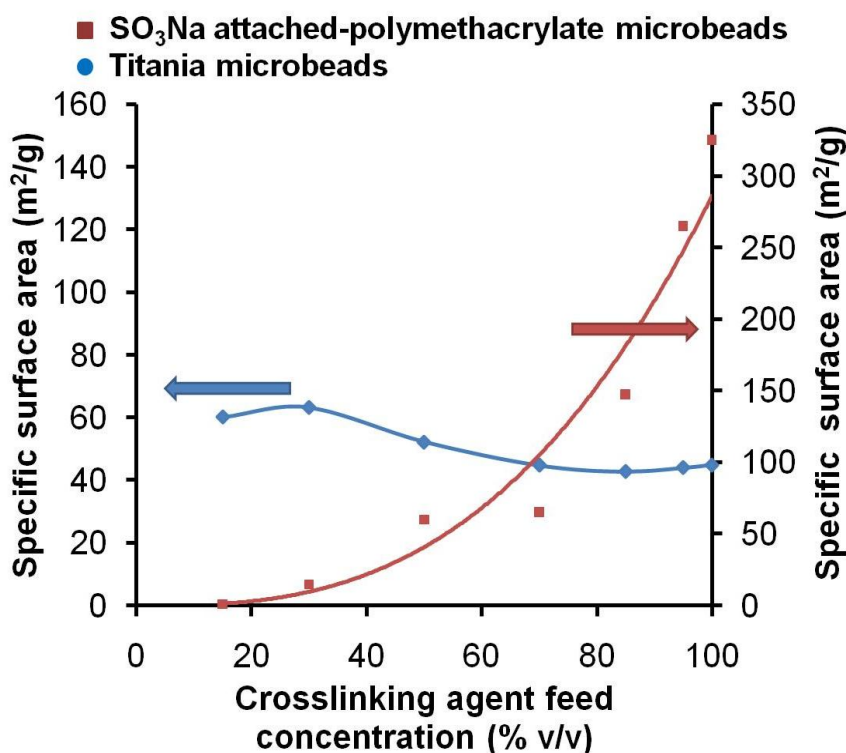


**Figure 4.4.** The effect of crosslinking agent feed concentration on the specific surface area of  $-\text{SO}_3\text{Na}$  attached-poly(HPMA-Cl-co-EDMA) microbeads and bare titania microbeads.

As seen from the Figure 4.4., the SSA of  $-\text{SO}_3\text{Na}$  attached-poly(HPMA-Cl-co-EDMA) microbeads increased with the increasing volume percent of EDMA. The

mean pore size decreased and the mesopore fraction became more dominant with the increasing feed concentration of crosslinking agent [188]. However, the tendency observed for bare titania microbeads in Figure 4.4. indicated that, SSA of bare titania microbeads was not strongly influenced by the porous properties of the  $-\text{SO}_3\text{Na}$  attached-poly(HPMA-Cl-co-EDMA) microbeads. Although the templates produced with high crosslinking agent feed concentrations (i.e. 95 % v/v and 100 % v/v) had reasonably high SSA values, no significant change was observed in the SSA of resulting bare titania microbeads (Figure 4.4.). This behaviour can be explained by the dominant control of calcination conditions on formation of three-dimensional porous structure of the titania microbeads.

#### 4.1.2.2. Effect of concentration of polymeric template on titania microbeads

The SEM photographs of bare titania microbeads synthesized with different concentrations of  $-\text{SO}_3\text{Na}$  attached-poly(HPMA-Cl-co-EDMA) microbeads (feed concentration of crosslinking agent: 30 % v/v) are shown in Figure 4.5. The size properties and SSAs of bare titania microbeads are given in Table 4.3.

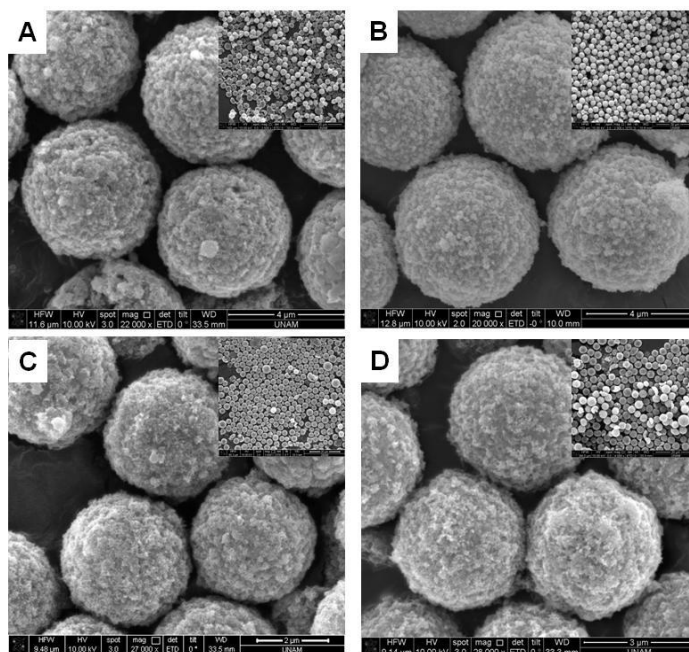


**Figure 4.5.** SEM photographs of bare titania microbeads prepared by using different concentrations of  $-\text{SO}_3\text{Na}$  attached-poly(HPMA-Cl-co-EDMA) microbeads (g/L) A: 3.3 g/L, B: 6.7 g/L, C: 10 g/L, D: 13.3 g/L. (feed concentration of crosslinking agent: 30 % v/v). Magnifications: Larger images: X25,000, Smaller images: X2500.

**Table 4.3.** The size and specific surface areas of bare titania microbeads obtained with different concentrations of poly(HPMA-Cl-co-EDMA) microbeads (volume percent of crosslinking agent: % 30).

<b>Mass of polymeric template/ Volume of solution (g/L)</b>	<b>Diameter (<math>\mu\text{m}</math>)</b>	<b>CV (%)</b>	<b>SSA (<math>\text{m}^2/\text{g}</math>)</b>
3.3	5.0	5.3	58.1
6.7	5.4	5.2	63.3
10.0	3.8	4.1	62.2
13.3	3.6	5.9	62.4

Calcination temperature: 550°C

As seen in Figure 4.5. and Table 4.3., bare titania microbeads with spherical shape were obtained with all feed concentrations of  $-\text{SO}_3\text{Na}$  attached-poly(HPMA-Cl-co-EDMA) microbeads. The average microbead size decreased with the increasing feed concentration of  $-\text{SO}_3\text{Na}$  attached-poly(HPMA-Cl-co-EDMA) microbeads since the constant amount of hydrous titania nanoparticles were distributed to higher number of polymeric template microbeads. Both the monodispersity and specific surface area of bare titania microbeads were not strongly influenced by the feed concentration of the template.

#### **4.1.2.3. Effect of calcination temperature on titania microbeads**

Thermal decomposition behaviour of poly(HPMA-Cl-co-EDMA) microbeads are important for the determination of calcination temperature to obtain bare titania microbeads from titania-polymer composite microbeads. Thermal Gravimetric Analysis (TGA) of poly(HPMA-Cl-co-EDMA) microbeads is given in Figure 4.6.



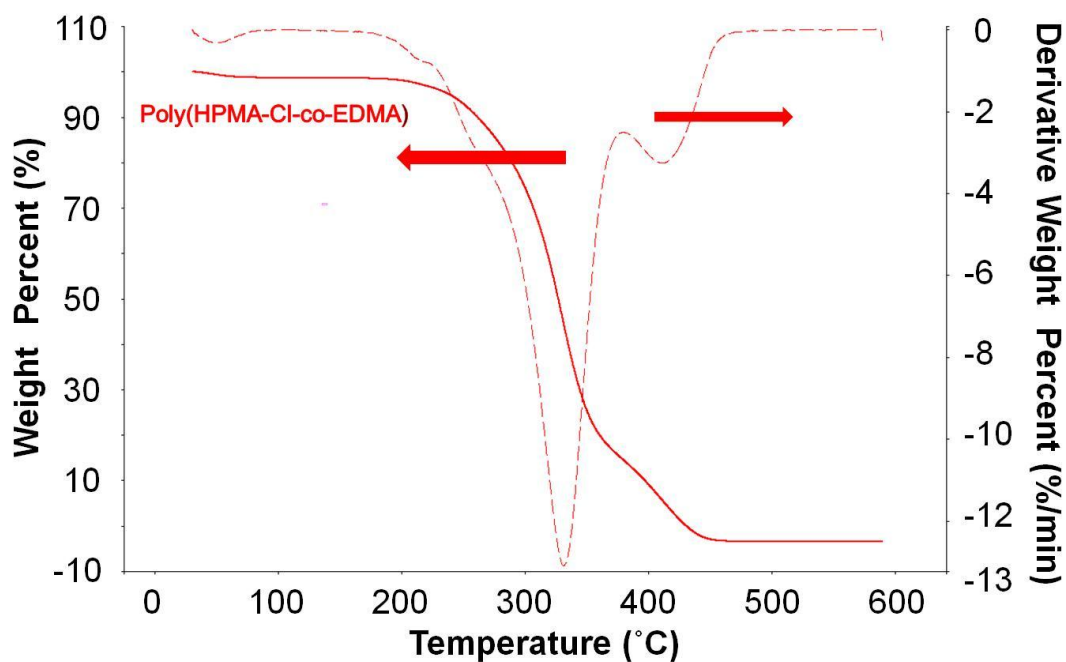


**Figure 4.6.** TGA curves of monodisperse-porous poly(HPMA-Cl-co-EDMA) microbeads.

TGA clearly showed that the thermal decomposition of poly(HPMA-Cl-co-EDMA) microbeads was almost completed at 450°C. Additionally, the peak temperature of the derivative curve of poly(HPMA-Cl-co-EDMA) microbeads was 335°C. The decomposition behaviour obtained by TGA were also supported by Differential Scanning Calorimetry (DSC) curve of poly(HPMA-Cl-co-EDMA) microbeads. The DSC curve is given in Figure 4.7 .

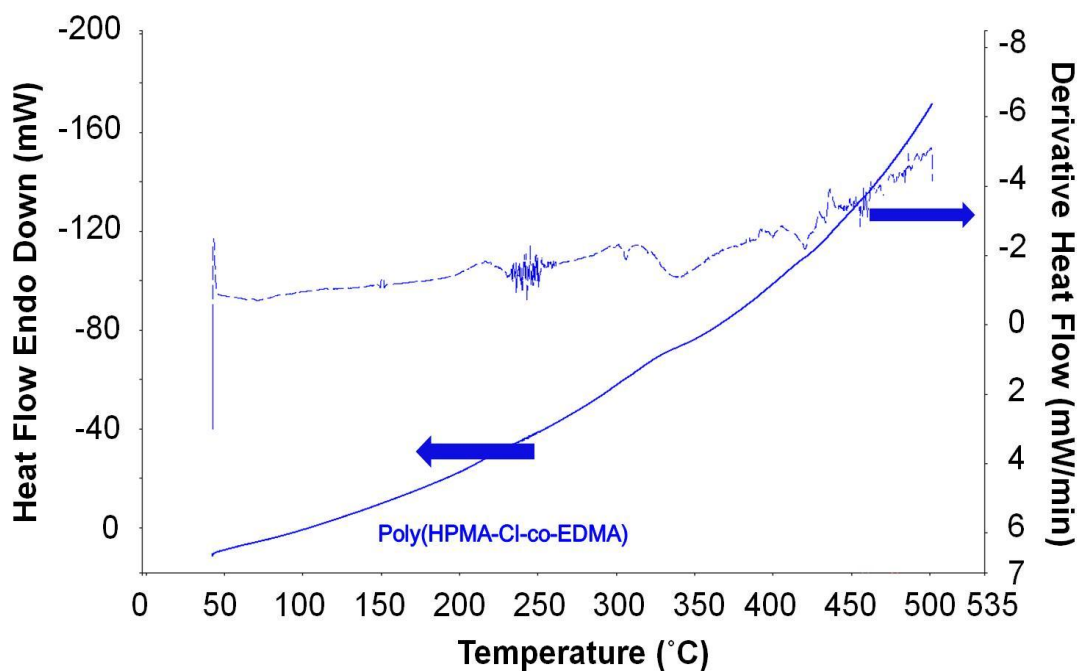


**Figure 4.7.** DSC curve of monodisperse-porous poly(HPMA-Cl-co-EDMA) microbeads.

DSC showed that thermal decomposition of poly(HPMA-Cl-co-EDMA) microbeads started at the temperatures higher than 200°C and continued till 450°C. Thermal analysis results obtained by both methods showed that the complete removal of poly(HPMA-Cl-co-EDMA) microbeads was achieved by performing the calcination of titania-polymer composite microbeads at a minimum temperature of 450°C.

Titania-polymer composite microbeads prepared by using -SO<sub>3</sub>Na attached-poly(HPMA-Cl-co-EDMA) microbeads (feed concentration of crosslinking agent: % 30 v/v, mass of particle/volume of solution ratio: 6.7 g/mL) were calcined at 450°C, 500°C, 550°C, 600°C to determine the effect of calcination temperature on SSA of titania microbeads.

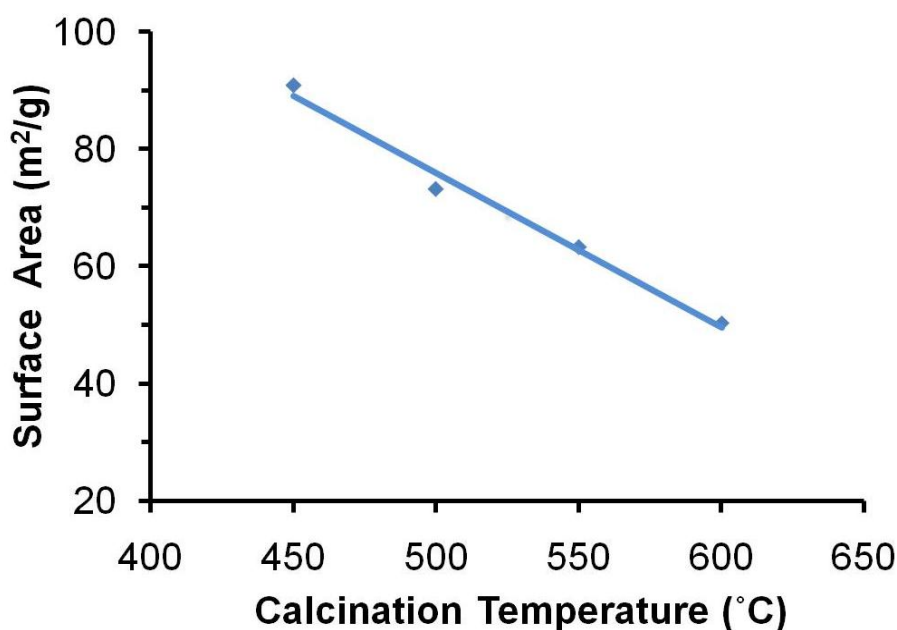


**Figure 4.8.** The variation of specific surface area of bare titania microbeads with the calcination temperature. Template:  $-\text{SO}_3\text{Na}$  attached-poly(HPMA-Cl-co-EDMA) microbeads.

Using poly(HPMA-Cl-co-EDMA) microbeads gave an opportunity to perform the calcination of titania-polymer composite microbeads at lower temperatures (450°C), which resulted in higher specific surface area of bare titania microbeads as shown in Figure 4.8. As seen in Figure 4.8., the SSA of bare titania microbeads linearly decreased with increasing calcination temperature [36, 37]. The highest SSA was obtained with the lowest calcination temperature. Various shape templated sol-gel protocols were proposed for the synthesis of porous titania microbeads using monodisperse-porous poly(styrene-co-divinylbenzene), poly(S-co-DVB) microbeads as the template material [32-36]. Due to its aromatic nature, the thermal degradation of the poly(S-co-DVB) microbeads could be achieved at higher temperatures with respect to those used for the new polymethacrylate based template material proposed in this thesis. TGA analysis of poly(S-co-DVB) beads showed that the lowest temperature that could be utilized for complete thermal degradation was 550°C. Hence, the template removal could be performed at an extremely lower temperature (i.e. 450°C) by the use of new template proposed (i.e. poly(HPMA-Cl-co-EDMA)). The calcination at lower temperature resulted in a significant increase in SSA with respect to the titania microbeads obtained from poly(S-co-DVB) based template materials [32-36].

XRD patterns for monodisperse-porous bare titania microbeads calcined at 450°C, 500°C, 550°C, 600°C are given in Figure 4.9. As seen here, the calcination temperature significantly affected the crystalline structure of bare titania microbeads. It was reported that, the amorphous-anatase transformation of titania was completed in the temperature range of 350-450 °C [37].

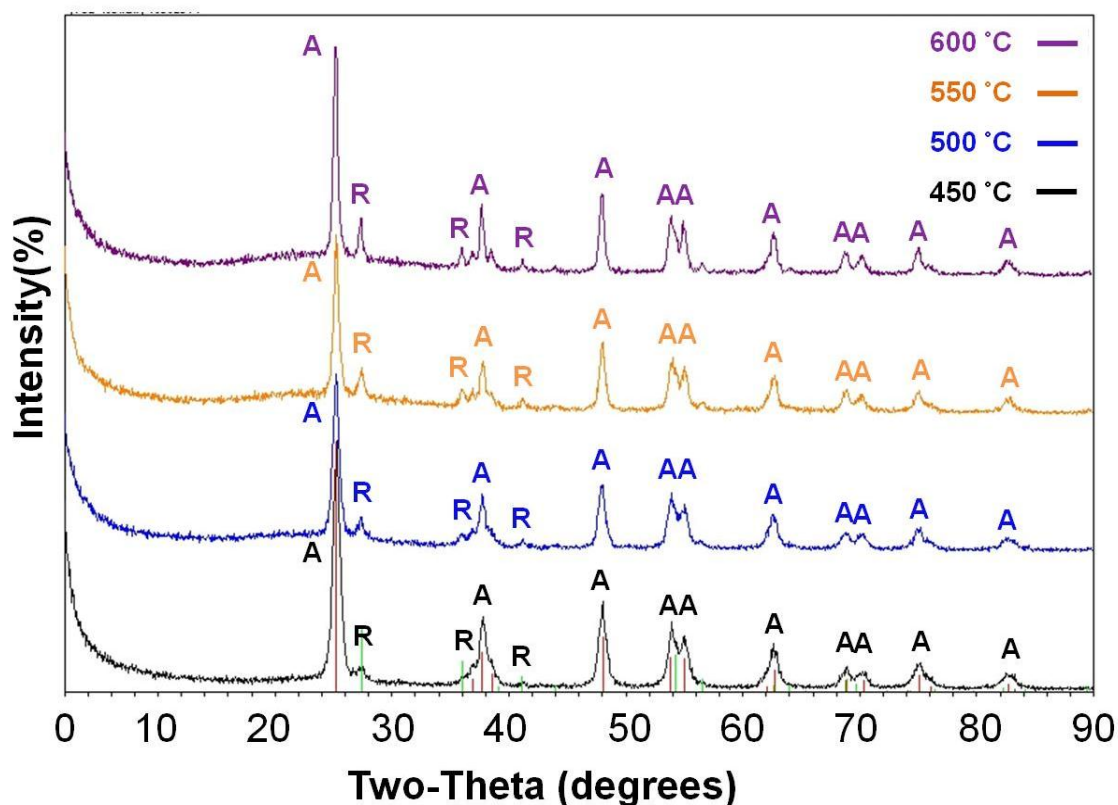


**Figure 4.9.** XRD patterns for monodisperse-porous bare titania microbeads calcined at different temperatures (450°C, 500°C, 550°C, 600°C). Template: -SO<sub>3</sub>Na attached poly(HPMA-Cl-co-EDMA) microbeads.

It was reported that anatase-rutile transformation occurred in different temperature ranges from 450°C to 1100°C [37]. The anatase/rutile ratio was particularly critical in the photocatalytic applications of porous TiO<sub>2</sub> beads [37]. As seen from XRD patterns amorphous titania transformed to anatase at each calcination temperature (Figure 4.9.). The rutile content of titania microbeads clearly increased with increasing calcination temperature.

Based on the evaluation of the results obtained with bare titania microbeads, the poly(HPMA-Cl-co-EDMA) microbeads produced with the crosslinking agent feed concentration of % 30 v/v were chosen as the most appropriate template to obtain monodisperse-porous and spherical titania microbeads. The ratio of mass of poly(HPMA-Cl-co-EDMA) microbeads /volume of  $\text{TiCl}_4$  solution was chosen as 6.7 g/mL considering the SSA values of titania microbeads.

## **4.2. Synthesis and Characterization of Monodisperse-Porous and Magnetic Titania Microbeads**

In this thesis a new protocol was developed for the synthesis of magnetic titania microbeads. The magnetic titania microbeads were obtained by starting from the magnetic poly(HPMA-Cl-co-EDMA) microbeads. For this purpose, the poly(HPMA-Cl-co-EDMA) microbeads produced with the crosslinking agent feed concentration of % 30 v/v was chosen as the most appropriate template and the magnetic form of this material was synthesized as the starting material. The protocol developed for the synthesis of magnetic titania microbeads is discussed below in detail.

### **4.2.1. Synthesis and Characterization of Amine Functionalized Poly(HPMA-Cl-co-EDMA) Microbeads**

The amine functionalized form of poly(HPMA-Cl-co-EDMA) microbeads (volume percent of crosslinking agent: 30 % (% v/v)) was easily obtained via a simple reaction between reactive chloropropyl groups of poly(HPMA-Cl-co-EDMA) microbeads and EDA. The amine content of EDA treated-poly(HPMA-Cl-co-EDMA) microbeads was determined as 5 % w/w by the elemental analysis.

### **4.2.2. Synthesis and Characterization of Magnetic poly(HPMA-Cl-co-EDMA) Microbeads**

Magnetic poly(HPMA-Cl-co-EDMA) microbeads were obtained by the impregnation of iron ions on amine attached-poly(HPMA-Cl-co-EDMA) microbeads (feed concentration of crosslinking agent: 30 % (% v/v)) by in-situ co-precipitation method. The SEM photographs of plain poly(HPMA-Cl-co-EDMA) and magnetic poly(HPMA-Cl-co-EDMA) microbeads are shown in Figure 4.10. As seen here, the surface morphology of poly(HPMA-Cl-co-EDMA) microbeads was changed

apparently after magnetization step. This view showed the presence of magnetite layer on the magnetic polymeric template on the outer surface of the microbeads.

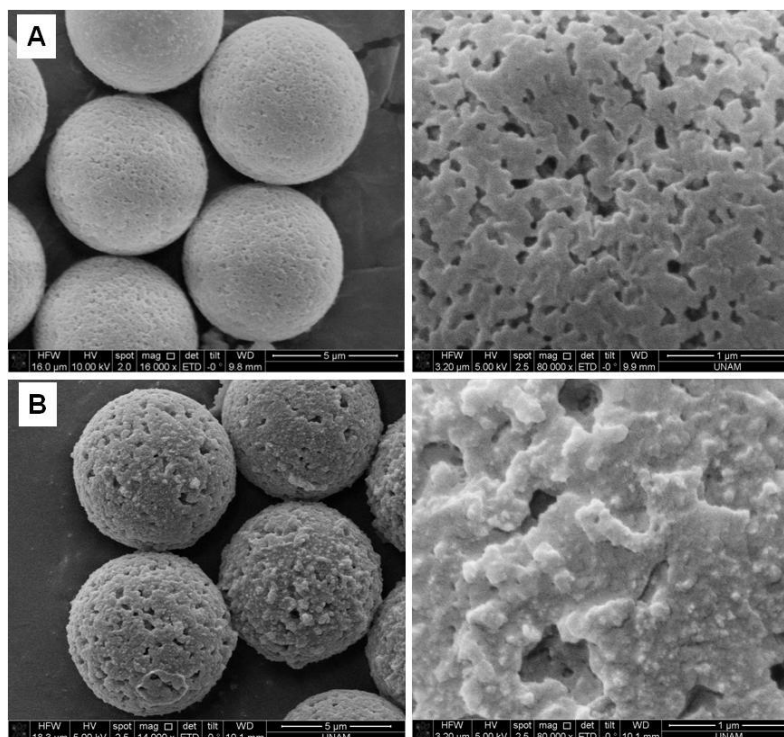


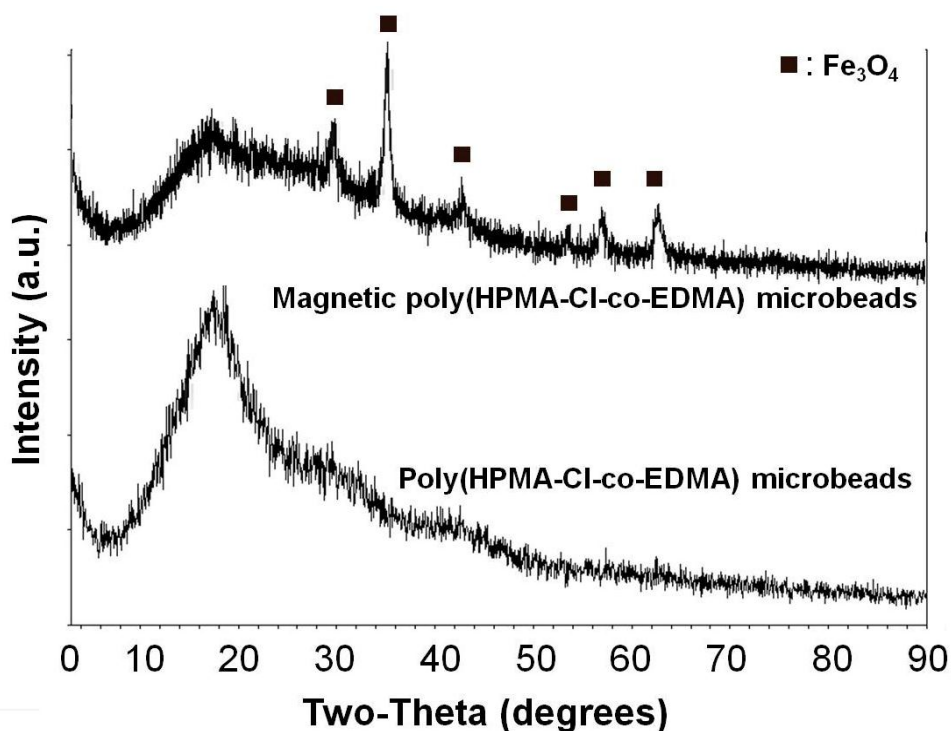
**Figure 4.10.** SEM photographs of (A): poly(HPMA-Cl-co-EDMA) microbeads, (B): magnetic poly(HPMA-Cl-co-EDMA) microbeads. Magnifications: Images on the left side: X16000, Images on the right side: X80000.

The size properties and SSA values of plain poly(HPMA-Cl-co-EDMA) and magnetic poly(HPMA-Cl-co-EDMA) microbeads are given in Table 4.4.

**Table 4.4.** Size properties and specific surface areas of poly(HPMA-Cl-co-EDMA) and magnetic poly(HPMA-Cl-co-EDMA) microbeads.

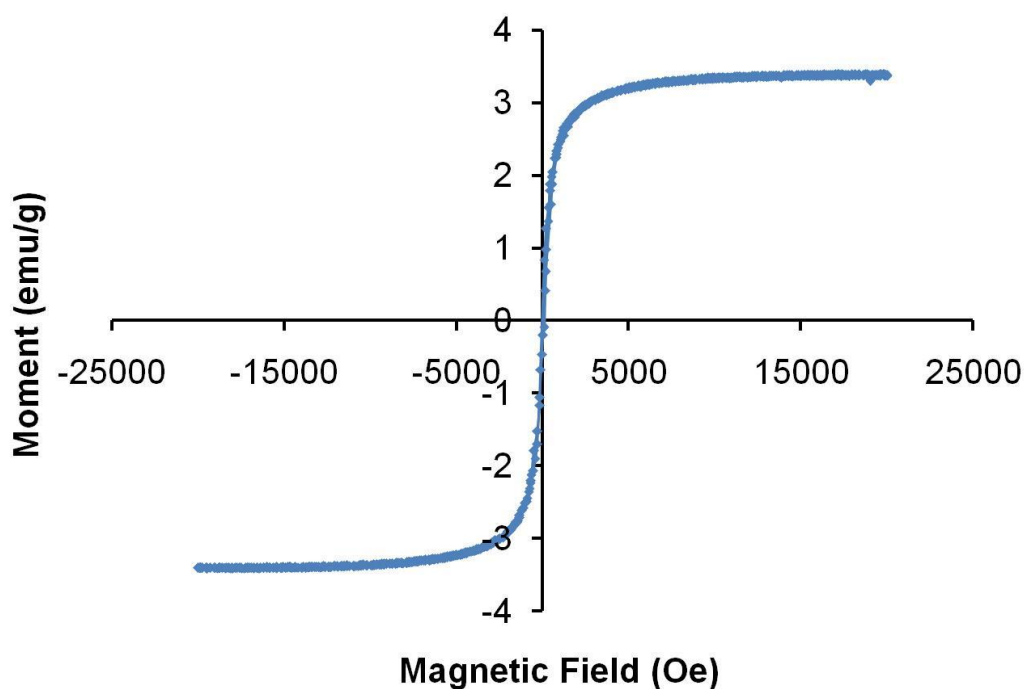
<b>Microbeads</b>	<b>Diameter (<math>\mu\text{m}</math>)</b>	<b>CV (%)</b>	<b>SSA (<math>\text{m}^2/\text{g}</math>)</b>
Poly(HPMA-Cl-co-EDMA) Microbeads	6.3	4.9	14.7
Magnetic Poly(HPMA-Cl-co-EDMA) microbeads	6.5	4.8	8.3

As seen in Table 4.4., the average size and the coefficient of variation for size distribution for poly(HPMA-Cl-co-EDMA) microbeads did not markedly change after magnetization. However, SSA significantly decreased since a certain portion of the micropores were filled with the iron oxide nanoparticles generated during magnetization. The structure of poly(HPMA-Cl-co-EDMA) and magnetic poly(HPMA-Cl-co-EDMA) microbeads were investigated by XRD and the related patterns are given in Figure 4.11.



**Figure 4.11.** XRD patterns of poly(HPMA-Cl-co-EDMA) and magnetic poly(HPMA-Cl-co-EDMA) microbeads.

Only a broad peak ( $2\theta$ :  $18^\circ$ ) corresponding to the amorphous poly(HPMA-Cl-co-EDMA) was observed as seen from XRD pattern of poly(HPMA-Cl-co-EDMA) microbeads in Figure 4.11. In the XRD pattern of magnetic poly(HPMA-Cl-co-EDMA) microbeads, additional to the broad peak ( $2\theta$ :  $18^\circ$ ) of the amorphous poly(HPMA-Cl-co-EDMA), the characteristic peaks (at  $2\theta$ :  $30.4$ ,  $35.7$ ,  $43.4$ ,  $57.4$ ,  $63.0$  and  $66.0^\circ$ ) of cubic spinel structure phase of  $\text{Fe}_3\text{O}_4$  nanoparticles were observed. This difference between the XRD patterns in Figure 4.11. is an evidence that the magnetization of plain poly(HPMA-Cl-co-EDMA) microbeads was performed successfully.



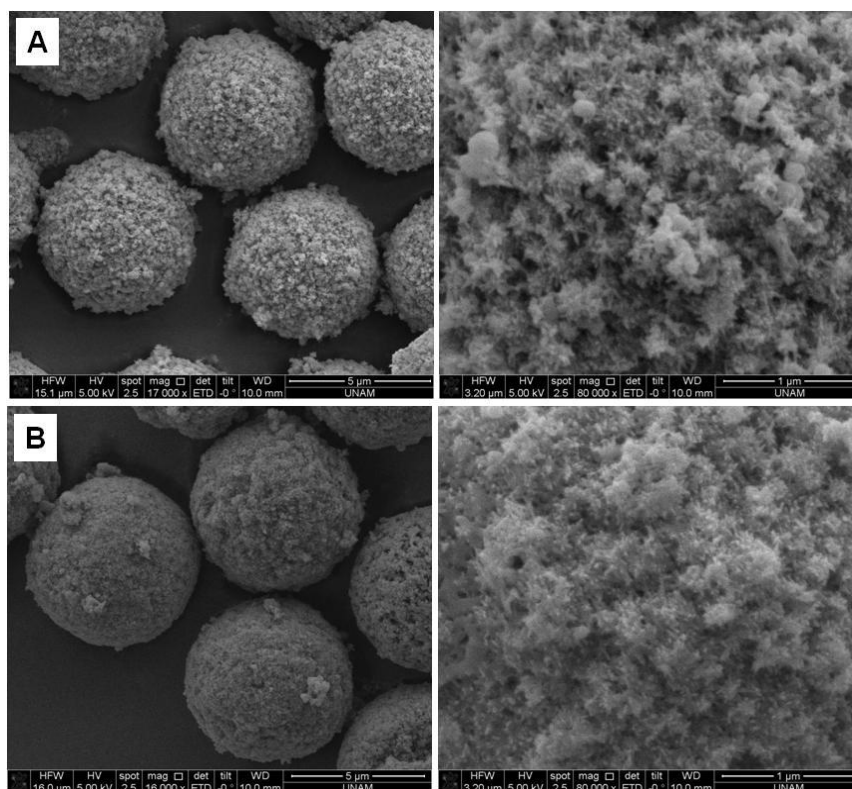
**Figure 4.12.** VSM curve of magnetic poly(HPMA-Cl-co-EDMA) microbeads.

Figure 4.12. shows the magnetization curve of magnetic poly(HPMA-Cl-co-EDMA) microbeads measured at 300K. The magnetic saturation ( $M_s$ ) value is 3.3 emu/g for magnetic poly(HPMA-Cl-co-EDMA) microbeads. The magnetic microbeads exhibit superparamagnetic behavior at room temperature as the value of remanent magnetization ( $M_r$ ) and coercivity ( $H_c$ ) were low [144]. The superparamagnetic behavior gives the opportunity to separate magnetic microbeads by a magnet or an applied magnetic field.

#### 4.2.3. Properties of Magnetic Titania Microbeads

Magnetic titania microbeads were obtained by a new via sol-gel templating method, in which magnetic poly(HPMA-Cl-co-EDMA) microbeads [feed concentration of crosslinking agent: 30 % (% v/v), mass of particle/volume of solution ratio: 6.7 g/mL] were interacted with the titania precursor,  $TiCl_4$  in the aqueous solution and then washed with aqueous ammonia solution to remove chloride ions generated by the hydrolysis of the precursor. Hence, magnetic titania-polymer composite microbeads obtained in the spherical form were calcined at 450°C to obtain monodisperse-porous and magnetic titania microbeads. The SEM photographs of bare and magnetic titania microbeads obtained by  $-SO_3Na$  attached-poly(HPMA-Cl-co-EDMA) microbeads and magnetic poly(HPMA-Cl-co-EDMA) microbeads, respectively are shown in Figure 4.13.





**Figure 4.13.** SEM photographs of (A): bare titania microbeads, (B): magnetic titania microbeads. Magnifications: Images on the left side (microbeads): X16.000, Images on the right side (surface): X80.000.

As seen in Figure 4.13., the surface morphologies of monodisperse-porous bare and magnetic titania microbeads were similar. The reason of this similarity could be the successful integration of magnetic nanoparticles into the structure of titania microbeads during the calcination. The size properties and specific surface areas of bare and magnetic titania microbeads are given in Table 4.5.

**Table 4.5.** Size properties and specific surface areas of monodisperse-porous bare and magnetic titania microbeads.

Microbeads	Diameter (μm)	CV (%)	SSA (m <sup>2</sup> /g)
Titania microbeads	5.4	5.2	91.0
Magnetic titania microbeads	5.5	5.4	72.4

As seen from Table 4.5., the average size and the coefficient of variation for size distribution for bare and magnetic titania microbeads were nearly the same.

However, the SSA of magnetic titania microbeads was slightly lower than the bare titania microbeads. The reason of lower SSA is likely partial filling of mesopores of the titania microbeads with the magnetic nanoparticles. The structure of bare and magnetic titania microbeads were investigated by XRD and the related patterns are given in Figure 4.14.

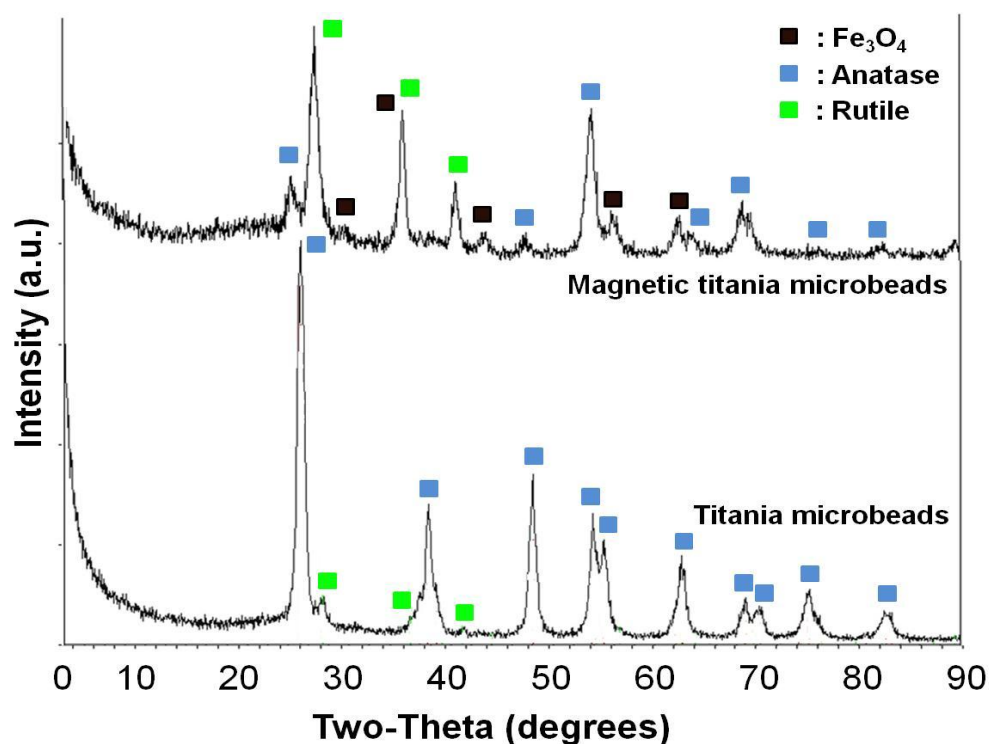


**Figure 4.14.** XRD patterns of bare and magnetic titania microbeads.

The XRD patterns of bare and magnetic titania microbeads calcined at 450°C are presented in Figure 4.14., which reveals that the use of magnetic poly(HPMA-Cl-co-EDMA) microbeads as template influenced the crystal structure of titania microbeads. The rutile phase in the crystal structure of magnetic titania microbeads was more apparent when compared with bare titania microbeads. In the XRD pattern of magnetic titania microbeads, in addition to the anatase and rutile peaks, the characteristic peaks of cubic spinel structure phase of  $\text{Fe}_3\text{O}_4$  nanoparticles were observed (at  $2\theta$ : 30.4, 43.4, 57.4 and 63.0°). The existence of these characteristic peaks is a clear evidence for the presence of  $\text{Fe}_3\text{O}_4$  nanoparticles within the crystal structure of titania microbeads.

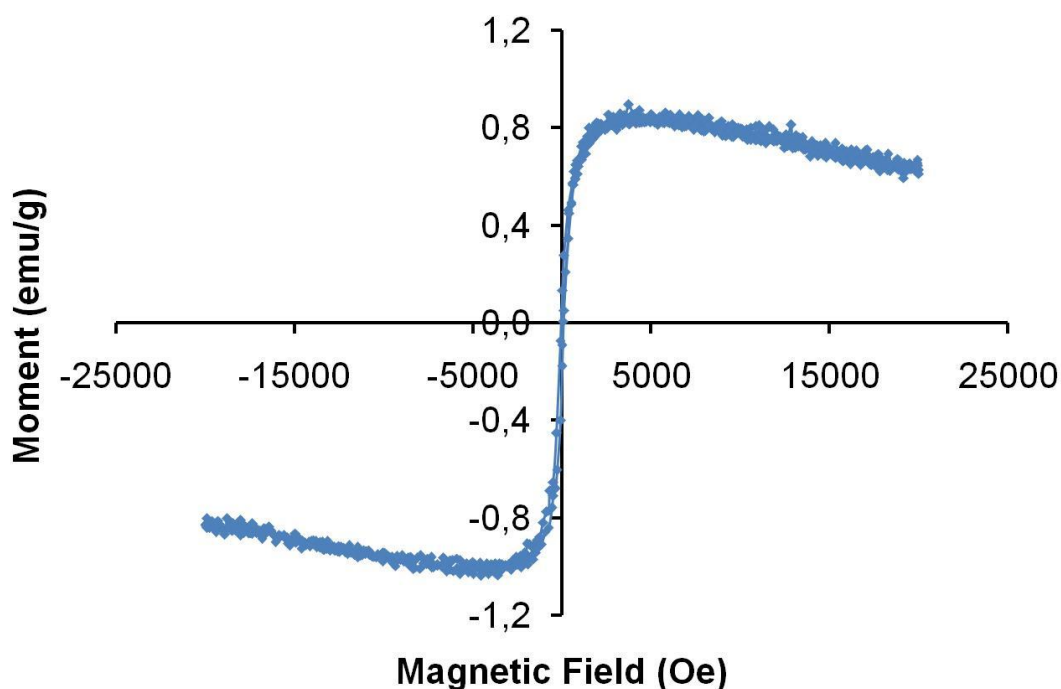


**Figure 4.15.** VSM curve of magnetic titania microbeads.

Figure 4.15. shows the magnetization curve of magnetic titania microbeads measured at 300K. The magnetic saturation ( $M_s$ ) value of magnetic titania microbeads is 0.6 emu/g, which is lower than the magnetic saturation ( $M_s$ ) value of magnetic poly(HPMA-Cl-co-EDMA) microbeads. The decrease should be probably due to the high temperature used in calcination since the saturation magnetization is inversely proportional with synthesis temperature of the magnetic material. However, magnetic titania microbeads still exhibit superparamagnetic behavior at room temperature as the value of remanent magnetization ( $M_r$ ) and coercivity ( $H_c$ ) were low.

### **4.3.Synthesis and Characterization of AuNP Decorated Bare/Magnetic Titania Microbeads**

#### **4.3.1. Synthesis and Characterization of Amine Functionalized Bare/Magnetic Titania Microbeads**

The amine functionalized forms of bare and magnetic titania microbeads were obtained via a simple reaction between hydroxyl groups of bare/magnetic titania microbeads and methoxysilane groups of APTES. The elemental analysis showed that the amine functionalization was achieved both for bare and magnetic titania

microbeads. The amine contents of resulting bare and magnetic titania microbeads were determined as 3.2 and 2.7 % w/w, respectively.

#### 4.3.1.1. Properties of AuNP Decorated Bare Titania Microbeads

Decoration of bare titania microbeads with Turkevich and Martin AuNPs was assured by firm contact between the amine attached bare titania microbeads and AuNP solutions synthesized with Turkevich and Martin methods, respectively. Au loading (% w/w) on bare titania microbeads was varied (2.5, 5.0, 10.0 (%w/w)) by changing the amount of amine attached bare titania microbeads interacted with the same volume of AuNP solution obtained with Turkevich and Martin methods. To present an example of surface morphology for AuNP decorated bare titania microbeads, the SEM photograph of Turkevich AuNP decorated bare titania microbeads with an Au loading of 5 % (%w/w) is shown in Figure 4.16.

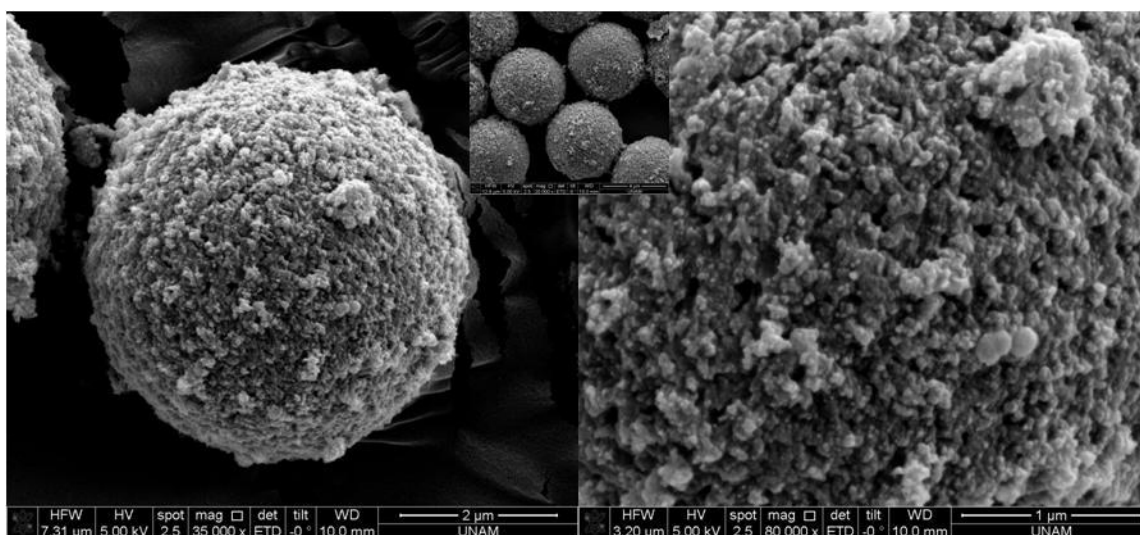


**Figure 4.16.** SEM photograph of Turkevich AuNP decorated bare titania microbeads with an Au loading of 5 % (%w/w).

The surface morphology of Turkevich AuNP decorated bare titania microbeads shown in SEM photographs (Figure 4.16.) is the convincing proof of the decoration of AuNPs on the amine attached bare titania microbeads. The UV-Vis spectra of Turkevich and Martin AuNP solutions are given in Figure 4.17. The characteristic surface plasmon bands for the AuNPs 3 nm and 10 nm in size, synthesized with Martin and Turkevich method, were observed at 509 and 521 nm in the UV-Visible

spectrums (Figure 4.17.), respectively. The SSA values of Turkevich and Martin AuNP decorated bare titania microbeads are given in Table 4.6.

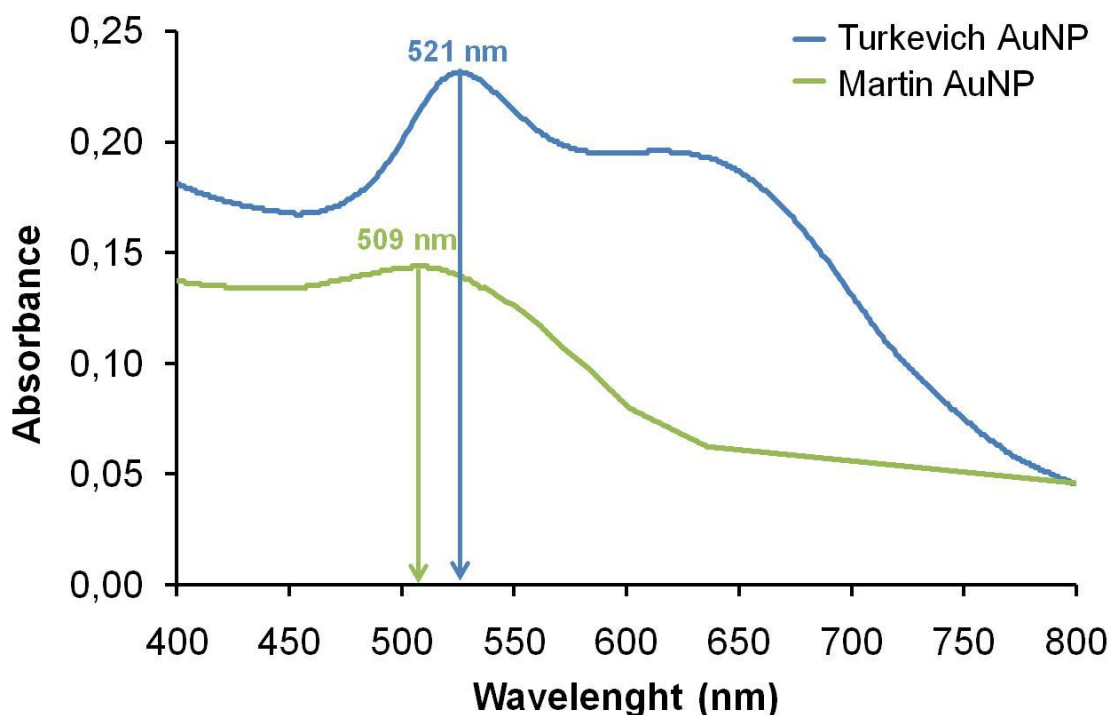


**Figure 4.17.** UV-Vis spectra of Turkevich and Martin AuNP solutions.

**Table 4.6.** Specific surface areas of Turkevich and Martin AuNP decorated bare titania microbeads with different Au loadings.

Turkevich Method		Martin Method	
Au loading on bare TiO <sub>2</sub> microbeads (% w/w)	SSA (m <sup>2</sup> /g)	Au loading on bare TiO <sub>2</sub> microbeads (% w/w)	SSA (m <sup>2</sup> /g)
2.5	71.2	2.5	63.2
5.0	72.2	5.0	66.2
10.0	71.6	10.0	65.1

Calcination temperature: 450°C

The SSA values of Turkevich and Martin AuNP decorated bare titania microbeads with all Au loadings, shown in Table 4.6., were lower than the SSA of bare titania microbeads. The decrease in SSA can be explained by the partial filling of mesopores by the AuNPs diffused into the bare titania microbeads. Note that the SSA values obtained for Martin AuNP decorated titania microbeads were slightly lower with respect to the Turkevich AuNP decorated microbeads. This result can be explained by more effective diffusion of smaller AuNPs into the mesopores of titania microbeads for Martin AuNP decorated sample. As also seen in Table 4.6., the SSA of Turkevich or Martin AuNP decorated bare titania microbeads was not correlated with the Au loading. The structure of bare titania microbeads, Turkevich and Martin AuNP decorated bare titania microbeads were investigated by XRD and the related patterns are given in Figure 4.18.

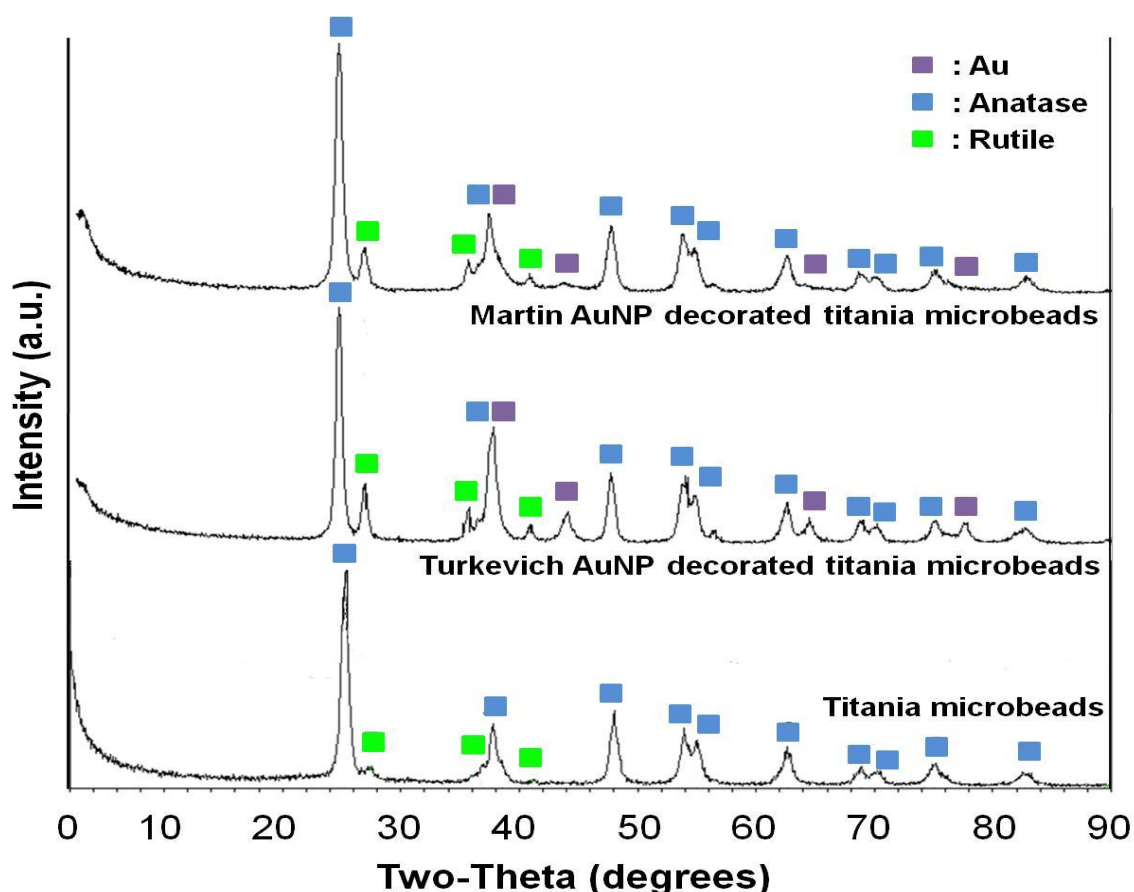


**Figure 4.18.** XRD patterns of bare titania microbeads, Turkevich and Martin AuNP decorated bare titania microbeads.

As seen in Figure 4.18., the characteristic peaks (at  $2\Theta$ :  $38^\circ$ ,  $44^\circ$ ,  $64^\circ$  and  $77^\circ$ ) of cubic structure of metallic gold were observed in the XRD patterns of Turkevich and Martin AuNP decorated-bare titania microbeads, in addition to the anatase and rutile peaks of titania. The results showed that AuNPs were successfully incorporated into the bare titania microbeads by both methods without performing a significant change in the crystal structure of bare titania. The intensities of the peaks at  $2\Theta$ :  $38^\circ$ ,  $44^\circ$ ,  $64^\circ$  decreased and the peak at  $2\Theta$ :  $77^\circ$  disappeared in the XRD patterns of Martin AuNP decorated bare titania microbeads compared to the Turkevich AuNP decorated bare titania microbeads. These results were consistent with the results obtained by Moreau and Bond [191], who reported that the intensity of characteristic peaks of metallic gold decreased by lowering the size of AuNPs.

#### **4.3.2. Properties of AuNP Decorated Magnetic Titania Microbeads**

Decoration of magnetic titania microbeads with Turkevich and Martin AuNPs was performed by firm contact between the primary amine functionalized magnetic titania microbeads and AuNP solutions synthesized with both Turkevich and Martin methods. The Au loading on magnetic titania microbeads was varied (2.5, 5.0, 10.0 (%w/w)) by changing the amount of amine attached magnetic titania microbeads interacted with the same volume of AuNP solution synthesized with both Turkevich and Martin methods. To present an example of surface morphology of AuNP decorated magnetic titania microbeads, the SEM photograph of monodisperse-porous Turkevich AuNP decorated magnetic titania microbeads with an Au loading of 5.0 % (%w/w) is shown in Figure 4.19.



**Figure 4.19.** SEM photograph of monodisperse-porous Turkevich AuNP decorated magnetic titania microbeads with an Au loading of 5.0 % (%w/w).

The surface morphology of Turkevich AuNP decorated magnetic titania microbeads shown in SEM photographs (Figure 4.19.), is the convincing proof of the decoration Turkevich AuNPs on the amine attached magnetic titania microbeads. When compared with the Turkevich AuNP decorated bare titania microbeads, the surface coverage by AuNPs was more dense for the magnetic microbeads. The SSA values of Turkevich and Martin AuNP decorated magnetic titania microbeads are given in Table 4.7.

**Table 4.7.** Specific surface area values of Turkevich and Martin AuNP decorated magnetic titania microbeads with different with different Au loadings.

<b>Turkevich Method</b>		<b>Martin Method</b>	
<b>Au loading on magnetic TiO<sub>2</sub> microbeads (% w/w)</b>	<b>SSA (m<sup>2</sup>/g)</b>	<b>Au loading on magnetic TiO<sub>2</sub> microbeads (% w/w)</b>	<b>SSA (m<sup>2</sup>/g)</b>
2.5	71.5	2.5	65.3
5.0	70.2	5.0	69.8
10.0	72.6	10.0	64.9

Calcination temperature: 450°C.



No significant change was observed in SSA with Au loading for magnetic titania microbeads decorated with both Turkevich and Martin AuNPs. However, the SSA values of Turkevich AuNP decorated titania microbeads were slightly higher with respect to those obtained by Martin method. This difference can be explained by the partial filling of mesopores more effectively by the smaller AuNPs produced by Martin method. The structure of magnetic titania microbeads, Turkevich and Martin AuNP decorated magnetic titania microbeads were investigated by XRD and related patterns are given in Figure 4.20.

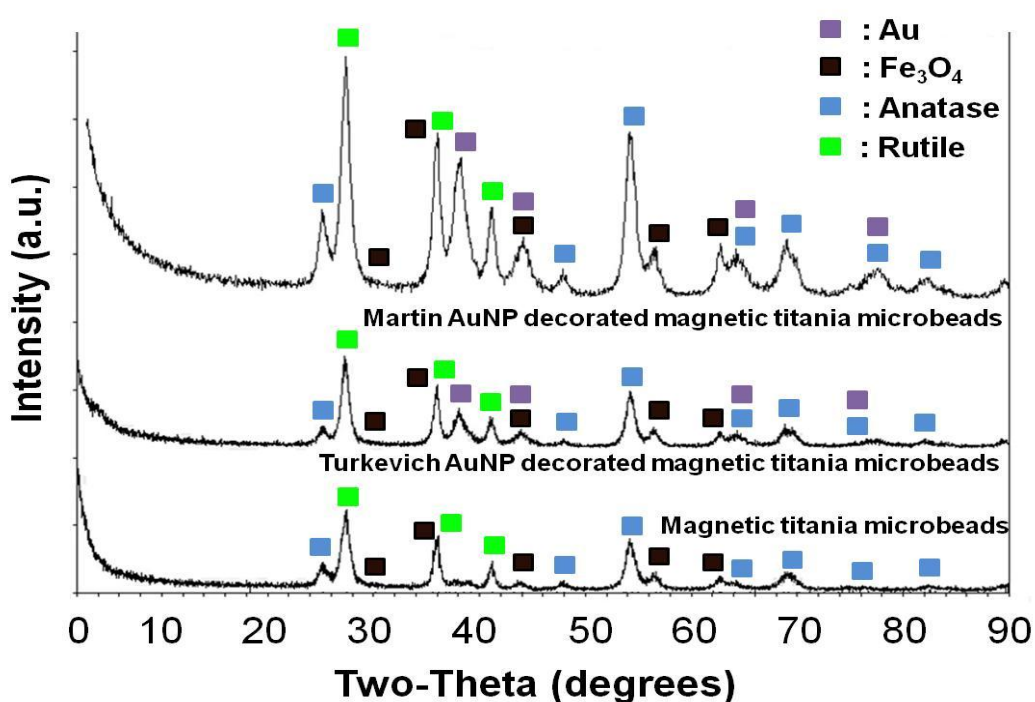


**Figure 4.20.** XRD patterns of magnetic titania microbeads, Turkevich and Martin AuNP decorated magnetic titania microbeads.

In addition to the anatase, rutile and Fe<sub>3</sub>O<sub>4</sub> peaks in the XRD patterns of the Turkevich and Martin AuNP decorated magnetic titania microbeads, the characteristic peaks at  $2\theta$ : 38°, 44°, 64° and 77° can be indexed to the (111), (200), (220) and (311) Bragg's reflections of cubic structure of metallic gold, respectively (Figure 4.20.).

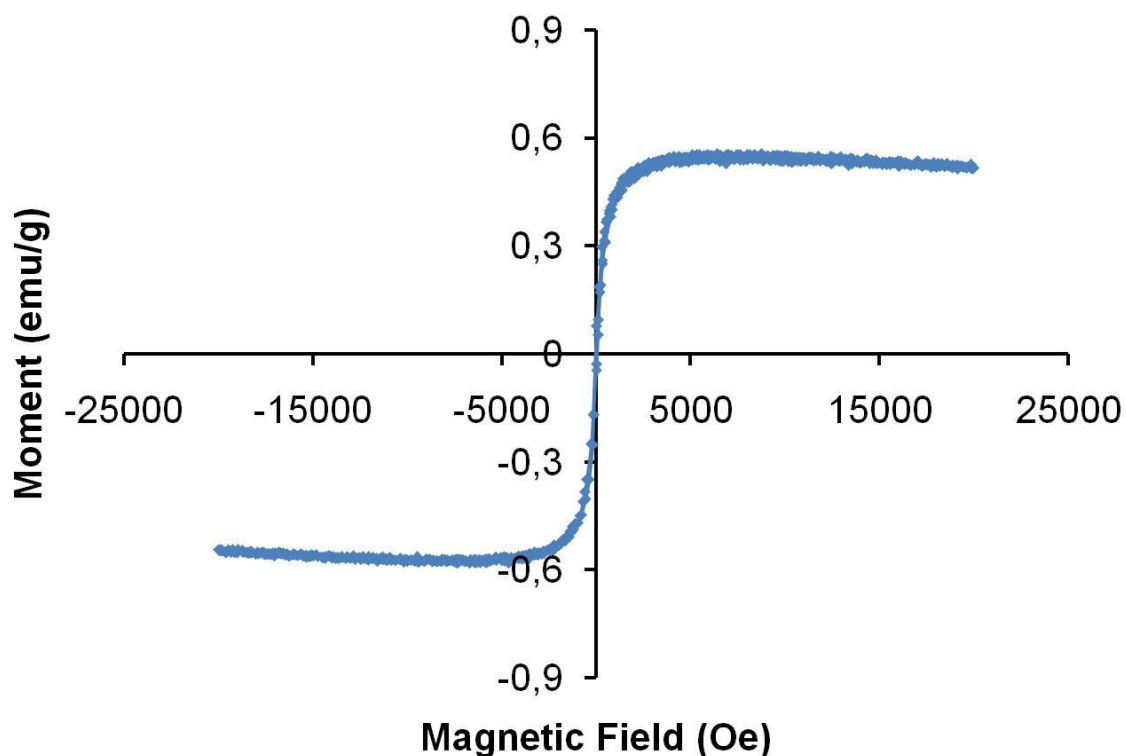


**Figure 4.21.** VSM curve of Turkevich and Martin GNP decorated magnetic titania microbeads.

Figure 4.21. showed that the magnetization curves of Turkevich and Martin AuNP decorated magnetic titania microbeads measured at 300K were exactly the same, Hence the magnetic saturation ( $M_s$ ) values of Turkevich and Martin AuNP decorated magnetic titania microbeads were the same (i.e. 0.5 emu/g). This value was also slightly lower than the magnetic saturation ( $M_s$ ) value of magnetic titania microbeads. This decrease should be probably due to the mass increase occurred depending upon the Au loading onto the magnetic titania microbeads. Turkevich and Martin AuNP decorated magnetic titania microbeads still exhibited superparamagnetic behaviors at room temperature.

#### 4.4. Photocatalytic Activity Measurements

TiO<sub>2</sub> is the most common photocatalyst that is used for the degradation of organic molecules particularly for phenolic compounds and textile dyes due to its high photocatalytic activity. Photocatalytic degradation rates of organic molecules are affected by many parameters like pH, catalyst concentration, crystal composition, specific surface area, initial reactant concentration and temperature. The photocatalytic activity of titania microbeads was examined by the photocatalytic degradations of an azo dye, RB5 and phenol as organic compounds.

##### 4.4.1. Photocatalytic Degradation of Remazol Black 5 Dye with Bare Titania Microbeads

RB5 is an azo dye which is non-biodegradable under aerobic conditions and is very stable due to its complex molecular structure [192,193]. Under anaerobic conditions azo dyes can be degraded but hazardous and carcinogenic aromatic amines are formed as degradation products [193,194]. However, by using titania microbeads as photocatalyst complete degradation of RB5 in the aqueous medium was achieved using Degussa TiO<sub>2</sub> nanoparticles ca. 21 nm in size [14]. In our case, a micron-size, monodisperse-porous TiO<sub>2</sub> microbeads were first tried as a potential packable photocatalyst. The molecular structure of RB5 is given in Figure 4.22.

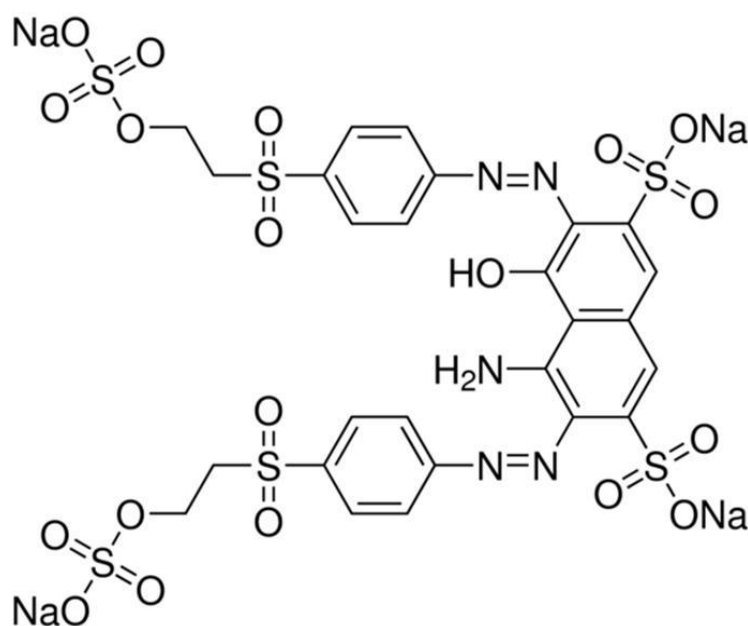


**Figure 4.22.** Molecular structure of RB5.

As seen in Figure 4.22., nitrogen to nitrogen double bonds (-N=N-) are the typical groups of azo dyes. Azo-bonds are the most active bonds in RB5 and can be oxidized either by positive holes or hydroxyl radicals which results in photocatalytic degradation of RB5 [195, 196].

The decolorization of RB5 dye solution with titania microbeads was monitored by UV-Vis spectroscopy. The concentration of RB5 was calculated based on the decrease in the absorbance peak at 598 nm, which was directly proportional to the decrease in the concentration of RB5. The UV-Vis spectra obtained at different time intervals during decolorization of RB5 dye solution (25 ppm, 100 mL) with titania microbeads (80 mg, calcination temperature: 450°C) at pH 7 are shown in Figure 4.23.

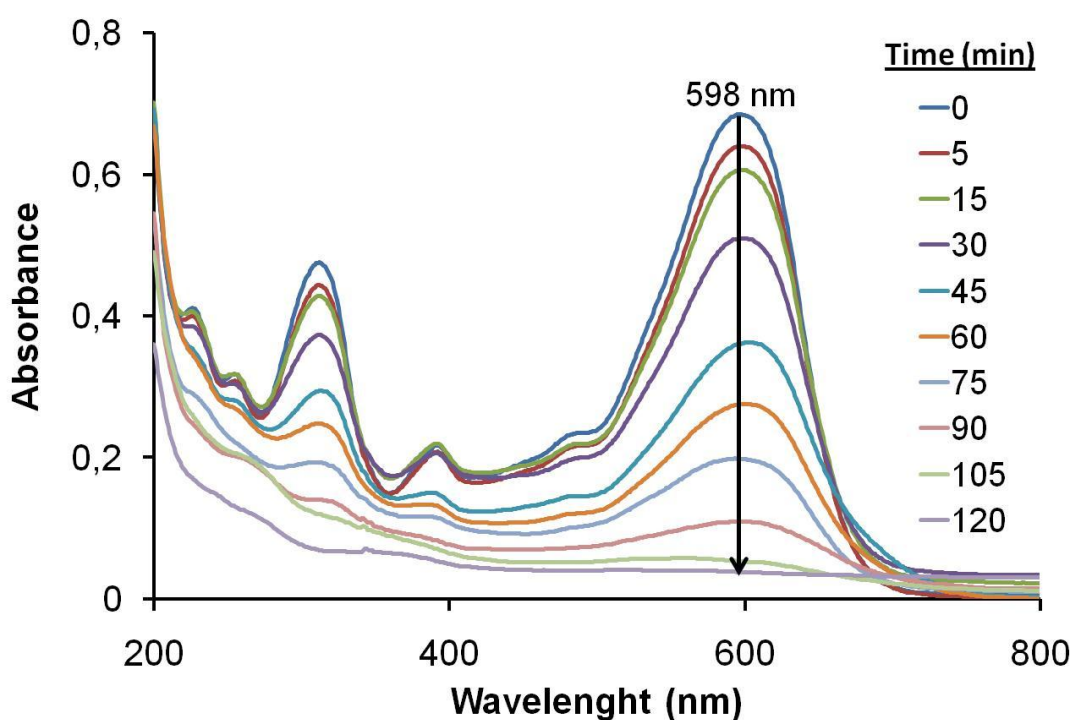


**Figure 4.23.** UV-Vis spectra at different times during the decolorization of RB5 dye solution. (Conditions: pH: 7, catalyst amount: 80 mg, calcination temperature: 450°C, RB dye solution: 25 ppm, 100 mL)

The decrease in the absorbance at 598 nm due to photocatalytic degradation can be clearly seen from Figure 4.23. The complete decolorization of RB5 dye solution was achieved within 120 min. The concentration of RB5 dye in the solution at

certain times was determined according to the absorbance peak of RB5 dye and is given in Figure 4.24.

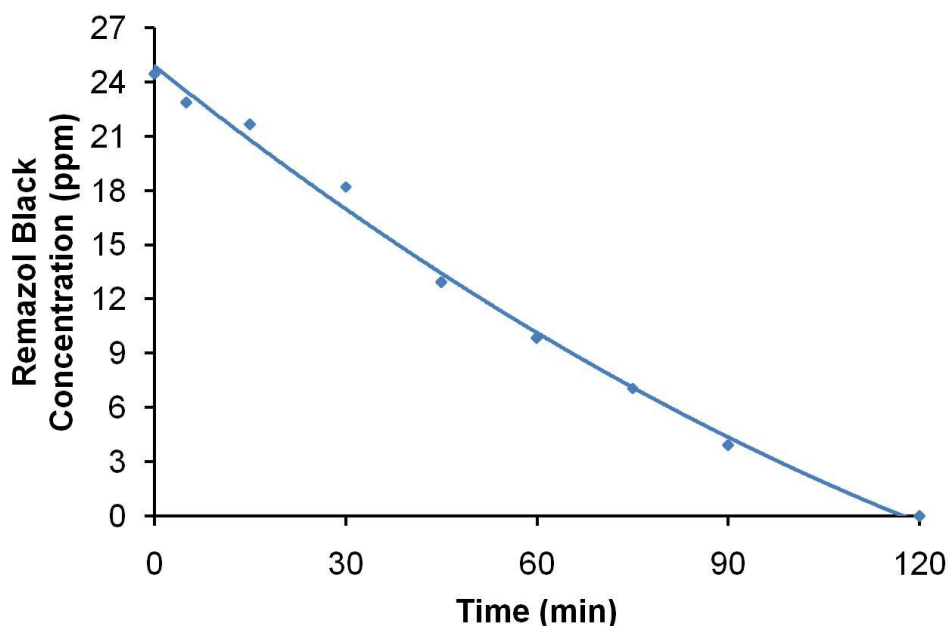


**Figure 4.24.** The variation of RB5 dye concentration with the time during the photocatalytic degradation. (Conditions: pH: 7, catalyst amount: 80 mg, calcination temperature: 450°C, RB5 dye solution: 25 ppm, 100 mL).

#### 4.4.1.1. Effect of Calcination Temperature

Titania photocatalysts in anatase phase show the highest photocatalytic activity. However, in some studies it was reported that pure anatase not always lead to the best photocatalytic performance [56, 57, 154]. The photocatalytic activity is also increased with higher surface area of the titania photocatalyst since the adsorption of higher amounts of reactant promotes the photodegradation reaction. Considering that the initial step of the photocatalytic degradation is the hydroxyl radical attack on the dye adsorbed onto the catalyst. Hence, the adsorption capacity of the photocatalyst is quite important. Higher surface area of the photocatalyst provides higher amounts of adsorbed dye which promotes the photocatalytic degradation. In order to obtain maximum photocatalytic activity, the surface area and the crystallinity of the titania photocatalyst should be considered together. The specific surface area and the crystallinity of titania microbeads significantly depend on the calcination temperature of titania-polymer composite

microbeads as discussed in Section 4.1.3.3. It was found that the specific surface area of monodisperse-porous titania microbeads decreased while the rutile form in the crystal structure increased with the increasing calcination temperature.

The effect of calcination temperature on the photocatalytic degradation of RB5 dye was investigated by the decolorization of RB5 solution (25 ppm, 100 mL, pH 3.5) with the bare titania microbeads (80 mg) calcined at different temperatures (450°C, 500°C, 550°C, 600°C). The variation of RB5 concentration during the decolorization with the bare titania microbeads calcined at different temperatures are given in Figure 4.25.

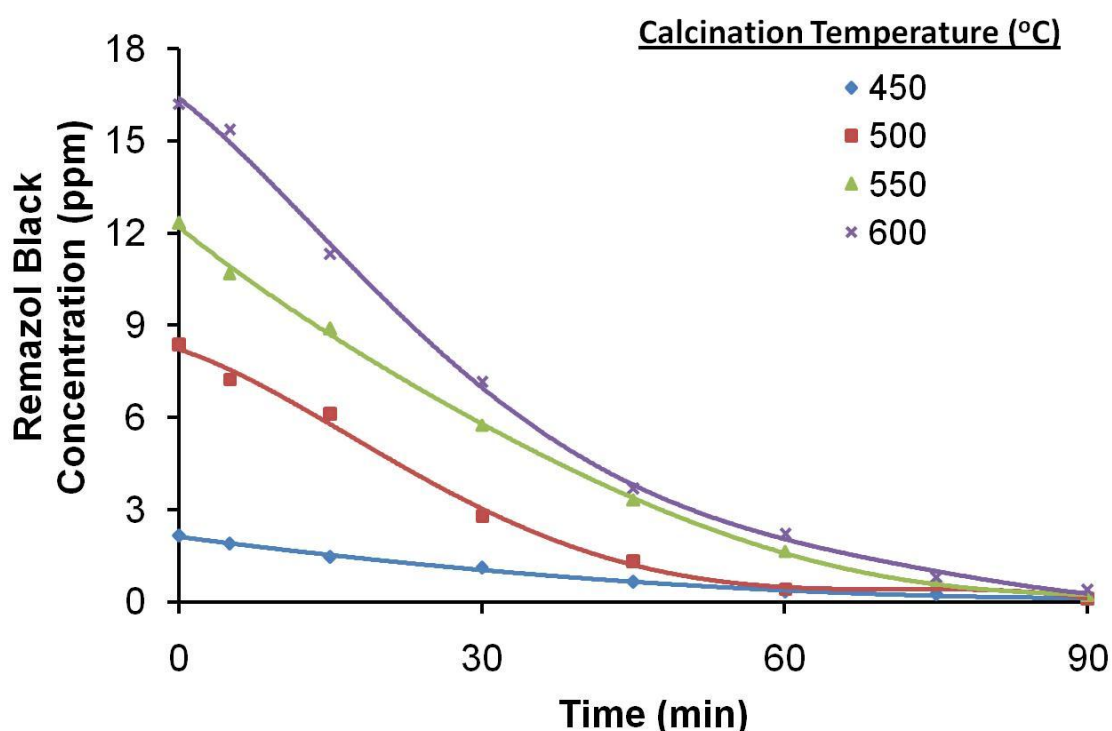


**Figure 4.25.** Effect of calcination temperature on the photocatalytic degradation of RB5 dye with bare titania microbeads. (Conditions: catalyst amount: 80 mg, RB5 dye solution: 25 ppm, 100 mL, pH: 3.5).

As a result of its highest specific surface area, almost 90 % w/w of RB5 dye was adsorbed by the bare titania microbeads calcined at 450°C in the solution before irradiation with a UV light-source. As seen in Figure 4.25., the adsorption of RB5 on bare titania microbeads decreased, with increasing the calcination temperature of the microbeads. This decrease should be related to the decreasing surface area

with the increasing calcination temperature. However, the time needed for the complete decolorization of RB5 dye solution was 90 min for all microbeads calcined at different temperatures. This result exposed that the crystalline structure of bare titania microbeads was not effective on the photocatalytic degradation of RB5 dye. By considering the behaviour in Figure 4.25., the titania microbeads produced at the calcination temperature of 450°C were selected as the most suitable photocatalyst among the tried samples since the highest initial decolorization rate was achieved with this sample.

#### **4.4.1.2. Effect of pH**

Due to the amphoteric nature of titania, the surface charge of titania microbeads directly changes depending on pH. Then the adsorption of RB5 onto the titania microbeads accordingly the photocatalytic degradation of RB5 are affected by the surface charge. The point of zero-charge for titania is obtained at pH 6.5. Under acidic conditions ( $\text{pH} \leq 6.5$ ), the titania microbeads are protonated, while under alkaline conditions ( $\text{pH} \geq 6.5$ ) they are deprotonated. Considering the  $\text{SO}_3^-$  groups of RB5 (Figure 4.22.), a strong interaction occurs with positively charged titania microbeads in an acidic medium which results in higher adsorption of RB onto titania microbeads. However, negatively charged titania microbeads repels RB5 and the adsorption decreases in an alkaline medium.

The effect of pH on the photocatalytic degradation rate of RB5 was investigated by the decolorization of RB5 dye solution (25 ppm, 100 mL) containing titania microbeads (80 mg, calcined at 450°C). The variation of RB5 concentration with the time during the decolorization of RB5 dye solution containing bare titania microbeads are given in Figure 4.26.

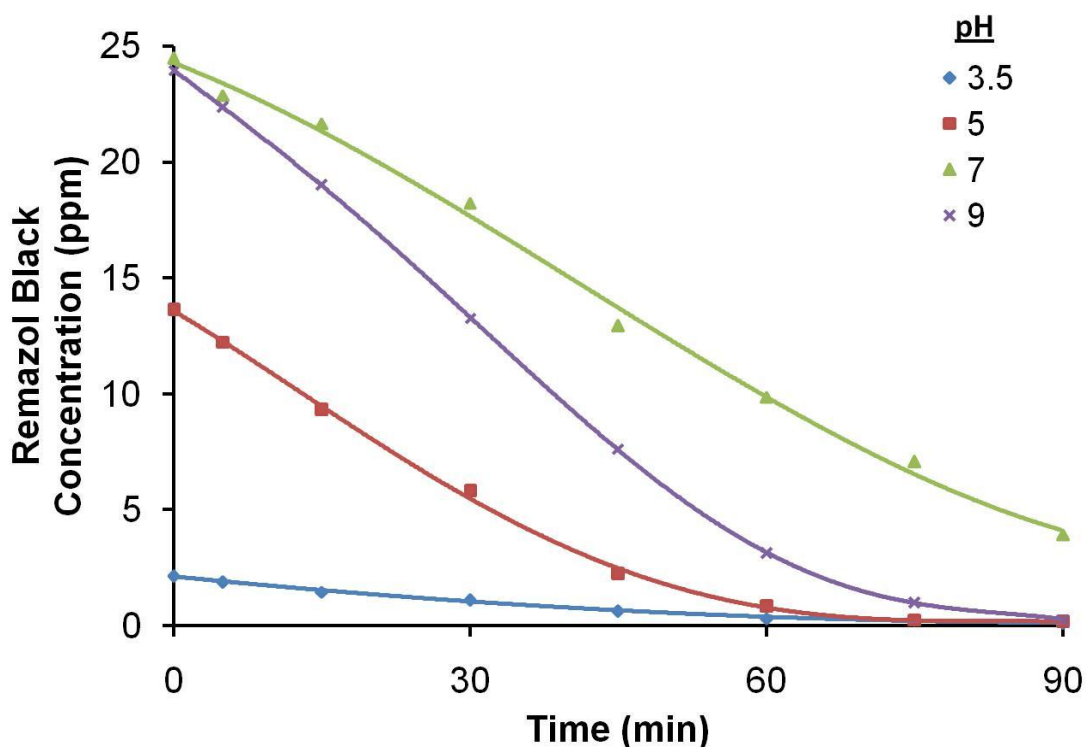


**Figure 4.26.** Effect of pH on the photocatalytic degradation rate of RB5 with bare titania microbeads.(Conditions: catalyst amount: 80 mg, calcination temperature: 450°C, RB5 dye solution: 25 ppm, 100 mL).

Before the irradiation with a UV light-source, nearly 90 % of RB5 dye in the solution was adsorbed by the titania microbeads at pH 3.5 due to the positively charged nature of titania microbeads (Figure 4.26.). Then highest decolorization rate was achieved at pH 3.5. The lowest adsorption and the lowest decolorization rate were obtained at pH 7. However, the decolorization rate at pH 9 was higher with respect to pH 7. This behaviour can be explained by the the higher concentration of hydroxyl radicals attacking to RB5 in the alkaline medium.

#### 4.4.1.3. Effect of Catalyst Amount

In the photocatalytic degradations, the determination of the most appropriate amount of photocatalyst is crucial to ensure the total absorption of efficient photons . Hence, the use of redundant catalyst is prevented [147]. On the other hand, the amount of photocatalyst at which all particles are fully illuminated depends on the geometry of the reactor and the conditions of the reaction.



The effect of catalyst amount on the photocatalytic degradation rate of RB5 was investigated by the decolorization of RB5 dye solution (25 ppm, 100 mL) with different amounts of bare titania microbeads (20 mg, 40 mg, 80 mg, calcined at 450°C). The variation of RB5 concentration with the time during the decolorization with different amounts of bare titania microbeads are given in Figure 4.27.

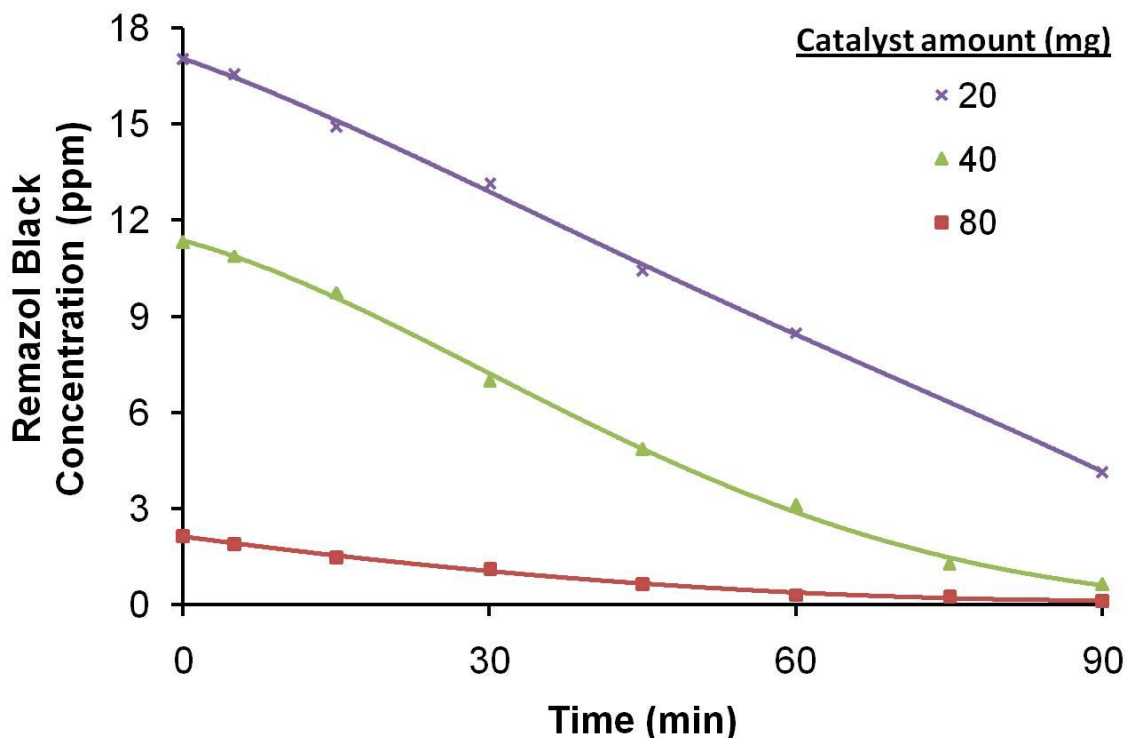


**Figure 4.27.** Effect of catalyst amount on the photocatalytic degradation rate of RB5 with bare titania microbeads.(Conditions: calcination temperature: 450°C, RB5 dye solution: 25 ppm, 100 mL, pH: 3.5).

Here, the decolorization of dye solution should be evaluated as a process progressing based on both adsorption and photocatalytic degradation. Hence, the rate of dye removal from the aqueous medium should be considered as a magnitude depending upon both the rate of dye adsorption and the rate of photocatalytic decomposition. Hence, the observed dye removal rate should be controlled by the stage progressing with lower rate. As seen in Figure 4.27., the amount of dye adsorbed onto the titania microbeads increased with the increasing amount of titania microbeads before the UV-irradiation. The increase in the total surface area of the photocatalyst is of course the reason of this behaviour. Although the time for the complete decolorization was nearly same for the

photocatalyst amounts of 40 and 80 mg, the dye adsorption onto the photocatalyst at the beginning of decolorization was extremely lower for the photocatalyst amount of 40 mg. Note that, the complete decolorization was not achieved within 90 min using 20 mg of bare titania microbeads. Although almost the same decolorization rates were achieved with 20 and 40 mg of bare titania microbeads, the concentration of RB5 was still high at the end of 90 min period for the photocatalyst amount of 20 mg since the initial dye removal via adsorption was too low with this amount.

#### **4.4.1.4. Effect of Initial RB5 Dye Concentration**

In photocatalytic degradations, the decolorization rate decreases with the increasing initial concentration of organic contaminant. All the catalytic sites of photocatalyst are occupied at high initial concentrations of organic molecules, which results in low degradation rate as the photocatalytic degradation takes place on the surface of the non-porous photocatalyst [15, 197, 198]. The effect of initial RB5 dye concentration on the photocatalytic degradation rate of RB5 dye was investigated by the decolorization of RB5 dye solution with different concentrations (25 ppm, 50 ppm, 100 ppm, 100 mL) with bare titania microbeads (80 mg, calcined at 450°C). The variation of RB5 dye concentration with the time during the decolorization of RB5 dye solution with bare titania microbeads are given in Figure 4.28.

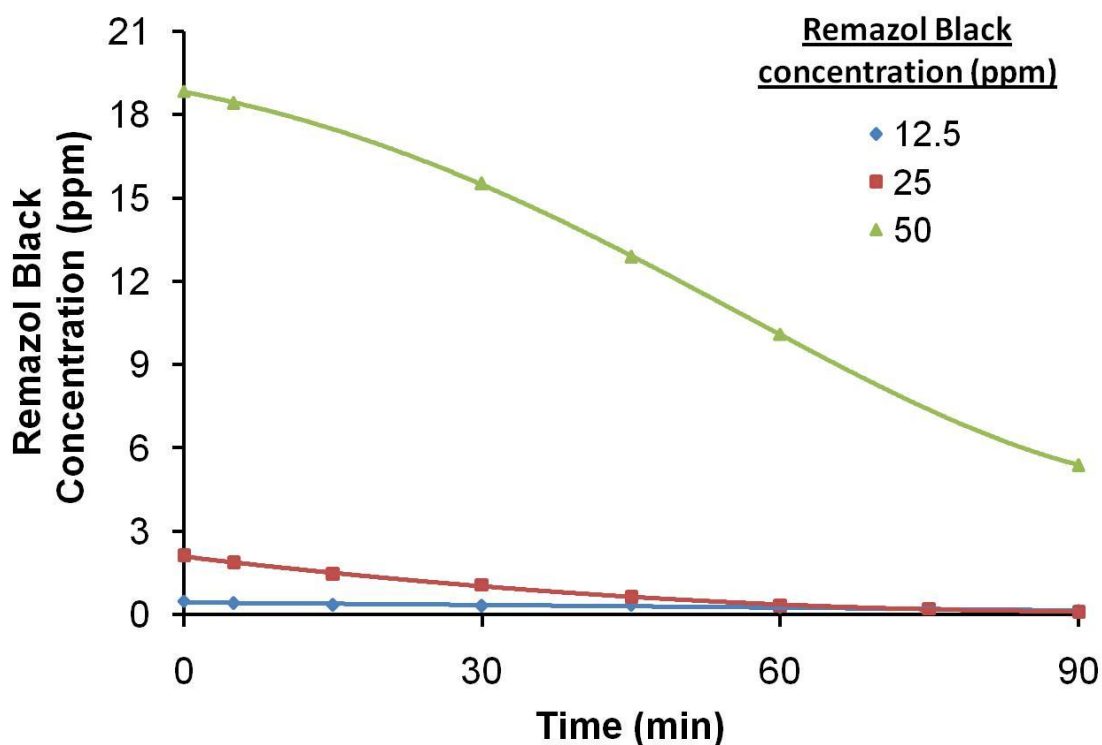


**Figure 4.28.** Effect of initial RB5 dye concentration on the photocatalytic degradation rate of RB5 dye with bare titania microbeads. (Conditions: catalyst amount: 80 mg, calcination temperature: 450°C, pH: 3.5).

The results showed that the decolorization rate of RB5 dye solution strongly depends on the initial RB5 dye concentration. As seen in Figure 4.28., the photocatalytic degradation rate (i.e. the variation rate of RB5 concentration with the time) significantly increased with the increasing initial concentration of RB5 dye. This result should be explained by the higher intraparticle diffusion rate of RB5 depending upon its higher solution concentration. It should be also noted that although the photocatalytic degradation rate was higher, the time necessary for complete decolorization was longer at higher RB5 concentration.

#### 4.4.1.5. Effect of Au Loading

It is expected that loading of AuNPs on titania microbeads will increase the photocatalytic activity by decreasing the band-gap of titania microbeads. As the band-gap of the titania microbeads decreases, the absorption of visible light increases which results in an enhancement in the photocatalytic activity of the photocatalyst. Photocatalytic activity of Au loaded titania microbeads depends on various factors like pH, AuNP size, and Au loading. To determine the effect of

AuNP loading on the photocatalytic activity, the most appropriate values for pH and AuNP size were determined. These studies are described below:

#### 4.4.1.5.1. Determination of appropriate pH

The effect of pH on the photocatalytic degradation rate of RB5 with Turkevich AuNP decorated bare titania microbeads (80 mg, Au loading (w/w): 5 %) was investigated by decolorization of RB5 dye solution (25 ppm, 100 mL). The variation of RB5 concentration at different pH in the presence of Turkevich AuNP decorated titania microbeads is given in Figure 4.29.

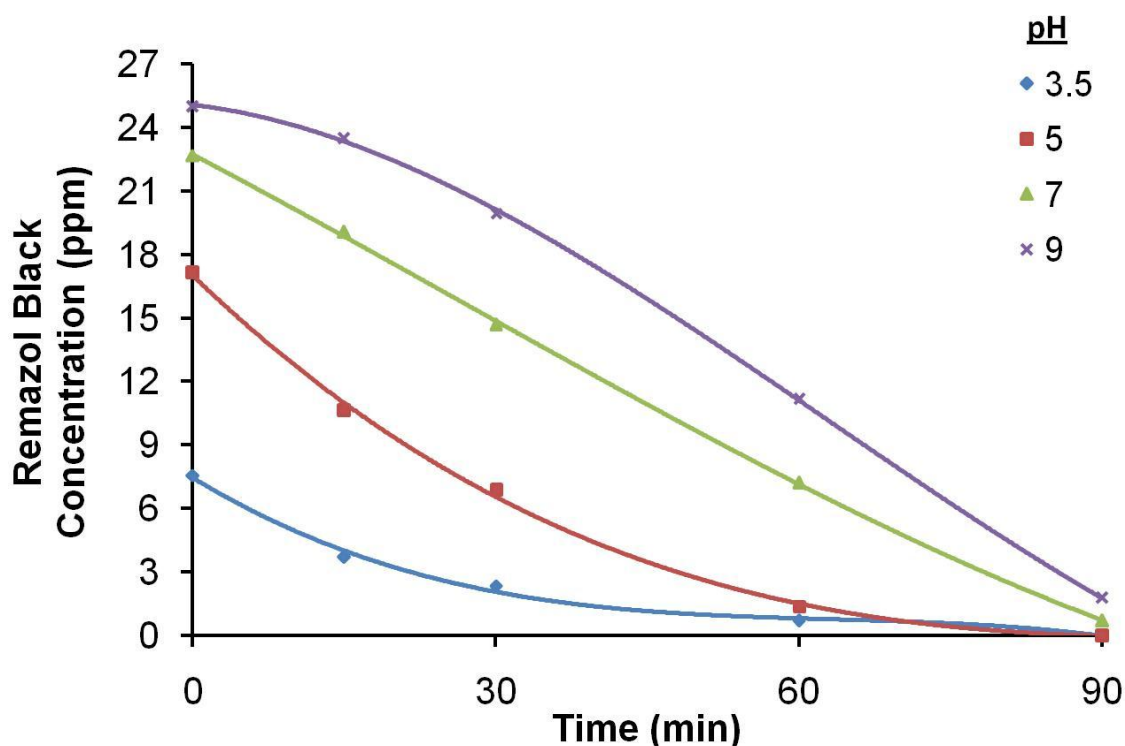


**Figure 4.29.** Effect of pH on the photocatalytic degradation rate of RB5 dye with Turkevich AuNP decorated bare titania microbeads. (Conditions: catalyst amount: 80 mg, Au loading (w/w): 5 %, RB5 dye solution: 25 ppm, 100 mL).

When compared with bare titania microbeads (Figure 4.26.), less amount of RB5 was adsorbed by Turkevich AuNP decorated bare titania microbeads particularly in acidic region (i.e. pH 3 and 5) before irradiation with a UV light-source. The reasons of lower adsorption are: 1) less positively charged microbeads due to the negatively charged citrate ions on AuNPs and 2) lower SSA because of loading Turkevich AuNPs particularly into the mesopores of bare titania microbeads.

Complete decolorization of RB5 in solution was again obtained within 90 min with acidic pHs. While complete decolorization was not obtained at pH 7 with bare titania microbeads in 90 min, it was achieved with the Turkevich AuNP decorated titania microbeads in 90 min, it was achieved with the Turkevich AuNP decorated titania microbeads. The reason for lower decolorization rate at pH 9 compared to the bare titania microbeads can be attributed to the higher negative charge on the microbeads in the alkaline medium because of the citrate ions on immobilized AuNPs. As a result, only an enhancement in the photocatalytic activity was observed at pH 7, by loading citrate stabilized Turkevich AuNPs onto the bare titania microbeads.

#### 4.4.1.5.2. Determination of appropriate AuNP size

The effect of AuNP size on the photocatalytic degradation rate of RB5 was investigated by the decolorization of RB5 dye solution (25 ppm, 100 mL) with AuNP decorated bare titania microbeads (80 mg, Au loading (w/w): 5 %) with different AuNP sizes. The variation of RB5 concentration with the time during the decolorization of RB5 dye solution with bare titania microbeads and AuNP decorated bare titania microbeads with different AuNP sizes are comparatively given in Figure 4.30.

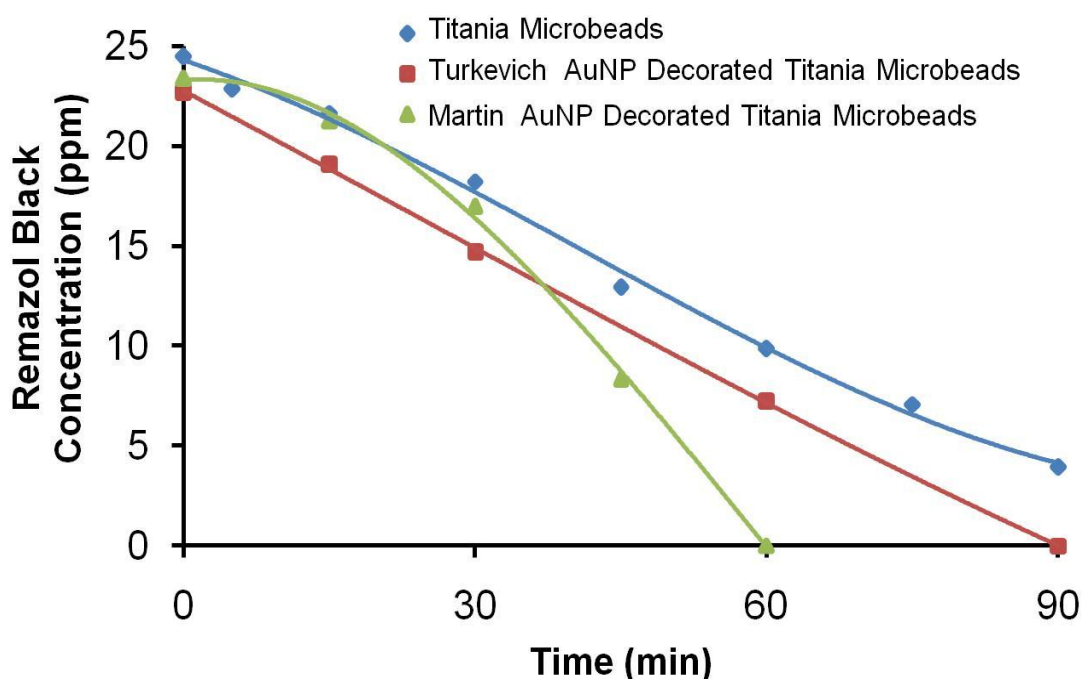


**Figure 4.30.** Effect of AuNP size on the photocatalytic degradation rate of RB5 dye. (Conditions: catalyst amount: 80 mg, Au loading (w/w): 5 %, RB dye solution: 25 ppm, 100 mL, pH: 7).

As seen in Figure 4.30., the loading of AuNPs onto the bare titania microbeads did not significantly affect on the amount of RB5 dye adsorbed onto the titania microbeads before irradiation as the surface charge of bare titania microbeads was zero at pH 7. However, the enhancement in the decolorization rate of RB5 dye solution was observed with both Martin and Turkevich AuNP decorated bare titania microbeads compared to the bare titania microbeads. Under these conditions, the highest decolorization rate was observed with the Martin AuNP decorated bare titania microbeads in which the AuNP size was smaller. Kamat et al. also reported that small AuNPs induce larger shifts in the Fermi level than the large particles do, which means that the size of AuNPs directly effects photocatalytic activity [199].

#### **4.4.1.5.3. Effect of AuNP loading at the appropriate pH and appropriate AuNP size**

The effect of Au loading on the photocatalytic degradation rate of RB5 dye was investigated by the decolorization of RB5 dye solution (25 ppm, 100 mL) at pH 7 with Turkevich AuNP decorated bare titania microbeads (80 mg) with different Au loadings. The variation of RB5 concentration with the time during the decolorization of RB5 dye solution with Turkevich AuNP decorated bare titania microbeads with different Au loadings are given in Figure 4.31.

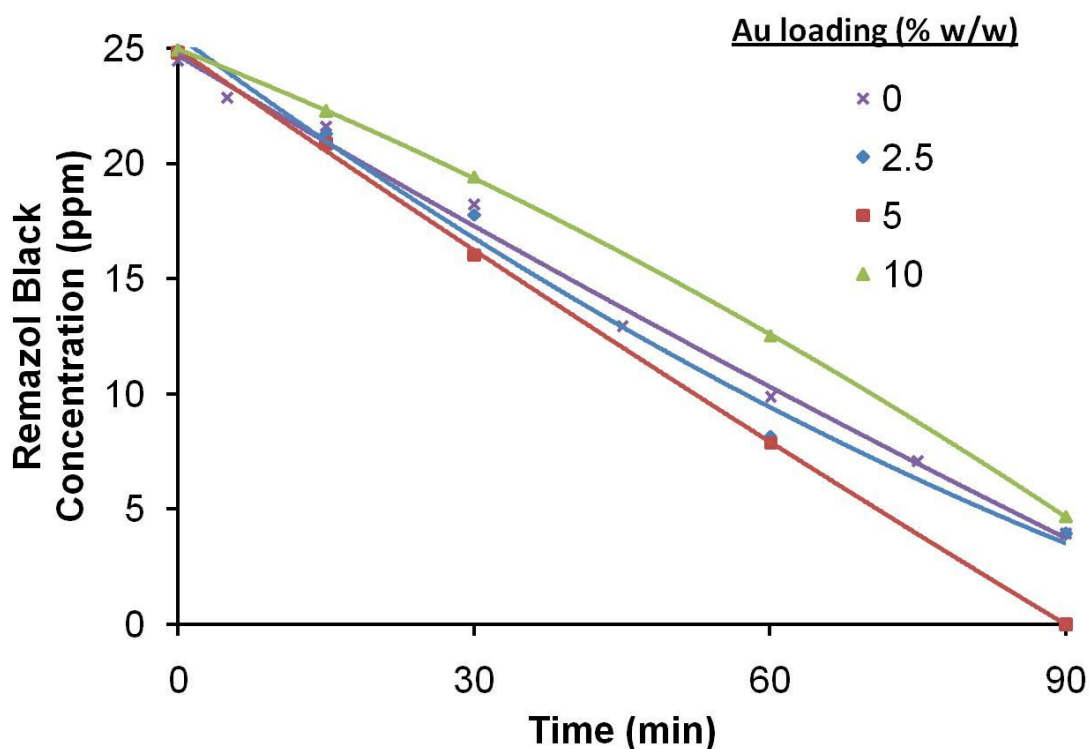


**Figure 4.31.** Effect of weight percent of Au loading on the photocatalytic degradation rate of RB5 dye with Turkevich AuNP decorated bare titania microbeads. (Conditions: catalyst amount: 80 mg, RB5 dye solution: 25 ppm, 100 mL, pH: 7).

10 % of Au loading with the Turkevich AuNPs onto bare titania microbeads did not provide an enhancement in the decolorization rate of RB5 dye solution. The possible reasons of this behaviour 1) the blocking of catalytic active sites on titania microbeads by the AuNPs with high surface concentration of AuNPs and 2) the decrease in the light permeability within the titania microbeads due to the high surface concentration of AuNPs. As seen in Figure 4.31., the rate of decolorization with Turkevich AuNP decorated bare titania microbeads with 5 % of Au loading was slightly higher compared to 2.5 % of Au loading. The most appropriate Au loading was chosen as 5 % for the Turkevich AuNP decorated bare titania microbeads. The effect of Au loading on the photocatalytic degradation rate of RB5 dye was investigated by the decolorization of RB5 dye solution (25 ppm, 100 mL) at pH 7 with Martin AuNP decorated bare titania microbeads (80 mg) with different Au loadings. The variation of RB5 concentration with time during the decolorization of RB5 dye solution with Martin AuNP decorated-bare titania microbeads with different Au loadings are given in Figure 4.32.

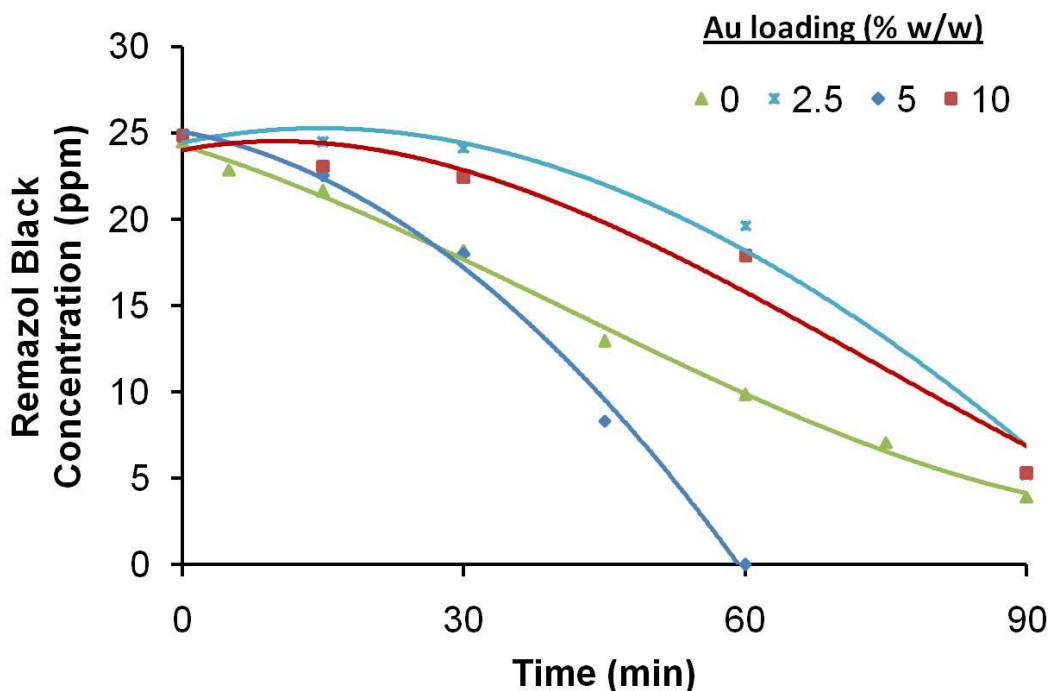


**Figure 4.32.** Effect of weight percent of Au loading on the photocatalytic degradation rate of RB5 dye with Martin AuNP decorated bare titania microbeads. (Conditions: catalyst amount: 80 mg, RB dye solution: 25 ppm, 100 mL, pH: 7).

As seen in Figure 4.32., only an enhancement in the photocatalytic activity was achieved with the Au loading of 5 % using Martin AuNP decorated titania microbeads. The complete decolorization of RB5 dye solution was observed in a shorter time (60 min) with respect to the bare titania microbeads under the same conditions. The enhancement in the photocatalytic degradation rate of RB5 could not be observed with the other Au loadings. 2.5 % of AuNP loading was probably insufficient for the enhancement. The blocking of photocatalytic active sites and the decrease in the light permeability due to the high surface concentration of AuNPs should be evaluated as the reasons involving lower decolorization rate with 10 % of Au loading.



#### 4.4.1.6. Reusability

The reusability was investigated only with the Martin AuNP decorated titania microbeads which has the highest photocatalytic activity. To obtain the reusability of Martin AuNP decorated bare titania microbeads (80 mg, Au loading: 5 % (%w/w)), the decolorization of RB5 dye solution (25 ppm, 100 mL) at pH 7 was repeated for five times under the same conditions. The total decolorization time was 60 min. After each experiment, the photocatalyst was recovered by rinsing with water for several times for reuse. The percent of removal values for RB5 dye achieved after each cycle are given in Figure 4.33.

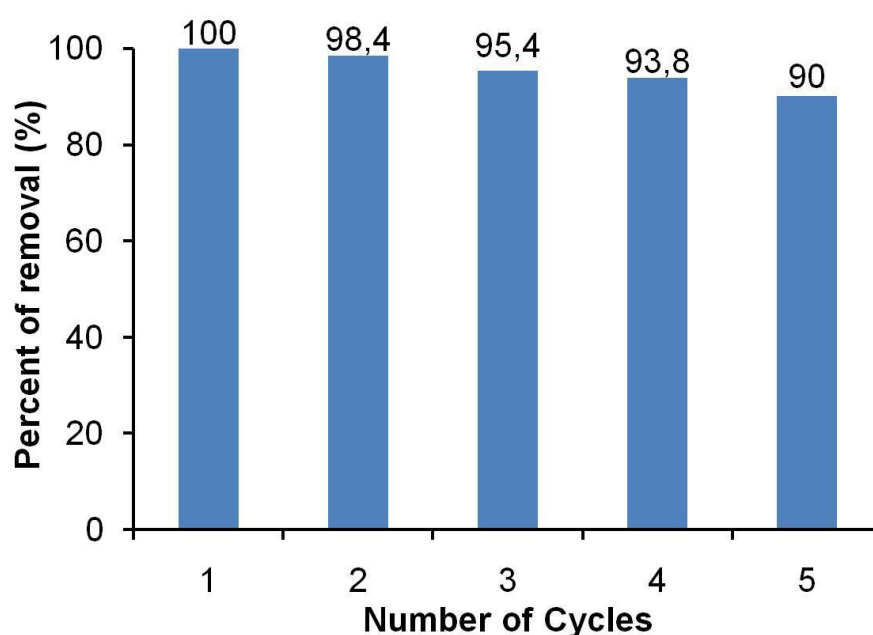


**Figure 4.33.** Reusability of Martin AuNP decorated bare titania microbeads in decolorization of RB5 dye solution. (Conditions: catalyst amount: 80 mg, Au loading (%w/w): 5 %, RB5 dye solution: 25 ppm, 100 mL, pH: 7).

The percent of removal decreased about 5 % after the third cycle. At the end of the fifth cycle, only 10 % of decrease in the percent removal was observed (Figure 4.33.). This decrease could be ascribed to the adsorption of degradation products on the photoactive sites of the Martin AuNP decorated titania microbeads.

#### **4.4.2. Photocatalytic Degradation of RB5 with Magnetic Titania Microbeads**

It is important to achieve the photocatalytic degradation of RB5 dye with magnetic titania microbeads because photocatalyst can be easily recovered from the reaction medium by applying an external magnetic field.

##### **4.4.2.1. Effect of pH**

Due to the amphoteric nature of titania and magnetic nanoparticles, the surface charge of magnetic titania microbeads directly changes with the pH of the reaction medium. Surface charge affects on the adsorption of RB5 onto the magnetic titania microbeads accordingly the photocatalytic degradation of RB5 dye. The points of zero charge for  $\text{TiO}_2$  and  $\text{Fe}_3\text{O}_4$  are about at pH 6.5 and pH 7.9, respectively [161]. As mentioned in chapter 4.4.1.2, magnetic titania microbeads are protonated under acidic conditions ( $\text{pH} \leq 6.5$ ), while they are deprotonated under alkaline conditions ( $\text{pH} \geq 6.5$ ). The addition of  $\text{Fe}_3\text{O}_4$  nanoparticles into the structure of titania microbeads increases the surface charge in both acidic and alkaline conditions. In the acidic medium, the interaction between RB5 molecules containing  $\text{SO}_3^-$  groups and magnetic titania microbeads should be stronger due to the higher positive charge originating from magnetic nanoparticles on the microbeads with respect to the bare titania microbeads. Hence, higher RB5 adsorption onto the magnetic titania microbeads should be observed. However, in the alkaline medium, the electrostatic repulsion between the RB5 molecules and more negatively charged magnetic titania microbeads should be stronger which diminishes the adsorption of RB5 dye onto the microbeads.

The effect of pH on the photocatalytic degradation rate of RB5 was investigated by the decolorization of RB5 dye solution (25 ppm, 100 mL) at different pH with magnetic titania microbeads (80 mg, calcined at  $450^\circ\text{C}$ ). The variation of RB5 concentration with the time with magnetic titania microbeads are given in Figure 4.34. for different pH values.

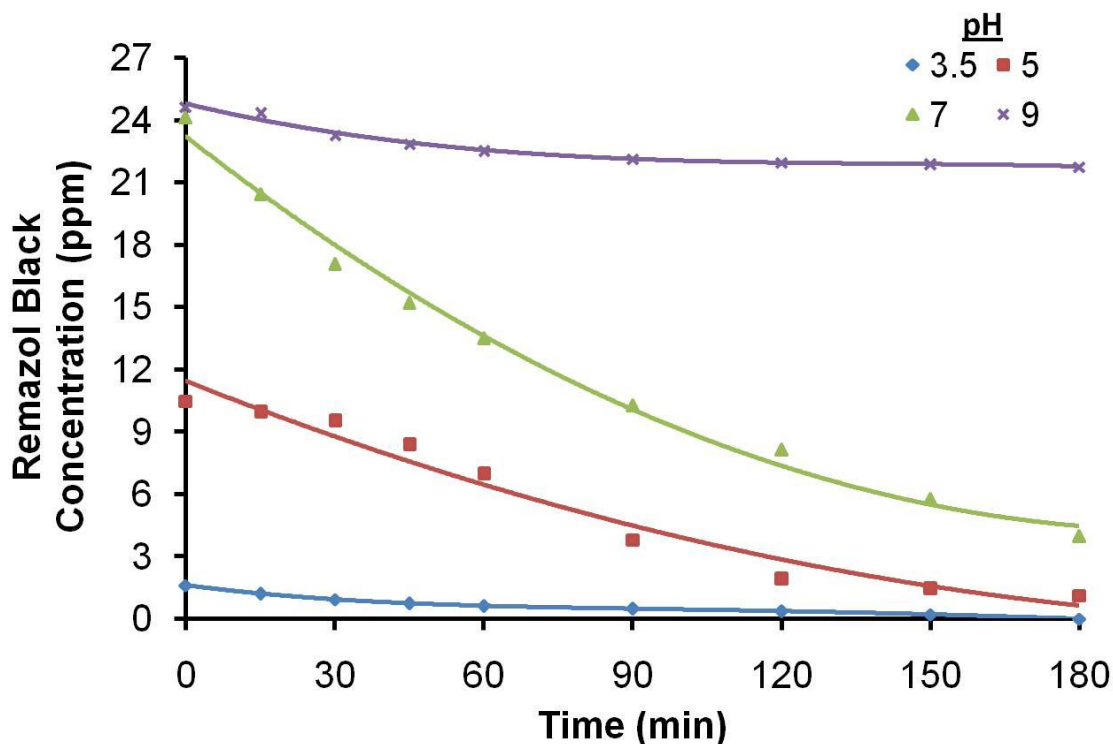


**Figure 4.34.** Effect of pH on the photocatalytic degradation rate of RB5 dye with magnetic titania microbeads. (Conditions: catalyst amount: 80 mg, calcination temperature: 450°C, RB dye solution: 25 ppm, 100 mL).

When compared with the bare titania microbeads (Figure 4.26.), higher RB5 adsorption onto the magnetic titania microbeads was observed in the acidic medium before the irradiation. As expected the initial concentrations of RB5 dye in the solutions was nearly same at pH 7 and pH 9 as there was no significant interaction between the RB5 dye and magnetic titania microbeads. The complete decolorization with the magnetic titania microbeads was achieved only in the acidic medium at extended times (180 min). Hence, a decrease in the photocatalytic activity was observed by the magnetization with respect to the bare titania microbeads. The transfer of electrons and holes from TiO<sub>2</sub> to magnetic iron oxide nanoparticles and their recombination on the magnetic iron oxide core and the decrease in the light permeability within the titania microbeads due to the magnetic iron oxide nanoparticles are probably the reasons for the decrease in the photocatalytic activity with respect to the bare titania microbeads. The decolorization of RB5 dye solution at pH 9 could not be achieved probably due to

high electrostatic repulsion between the negatively charged magnetic titania microbeads and RB5.

#### 4.4.2.2. Effect of Catalyst Amount

The effect of catalyst amount on the photocatalytic degradation rate was investigated by the decolorization of RB5 dye solution (25 ppm, 100 mL) with different amounts of magnetic titania microbeads (20 mg, 40 mg, 80 mg, calcined at 450°C). The variation of RB5 concentration with the time during the decolorization of RB5 dye solution in the presence of magnetic titania microbeads are given in Figure 4.35.

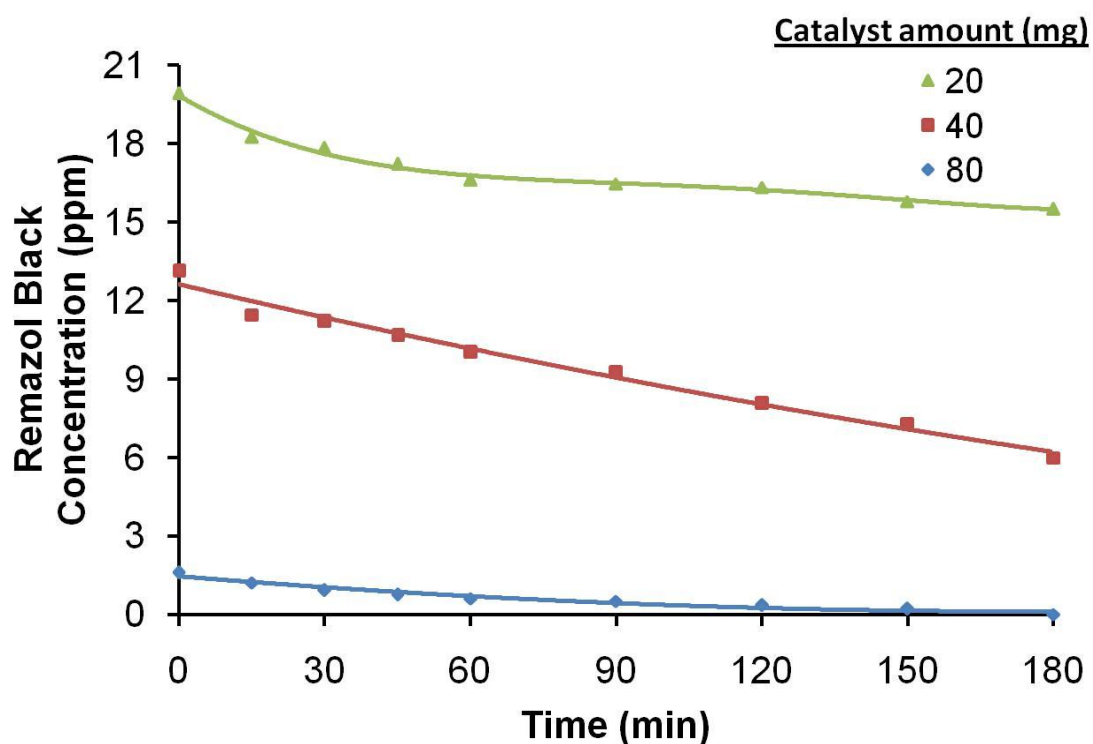


**Figure 4.35.** Effect of catalyst amount on the photocatalytic degradation rate of RB5 dye with magnetic titania microbeads. (Conditions: calcination temperature: 450°C, RB dye solution: 25 ppm, 100 mL, pH: 3.5).

As seen in Figure 4.35., RB5 adsorption onto the magnetic titania microbeads increased by increasing the amount of photocatalyst. The complete decolorization was only achieved with 80 mg of magnetic titania microbeads within 180 min. Lower amounts of magnetic titania microbeads was not enough to obtain complete decolorization.

#### 4.4.2.3. Effect of RB5 Dye Concentration

The effect of initial dye concentration on the photocatalytic degradation rate was investigated by the decolorization of RB dye solution with different concentrations (25 ppm, 50 ppm, 100 ppm, 100 mL) in the presence of magnetic titania microbeads (80 mg, calcined at 450°C). The variation of RB5 concentration with the time during the decolorization of RB5 dye solution with different concentrations in the presence of magnetic titania microbeads are given in Figure 4.36.

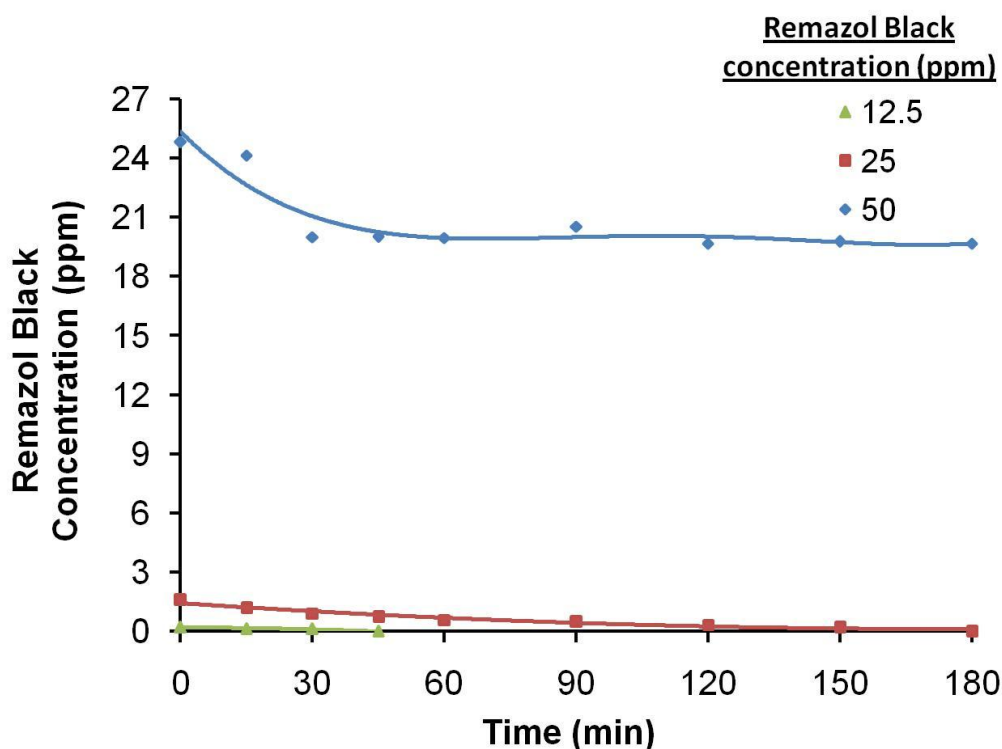


**Figure 4.36.** Effect of initial dye concentration on the photocatalytic degradation rate of RB5 dye in the presence of magnetic titania microbeads (Conditions: catalyst amount: 80 mg, calcination temperature: 450°C, pH: 3.5).

The results showed that the decolorization rate strongly depended on the initial RB5 dye concentration. Increasing the initial concentration increased the time needed for the complete decolorization of RB5 dye solution. The generation rate of hydroxyl radicals was reduced since some of the photocatalytic active sites were occupied by the adsorbed RB5 dye molecules. The transfer of electrons and holes from  $\text{TiO}_2$  to magnetic iron oxide nanoparticles could be the other possible reasons explaining this behaviour.

#### **4.4.2.4. Effect of Au Loading**

The photocatalytic activity of AuNP loaded magnetic titania microbeads was investigated by changing pH, AuNP size and AuNP loading onto the magnetic titania microbeads. The results of these studies are given below:

##### **4.4.2.4.1. Effect of pH**

The effect of pH on the photocatalytic degradation rate was investigated by the decolorization of RB5 dye solution (25 ppm, 100 mL) with Turkevich AuNP decorated magnetic titania microbeads (80 mg, Au loading (w/w): 5 %). The variation of RB5 concentration with the time during the decolorization of RB5 dye solution at different pH values containing Turkevich AuNP decorated magnetic titania microbeads are given in Figure 4.37.

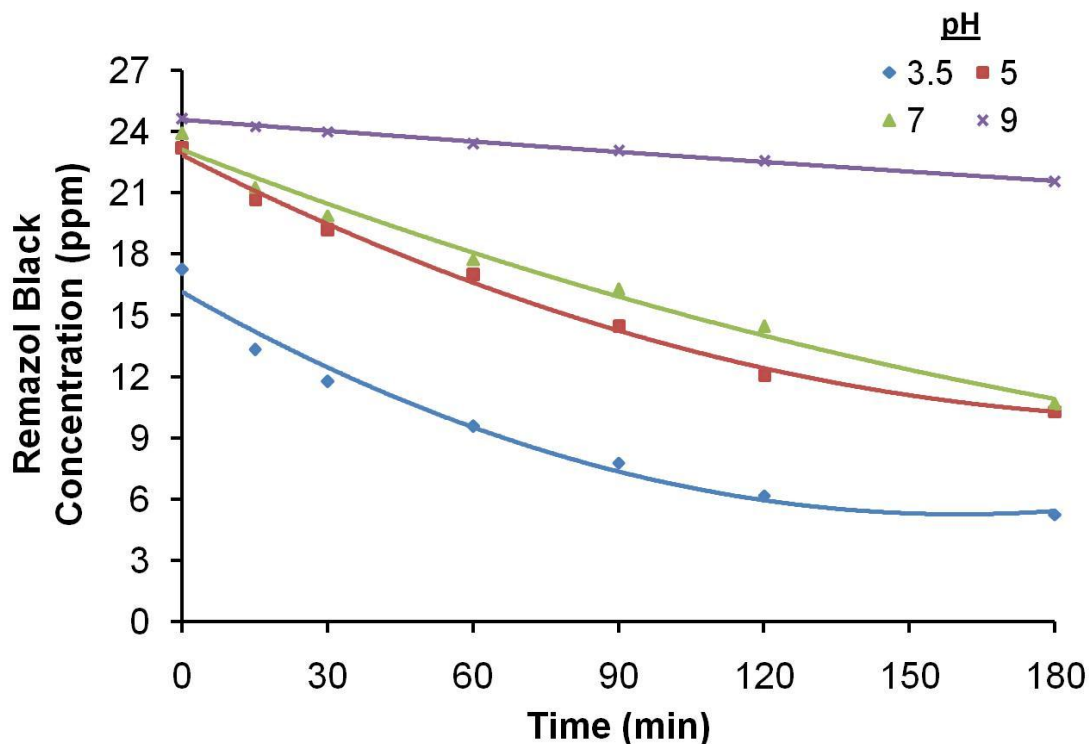


**Figure 4.37.** Effect of pH on the photocatalytic degradation rate of RB5 dye with Turkevich AuNP decorated magnetic titania microbeads. (Conditions: catalyst amount: 80 mg, Au loading (w/w): 5 %, RB dye solution: 25 ppm, 100 mL).

Detrimental effects were observed on the adsorption of RB5 dye before irradiation and photocatalytic degradation of RB5 dye at all pH values by decorating magnetic titania microbeads with the Turkevich AuNPs. As seen in Figure 4.37., the complete decolorization could not be achieved at all pH values. The reasons of these detrimental effects could be: 1) the formation of less positively charged microbeads due to the negatively charged citrate ions of AuNPs, 2) the generation of less hydroxyl radicals due to the transfer of electrons and holes from titania to magnetic iron oxide nanoparticles and 3) the decrease in the light permeability of titania microbeads by the incorporation of Turkevich AuNPs.

#### 4.4.2.4.2. Effect of Gold Nanoparticle Size

The effect of AuNP size on the photocatalytic degradation rate was investigated by the decolorization of RB5 dye solution (25 ppm, 100 mL) with the magnetic titania microbeads carrying AuNPs with different sizes (80 mg, Au loading (w/w): 5

%). The variation of RB5 concentration with the time during the decolorization of RB5 dye solution with magnetic titania microbeads and AuNP decorated magnetic titania microbeads are comparatively given in Figure 4.38.

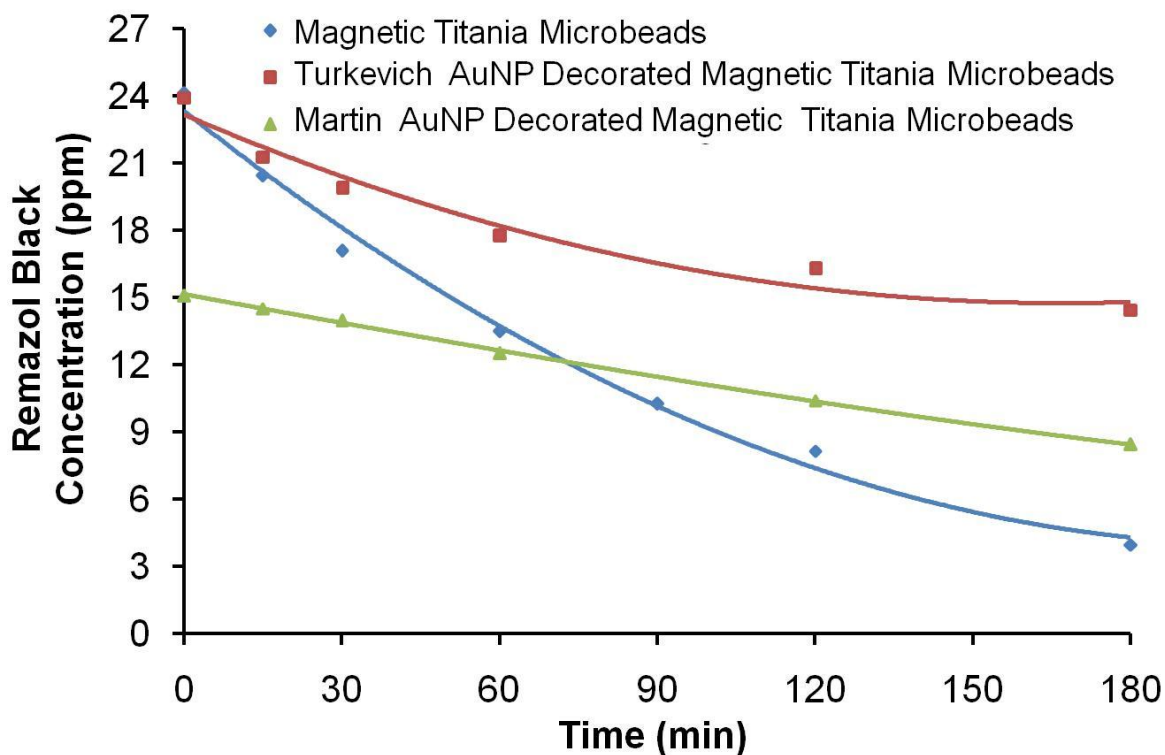


**Figure 4.38.** Effect of AuNP size on the photocatalytic degradation rate of RB5 dye. (Conditions: catalyst amount: 80 mg, Au loading (w/w): 5 %, RB5 dye solution: 25 ppm, 100 mL, pH: 7).

As seen in Figure 4.38., no significant enhancement was observed in the photocatalytic degradation rate of RB5 at pH 7 by loading Martin and Turkevich AuNPs onto the magnetic titania microbeads. The complete decolorization of RB5 dye solution could not be achieved in 180 min with all magnetic photocatalysts.

#### 4.4.2.4.3. Effect of of Au Loading

The effect of Au loading on the photocatalytic degradation rate was investigated by the decolorization of RB5 dye solution (25 ppm, 100 mL) at pH 7 with Martin AuNP decorated magnetic titania microbeads (80 mg) with different Au loadings. The variation of RB5 concentration with the time during the decolorization with Martin



AuNP decorated magnetic titania microbeads with different Au loadings are given in Figure 4.39.

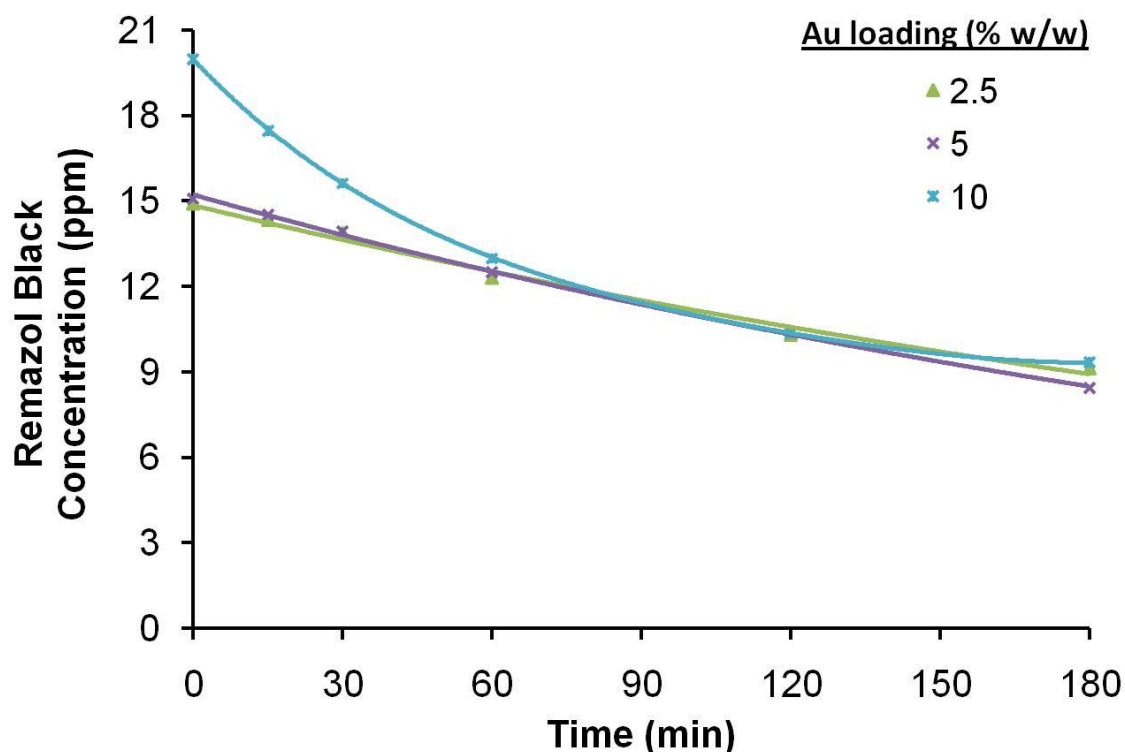


**Figure 4.39.** Effect of Au loading on the photocatalytic degradation rate of RB5 with Martin AuNP decorated magnetic titania microbeads. (Conditions: catalyst amount: 80 mg, RB dye solution: 25 ppm, 100 mL, pH: 7).

As seen in Figure 4.39., a certain effect of weight percent of Au loading on photocatalytic activity of Martin AuNP decorated magnetic titania microbeads could not be obtained. The complete decolorization of RB5 dye solution could not be achieved with none of the weight percents of Au loading.

#### 4.4.2.5. Reusability

The reusability was investigated only for magnetic titania microbeads which has the highest photocatalytic activity. To obtain the reusability of magnetic titania microbeads (80 mg), the photocatalytic degradation of RB5 dye solution (25 ppm, 100 mL) at pH 3.5 was repeated for five times under the same conditions. After each experiment, the photocatalyst was recovered by rinsing with water for several times for reuse. The percent of dye removal in each run is given in Figure 4.40.

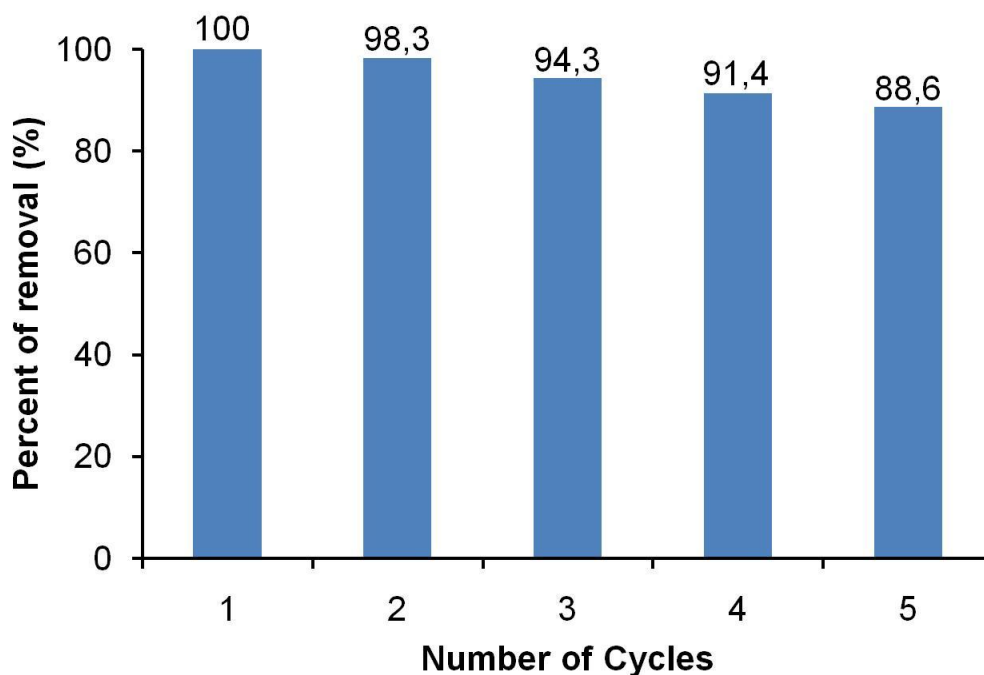


**Figure 4.40.** Reusability of magnetic titania microbeads in the decolorization of RB5 dye solution. (Conditions: catalyst amount: 80 mg, calcination temperature: 450°C, RB5 dye solution: 25 ppm, 100 mL, pH: 3.5)

The percent of dye removal decreased nearly 6 % after 3 cycles and was 88.6 % after being reused five times (Figure 4.40.). This decrease could be ascribed to the adsorption of degradation products onto the photocatalytically active sites of the magnetic titania microbeads.

#### **4.4.3. Photocatalytic Degradation of Phenol with Bare Titania Microbeads**

Phenol is a highly toxic and carcinogenic compound which can cause serious damage to human health. Therefore, numerous studies on the photocatalytic degradation of phenol were already published [18-23].

The parameters controlling the photocatalytic degradation of phenol with titania microbeads are the crystalline structure and the surface area of catalyst, the amount of catalyst, pH, initial phenol concentration, light intensity, and the partial pressure of oxidation agent, mostly oxygen. Figure 4.41. shows a typical reaction pathway for the photocatalytic degradation of phenol and the formation of intermediates. During the photocatalytic degradation, the reaction occurs by the

attack of hydroxyl radicals onto the phenyl ring of phenol which results in major intermediates like catechol, hydroquinone, and benzoquinone [200]. Additionally, some carboxylic acids like oxalic acid, lactic acid, fumaric acid, maleic acid, and formic acid could be formed as intermediates [200-206]. At the end of the degradation with optimum conditions, all intermediates turn into CO<sub>2</sub> and H<sub>2</sub>O.

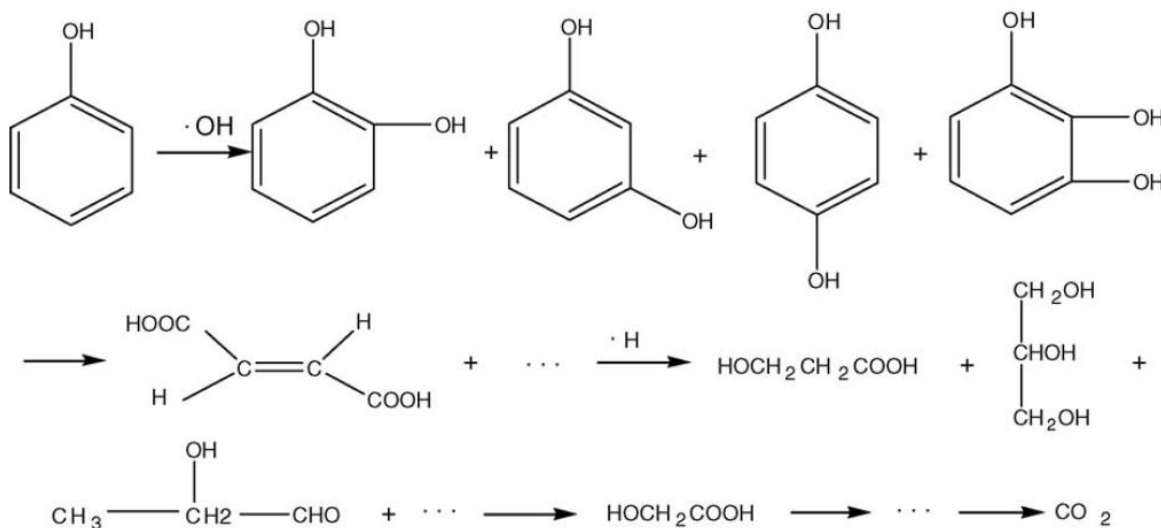


**Figure 4.41.** A proposed model for the photocatalytic degradation of phenol.

The HPLC chromatograms obtained at different reaction times during the photocatalytic degradation of phenol (50 ppm, 100mL) with the bare titania microbeads (160 mg, calcination temperature: 450°C) at pH 7 are shown in Figure 4.42.

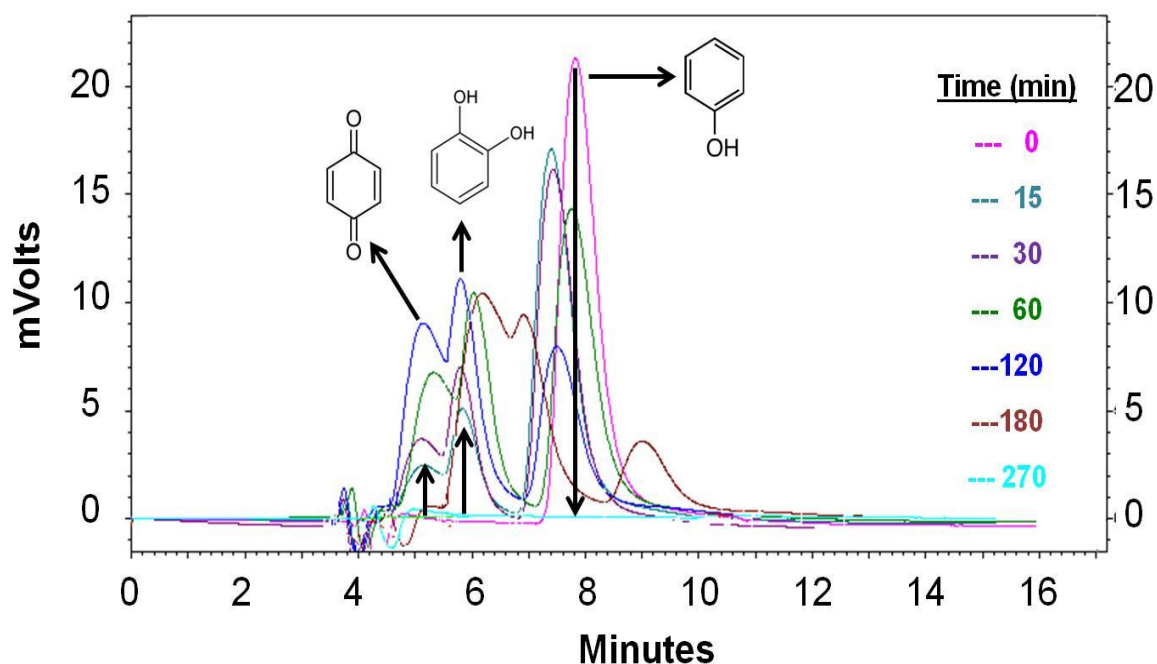


**Figure 4.42.** HPLC chromatograms obtained at different times during the photocatalytic degradation of phenol. (Conditions: catalyst amount: 160 mg, calcination temperature: 450°C, phenol solution: 50 ppm, 100 mL, pH: 7).

The decrease in the phenol peak due to photocatalytic degradation can be clearly seen from Figure 4.42. The major intermediates formed by the photocatalytic degradation of phenol with bare titania microbeads were detected as benzoquinone and hydroquinone, respectively. Depending on the degradation of phenol, the intensities of the peaks belonging to benzoquinone and hydroquinone increased till 180 min. As the photocatalytic degradation continued, the areas of intermediate peaks also started to decrease due to their degradation into CO<sub>2</sub> and H<sub>2</sub>O. The complete photocatalytic degradation of phenol and the intermediates was achieved within 270 min. The concentration of phenol in the solution at a certain time was determined according to the area under the peak of phenol and is given in Figure 4.43.

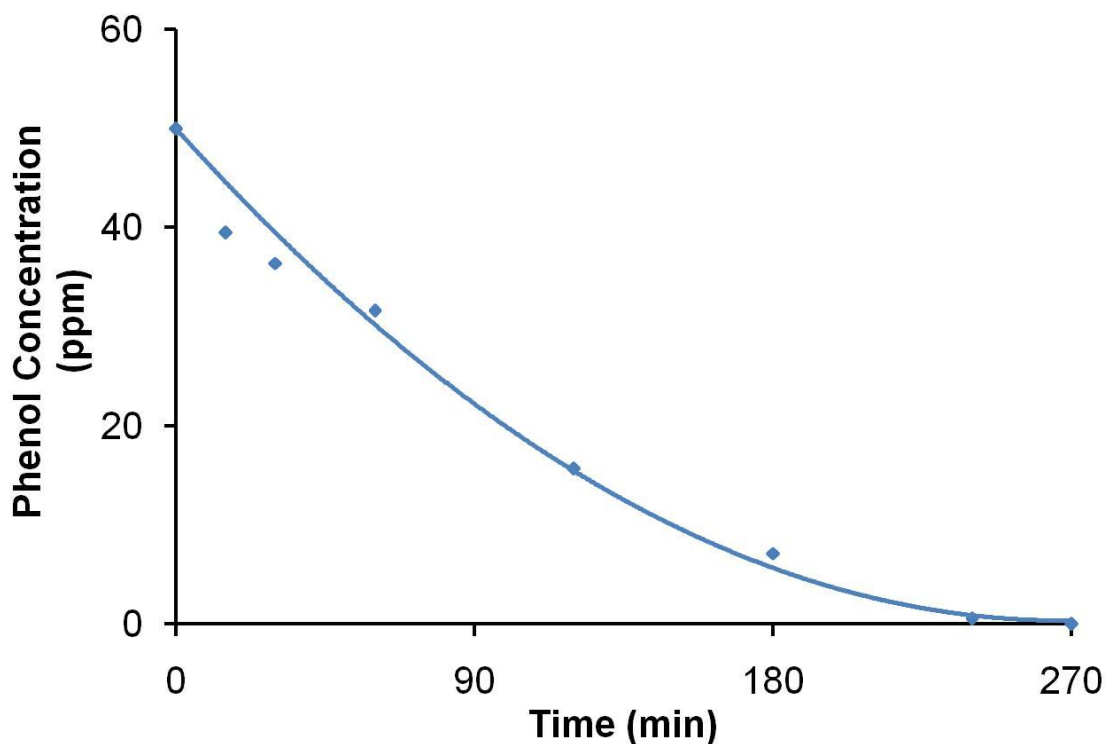


**Figure 4.43.** The variation of phenol concentration with the time in the degradation of phenol with bare titania microbeads. (Conditions: catalyst amount: 160 mg, calcination temperature: 450°C, Phenol solution: 50 ppm, 100 mL, pH: 7).

#### 4.4.3.1. Effect of pH

The charge characteristics of titania microbeads and phenol have a significant effect on the adsorption of phenol onto the titania microbeads. At a pH lower than the pKa of phenol (i.e. 9), phenol acts as neutral compound. However, phenol is negatively charged above this value. The effect of pH on the photocatalytic degradation rate was investigated by the photocatalytic degradation of phenol solution (50 ppm, 100 mL) with bare titania microbeads (160 mg, calcined at 450°C). The variation of phenol concentration with the time during the photocatalytic degradation with the bare titania microbeads at different pH values are given in Figure 4.44.

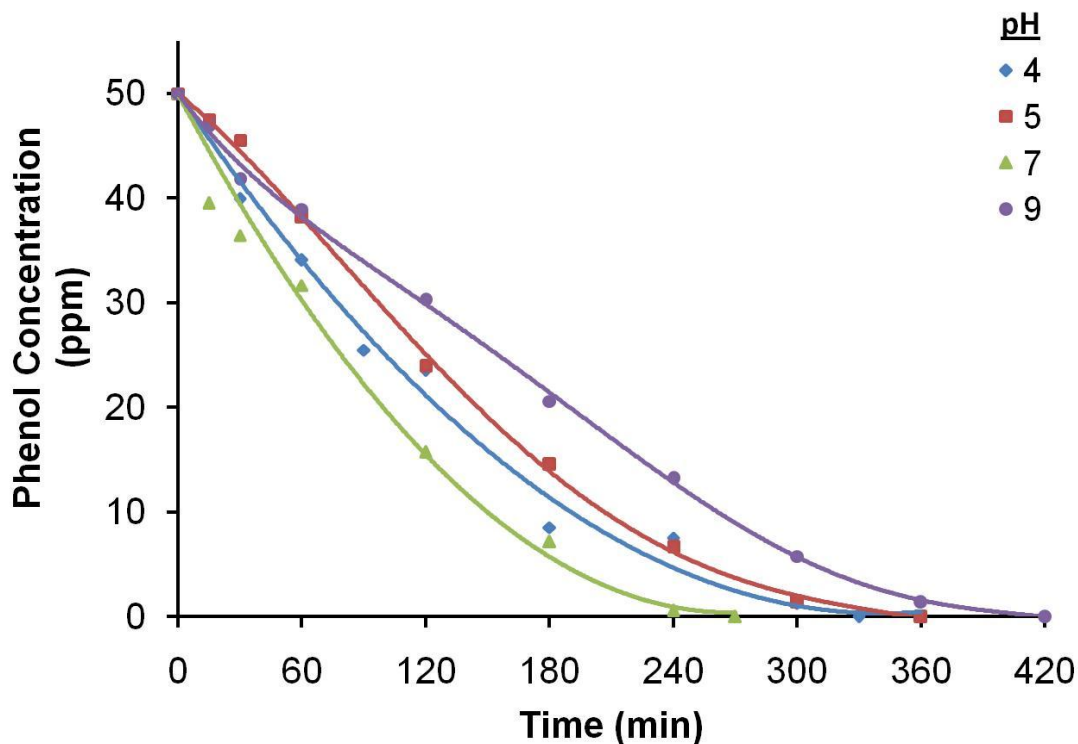


**Figure 4.44.** Effect of pH on the photocatalytic degradation rate of phenol with bare titania microbeads. (Conditions: catalyst amount: 160 mg, calcination temperature: 450°C, phenol solution: 50 ppm, 100 mL).

After addition of bare titania microbeads, phenol solution was equilibrated in dark under magnetic stirring for 20 min. The change in the phenol concentration before the irradiation was negligible at each pH. Hence, the adsorption of phenol onto the bare titania microbeads was inconsiderable (Figure 4.44.). Because no specific interaction was occurred between the positively charged or neutral bare titania microbeads and neutral phenol molecules at acidic pH and pH 7, which are lower than the pKa value of phenol. At pH 9, negatively charged bare titania microbeads repels the negatively charged phenol which diminishes the phenol adsorption.

When the effect of pH on the photocatalytic degradation rate of phenol was investigated, it was observed that the highest degradation rate was observed at pH 7. The complete photodegradation of phenol at pH 7 was achieved in a shorter time (270 min) compared to the other pH values. The reason of the higher degradation rate at pH 7 probably should be the higher hydroxyl ion concentration leading to higher number of hydroxyl radicals ( $\cdot\text{OH}$ ) per volume with respect to acidic pH region [207]. Despite the highest number of hydroxyl radicals per volume

( $\cdot\text{OH}$ ), the photocatalytic degradation rate of phenol was lowest at pH 9 because both phenol and bare titania microbeads were negatively charged at this pH.

#### **4.4.3.2. Effect of Catalyst**

It was reported that photocatalytic degradation rate increases with increasing the catalyst amount up to a certain value [147]. After this value, the photocatalytic degradation rate decreases because of the light scattering and screening effects [147]. Although the photocatalytic active sites in the solution increase with the increase in the catalyst amount, the excessive particle concentration seriously prevents the light penetration which causes non-uniform distribution of light intensity in the solution. Therefore it is important to use the most appropriate amount of photocatalyst.

The effect of catalyst amount on the photocatalytic degradation rate was investigated by the photocatalytic degradation of phenol solution (50 ppm, 100 mL) with different amounts of bare titania microbeads (80 mg, 160 mg, 240 mg, calcined at 450°C). The variation of phenol concentration with the time during the photocatalytic degradation with different amounts of bare titania microbeads are given in Figure 4.45. As seen in Figure 4.45., increasing the amount of bare titania microbeads increased the photocatalytic degradation rate and decreased the time needed for the complete degradation of phenol. However, increasing the amount over 160 mg resulted in a decrease in the photocatalytic degradation rate, which can be attributed to the light scattering due to the substantial amount of photocatalyst. In order to obtain the total absorption of efficient photons, 160 mg of bare titania microbeads was decided as the optimum catalyst amount for the photocatalytic degradation of phenol in a 100 mL of reaction volume.

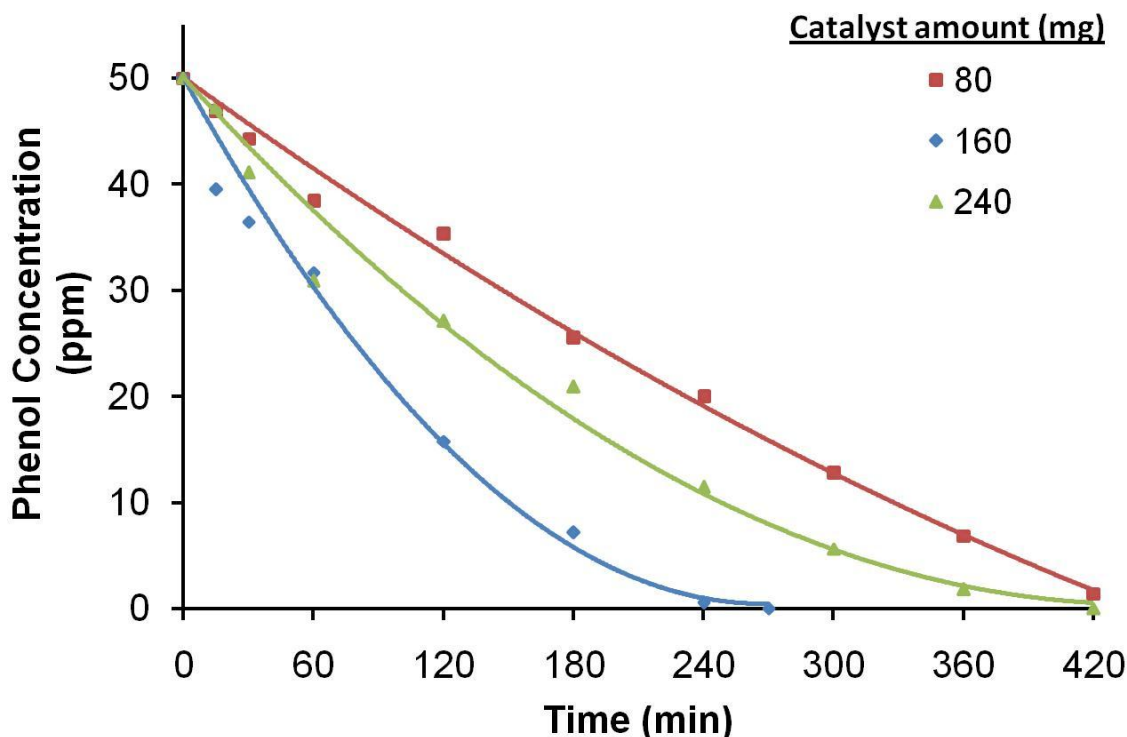


**Figure 4.45.** Effect of catalyst amount on the photocatalytic degradation rate of phenol with bare titania microbeads. (Conditions: Calcination temperature: 450°C, phenol solution: 50 ppm, 100 mL, pH : 7).

#### 4.4.3.3. Effect of Phenol Concentration

As reported in several studies, higher amounts of hydroxyl radicals are needed at higher concentrations of phenol for the photocatalytic degradation [207-209]. When the other reaction conditions (i.e. light intensity, catalyst amount and duration of irradiation) are kept constant, the formation rate of hydroxyl radicals on the catalyst surface is the same. In such a case, the number of hydroxyl radicals is not enough to attack all of the phenol molecules. Consequently, the photocatalytic degradation decreases at higher phenol concentrations. The effect of phenol concentration on the photocatalytic degradation rate was investigated by the photocatalytic degradation of phenol solutions with different concentrations (25 ppm, 50 ppm, 100 ppm) with bare titania microbeads (160 mg, calcined at 450°C). The variation of phenol concentration with the time during the photocatalytic degradation at different concentrations are given in Figure 4.46.



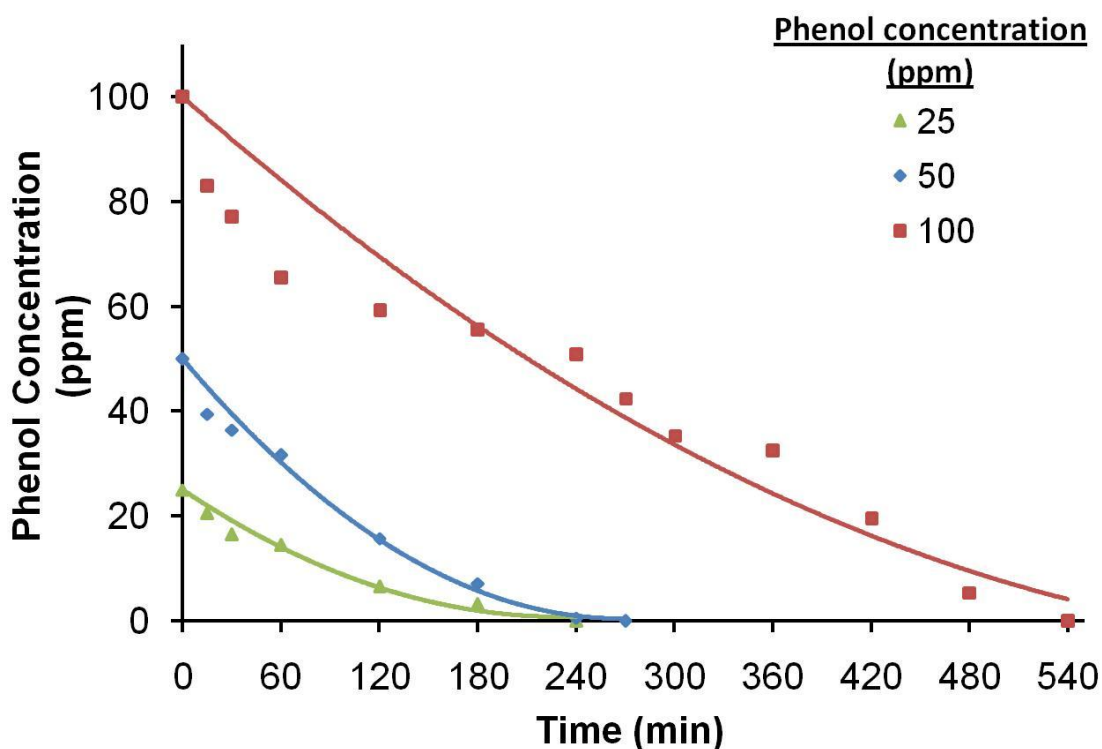


**Figure 4.46.** Effect of initial phenol concentration on the photocatalytic degradation rate of phenol with bare titania microbeads. (Conditions: Catalyst amount: 160 mg, Calcination temperature: 450°C, pH :7).

The results showed that the number of hydroxyl radicals formed with 160 mg of bare titania microbeads was adequate for the photocatalytic degradation of phenol with the initial concentrations of 25 ppm and 50 ppm. As expected, by increasing the phenol concentration over 50 ppm the photocatalytic degradation rate decreased (Figure 4.46.).

#### 4.4.3.4. Effect of Au Loading

For the enhancement of photocatalytic activity of the titania photocatalysts, AuNPs were doped as reported in many researches [166-169]. The effect of AuNPs on the photocatalytic activity depends on some parameters like size of AuNPs, AuNP loading and other photocatalytic degradation conditions. Both enhancement and inhibition on the photocatalytic activity of titania photocatalysts have been reported by doping AuNPs [167-169].

#### 4.4.3.4.1. Effect of AuNP Size

The effect of AuNP size on the photocatalytic degradation rate was investigated by photocatalytic degradation of phenol solution (50 ppm, 100 mL) with decorated bare titania microbeads with AuNPs in different sizes. The variation of phenol concentration with the time during the photocatalytic degradation with bare titania microbeads and decorated bare titania microbeads with AuNPs in different sizes are given in Figure 4.47.

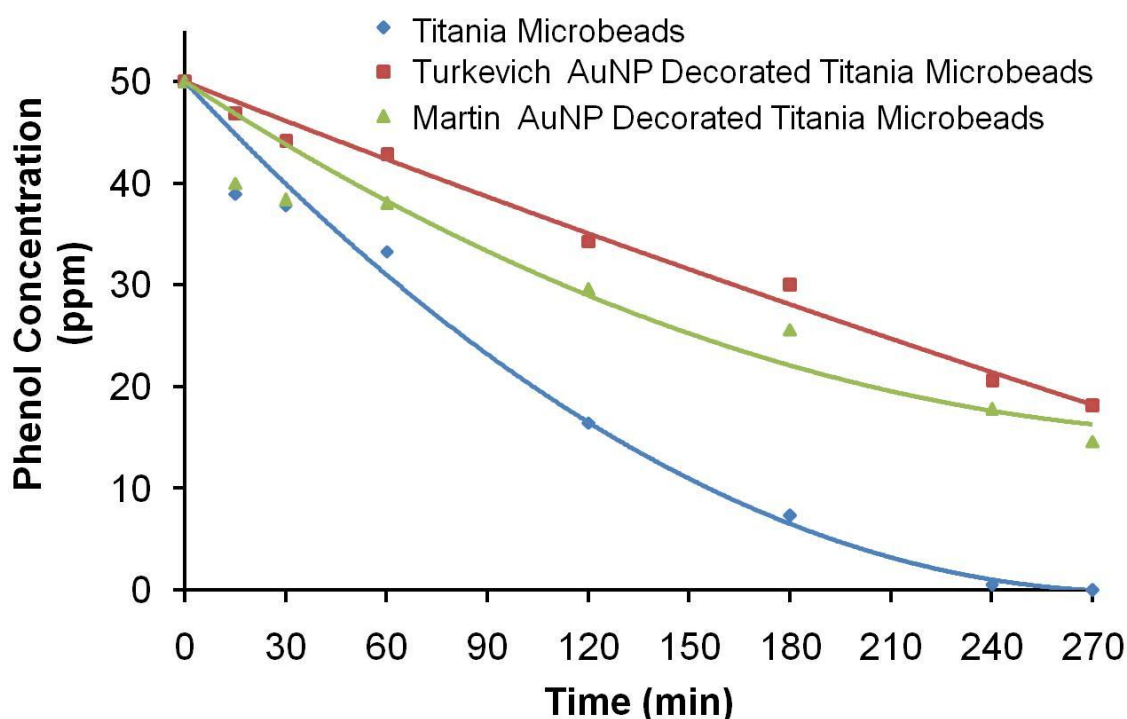


**Figure 4.47.** Effect of AuNP size on the photocatalytic degradation rate of phenol. (Conditions: Catalyst amount: 160 mg; Calcination temperature: 450°C; Au loading (w/w %) : 5 %; Phenol solution: 50 ppm, 100 mL; pH : 7).

As seen in Figure 4.47., inhibition was observed instead of enhancement on photocatalytic degradation rate of phenol by loading Martin and Turkevich AuNPs onto the bare titania microbeads. When the photocatalytic degradation rates of Martin and Turkevich AuNP decorated bare titania microbeads are compared, it was observed that AuNPs in lower size provided a slightly better photocatalytic activity. From these results, it can be concluded that bare titania microbeads performed higher photocatalytic activity compared to the AuNP decorated bare titania microbeads under these conditions.

#### 4.4.3.4.2. Effect of Au Loading

The effect of Au loading on the photocatalytic degradation rate was investigated by the photocatalytic degradation of phenol solution (50 ppm, 100 mL, pH 7) with Martin AuNP decorated titania microbeads (160 mg, calcined at 450°C) with different Au loadings. The variation of phenol concentration with the time during the photocatalytic degradation with Martin AuNP decorated titania microbeads with different Au loadings are given in Figure 4.48.

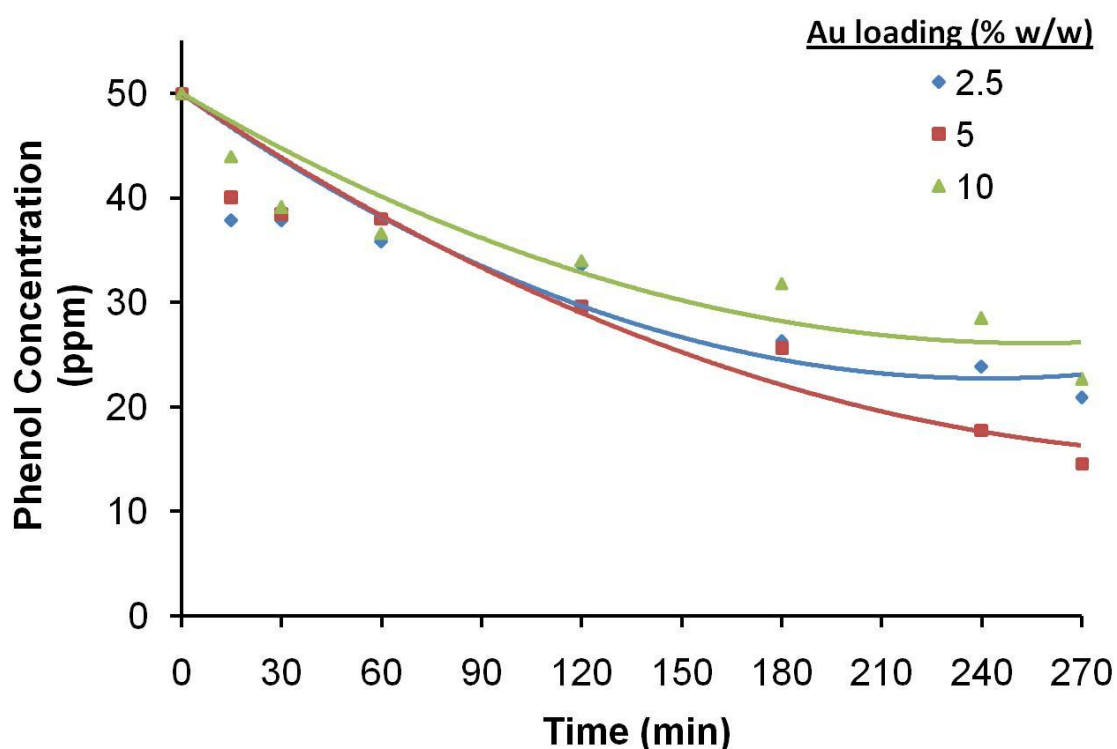


**Figure 4.48.** Effect of Au loading on the photocatalytic degradation rate of phenol with Martin AuNP decorated bare titania microbeads. (Conditions: Catalyst amount: 160 mg; Calcination temperature: 450°C; Phenol solution: 50 ppm, 100 mL; pH :7).

As seen in Figure 4.48., the amount of phenol degraded with 5 % of Au loading was higher with respect to the other preparations. Unfortunately, changing the Au loading did not provide an enhancement on the photocatalytic activity of titania microbeads.

#### 4.4.3.5. Reusability

The reusability experiments were done only with bare titania microbeads which has the highest photocatalytic activity. To obtain the reusability of bare titania microbeads (160 mg), the photocatalytic degradation of phenol solution (50 ppm, 100 mL) was repeated for five times at optimum conditions. After each experiment, the photocatalyst was recovered by rinsing with water for several times for reuse. The percent of removal in each run is given in Figure 4.49.

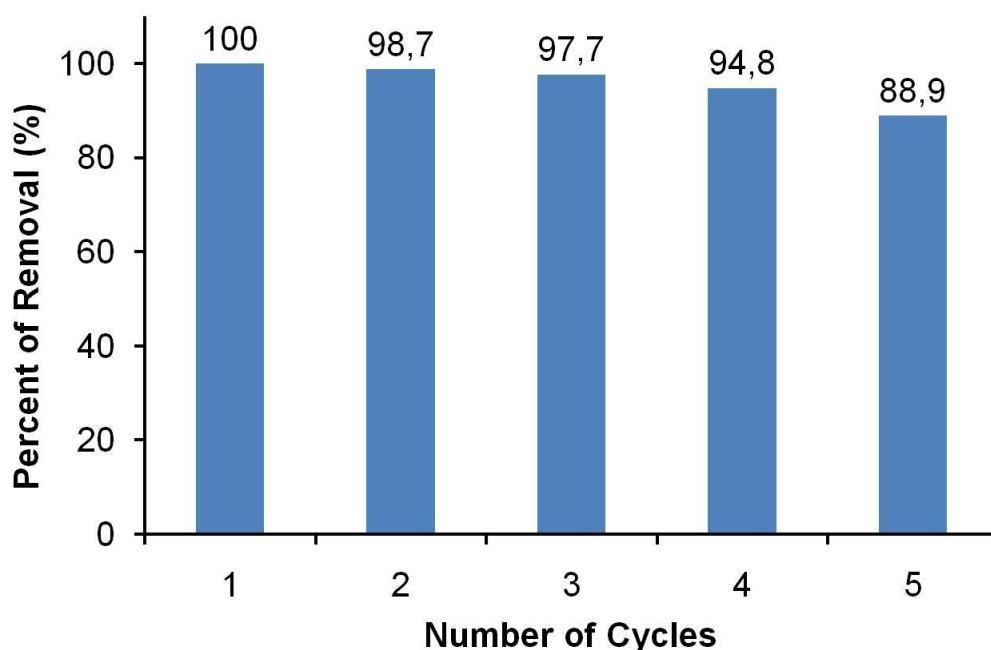


**Figure 4.49.** Reusability of bare titania microbeads in the photocatalytic degradation of phenol. (Conditions: Catalyst amount: 160 mg; Calcination temperature: 450°C; Phenol solution: 50 ppm, 100 mL; pH :7).

The phenol removal decreased only 2.3 % after 3 cycles. In the fifth cycle, the decrease in the percent removal of phenol was 11.1 % (Figure 4.49.). The adsorption of degradation products onto the photoactive sites of bare titania microbeads is probably the decrease in the photocatalytic activity of bare titania microbeads.

#### 4.4.4. Photocatalytic Degradation of Phenol with Magnetic Titania Microbeads

It is important to achieve the photocatalytic degradation of phenol with magnetic titania microbeads as it provides the ease of recovering the photocatalyst from the reaction solution by applying only an external magnetic field. To obtain the photocatalytic activity of magnetic titania microbeads, photocatalytic degradation of phenol solution was performed under the same experimental conditions used with bare titania microbeads. The variation of phenol concentration with the time during the photocatalytic degradation with bare and magnetic titania microbeads are comparatively given in Figure 4.50.

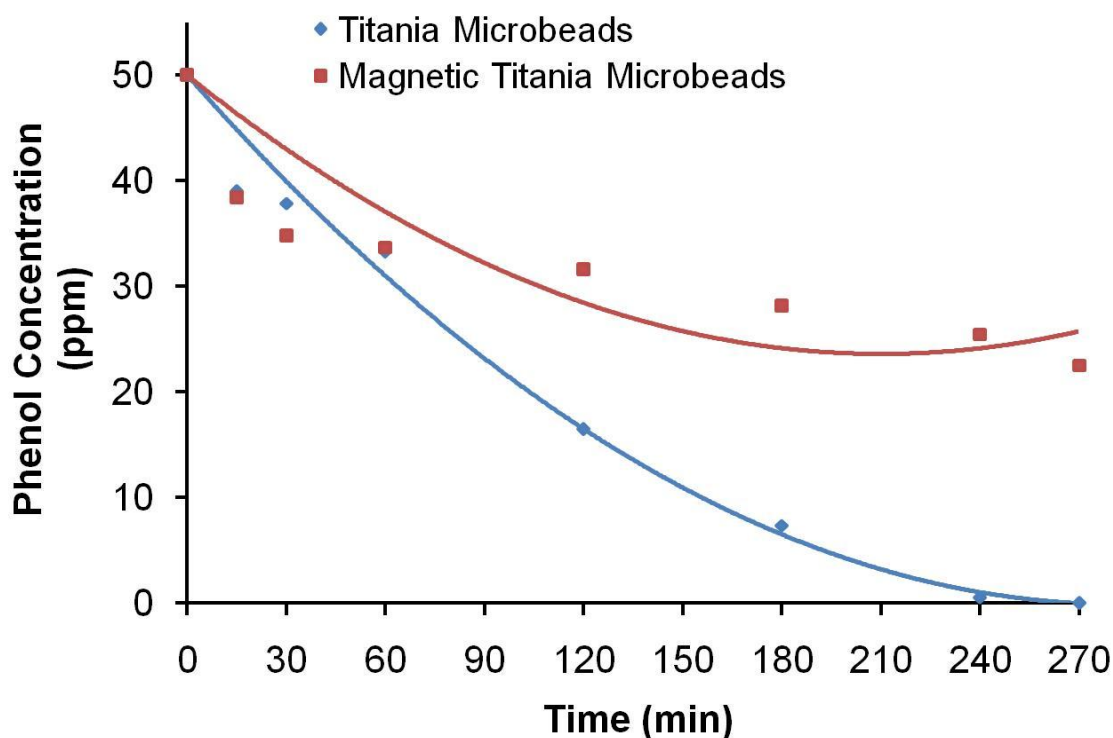


**Figure 4.50.** Comparison of the photocatalytic activity of bare and magnetic titania microbeads. (Conditions: Catalyst amount: 160 mg; Calcination temperature: 450°C; Phenol solution: 50 ppm, 100 mL; pH :7).

The results showed that magnetic titania microbeads could not perform such a good photocatalytic activity like bare titania microbeads under the same experimental conditions (Figure 4.50.). The reason of poor photocatalytic activity

could be ascribed to the transfer of electrons and holes from TiO<sub>2</sub> to magnetic iron oxide nanoparticles and their recombination at the iron oxide core.

#### 4.4.4.1. Effect of Au Loading

To obtain a better photocatalytic activity with the magnetic titania microbeads, AuNPs with different sizes were loaded on the magnetic titania microbeads. The effect of Au loading on the photocatalytic degradation rate of phenol was investigated by photocatalytic degradation of phenol solution (50 ppm, 100 mL) with decorated magnetic titania microbeads with AuNPs in different sizes. The variation of phenol concentration with the time using magnetic titania microbeads and decorated magnetic titania microbeads with AuNPs in different sizes are given in Figure 4.51.

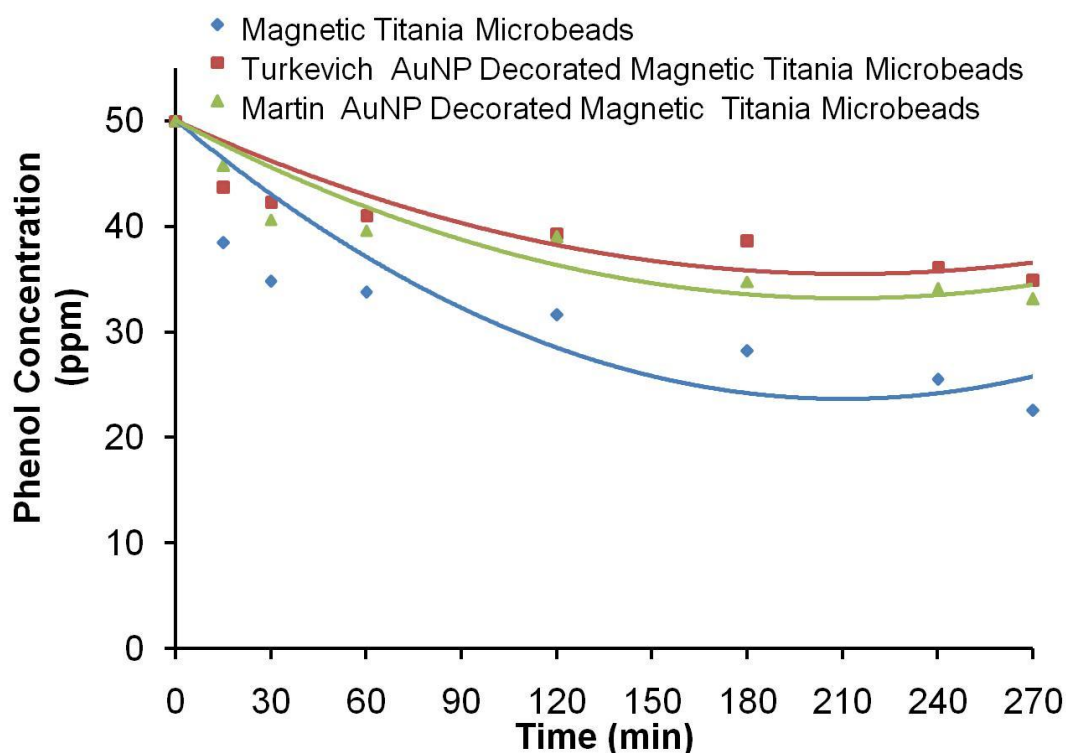


**Figure 4.51.** Effect of Au loading on the photocatalytic degradation rate of phenol with magnetic titania microbeads. (Conditions: Catalyst amount: 160 mg; Calcination temperature: 450°C; Au loading (w/w %) : 5 %; Phenol solution: 50 ppm, 100 mL; pH :7).

As seen in Figure 4.51., the loading AuNPs synthesized with both Martin and Turkevich methods, onto the magnetic titania microbeads resulted in the inhibition of photocatalytic activity. When the photocatalytic degradation rates of Martin and Turkevich AuNP decorated titania microbeads are compared, it was observed that the loading AuNPs in lower size provided slightly better photocatalytic activity. It can be concluded that an enhancement in the photocatalytic activity of magnetic titania microbeads could not be achieved by loading AuNPs with different sizes.

#### 4.5. Plasmonic Catalytic Activity Measurements

Au catalysts exhibit high plasmonic catalytic activity on many reactions like oxidation of carbon monoxide, alcohols and diols, reduction of organic compounds with borohydride [210, 211]. Although AuNPs perform their plasmonic catalytic activity without a solid support, the agglomeration of AuNPs in the reaction medium is a major disadvantage. To overcome this instability, different approaches have been tried in the literature like supporting gold nanoparticles on porous solids like polymers and metal oxides. In addition to the stability, the supporting of AuNPs on porous solids provides easy removal of catalyst from the reaction medium. Plasmonic catalytic activity of Au supported catalysts depends on some parameters like AuNP size and Au loading, catalyst amount, initial reactant concentration and temperature.

##### 4.5.1. Reduction of 4-Nitrophenol

The model reaction for the reduction of 4-nitrophenol (4-NP) to 4-aminophenol (4-AP) with AuNPs by using excess amount of sodium borohydride is given in Figure 4.52.

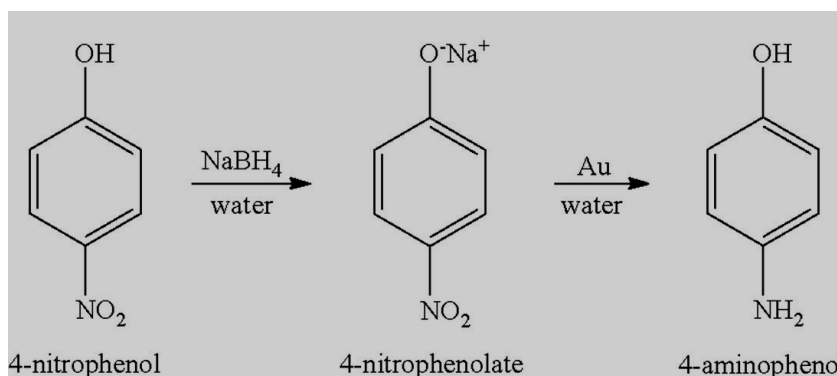


**Figure 4.52.** Model reaction for the reduction of 4-NP to 4-AP.

As shown in Figure 4.52., 4-nitrophenolate ion is formed by the addition of  $\text{NaBH}_4$  into 4-NP solution. The absorption peak of 4-NP shifts from 313 nm to 400 nm after the addition of  $\text{NaBH}_4$  due to the formation of 4-nitrophenolate ion with a color change from light yellow to dark yellow. The absorption peak at 400 nm remains the same after several days in spite of excess  $\text{NaBH}_4$ . Hence, no reduction occurs without Au supported catalyst.

#### 4.5.2. Plasmonic catalysis of 4-NP with Turkevich AuNP Decorated Bare and Magnetic Titania Microbeads

The plasmonic catalytic activity of Turkevich AuNP decorated bare and magnetic titania microbeads were obtained by the reduction of 4-NP solution. The reduction of 4-NP to 4-AP (the change in the intensity of absorption of nitrophenolate) was monitored by UV-Vis spectroscopy.

The UV-Vis spectra obtained at different time intervals during the reduction of 4-NP solution (7.5 ppm, 24 mL) with Turkevich AuNP decorated magnetic titania microbeads (1 mg, Calcination temperature:  $450^\circ\text{C}$ ) by using excess amount of sodium borohydride at  $20^\circ\text{C}$  are shown in Figure 4.53.

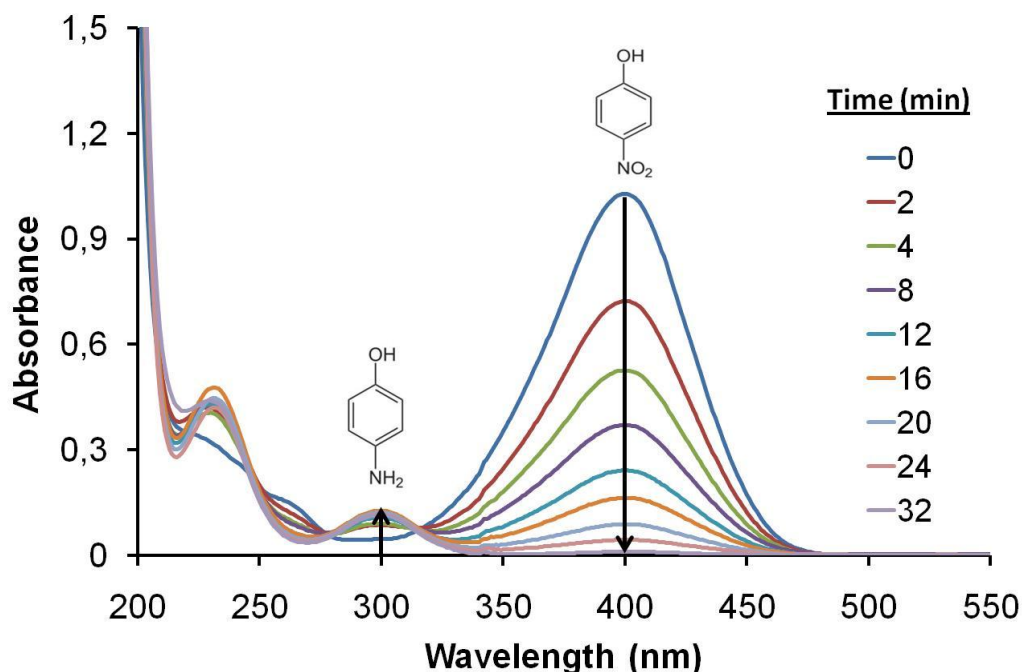


**Figure 4.53.** UV-Vis spectra at different times during the reduction of 4-NP. (Conditions: Catalyst: Turkevich AuNP decorated magnetic titania microbeads, Catalyst amount: 1 mg, Calcination temperature:  $450^\circ\text{C}$ , Au loading (w/w %) : 5 %; 4-NP solution: 7.5 ppm, 24 mL, Temperature:  $20^\circ\text{C}$ )



UV–Vis spectra shown in Figure 4.53. exposed that the peak at 400 nm corresponded to the formation of 4-nitrophenolate anion by the addition of  $\text{NaBH}_4$ . Due to the reduction of 4-NP with Turkevich AuNP decorated magnetic titania microbeads, the intensity of the 4-NP peak at 400 nm decreased continuously, while the intensity of 4-AP peak at 300 nm increased. As a result, the complete reduction of 4-NP at given conditions was achieved within 32 min.

The concentration of 4-NP was calculated according to the decrease in the absorbance peak at 400 nm, which was directly proportional to the reduction in 4-NP concentration. The variation of 4-NP concentration during the reduction of 4-NP solution (7.5 ppm, 24 mL) containing Turkevich AuNP decorated bare and magnetic titania microbeads is given in Figure 4.54.

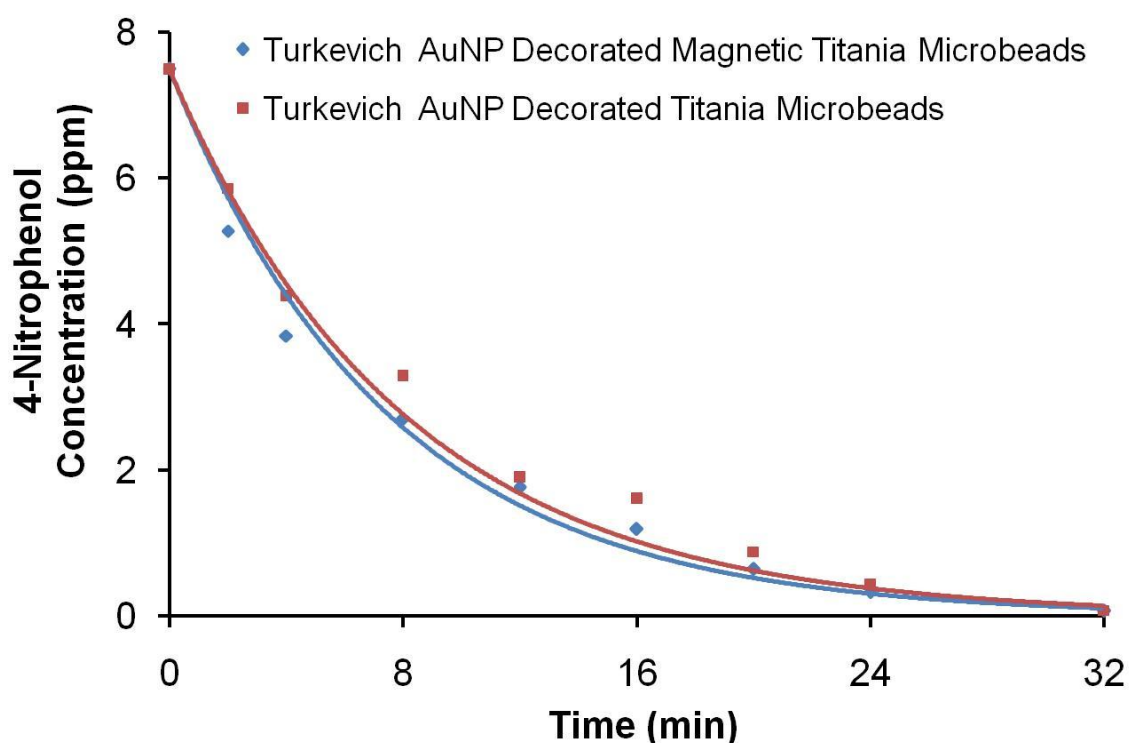


**Figure 4.54.** 4-NP concentration with time. (Conditions: Catalysts: Turkevich AuNP decorated bare and magnetic titania microbeads, Catalyst amount: 1 mg, Calcination temperature:  $450^{\circ}\text{C}$ , Au loading (w/w %) : 5 %; 4-NP solution: 7.5 ppm, 24 mL, Temperature:  $20^{\circ}\text{C}$ )

As seen in Figure 4.54., similar reduction rates of 4-NP were observed with both Turkevich AuNP decorated bare and magnetic titania microbeads. So, it can be concluded that using bare or magnetic titania microbeads as a support for AuNPs did not effect the reduction rate of 4-NP. Therefore, only the magnetic titania microbeads was used as support due to easy removal from the reaction medium.

#### 4.5.2.1. Plasmonic catalysis of 4-NP with Turkevich AuNP Decorated Magnetic Titania Microbeads

##### 4.5.2.1.1. Effect of Catalyst Amount

The effect of catalyst amount on the plasmonic catalytic degradation rate of 4-NP was investigated with reduction of 4-NP solution (7.5 ppm, 24 mL) with different amounts of Turkevich AuNP decorated magnetic titania microbeads (1 mg, 2.5 mg, 5 mg, 10 mg, Au loading (w/w %) : 5 %). The variation of 4-NP concentration with the time during the reduction of 4-NP with different amounts of Turkevich AuNP decorated magnetic titania microbeads are given in Figure 4.55.

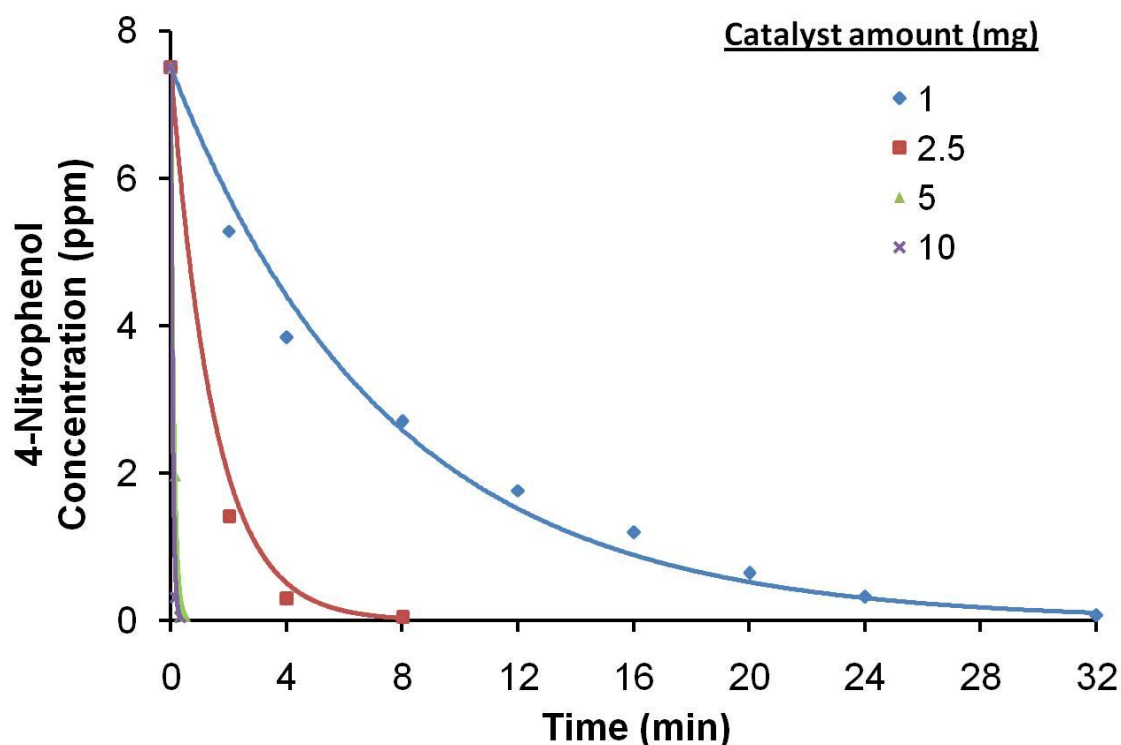


**Figure 4.55.** Effect of catalyst amount on the plasmonic catalytic degradation rate of 4-NP with Turkevich AuNP decorated magnetic titania microbeads. (Conditions: Calcination temperature: 450°C, Au loading (w/w %): 5 %; 4-NP solution: 7.5 ppm, 24 mL, Temperature: 20°C).

Figure 4.55. shows that the reduction rate of 4-NP increased evidently by increasing the amount of Turkevich AuNP decorated magnetic titania microbeads till 5 mg. However, the reduction rate did not increase for the catalyst amounts higher than 5 mg. This result can be explained by the effect of internal mass-transfer limitation on the observed rate depending upon the initial bulk-concentration of 4-NP (i.e. intraparticle diffusion of 4-NP within the porous-magnetic titania microbeads). Based on these results, 1 mg of Turkevich AuNP decorated magnetic titania microbeads was used in scanning other experimental parameters to observe the effects clearly.

#### **4.5.2.1.2. Effect of Temperature**

To obtain the effect of temperature, the plasmonic catalytic degradation rate of 4-NP solution (7.5 ppm, 24 mL) with Turkevich AuNP decorated magnetic titania microbeads (1 mg, Au loading (w/w %): 5 %) was performed at different temperatures (10°C, 20°C, 30°C, and 40°C). The variation of 4-NP concentration with the time during the reduction of 4-NP with Turkevich AuNP decorated magnetic titania microbeads at different temperatures are given in Figure 4.56. As seen in Figure 4.56., the reduction rate of 4-NP increased with increasing temperature due to the increase in the reaction rate constant.

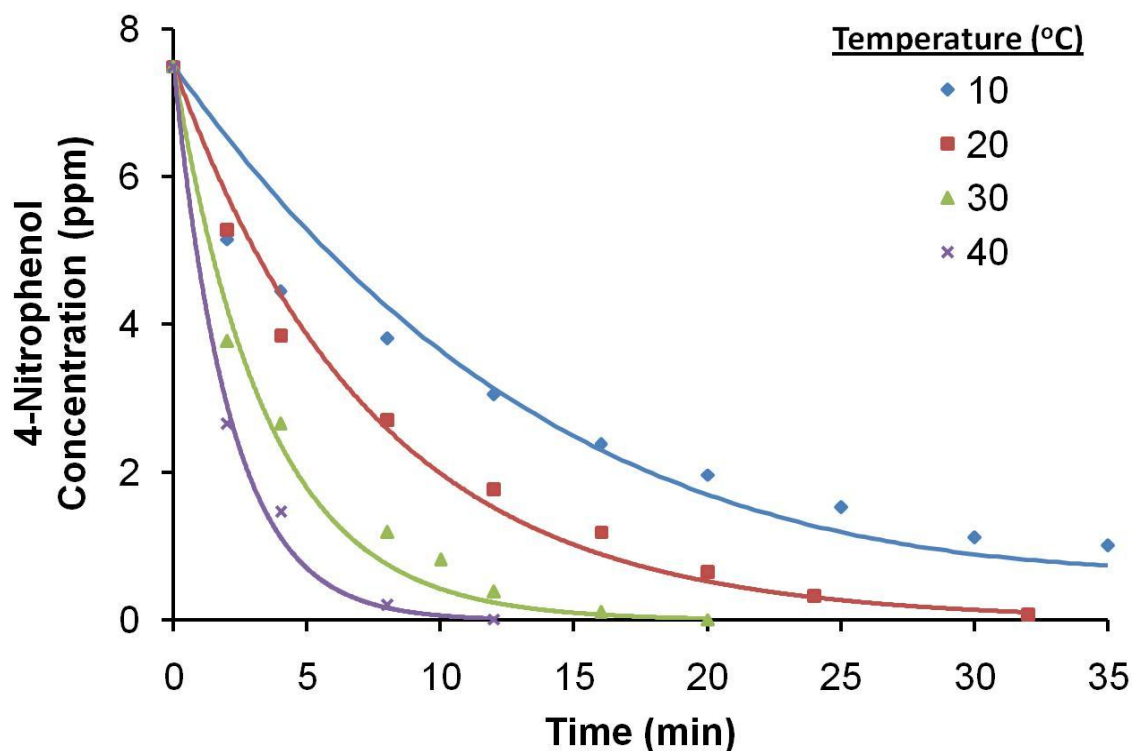


**Figure 4.56.** Effect of temperature on the plasmonic catalytic degradation rate of 4-NP with Turkevich AuNP decorated magnetic titania microbeads. (Conditions: Catalyst amount: 1 mg; Calcination temperature: 450°C; Au loading (w/w %) : 5 %; 4-NP solution: 7.5 ppm, 24 mL).

#### 4.5.2.1.3. Effect of Initial 4-NP Concentration

To obtain the effect of initial 4-NP concentration, the plasmonic catalytic degradation rate of 4-NP solutions at different concentrations (3.75 ppm, 7.5 ppm and 15 ppm) with Turkevich AuNP decorated magnetic titania microbeads (1 mg, Au loading (w/w %): 5 %) was performed at 20°C. The variation of 4-NP concentration with the time at different initial concentrations of 4-NP with Turkevich AuNP decorated magnetic titania microbeads are given in Figure 4.57.

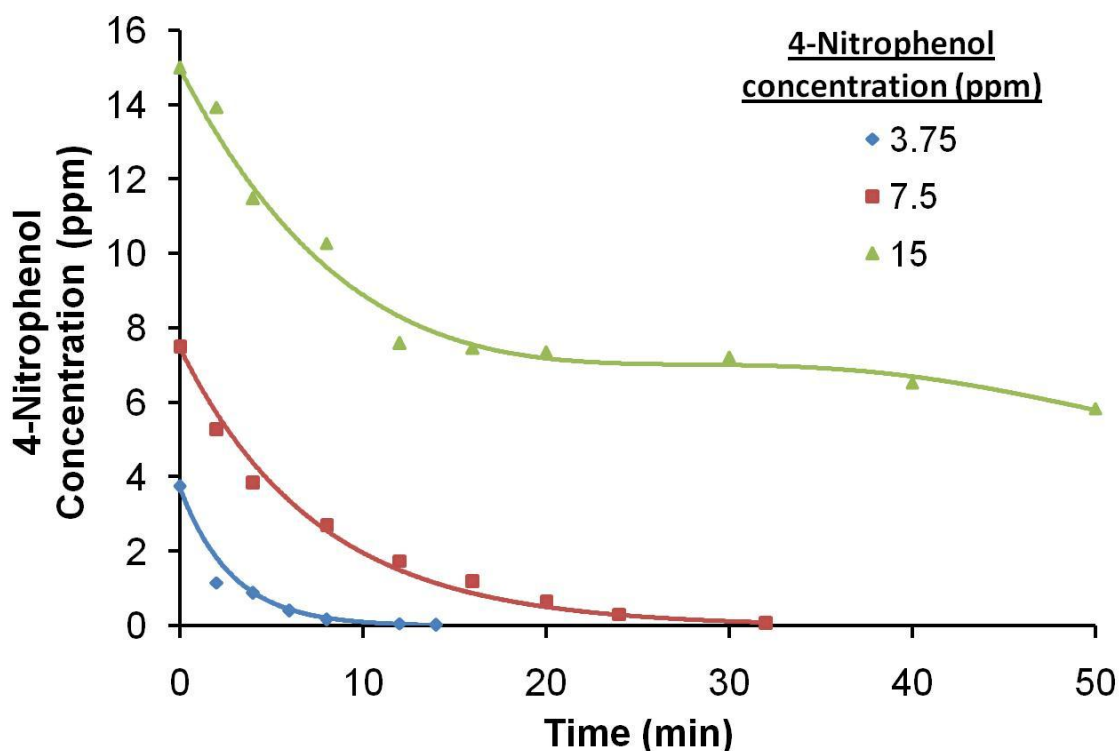


**Figure 4.57.** Effect of initial 4-NP concentration on the plasmonic catalytic degradation rate of 4-NP with Turkevich AuNP decorated magnetic titania microbeads. (Conditions: Catalyst amount: 1 mg; Calcination temperature: 450°C; Au loading (w/w %) : 5 %; Temperature: 20°C).

The results showed that the reduction rate of 4-NP decreased with the increase in the initial concentration of 4-NP solution (Figure 4.57.). The reason of this decrease could be ascribed to the inadequate amount of Turkevich AuNPs for the reduction of more 4-NP molecules.

### 4.5.3. Enhancement on the Plasmonic Catalytic Activity

#### 4.5.3.1. Effect of AuNP Size

It was reported that AuNPs at lower size have higher redox potential which accelerates the electron transfer and thereby increases the reaction rate of catalytic reactions. The effect of AuNP size on the plasmonic catalytic degradation rate of 4-NP was investigated by reduction of 4-NP solution (7.5 ppm, 24 mL) with AuNP decorated magnetic titania microbeads carrying AuNP with different sizes (1 mg, Au loading (w/w): 5 %). The variation of 4-NP concentration with the time using magnetic titania microbeads carrying AuNPs in different sizes are given in Figure 4.58.

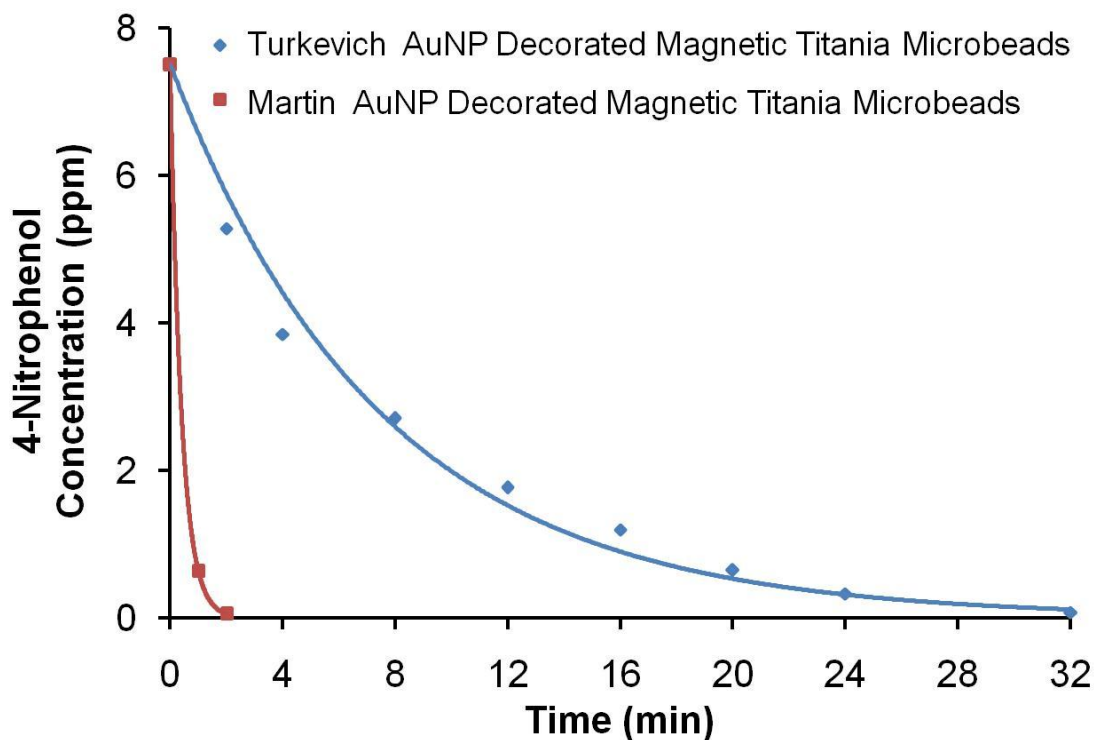


**Figure 4.58.** Effect of AuNP size on the plasmonic catalytic degradation rate 4-NP. (Conditions: Catalyst amount: 1 mg; Calcination temperature: 450°C; Au loading (w/w %) : 5 %; 4-NP solution: 7.5 ppm, 24 mL; Temperature: 20°C).

As seen in Figure 4.58., an enhancement in the reduction of 4-NP was observed by using Martin AuNP decorated magnetic titania microbeads, in which the AuNP size was smaller, compared to Turkevich AuNP decorated magnetic titania microbeads. The time needed for the complete reduction of 4-NP solution decreased from 32 min to 2 min due to higher redox potential of low size AuNPs supported on magnetic titania microbeads. As the reduction rate of 4-NP increased dramatically by changing AuNP size on the magnetic titania microbeads, the reduction of 4-NP solution with a higher concentration (15 ppm) was performed with Martin AuNP decorated magnetic titania microbeads. The variation of 4-NP concentration with the time using the initial 4-NP concentrations of 7.5 and 15 ppm with Martin AuNP decorated magnetic titania microbeads are given in Figure 4.59.

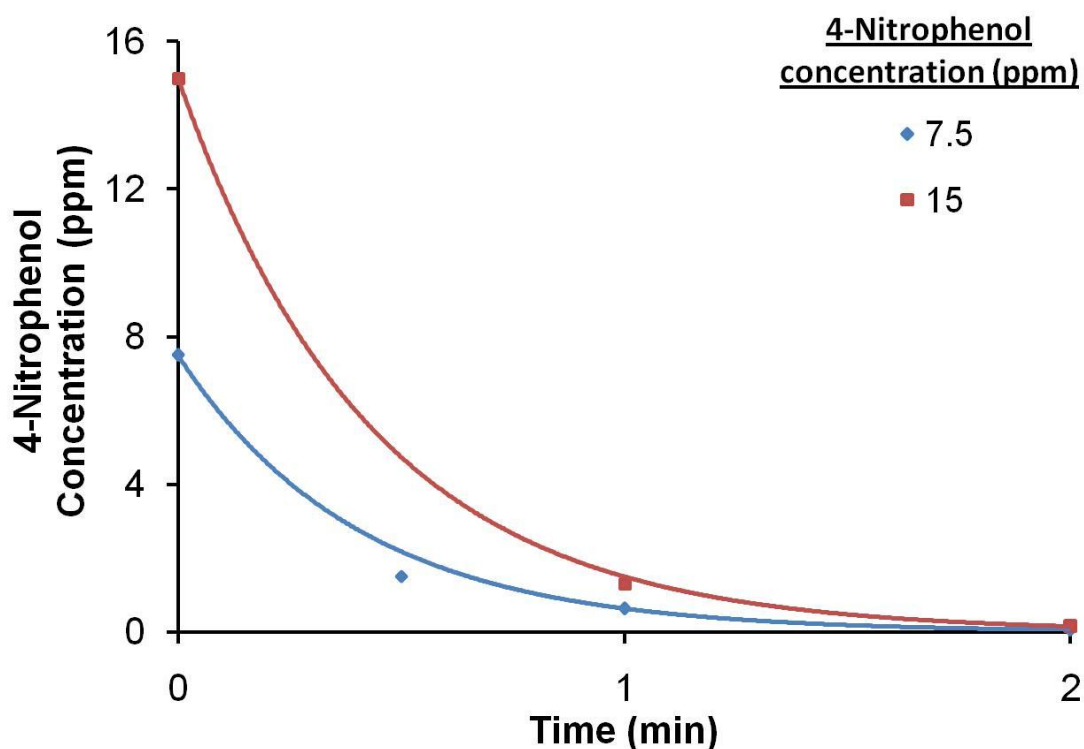


**Figure 4.59.** The variation of 4-NP concentration during the reduction of 4-NP with initial concentrations of 7.5 and 15 ppm with Martin AuNP decorated magnetic titania microbeads. (Conditions: Catalyst amount: 1 mg, Calcination temperature: 450°C, Au loading (w/w %) : 5 %; Temperature: 20°C)

As seen in Figure 4.59., although the initial concentration was increased two fold, the complete reduction of 4-NP solution was achieved at the same time (2 min). It should be reminded that the complete reduction of 4-NP with the concentration of 15 ppm could not be achieved with Turkevich AuNP decorated magnetic titania microbeads under the experimental conditions (Figure 4.57.). This is the proof of enhancement on the plasmonic catalytic activity of AuNP decorated magnetic titania microbeads by changing the AuNP size.

#### 4.5.3.2. Effect of Au loading

The effect of Au loading on the plasmonic catalytic degradation rate of 4-NP was investigated by reduction of 4-NP solution (7.5 ppm, 24 mL) with Martin AuNP decorated magnetic titania microbeads (1 mg) with different Au loadings. The variation of 4-NP concentration solution with the time during the reduction of 4-NP with Martin AuNP decorated magnetic titania microbeads prepared with different Au loadings are given in Figure 4.60.

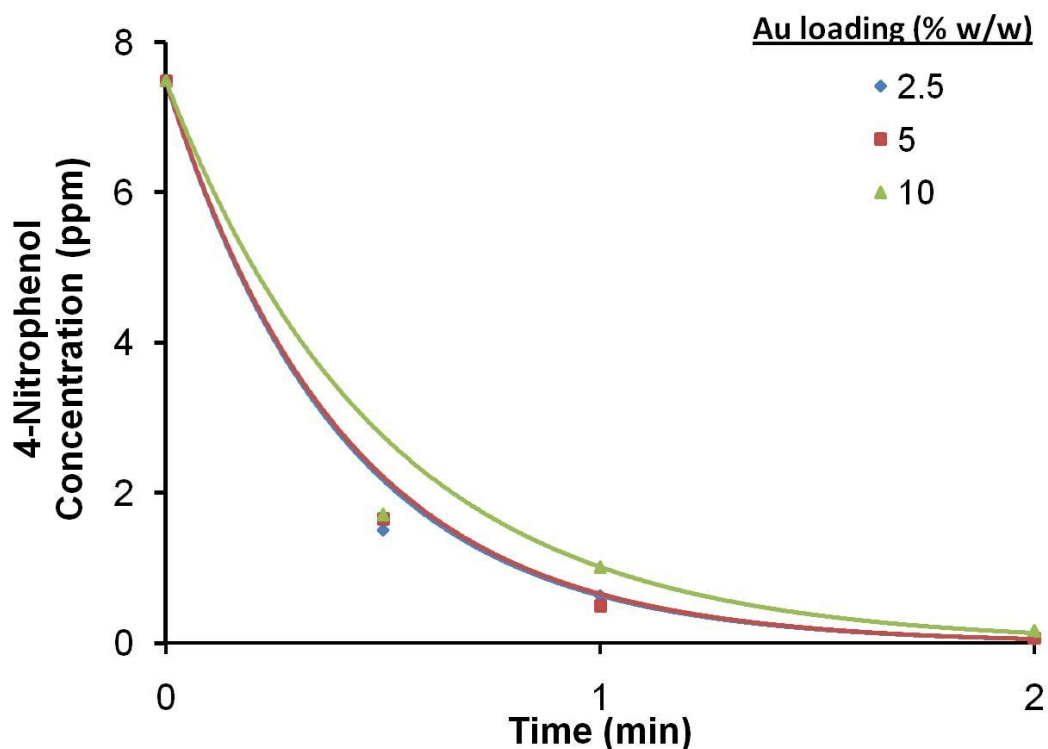


**Figure 4.60.** Effect of Au loading on the plasmonic degradation rate of 4-NP with Martin AuNP decorated magnetic titania microbeads. (Conditions: Catalyst amount: 1 mg; Calcination temperature: 450°C; 4-NP solution: 7.5 ppm, 24 mL; Temperature: 20°C).

As seen from Figure 4.60., the complete reduction of 4-NP solution was achieved at the same time with all Au loadings. An apparent effect of Au loading on the plasmonic catalytic activity of Martin AuNP decorated magnetic titania microbeads was not observed.

#### 4.5.4. Reusability

The reusability was investigated only for Martin AuNP decorated magnetic titania microbeads which has the highest plasmonic catalytic activity. To obtain the reusability of Martin AuNP decorated titania microbeads (1 mg), the reduction of 4-NP (7.5 ppm, 24 mL) at 20°C was repeated for five times under the same conditions. After each experiment, the plasmonic catalyst was recovered by rinsing with water for several times for reuse. The percent of removal in each cycle is given in Figure 4.61.



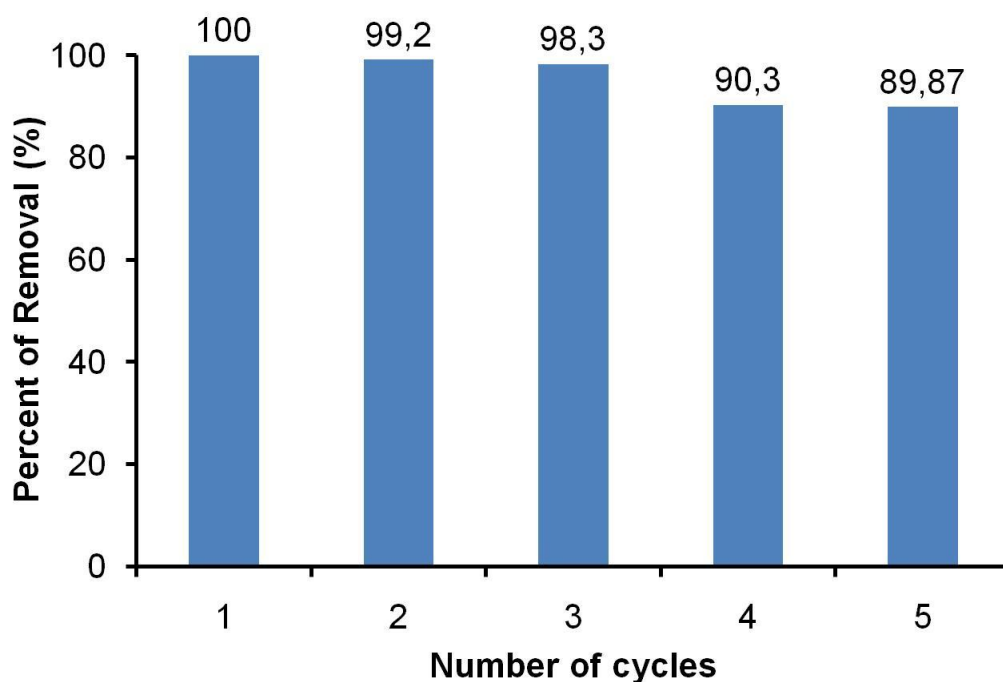


**Figure 4.61.** Reusability of Martin AuNP decorated magnetic titania microbeads in the reduction of 4-NP solution. (Conditions: Catalyst amount: 1 mg; Calcination temperature: 450°C; Au loading (w/w %) : 5 %; 4-NP solution: 7.5 ppm, 24 mL; Temperature: 20°C).

The percent removal of 4-NP decreased 1.7 % after 3 cycles and it was 89.9 % after being reused five times (Figure 4.61.). This decrease could be ascribed to the adsorption of 4-AP formed during plasmonic degradation onto the Martin AuNP decorated magnetic titania microbeads.

## 5. CONCLUSION

In the scope of this thesis, new sol-gel templating methods for the synthesis of bare and magnetic titania microbeads in the monodisperse-porous form were developed using  $-\text{SO}_3\text{Na}$  attached and magnetic polymethacrylate microbeads as templates, respectively. The decoration of AuNPs on bare and magnetic titania microbeads was performed by appropriate derivatizations. In the second part of this thesis, the photocatalytic activities of titania based catalysts were investigated by photocatalytic degradation of RB5 dye and phenol. The plasmonic catalytic activity of AuNP decorated bare and magnetic titania microbeads were also studied by plasmonic catalytic degradation of 4-NP by using excess amount of  $\text{NaBH}_4$ . The conclusions obtained from the synthesis, characterization and catalytic activity measurements of the titania based catalysts were given below:

- Monodisperse-porous bare titania microbeads in the size range of 3.0-5.0  $\mu\text{m}$  with different porous structures with specific surface areas ranging between 50-91  $\text{m}^2/\text{g}$  were obtained by a new sol-gel templating method using  $-\text{SO}_3\text{Na}$  attached-polymethacrylate microbeads with different porous structures as the template material.
- $-\text{SO}_3\text{Na}$  attached-polymethacrylate microbeads were obtained via a simple reaction between reactive chloropropyl group of poly(HPMA-Cl-co-EDMA) microbeads and  $\text{NaHSO}_3$ . The increase in the chloropropyl content of poly(HPMA-Cl-co-EDMA) microbeads resulted in increase in the  $-\text{SO}_3\text{H}$  content of polymethacrylate template.
- It was shown that surface morphology, size, porous structure and specific surface area of the monodisperse-porous bare titania microbeads did not strongly depend on the porous properties of  $-\text{SO}_3\text{Na}$  attached-poly(HPMA-Cl-co-EDMA) microbeads. The sphericity of titania microbeads decreased with the increasing feed concentration of the crosslinking agent of polymeric template.
- When the characterization studies for  $-\text{SO}_3\text{Na}$  attached poly(HPMA-Cl-co-EDMA) and titania microbeads were evaluated together, 30 % v/v was chosen as the most appropriate feed concentration of crosslinking agent for polymeric template to obtain monodisperse-porous titania microbeads in the spherical

form. The most appropriate value for ratio of  $\text{-SO}_3\text{Na}$  attached poly(HPMA-Cl-co-EDMA) microbeads/ $\text{TiCl}_4$  solution (g/mL) was chosen as 6.7 based on the SSAs of titania microbeads obtained.

- The selection of polymethacrylate template material instead of commonly used polystyrenic template materials allowed to perform the calcination of titania-polymer composite microbeads at a lower temperature with respect to the previously used template materials. Hence, the highest specific surface area of bare titania microbeads was observed by the calcination of titania-polymer composite microbeads at the lowest calcination temperature (i.e.  $450^\circ\text{C}$ ). As seen from XRD patterns, bare titania microbeads calcined at  $450^\circ\text{C}$  exhibited both anatase and rutile crystalline structure depending on the synthesis conditions.
- Monodisperse-porous magnetic titania microbeads were obtained by a new sol-gel templating method using magnetic poly(HPMA-Cl-co-EDMA) as template. Magnetic poly(HPMA-Cl-co-EDMA) microbeads were synthesized by the impregnation of iron ions on amine attached-poly(HPMA-Cl-co-EDMA) microbeads.
- The surface morphologies of monodisperse-porous bare and magnetic titania microbeads were similar. However, the SSA of magnetic titania microbeads was slightly lower than the SSA of bare titania microbeads due to the incorporation of iron oxide nanoparticles into the mesopores of titania microbeads.
- AuNPs with different sizes (obtained with Turkevich and Martin methods) were decorated successfully onto the amine functionalized bare and magnetic titania microbeads.
- The SSAs of Turkevich and Martin AuNP decorated bare and magnetic titania microbeads with all Au loadings were slightly lower than SSAs of corresponding bare and magnetic titania microbeads, respectively.
- The photocatalytic activity of bare and magnetic titania microbeads and their AuNP decorated forms was investigated in aqueous media using a textile dye, RB5 as an organic contaminant in batch fashion. Operational parameters such as pH, catalyst amount, crystal composition and surface area, initial

substrate concentration have been shown to play an important role in the photocatalytic degradation of RB5 dye with bare and magnetic titania microbeads. The complete removal of RB5 dye solution was obtained successfully with both bare and magnetic titania microbeads. Depending on the AuNP size, decoration of Martin AuNPs instead of Turkevich AuNPs markedly enhanced the photocatalytic activity of titania microbeads. Hence the decoration with AuNPs with lower size resulted in a significant increase in the photocatalytic degradation rate due to electron transfer characteristics of AuNPs with lower size. However, an enhancement could not be obtained with the Martin AuNP decorated magnetic titania microbeads.

- The photocatalytic activity behaviours of bare and magnetic titania microbeads and their AuNP decorated forms were also investigated using phenol as a common organic contaminant in batch fashion. The effects of pH, catalyst amount, initial substrate concentration on the photocatalytic degradation of phenol with bare titania microbeads were investigated. The complete photocatalytic degradation of phenol was obtained with the bare titania microbeads. Unlike bare titania microbeads, complete degradation could not be achieved with magnetic photocatalyst. The decoration of Martin and Turkevich AuNPs on bare and magnetic titania microbeads resulted in an inhibition of photocatalytic activity.
- The plasmonic catalytic activity of AuNP decorated magnetic titania microbeads was investigated by the reduction of 4-NP by changing AuNP size, Au loading, catalyst amount, initial substrate concentration and temperature. A significant enhancement in the plasmonic catalytic activity of was observed with Martin AuNP decorated magnetic titania microbeads, in which the gold nanoparticle size was smaller, compared to Turkevich AuNP decorated magnetic titania microbeads. 4-NP in solution could be converted into 4-AP in the reaction periods lower than 2 min.

## REFERENCES

- [1] Slokar, Y.M., Majcen Le Marechal, A., Methods of Decoloration of Textile Wastewaters, *Dyes and Pigment*, 37, 335-356, **1998**.
- [2] Andreozzi, R., Caprio, V., Insola, A., Marotta, R., Advanced oxidation processes (AOP) for water purification and recovery, *Catalysis Today*, 53, 51-59, **1999**.
- [3] Fox, M.A.; Dulay, M.T., Heterogeneous Photocatalysis, *Chemical Reviews*, 93, 341-357, **1993**.
- [4] Herrmann, J.M., Heterogeneous photocatalysis: Fundamentals and applications to the removal of various types of aqueous pollutants, *Catalysis Today*, 53, 115-129, **1999**.
- [5] Esplugas, S., Gimenez, J., Contreras, S., Pascual, E., Rodriguez, M., Comparison of different advanced oxidation processes for phenol degradation, *Water Research*, 36, 1034–1042, **2002**.
- [6] Chen, D., Ray, A.K., Photocatalytic kinetics of phenol and its derivatives over UV irradiated TiO<sub>2</sub>, *Applied Catalysis B Environmental*, 23, 143–157, **1999**.
- [7] Fujishima, A., Zhang, X., Titanium dioxide photocatalysis: present situation and future approaches, *Comptes Rendus Chimie*, 9, 750-760, **2006**.
- [8] Reutergardh, L.B., Ilangphasuk, M., Photocatalytic decolourization of reactive azo dye: a comparison between TiO<sub>2</sub> and CdS photocatalysis, *Chemosphere*, 35, 585-596, **1997**.
- [9] Hu, C., Tang, Y., Jiang, Z., Hao, Z., Tang, H., Wong, P. K., Characterization and photocatalytic activity of noble-metal-supported surface TiO<sub>2</sub>/SiO<sub>2</sub>. *Applied Catalysis A: General*, 253, 389–396, **2003**.

- [10] Linsebigler, A.L., Lu, G., Yates, J.T., Photocatalysis on TiO<sub>2</sub> Surfaces: Principles, Mechanisms, and Selected Results, *Chemical Reviews*, 95, 735-758, **1995**.
- [11] Qu, P., Zhao, J., Shen, T., Hidaka, H., TiO<sub>2</sub>-assisted photodegradation of dyes: a study of two competitive primary processes in the degradation of RB in an aqueous TiO<sub>2</sub> colloidal solution, *Journal of Molecular Catalysis A: Chemical*, 129, 257-268, **1998**.
- [12] Tang, W.Z., Zhang, Z., An, H., Quintana, M.O., Torres, D.F., TiO<sub>2</sub>/UV photodegradation of azo dyes in aqueous solutions, *Environmental Technology*, 18, 1-12, **1997**.
- [13] Shourong, Z., Qingguo, H., Jun, Z., Bingkun, W.,. A study on dye photoremoval in TiO<sub>2</sub> suspension solution, *Journal of Photochemistry and Photobiology A: Chemistry*, 108, 235-238, **1997**.
- [14] Zielinska, B., Grzechulska, J., Grzmil, B., Morawski, A.W., Photocatalytic degradation od Reactive Black 5 A comparison between TiO<sub>2</sub>-Tytanpol A11 and TiO<sub>2</sub>-Degussa P25 photocatalysts, *Applied Catalysis B*, 35, L1-L7, **2001**.
- [15] Alaton, I.A., Balcioglu, I.A., Photochemical and heterogeneous photocatalytic degradation of waste vinyl sulphone dyes: A case study with hydrolysed Reactive Black 5, *J Journal of Photochemistry and Photobiology A: Chemistry*, 141, 247-254, **2001**.
- [16] Bergamini, R.B.M., Azevedo, E.B., Araújo, L.R.R., Heterogeneous photocatalytic degradation of reactive dyes in aqueous TiO<sub>2</sub> suspensions: Decolorization kinetics, *Chemical Engineering Journal*, 149, 215-220, **2009**.
- [17] Saggiaro, E.M., Oliveira, A.S., Pavesi, T., Maia, C.G., Ferreira, L.F.V., Moreira, J.C., Use of Titanium Dioxide Photocatalysis on the Remediation

- of Model Textile Wastewaters Containing Azo Dyes, *Molecules*, 16, 10370-10386, **2011**.
- [18] Ahmed, S., Rasul, M.G., Martens, W.N., Brown, R., Hashib, M.A., Advances in Heterogeneous Photocatalytic Degradation of Phenols and Dyes in Wastewaters: A Review, *Water Air and Soil Pollution*, 215, 3-29, **2011**.
- [19] Ahmed, S., Rasul, M.G., Martens, W.N., Brown, R., Hashib, M.A., Heterogeneous photocatalytic degradation of phenols in wastewater: A review on current status and developments, *Desalination*, 261, 3-18, **2010**.
- [20] Ksibi, M., Zemzemi, A., Boukchina, R., Photocatalytic degradability of substituted phenols over UV irradiated TiO<sub>2</sub>, *Journal of Photochemistry and Photobiology A: Chemistry*, 159, 61-70, **2003**.
- [21] Salaices, M., Serrano, B., de Lasa, H.I., Photocatalytic conversion of phenolic compounds in slurry reactors, *Chemical Engineering Science*, 59, 3-15, **2004**.
- [22] Trillas, M., Pujol, M., Domenech, X., Phenol Photodegradation over Titanium Dioxide, *Journal of Chemical Technology and Biotechnology*, 55, 85-90, **1992**.
- [23] Peiro, A.M., Ayllon, J.A., Peral, J., Domenech, X., TiO<sub>2</sub>-photocatalyzed degradation of phenol and ortho-substituted phenolic compounds, *Applied Catalysis B: Environmental*, 30, 359-373, **2001**.
- [24] Kusvuran, E., Samil, A., Atanur, O.M., Erbatur, O., Photocatalytic degradation of di- and trisubstituted phenolic compounds in aqueous solution by TiO<sub>2</sub>/UV, *Applied Catalysis B: Environmental*, 58, 211-216, **2005**.

- [25] Lee, J., Orilall, M., Warren, S., Kamperman, M., DiSalvo, F., Wiesner, U., Direct access to thermally stable and highly crystalline mesoporous transition-metal oxides with uniform pores, *Nature Materials*, 7, 222-228, **2008**.
- [26] Testino, A., Bellobono, I.R., Buscaglia, V., Canevali, C., D'Arienzo, M., Polizzi, S., Scotti, R., Morazzoni, F., Optimizing the photocatalytic properties of hydrothermal TiO<sub>2</sub> by the control of phase composition and particle morphology. A systematic approach, *Journal of the American Chemical Society*, 129, 3564-3575, **2007**.
- [27] Agrawal, M., Gupta, S., Pich, A., Zafeiropoulos, N.E., Rubio-Retama, J., Jehnichen, D., Stamm, M., Template-Assisted Fabrication of Magnetically Responsive Hollow Titania Capsules, *Langmuir*, 26, 17649–17655, **2010**.
- [28] Shen, P., Jiang, W., Wang, F., Chen, M., Ma, P., Li, F., Preparation and characterization of Fe<sub>3</sub>O<sub>4</sub>@TiO<sub>2</sub> shell on polystyrene beads, *Journal of Polymer Research*, 20, 252, **2013**.
- [29] Gao, Q., Wang, S., Luo, W.J., Feng, Y.Q., Facile synthesis of magnetic mesoporous titania and its application in selective and rapid enrichment of phosphopeptides, *Materials Letters*, 107, 202–205, **2013**.
- [30] Yao, S., Song, S., Shia, Z., Wang, S., Photocatalytic degradation of methylene blue by visible-light-driven yttrium-doped mesoporous titania coated magnetite photocatalyst, *Desalination and Water Treatment*, 51, 7101–7108, **2013**.
- [31] Caruso, R.A., Nanocasting and Nanocoating, *Topics in Current Chemistry*, 226, 91-118, **2003**.
- [32] Shchukin, D.G., Caruso, R.A., Template Synthesis and Photocatalytic Properties of Metal Oxide Spheres Formed by Nanoparticle Infiltration, *Chemistry of Materials*, 16, 2287-2292, **2004**.



- [33] Deshpande, A.S., Shchukin, D.G., Ustinovich, E., Antonietti, M., Caruso, R. A., Titania and mixed titania/aluminum, gallium, or indium oxide spheres: sol-gel/template synthesis and photocatalytic properties, *Advanced Functional Materials*, 15, 239-245, **2005**.
- [34] Meyer, U., Larsson, A., Hentze, H.P., Caruso, R. A., Templating of Porous Polymeric Beads to form Porous Silica and Titania Spheres, *Advanced Materials*, 14, 1768-1772, **2002**.
- [35] Wang, M.L., Wang, C.H., Wang, W., Porous macrobeads composed of metal oxide nanocrystallites and with percolated porosity, *Journal of Materials Chemistry*, 17, 2133–2138, **2007**.
- [36] Zhang, D., Yang, D., Zhang, H., Lu, C., Qi, L., Synthesis and photocatalytic properties of hollow microparticles of titania and titania/carbon composites templated by Sephadex G-100, *Chemistry of Materials*, 18, 3477-3485, **2006**.
- [37] Zhang, Q., Gao, L., Guo, J., Effect of hydrolysis conditions on morphology and crystallization of nanosized TiO<sub>2</sub> powder, *Journal of the European Ceramic Society*, 20, 2153-2158, **2000**.
- [38] Callister, W. D., *Materials Science and Engineering an Introduction*, John Wiley & Sons, **1996**.
- [39] De Lasa, H., Serrano, B., Salices, M., *Photocatalytic Reaction Engineering*, Springer, **2005**.
- [40] Köhler, K., Simmendinger, P., Roelle, W., Scholz, W., Valet A., Slongo, M. , Paints and Coatings, Pigments, Extenders, and Additives, *Ullmann's Encyclopedia of Industrial Chemistry*, Wiley-VCH, **2010**.

- [41] Music, S., Gotic, M., Ivanda, M., Popovic, S., Turkovic, A., Trojko, R., Sekulic, A., Furic, K., Chemical and microstructural properties of TiO<sub>2</sub> synthesized by sol–gel procedure, *Materials Science and Engineering: B*, 47, 33–40, **1997**.
- [42] Schneider, M., Baiker, A., Titania–based aerogel, *Catalysis Today*, 35, 339–365, **1997**.
- [43] Rana, S., Srivastava, R.S., Sorensson, M.M., Misra, R.D.K., *Materials Science and Engineering: B*, 119, 144-151, **2005**.
- [44] Fu, W., Yang, H., Changa, L., Bala, H., Li, M., Zou, G., Anatase TiO<sub>2</sub> nanolayer coating on strontium ferrite nanoparticles for magnetic photocatalyst, *Colloids and Surfaces A*, 289, 47-52, **2006**.
- [45] Carp, O., Huisman, C.L., Reller, A., Photoinduced reactivity of titanium dioxide, *Progress in Solid State Chemistry*, 32, 33-177, **2004**.
- [46] Cheng, P., Zheng, M., Jin, Y., Huang, Q., Gu, M., Preparation and characterization of silica-doped titania photocatalyst through sol-gel method, *Materials Letters*, 57, 2989-2994, **2003**.
- [47] Reck, E., Richards, M., TiO<sub>2</sub> manufacture and life cycle analysis, *Pigment and Resin Technology*, 28, 149-157, **1999**.
- [48] Landmann, M., Rauls, E., Schmidt, W.G., The electronic structure and optical response of rutile, anatase and brookite TiO<sub>2</sub>, *Journal of Physics: Condensed Matter*, 24, 195503, **2012**.
- [49] Mo, S.D., Ching, W.Y., Electronic and optical properties of three phases of titanium dioxide: Rutile, anatase, and brookite, *Physical Review B*, 51, 13023–13032, **1995**.

- [50] Fujishima, A., Zhang, X., Tryk, D.A., TiO<sub>2</sub> photocatalysis and related surface phenomena, *Surface Science Reports*, 63, 515-582, **2008**.
- [51] Liu, G., Wang, L., Yang, H.G., Cheng, H.M., Lu, G.Q., Titania-based photocatalysts—crystal growth, doping and heterostructuring, *Journal of Materials Chemistry*, 20, 831–843, **2010**.
- [52] Yu, J.G., Zhao, X.J., Zhao, Q.N., Effect of surface structure on photocatalytic activity of TiO<sub>2</sub> thin films prepared by sol-gel method, *Thin Solid Films*, 379, 7-14, **2000**.
- [53] Kolen'ko, Y.V., Churagulov, B.R., Kunst, M., Mazerolles, L., Colbeau-Justin, C., Photocatalytic Properties of Titania Powders Prepared by Hydrothermal Method, *Applied Catalysis B: Environmental*, 54 , 51-58, **2004**.
- [54] O'Regan, B., Gratzel, M., A low-cost, high-efficiency solar cell based on dye sensitized colloidal TiO<sub>2</sub> Films, *Nature*, 353, 737-740, **1991**.
- [55] Wang, G., Hydrothermal synthesis and photocatalytic activity of nanocrystalline TiO<sub>2</sub> powders in ethanol–water mixed solutions, *Journal of Molecular Catalysis A: Chemical*, 274, 185-191, **2007**.
- [56] Jing, L., Li, S., Song, S., Xue, L., Fu, H., Investigation on the electron transfer between anatase and rutile in nano-sized TiO<sub>2</sub> by means of surface photovoltage technique and its effects on the photocatalytic activity, *Solar Energy Materials and Solar Cells*, 92, 1030-1036, **2008**.
- [57] Francisco, M.S.P., Mastelaro, V.R., Inhibition of the anatase-rutile phase transformation with addition of CeO<sub>2</sub> to CuO-TiO<sub>2</sub> system: Raman spectroscopy, X-ray diffraction, and textural studies, *Chemistry of Materials*, 14, 2514-2518, **2002**.

- [58] Sun, H., Wang, C., Pang, S., Li, X., Tao, Y., Tang, H., Liu, M., Photocatalytic TiO<sub>2</sub> films prepared by chemical vapor deposition at atmosphere pressure, *Journal of Non-Crystalline Solids*, 354, 1440-1443, **2008**.
- [59] Giolli, C., Borgioli, F., Credi, A., Fabio, A.D., Fossati, A., Miranda, M.M., Parmeggiani, S., Rizzi, G., Scrivani, A., Troglio, S., Tolstoguzov, A., Zoppi, A., Bardi, U., Characterization of TiO<sub>2</sub> coatings prepared by a modified electric arc-physical vapour deposition system, *Surface and Coatings Technology*, 202, 13-22, **2007**.
- [60] Zhao, X., Liu, X., Ding, C., Chu, P.K., Effects of plasma treatment on bioactivity of TiO<sub>2</sub> coatings, *Surface and Coatings Technology*, 201, 6878-6881, **2007**.
- [61] Turkevych, I., Pihosh, Y., Goto, M., Kasahara, A., Tosa, M., Kato, S., Takehana, K., Takamasu, T., Kido, G., Koguchi, N., Photocatalytic properties of titanium dioxide sputtered on a nanostructured substrate, *Thin Solid Films*, 516, 2387-2391, **2008**.
- [62] Weng, X., Fisher, P., Skowronski, M., Salvador, P.A., Maksimov, O., Structural characterization of TiO<sub>2</sub> films grown on LaAlO<sub>3</sub> and SrTiO<sub>3</sub> substrates using reactive molecular beam epitaxy, *Journal of Crystal Growth*, 310, 545-550, **2008**.
- [63] Huang, N.K., Wang, D.Z., Lu, Z., Lin, L.B., X-Ray photoelectronspectroscopy characterization of TiO<sub>2</sub> films deposited by dynamic ion-beam mixing, *Surface and Coatings Technology*, 70, 69-71, **1994**.
- [64] Lee, J.H., Yang, Y.S., Effect of hydrolysis conditions on morphology and phase content in the crystalline TiO<sub>2</sub> nanoparticles synthesized from aqueous TiCl<sub>4</sub> solution by precipitation, *Materials Chemistry and Physics*, 93, 237-242, **2005**.

- [65] Bellardita, M., Addamo, M., Di Paola, A., Palmisano, L., Photocatalytic behaviour of metal-loaded TiO<sub>2</sub> aqueous dispersions and films, *Chemical Physics*, 339, 94-103, **2007**.
- [66] Hidalgo, M.C., Aguilar, M., Maicu, M., Navío, J.A., Colón, G., Hydrothermal preparation of highly photoactive TiO<sub>2</sub> nanoparticles, *Catalysis Today*, 129 50-58, **2007**.
- [67] Xie, R.C., Shang, J.K., Morphological control in solvothermal synthesis of titanium oxide, *Journal of Materials Science*, 42, 6583-6589, **2007**.
- [68] Andersson, M., Kiselev, A., Osterlund, L., Palmqvist, A.E.C., Microemulsion mediated room-temperature synthesis of high-surface-area rutile and its photocatalytic performance, *Journal of Physical Chemistry C*, 111 6789-6797, **2007**.
- [69] Kitamura, Y., Okinaka, N., Shibayama, T., Mahaney, O.O.P., Kusano, D., Ohtani, B., Akiyama, T., Combustion synthesis of TiO<sub>2</sub> nanoparticles as photocatalyst, *Powder Technology*, 176, 93-98, **2007**.
- [70] Sankapal, B.R., Sartale, S.D., Lux-Steiner, M.C., Ennaoui, A., Chemical and electrochemical synthesis of nanosized TiO<sub>2</sub> anatase for large-area photon conversion, *Comptes Rendus Chimie*, 9, 702-707, **2006**.
- [71] Kolen'ko, Y.V., Garshev, A.V., Churagulov, B.R., Boujday, S., Portes, P., Colbeau-Justin, C., Photocatalytic activity of sol-gel derived titania converted into nanocrystalline powders by supercritical drying, *Journal of Photochemistry and Photobiology A: Chemistry*, 172, 19-26, **2005**.
- [72] Wang, W.D., Silva, C.G., Faria, J.L., Photocatalytic degradation of Chromotrope 2R using nanocrystalline TiO<sub>2</sub>/activated-carbon composite catalysts, *Applied Catalysis B: Environmental*, 70, 470-478, **2007**.

- [73] Tong, T., Zhang, J., Tian, B., Chen, F., He, D., Preparation of Fe<sup>3+</sup>-doped TiO<sub>2</sub> catalysts by controlled hydrolysis of titanium alkoxide and study on their photocatalytic activity for methyl orange degradation, *Journal of Hazardous Materials*, 155, 572-579, **2008**.
- [74] Schubert, U., Hüsing, N., Synthesis of inorganic materials, *Wiley-Vch Verlag GmbH & Co*, **2005**.
- [75] Brinker, C. J., Scherer, G.W., Sol-gel science, *Academic Press*, **1990**.
- [76] Zhang, Q.H., Gao, L., Guo, J.K., Preparation and characterization of nanosized TiO<sub>2</sub> powders from aqueous TiCl<sub>4</sub> solution, *Nanostructured Materials*, 11, 1293-1300, **1999**.
- [77] Sivakumar, S., Sibin, C.P., Mukundan, P., Pillai, P.K., Warriar, K.G.K., Nanoporous titania-alumina mixed oxides - an alkoxide free sol-gel synthesis, *Materials Letters*, 58, 2664-2669, **2004**.
- [78] Nag, M., Basak, P., Manorama, S.V., Low-temperature hydrothermal synthesis of phase-pure rutile titania nanocrystals: time temperature tuning of morphology and photocatalytic activity, *Materials Research Bulletin*, 42, 1691-1704, **2007**.
- [79] Hu, S., Wang, H., Cao, J., Liu, J., Fang, B., Zheng, M., Ji, G., Zhang, F., Yang, Z., Synthesis of mesostructure anatase TiO<sub>2</sub> particles in room-temperature ionic liquids, *Materials Letters*, 62, 2954-2956, **2008**.
- [80] Kanna, M., Wongnawa, S., Mixed amorphous and nanocrystalline TiO<sub>2</sub> powders prepared by sol-gel method: characterization and photocatalytic study, *Materials Chemistry and Physics*, 110: 166-175, **2008**.

- [81] Wu, L., Yu, J.C., Wang, X., Zhang, L., Yu, J., Characterization of mesoporousnanocrystalline TiO<sub>2</sub> photocatalysts synthesized via a sol–solvothermal process at a low temperature, *Journal of Solid State Chemistry*, 178, 321–328, **2005**.
- [82] Liu, T., Li, F., Li, X., Effects of peptizing conditions on nanometer properties and photocatalytic activity of TiO<sub>2</sub> hydrosols prepared by H<sub>2</sub>TiO<sub>3</sub>, *Journal of Hazardous Materials*, 155, 90–99, **2008**.
- [83] Liu, T., Li, F., Li, X., TiO<sub>2</sub> hydrosols with high activity for photocatalyticdegradation of formaldehyde in a gaseous phase. *Journal of Hazardous Materials*, 152, 347–355, **2008**.
- [84] Lee, D.S., Liu, T.K., Preparation of TiO<sub>2</sub> sol using TiCl<sub>4</sub> as a precursor, *Journal of Sol-Gel Science and Technology*, 25, 121–136, **2002**.
- [85] Addamo, M., Augugliaro, V., Di Paola, A., Garcia–Lopez, E., Loddo, V., Marc, G., Palmisano, L., Preparation and photoactivity of nanostructured TiO<sub>2</sub> particles obtained by hydrolysis of TiCl<sub>4</sub>, *Colloids and Surfaces A: Physicochemical and Engineering Aspects*, 265, 23– 31, **2005**.
- [86] Randorn, C., Wongnawa, S., Boonsin, P., Bleaching of methylene blue by hydrated titanium dioxide, *Science Asia*, 30,149–156, **2004**.
- [87] Deshpande, A. S., Niederberger, M., Synthesis of mesoporous ceria zirconia beads, *Microporous Mesoporous Materials*, 101, 413-418, **2007**.
- [88] Naydenov, V., Tosheva, L., Sterte, J., Vanadium modified AIPO-5 spheres through resin macrotemplating, *Microporous Mesoporous Materials*, 66, 321-329, **2003**.

- [89] Zhou, J. F., Zhou, M. F., Caruso, R. A., Agarose Template for the Fabrication of Macroporous Metal Oxide Structures, *Langmuir*, 22, 3332-3336, **2006**.
- [90] Huang, F., Zhou, M., Cheng, Y.B., Caruso, R. A., Al-Containing Porous Titanium Dioxide Networks: Sol-Gel Synthesis within Agarose Gel Template and Photocatalytic Activity, *Chemistry of Materials*, 18, 5835-5839, **2006**.
- [91] Du, K. F., Yang, D., Sun, Y., Controlled Fabrication of Porous Titania Beads by a Sol-Gel Templating Method, *Industrial & Engineering Chemistry Research*, 48, 755-762, **2009**.
- [92] Paine, A.J., Luymes, W., McNulty, J., Dispersion polymerization of styrene in polar Solvents. 6. Influence of reaction parameters on particle size and molecular weight in poly(N-vinylpyrrolidone)-stabilized reactions, *Macromolecules*, 23, 3104-3109, **1990**.
- [93] Kawaguchi, S., Winnik, M.A., Ito, K., Dispersion copolymerization of n-butyl methacrylate with poly(ethylene oxide) macromonomers in methanol-water. Comparison of experiment with theory, *Macromolecules*, 28, 1159-1166, **1995**.
- [94] Barrett, K.E.J., Dispersion Polymerization in Organic Media, *John Wiley & Sons, London*, **1975**.
- [95] Ellingsen, T., Aune, O., Ugelstad, J., Hagen, S., Monosized stationary phases for chromatography, *Journal of Chromatography*, 535, 147-161, **1990**.
- [96] Ugelstad, J., Berge, A., Ellingsen, T., Schmid, R., Nilsen, T.N., Mørk P.C., Sienstad, P., Hornes, E., Olsvik, Ø., Preparation and application of new monosized polymer particles, *Progress in Polymer Science*, 17, 87-161, **1992**.



- [97] Camli, S.T., Senel, S., Tuncel, A., Cibacron blue F3G-A-attached uniform and macroporous poly(styrene-co-divinylbenzene) particles for specific albumin adsorption, *Journal of Biomaterials Science: Polymer Edition*, 10, 875-889, **1999**.
- [98] Galperin, A., Margel, S., Synthesis and characterization of new radiopaque microspheres by the dispersion polymerization of an iodinated acrylate monomer for X-ray imaging applications, *Journal of Polymer Science, Part A: Polymer Chemistry*, 44, 3859-3868, **2006**.
- [99] Almog, Y., Reich, S., Levy, M., Monodisperse Polymeric Spheres In The Micron Size Range By A Single Step Process, *British Polymer Journal*, 14, 131-136, **1982**.
- [100] Bromberg, L., Polyether-Modified Poly(acrylic acid): Synthesis and Applications, *Industrial and Engineering Chemistry Research*, 37, 4267-4274, **1998**.
- [101] Kawaguchi, H., Functional polymer microspheres, *Progress in Polymer Science*, 25, 1171-1210, **2000**.
- [102] Paine, A.J., Dispersion polymerization of styrene in polar solvents. 7. A simple mechanistic model to predict particle size, *Macromolecules*, 23, 3109-3117, **1990**.
- [103] Deslandes, Y., Mitchell, D.F., Paine, A.J., X-ray photoelectron spectroscopy and static time-of-flight secondary ion mass spectrometry study of dispersion polymerized polystyrene latexes, *Langmuir*, 9, 1468-1472, **2002**.
- [104] Shen, S., Sudol, E.D., El-Aasser, M.S., Dispersion polymerization of methyl methacrylate: Mechanism of particle formation, *Journal of Polymer Science, Part A: Polymer Chemistry*, 32, 1087-1100, **1994**.

- [105] Lacroix-Desmazes, P., Guillot, J., Dispersion polymerization of styrene in ethanol-water media: Monomer partitioning behavior and locus of polymerization, *Journal of Polymer Science, Part B: Polymer Physics*, 36, 325-335, **1998**.
- [106] Lok, K.P., Ober, C.K., Particle-size control in dispersion polymerization of polystyrene, *Canadian Journal of Chemistry*, 63, 209-216, **1985**.
- [107] Ober, C. K., Hair, M. L., The effect of temperature and initiator levels on the dispersion polymerization of polystyrene, *Journal of Polymer Science Polymer Chemistry Edition*, 25, 1395-1407, **1987**.
- [108] Tseng, C.M., Lu, Y.Y., El-Aasser, M.S., Vanderhoff, J.W., Uniform polymer particles by dispersion polymerization in alcohol, *Journal of Polymer Science, Part A: Polymer Chemistry*, 24, 2995-3007, **1986**.
- [109] Shen, S., Sudol, E.D., El-Aasser, M.S., Control of particle size in dispersion polymerization of methyl methacrylate, *Journal of Polymer Science, Part A: Polymer Chemistry*, 31, 1393-1402, **1993**.
- [110] Fitch, R.M., The homogeneous nucleation of polymer colloids, *British Polymer Journal*, 5, 467-483, **1973**.
- [111] Becker, R., Döring, W., Kinetic treatment of the nucleation in supersaturated vapour, *Annalen Der Physik*, 24, 719-752, **1935**.
- [112] Harkins, W.D., A general theory of the mechanism of emulsion polymerization, *Journal of the American Chemical Society*, 69, 1428-1444, **1947**.
- [113] Barrett, K.E.J., Thomas, H.R., Kinetics of dispersion polymerization of soluble monomers. I. Methyl methacrylate, *Journal of Polymer Science Part A-1, Polymer Chemistry*, 7, 2621-2650, **1969**.

- [114] Paine, A.J., Dispersion polymerization of styrene in polar solvents. I. Grafting mechanism of stabilization by hydroxypropyl cellulose, *Journal of Colloid And Interface Science*, 138, 157-169, **1990**.
- [115] Gokmen, M.T., Du Prez, F.E., Porous polymer particles—A comprehensive guide to synthesis, characterization, functionalization and applications, *Progress in Polymer Science*, 37, 365– 405, **2012**.
- [116] Bamnolker, H., Margel, S., Dispersion polymerization of styrene in polar solvents: Effect of reaction parameters on microsphere surface composition and surface properties, size and size distribution, and molecular weight, *Journal of Polymer Science, Part A: Polymer Chemistry*, 34, 1857-1871, **1996**.
- [117] Sáenz, J.M., Asua, J.M., Dispersion polymerization in polar solvents, *Journal of Polymer Science, Part A: Polymer Chemistry*, 33:1511-1521, **1995**.
- [118] Ugelstad, J., Kaggerud, K.H., Hansen, F.K., Berge, A., Absorption of low molecular weight compounds in aqueous dispersions of polymeroligomer particles, 2. A two step swelling process of polymer particles giving an enormous increase in absorption capacity, *Makromolekulare Chemie*, 180, 737–44, **1979**.
- [119] Slater, M., Snauko, M., Svec, F., Fréchet, J.M.J., “Click chemistry” in the preparation of porous polymer-based particulate stationary phases for  $\mu$ -HPLC separation of peptides and proteins, *Analytical Chemistry*, 78, 4969–4975, **2006**.

- [120] Wang, Q. C., Svec, F., Fréchet, J. M. J., Fine Control of the Porous Structure and Chromatographic Properties of Monodisperse Macroporous Poly(styrene-co-divinylbenzene) Beads Prepared Using Polymer Porogens, *Journal of Polymer Science Part A: Polymer Chemistry*, 32, 2577- 2588, **1994**.
- [121] Camli, T., Tuncel, M., Şenel, S., Tuncel, A., Functional, uniform, and macroporous latex particles: preparation, electron microscopic characterization, and nonspecific protein adsorption properties, *Journal of Applied Polymer Science*, 84, 414–429, **2002**.
- [122] Caglayan, B., Unsal, E., Çamli, S.T., Tuncel, M., Tuncel, A., Monodisperse Porous Poly(vinylacetate-co-divinylbenzene) Particles by Single-Stage Seeded Polymerization: A Packing Material for Reversed Phase HPLC, *Separation Science*, 29, 936-944, **2006**.
- [123] Chen, X., Mao, S.S., Titanium dioxide nanomaterials: synthesis, properties, modifications, and applications, *Chemical Reviews*, 107, 2891-959, **2007**.
- [124] Peng, T., Zhao, D., Dai, K., Shi, W., Hirao, K., Synthesis of titanium dioxide nanoparticles with mesoporous anatase wall and high photocatalytic activity, *Journal of Physical Chemistry B*, 109, 4947-4952, **2005**.
- [125] Zhou, W., Sun, F., Pan, K., Tian, G., Jiang, B., Ren, Z., Tian, C., Fu, H., Well-Ordered Large-Pore Mesoporous Anatase TiO<sub>2</sub> with Remarkably High Thermal Stability and Improved Crystallinity: Preparation, Characterization, and Photocatalytic Performance, *Advanced Functional Materials*, 21, 1922-1930, **2011**.
- [126] Dai, K., Peng, T., Chen, H., Liu, J., Zan, L., Photocatalytic degradation of commercial phoxim over La-doped TiO<sub>2</sub> nanoparticles in aqueous suspension, *Environmental Science & Technology*, 43, 1540-1545, **2009**.

- [127] Oregan, B., Gratzel, M., A low-cost, high-efficiency solar cell based on dye-sensitized colloidal TiO<sub>2</sub> films, *Nature*, 353, 737-740, **1991**.
- [128] Uchida, S., Chiba, R., Tomiha, M., Masaki, N., Shirai, M., Application of Titania Nanotubes to a Dye-Sensitized Solar Cell, *Electrochemistry*, 70, 418-420, **2002**.
- [129] Adachi, M., Murata, Y., Takao, J., Jiu, J.T., Sakamoto, M., Wang, F.M., Highly Efficient Dye-Sensitized Solar Cells with a Titania Thin-Film Electrode Composed of a Network Structure of Single-Crystal-like TiO<sub>2</sub> Nanowires Made by the "Oriented Attachment" Mechanism, *Journal of American Chemical Society*, 126, 14943-14949, **2004**.
- [130] Song, M.Y., Kim, D.K., Ihn, K.J., Jo, S.M., Kim, D.Y., Electrospun TiO<sub>2</sub> electrodes for dyesensitized solar cells, *Nanotechnology*, 15, 1861-1865, **2004**.
- [131] Khan, M.A., Akhtar, M.S., Yang, O.B., Synthesis, characterization and application of sol-gel derived mesoporous TiO<sub>2</sub> nanoparticles for dye-sensitized solar cells, *Solar Energy*, 84, 2195-2201, **2010**.
- [132] Zhao, D., Peng, T., Lu, L., Cai, P., Jiang, P., Bian, Z., Effect of Annealing Temperature on the Photoelectrochemical Properties of Dye-Sensitized Solar Cells Made with Mesoporous TiO<sub>2</sub> Nanoparticles, *Journal of Physical Chemistry C*, 112, 8486-8494, **2008**.
- [133] Benkstein, K.D., Semancik, S., Mesoporous nanoparticle TiO<sub>2</sub> thin films for conductometric gas sensing on microhotplate platforms, *Sensors and Actuators B: Chemical*, 113, 445-453, **2006**.
- [134] Devi, G.S., Hyodo, T., Shimizu, Y., Egashira, M., Synthesis of mesoporous TiO<sub>2</sub>-based powders and their gas-sensing properties, *Sensors and Actuators B: Chemical*, 87, 122-129, **2002**.

- [135] Wu, K.C.W., Yamauchi, Y., Hong, C.Y., Yang, Y.H., Liang, Y.H., Funatsu, T., Tsunoda, M., Biocompatible, surface functionalized mesoporous titania nanoparticles for intracellular imaging and anticancer drug delivery, *Chemical Communications*, 47, 5232-5234, **2011**.
- [136] Serpone, N., Pelizzetti, E., Photocatalysis. Fundamentals and applications, *Wiley Interscience, New York*, **1989**.
- [137] Cardenas Lizana, F., Gomez Quero, S., Idriss, H., Keanne, M.A., Gold particle size effects in the gas-phase hydrogenation of m-dinitrobenzene over Au/TiO<sub>2</sub>, *Journal of Catalysis*, *Journal of Catalysis*, 268, 223-234, **2009**.
- [138] Nguyen, L.Q., Salim, C., Hinode, H., Performance of nano-sized Au/TiO<sub>2</sub> for selective catalytic reduction of NO<sub>x</sub> by propene, *Applied Catalysis A: General*, 94-99, **2008**.
- [139] Nguyen, L.Q., Salim, C., Hinode, H., Promotive Effect of MO<sub>x</sub> (M=Ce, Mn) Mechanically Mixed with Au/TiO<sub>2</sub> on the Catalytic Activity for Nitrogen Monoxide Reduction by Propene, *Topics in Catalysis*, 52, 779-783, **2009**.
- [140] Chang, Y.C., Chen, D.H., Catalytic reduction of 4-nitrophenol by magnetically recoverable Au nanocatalyst, *Journal of Hazardous Materials*, 165, 664-669, **2009**.
- [141] Damato, T.C., Oliveira, C.C.S., Ando, R.A., Camargo, P.H.C., A Facile Approach to TiO<sub>2</sub> Colloidal Spheres Decorated with Au Nanoparticles Displaying Well-Defined Sizes and Uniform Dispersion, *Langmuir*, 29, 1642-1649, **2013**.

- [142] Yazid, H., Adnan, R., Farrukh, M.A., Gold nanoparticles supported on titania for the reduction of p-nitrophenol, *Indian Journal of Chemistry*, 52A, 184-191, **2013**.
- [143] Fujishima, A., Honda, K., Electrochemical photolysis of water at a semiconductor electrode, *Nature*, 238, 37-38, **1972**.
- [144] Bean, C. P., Livingston, J. D., Superparamagnetism, *Journal of Applied Physics*, 30, 120-129, **1959**.
- [145] Chen, D., Ray, A.K., Photocatalytic kinetics of phenol and its derivatives over UV irradiated TiO<sub>2</sub>, *Applied Catalysis B: Environmental*, 23, 143–157, **1999**.
- [146] Herrmann, J.M., Heterogeneous photocatalysis: State of the art and present applications, *Topics in Catalysis*, 34, 49-65, **2005**.
- [147] Obuchi, E., Sakamoto, T., Nakano, K., Shiraishi, F., Photocatalytic decomposition of acetaldehyde over TiO<sub>2</sub>/SiO<sub>2</sub> catalyst, *Chemical Engineering Science*, 54, 1525–1530, **1999**.
- [148] Carey, J.H., Lawrence, J., Tosine, H.M., Photodechlorination of PCB's in the presence of titanium dioxide in aqueous suspensions, *Bulletin of Environmental Contamination and Toxicology*, 16, 697-701, **1976**.
- [149] Yu, K., Lee, G.W.M., Huang, W., Wu, C., Yang, S., The correlation between photocatalytic oxidation performance and chemical/physical properties of indoor volatile organic compounds, *Atmospheric Environment*, 40, 375–385, **2006**.
- [150] Herrmann, J.M., Heterogeneous photocatalysis: fundamentals and applications to the removal of various types of aqueous pollutants, *Catalysis Today*, 53, 115–129, **1999**.

- [151] Litter, M.I., Heterogeneous photocatalysis, transition metal ions in photocatalytic systems. *Applied Catalysis B: Environmental*, 23, 89–114, **1999**.
- [152] Puma, G.L., Bono, A., Krishnaiah, D., Collin, J.G., Preparation of titanium dioxide photocatalyst loaded onto activated carbon support using chemical vapor deposition: A review paper, *Journal of Hazardous Materials*, 157: 209–219, **2008**.
- [153] Oppenländer, T., Photochemical Purification of Water and Air. Advanced Oxidation Processes (AOPs): Principles, Reaction Mechanisms, Reactor Concepts, *Wiley-VCH, Berlin*, **2003**.
- [154] Bacsa, R.R., Kiwi, J., Effect of rutile phase on the photocatalytic properties of nanocrystalline titania during the degradation of p-coumaric acid, *Applied Catalysis B: Environmental*, 16, 19–29, **1998**.
- [155] Ayllón, J.A., Figueras, A., Garelik, S., Spirkova, L., Durand, J., Cot, L., Preparation of TiO<sub>2</sub> powder using titanium isopropoxide decomposition in a plasma enhanced chemical vapor deposition (PECVD) reactor, *Journal of Materials Science Letters*, 18, 1319-1321, **1999**.
- [156] Ohtani, B., Ogawa, Y., Nishimoto, S., Photocatalytic activity of amorphous anatase mixture of titanium(IV) oxide particles suspended in aqueous solutions, *The Journal of Physical Chemistry B*, 101, 3746-3752, **1997**.
- [157] Zhang, Z., Wang, C.C., Zakaria, R., Ying, J.Y., Role of particle size in nanocrystalline TiO<sub>2</sub>-based photocatalysts, *Journal of Physical Chemistry B*, 102, 10871-10878, **1998**.
- [158] Li, X., Quan, X., Kutal, C., Synthesis and photocatalytic properties of quantum confined titanium dioxide nanoparticle, *Scripta Materialia*, 50, 499-505, **2004**.



- [159] Stafford, U., Gray, K.A., Kamat, P.V., Radiolytic and TiO<sub>2</sub>-Assisted Photocatalytic Degradation of 4-Chlorophenol. A Comparative Study. *Journal of Physical Chemistry*, 98, 6343-6351, **1994**.
- [160] Turchi, C.S., Ollis, D.F., Photocatalytic Degradation of Organic Water Contaminants: Mechanisms Involving Hydroxyl Radical Attack, *Journal of Catalysis*, 122, 178-192, **1990**.
- [161] van Dyk, A.C., Heyns, A.M., Dispersion stability and photo-activity of rutile (TiO<sub>2</sub>) powders, *Journal of Colloid and Interface Science*, 206, 381-391, **1998**.
- [162] Ollis, D.F., Kinetics of liquid phase photocatalyzed reactions: an illuminating approach, *Journal of Physical Chemistry B*, 109, 2439-2444, **2005**.
- [163] Son, H.S., Choi, S.B., Zoh, K.D., Khan, E., Effects of ultraviolet intensity and wavelength on the photolysis of triclosan, *Water Science & Technology*, 55 209–216, **2007**.
- [164] Son, H.S., Ko, G., Zoh, K.D., Kinetics and mechanism of photolysis and TiO<sub>2</sub> photocatalysis of triclosan, *Journal of Hazardous Materials*, 166, 954-960, **2009**.
- [165] Gaya, U.I., Abdullah, A.H., Heterogeneous photocatalytic degradation of organic contaminants over titanium dioxide: A review of fundamentals, progress and problems, *Journal of Photochemistry and Photobiology C Photochemistry Reviews*, 9, 1-12, **2008**.
- [166] Cao, Y.A., Yang, W.S., Zhang, W.F., Liu, G.Z., Yue, P.L., Improved photocatalytic activity of Sn<sup>4+</sup> doped TiO<sub>2</sub> nanoparticulate films prepared by plasma-enhanced chemical vapor deposition, *New Journal of Chemistry*, 28, 218-222, **2004**.

- [167] Li, F.B., Li, X.Z., Photocatalytic properties of gold/gold ion-modified titanium dioxide for wastewater treatment, *Applied Catalysis A: General*, 228, 15-27, **2002**.
- [168] Venkatachalam, N., Palanichamy, M., Murugesan, V., Sol-gel preparation and characterization of alkaline earth metal doped nano TiO<sub>2</sub>: Efficient photocatalytic degradation of 4-chlorophenol, *Journal of Molecular Catalysis A: Chemical*, 273, 177-185, **2007**.
- [169] Yu, J., Liu, S., Xiu, Z., Yu, W., Feng, G., Combustion synthesis and photocatalytic activities of Bi<sup>3+</sup>-doped TiO<sub>2</sub> nanocrystals, *Journal of Alloys and Compounds*, 461, L17-L19, **2008**.
- [170] Low, A., Bansal, V., A visual tutorial on the synthesis of gold nanoparticles *Biomedical Imaging and Intervention Journal*, 6, e9, **2010**.
- [171] Lu, X., Tuan, H.Y., Korgelc, B.A., Xia, Y., Facile Synthesis of Gold Nanoparticles with Narrow Size Distribution by Using AuCl or AuBr as the Precursor, *Chemistry*, 14, 1584–1591, **2008**.
- [172] Mallick, K., Witcomb, M., Erasmus, R.M., Strydom, A.M., Low temperature magnetic property of polymer encapsulated gold nanoparticles, *Journal of Applied Physics*, 106, 074303-074209, **2009**.
- [173] Kimling, J., Maier, M., Okenve, B., Kotaidis, V., Ballot, H., Plech, A., Turkevich Method for Gold Nanoparticle Synthesis Revisited, *Journal of Physical Chemistry B*, 110, 15700–15707, **2006**.
- [174] Brust, M., Walker, M., Bethell, D., Schiffrin, D.J., Whyman, R., Synthesis of Thiol-derivatised Gold Nanoparticles in a Two-phase Liquid-Liquid System". *Chemical Communications*, 801-802, **1994**.

- [175] Martin, M.N., Basham, J.I., Chando, P., Eah, S.K., Charged gold nanoparticles in non-polar solvents: 10-min synthesis and 2D self-assembly, *Langmuir*, 26, 7410-7417, **2010**.
- [176] Turkevich, J., Stevenson, P.C., Hillier, J., A study of the nucleation and growth processes in the synthesis of colloidal gold, *Discussions of the Faraday Society*, 11, 55-75, **1951**.
- [177] Frens, G., Particle size and sol stability in metal colloids, *Colloid & Polymer Science*, 250, 736-741, **1972**.
- [178] Frens, G., Controlled nucleation for the regulation of the particle size in monodisperse gold suspensions, *Nature Physical Science*, 241, 20-22, **1973**.
- [179] Jiang, W.Q., Yang, H.C., Yang, S.Y., Horng, H.E., Hung, J.C., Chen, Y.C., Hong, C.Y., Preparation and properties of superparamagnetic nanoparticles with narrow size distribution and biocompatible, *Journal of Magnetism and Magnetic Materials*, 283, 210-214, **2004**.
- [180] Dacoata, G.M., Degrave, E., Debakker, P.M.A., Vandenberghe, R.E., Synthesis and Characterization of Some Iron-Oxides by Sol-Gel Method, *Journal of Solid State Chemistry*, 113, 405-412, **1994**.
- [181] Deng, Y., Wang, L., Yang, W., Fu, S., Elaissari, A., Preparation of magnetic polymeric particles via inverse microemulsion polymerization process, *Journal of Magnetism and Magnetic Materials*, 257, 69-78, **2003**.
- [182] Chen, D., Xu, R., Hydrothermal synthesis and characterization of nanocrystalline Fe<sub>3</sub>O<sub>4</sub> powders, *Materials Research Bulletin*, 33, 1015-1021, **1998**.

- [183] Hyeon, T., Lee, S.S., Park, J., Chung, Y., Na, H.B., Synthesis of Highly Crystalline and Monodisperse Maghemite Nanocrystallites without a Size-Selection Process, *Journal of American Chemical Society*, 123, 12798-12801, **2001**.
- [184] Kang, Y.S., Risbud, S., Rabolt, J.F., Stroeve, P., Synthesis and Characterization of Nanometer-Size  $\text{Fe}_3\text{O}_4$  and  $\gamma\text{-Fe}_2\text{O}_3$  Particles, *Chemistry Materials*, 8, 2209-2211, **1996**.
- [185] Massart, R., Preparation of aqueous magnetic liquids in alkaline and acidic media, *IEEE Transactions on Magnetics*, 17, 1247-1248, **1981**.
- [186] Boistelle, R., Astier, J.P., Crystallization Mechanisms in Solutions, *Journal of Crystal Growth*, 90, 14-30, **1988**.
- [187] Elmas, B., Tuncel, M., Yalcin, G., Senel, S., Tuncel, A., Synthesis of uniform, fluorescent poly(glycidyl methacrylate) based particles and their characterization by confocal laser scanning microscopy, *Colloids and Surfaces A*, 269, 125–134, **2005**.
- [188] Kip, C., Maras, B., Evirgen, O., Tuncel, A., A new type of monodisperse porous, hydrophilic microspheres with reactive chloroalkyl functionality: synthesis and derivatization properties, *Colloid and Polymer Science*, 292, 219–228, **2014**.
- [189] Ma, Z., Guan, Y., Liu, H., Synthesis and Characterization of Micron-Sized Monodisperse Superparamagnetic Polymer Particles with Amino Groups, *Journal of Polymer Science: Part A: Polymer Chemistry*, 43, 3433–3439 **2005**.
- [190] Hamaloğlu, K.Ö., Çelebi, B., Sağ, E., Tuncel, A., A new method for the synthesis of monodisperse-porous titania microbeads by using polymethacrylate microbeads as template, *Microporous and Mesoporous Materials*, 207, 17-26, **2015**.

- [191] Moreau, F., Bond, G.C., Preparation and reactivation of Au/TiO<sub>2</sub> catalysts, *Catalysis Today*, 122, 260-265, **2007**.
- [192] Habibi, M.H., Hassanzadeh, A., Mahdavi, S., The effect of operational parameters on the photocatalytic degradation of three textile azo dyes in aqueous TiO<sub>2</sub> suspensions, *Journal of Photochemistry and Photobiology A: Chemistry*, 172, 89-96, **2005**.
- [193] Bizani, E., Fytianos, K., Poullos, I., Tsiridis, V., Photocatalytic decolorization and degradation of dye solutions and wastewaters in the presence of titanium dioxide, *Journal of Hazardous Materials*, 136, 85-94, **2006**.
- [194] Chen, C., Lu, C., Chung, Y., Photocatalytic degradation of ethyl violet in aqueous solution mediated by TiO<sub>2</sub> suspensions, *Journal of Photochemistry and Photobiology A: Chemistry*, 181, 120-125, **2006**.
- [195] Feng, W., Nansheng, D., Helin, H., Degradation mechanism of azo dye C.I. reactive red 2 by iron powder reduction and photooxidation in aqueous solutions, *Chemosphere*, 41, 1233-1238, **2000**.
- [196] Karkmaz, M., Puzenat, E., Guillard, C., Herrmann, J.M., Photocatalytic degradation of the alimentary azo dye amaranth mineralization of the azo group to nitrogen, *Applied Catalysis B: Environmental*, 51, 183-194, **2004**.
- [197] Daneshvar, N., Salari, D., Khataee, A.R., Photocatalytic degradation of azo dye acid red 14 in water: investigation of the effect of operational parameters, *Journal of Photochemistry and Photobiology A: Chemistry*, 157, 111-116, **2003**.
- [198] Grzechulska, J., Morawski, A.W., Photocatalytic decomposition of azo-dye acid black 1 in water over modified titanium dioxide. *Applied Catalysis B: Environmental*, 36, 45-51, **2002**.

- [199] Kamat, P.V., Photophysical, Photochemical and Photocatalytic Aspects of Metal Nanoparticles, *Journal of Physical Chemistry B*, 106, 7729–7744, **2002**.
- [200] Sobczynski, A., Duczmal, L., Zmudzinski, W., Phenol destruction by photocatalysis on TiO<sub>2</sub>: An attempt to solve the reaction mechanism, *Journal of Molecular Catalysis A: Chemical*, 213, 225-230, **2004**.
- [201] He, Z.Q., Xie, L., Tu, J.J., Song, S., Liu, W.P., Liu, Z.W., Fan, J.Q., Liu, Q., Chen, J.M., Visible Light-Induced Degradation of Phenol over Iodine-Doped Titanium Dioxide Modified with Platinum: Role of Platinum and the Reaction Mechanism, *Journal of Physical Chemistry C*, 114, 526-532, **2010**.
- [202] Vinu, R., Madras, G., Environmental remediation by photocatalysis, *Journal of the Indian Institute of Science*, 90,189-230, **2010**.
- [203] Laoufi, N.A., Tassalit, D., Bentahar, F., The degradation of pheol in water solution by TiO<sub>2</sub> photocatalysis in a helical reactor, *Global NEST Journal*,10, 404-418, **2008**.
- [204] Ortiz-Gomez, A., Serrano-Rosales, B., de Lasa, H., Enhanced mineralization of phenol and other hydroxylated compounds in a photocatalytic process assited with ferric ions, *Chemical Engineering Science*, 63, 520-557, **2008**.
- [205] Chhor, K., Bocquet, J.F., Cobeau-Justin, C., Comparative studies of phenol and salicylic acid photocatalytic degradation: Influence of adsorbed oxygen, *Materials Chemistry and Physics*, 86, 123-131, **2004**.
- [206] Wang, Z., Cai, W., Hong, X., Zhao, X., Xu, F., Cai, C., Photocatalytic degradation of phenol in aqueous nitrogen-doped TiO<sub>2</sub> suspensions with various light sources, *Applied Catalysis B: Environmental*, 57, 223-231, **2005**.

- [207] Barakat, M.A., Schaeffer, H., Hayes, G., Ismat-Shah, S., Photocatalytic degradation of 2- Chlorophenol by Co-doped TiO<sub>2</sub> nanoparticles, *Applied Catalysis B: Environmental*, 57, 23-30, **2005**.
- [208] Hong, S.S., Ju, C.S., Lim, C.G., Ahn, B.H., Lim, K.T., Lee, G.D., A photocatalytic degradation of phenol over TiO<sub>2</sub> prepared by sol-gel method. *Journal of Industrial and Engineering Chemistry*, 7, 99-104, **2001**.
- [209] Chiou, C.H., Juang, R.S., Photocatalytic degradation of phenol in aqueous solutions by Prdoped TiO<sub>2</sub> nanoparticles, *Journal of Hazardous Materials*, 149, 1-7, **2007**.
- [210] Pradhan, N., Pal, A., Pal, T., Silver nanoparticle catalyzed reduction of aromatic nitro compounds, *Colloids and Surfaces A: Physicochemical and Engineering Aspects*, 196, 247-257, **2002**.
- [211] Esumi, K., Miyamoto, K., Yoshimura, T., Comparison of PAMAM-Au and PPI-Au nanocomposites and their catalytic activity for reduction of 4-nitrophenol, *Journal of Colloid and Interface Science*, 254, 402-405, **2002**.

## CURRICULUM VITAE

### Credentials

Name, Surname: Kadriye Özlem HAMALOĞLU  
Place of Birth: Ankara  
Marital Status: Married  
E-mail: ozlemnaz@hacettepe.edu.tr  
Address: Hacettepe University Chemical Engineering Department  
BEYTEPE/ ANKARA

### Education

High School: Ankara Atatürk Anatolian High School  
BSc. : Hacettepe University Chemical Engineering Department  
MSc. : Hacettepe University Chemical Engineering Department  
PhD.: Hacettepe University Chemical Engineering Department

### Foreign Languages

İngilizce: Advanced  
Almanca: Intermediate

### Work Experience

29/06/2010–Continues Reseach Assistant,  
Hacettepe University Chemical Engineering Department  
BEYTEPE/ANKARA  
06/2007 - 07/2007 TAI, ANKARA (internship)  
07/2006 – 08/2006 Çimsa Cement Factory (internship)  
07/2005 – 08/2005 MTA, ANKARA (internship)

### Areas of Experience

- Nanoparticle Synthesis
- Polymer Science
- Titania
- Surface Functionalization
- Material Characterization



- Photocatalysis

### Projects and Budgets

Synthesis of Monodisperse-Porous Titanium Dioxide Microparticles by Sol-gel Templating Method, BAP(014 D09 604 001-737), Project Period: 29/09/2014-29/06/2015, Budget: 18600 TL.

### Publications

1. **Nazli, Kadriye Özlem**; Pester, Christian W.; Konradi, Artjom; Böker, Alexander; van Rijn, Patrick, Cross-Linking Density and Temperature Effects on the Self-Assembly of SiO<sub>2</sub>—PNIPAAm Core–Shell Particles at Interfaces, *Chemistry - A European Journal*, 19, 5586–5594, **2013**.
2. van Rijn, Patrick; Park, Hyunji; **Nazli, Kadriye Özlem**; Mougín, Nathalie C.; Böker, Alexander, Self-Assembly Process of Soft Ferritin-PNIPAAm Conjugate Bionanoparticles at Polar–Apolar Interfaces, *Langmuir*, 29, 276–284, **2013**.
3. **Hamaloğlu, Kadriye Özlem**; Çelebi, Bekir; Sağ, Ebru; Tuncel, Ali, A new method for the synthesis of monodisperse-porous titania microbeads by using polymethacrylate microbeads as template, *Microporous and Mesoporous Materials*, 207, 17-26, **2015**.

### Oral and Poster Presentations

1. **Hamaloğlu, Kadriye Özlem**; Çelebi, Bekir; Kip, Çiğdem; Tuncel, Ali; Synthesis and characterization of monosized-porous titania beads, *HPLC 2014, 41st International Symposium on High Performance Liquid Phase Separations and Related Techniques*, New Orleans, USA, 11-15 May, **2014**.
2. **Hamaloğlu, Kadriye Özlem**; Sağ, Ebru; Kip, Çiğdem; Gökaltun, Aslıhan; Saraçoğlu, Berna; Tuncel, Ali; Synthesis and characterization of magnetic polyacrylate microspheres with reactive character, *HPLC 2014, 41st International Symposium on High Performance Liquid Phase Separations and Related Techniques*, New Orleans, USA, 11-15 May, **2014**.
3. **Hamaloğlu, Kadriye Özlem**; Akdağ, Cansu; Çelebi, Bekir; Gökaltun, Aslıhan; Tuncel, Ali; Photocatalytic behaviour of monosized-porous titania beads for dye removal in an aqueous medium, *HPLC 2014, 41st International Symposium on*

*High Performance Liquid Phase Separations and Related Techniques*, New Orleans, USA, 11-15 May, **2014**.